Investigating circuits underlying acetylcholine-evoked striatal dopamine release in health and disease

---

DPhil in Physiology, Anatomy and Genetics

Polina Kosillo

Trinity term 2014

Christ Church College, Oxford

Investigating circuits underlying acetylcholine-evoked striatal dopamine release in health and disease

DPhil in Physiology, Anatomy and Genetics, Trinity term 2014

Polina Kosillo, Christ Church College

Abstract

Dopamine (DA) is a key striatal neuromodulator central to normal functioning of the basal ganglia. Identifying and characterizing circuits governing striatal DA transmission is necessary for understanding DA involvement in adaptive behaviour and pathology. Properties of evoked striatal DA release can be examined using fast-scan cyclic voltammetry at carbon fibre microelectrodes, a technique enabling live monitoring of transmitter release events with sub-millisecond resolution. Experimental work presented in this thesis employed this approach to study regulation of striatal DA by acetylcholine (ACh) in health and disease in acute brain slices.

Synchronous activity in a small population of striatal cholinergic interneurons (ChIs) was previously shown to directly drive striatal DA release. Here using optogenetic approach I explore physiological relevance of ChI-evoked drive of striatal DA by examining whether corticostriatal and thalamostriatal afferents to ChIs can trigger ACh-evoked DA events. Following floxed vector injections in motor cortex or caudal intralaminar thalamus of CaMK2a-Cre mice I examine the properties of evoked DA upon light activation of channelrhodopsin-2-transduced inputs to striatal ChIs. These experiments revealed that both cortical and thalamic afferents are capable of driving ACh-evoked DA release, but operate using a different complement of post-synaptic ionotropic glutamate receptors and display distinct release recovery profiles. I further explore if rebound excitation in a population of striatal ChIs could drive DA events by examining whether ACh-evoked DA release follows optical inhibition of striatal ChIs selectively expressing hyperpolarizing halorhodopsin 3.0 or archaerhodopsin 3.0 in ChAT-Cre mice. This work showed that hyperpolarizing ion pumps were not successful in triggering ChI-evoked DA release. I also investigate whether cholinergic brainstem innervation of striatum could contribute to or drive ACh-evoked striatal DA events in

ChAT-Cre rat, concurrently showing that ChI-evoked DA release is not a species artefact, and is present in mouse and rat alike. Current results also suggest that cholinergic brainstem afferents do not drive or contribute to striatal ACh-evoked DA events.

Close interaction between DA and ACh systems further indicates that ACh could impact dopaminergic dysfunction. To explore this I examined the state of ACh transmission in a mouse model of Parkinson's disease overexpressing human wild type α–synuclein protein. These animals present with impaired striatal DA release from young age, but DA deficits could be mediated by changes in ACh tone. Here I show that impaired striatal DA release is the results of primary DA axon dysfunction, although in ventral striatum DA release deficits could be partially compensated by increased ACh tone at nicotinic receptors. I further show that the functional state of muscarinic ACh receptors in not altered following decreased DA transmission, although the data from aged animals suggest that α–synuclein-dependent changes in vesicle handling could contribute to impaired DA releasability. Finally, I show that vesicle handling may indeed be altered in this mouse model as impaired DA release is evident with short stimulation protocols, while with prolonged depolarization of DA axon terminals α–synuclein-overexpressor mice are better able to sustain evoked DA release.

Overall, the main body of work presented in this thesis examined the processes regulating striatal DA transmission via ACh system. In particular, I show that ChI-evoked drive of striatal DA release can be recruited physiologically and further establish that changes in ACh transmission are not the primary drivers of impaired DA releasability in a mouse model of Parkinson's disease overexpressing human α–synuclein protein.

Table of Contents

Acknowledgements

I would like to take this opportunity to formally thank my supervisors Prof Stephanie Cragg and Dr Sarah Threlfell for their patience, support and encouragement on this wonderful and perilous journey. Working with Steph and Sarah has been a great and rewarding experience, not the least because of their huge expertise and passion for rigorous scientific inquiry. Research enthusiasm and curiosity that my supervisors have shared with me will live on well beyond my thesis submission. I am particularly grateful for their sharing of experience, and teaching me that attention to details does not need to obscure the bigger picture. I have been very fortunate in my choice of group to join for DPhil, and in large part this is due to Steph and Sarah always being there to answer questions and to question me. I also would like to thank other members of Cragg group, past and present, for sharing resources and insights. I specifically want to thank Dr Katherine Brimblecombe for moral support and stimulating scientific discussions.

I would like to thank the Clarendon Fund and Christ Church College for their generous funding which made it possible for me to pursue a DPhil at Oxford.

Finally, the people who really made all of this possible are, of course, my parents and sister, whose faith in me and in my achieving any goal I choose gave me strength to preserve in the face of all challenges. I also want to thank Amin for his endless love, limitless support and great generosity in supplying me with chocolates that kept me going for the past few months. Now that this thesis is almost ready to make its way to the submission desk at the Exam Schools, I am yet again realizing how blessed I am, for my wonderful family, supportive friends, knowledgeable and generous colleagues, and my amazing boy really helped me to achieve this new step in my quest for knowledge.

Abbreviations

5-HT	serotonin
6-OHDA	6-hydroxydopamine
AAV	adeno-associated virus
ACh	acetylcholine
AChE	acetylcholinesterase
aCSF	artificial cerebrospinal fluid
AP	action potential
AMPARs	α-amino-3-hydroxy-5-methyl-4-isoxazolepropionic acid receptors
AP	anterior-posterior
Arch	archaerhodopsin
BAC	bacterial artificial chromosome
BG	basal ganglia
BSA	bovine serum albumin
CaMK2	calcium calmodulin kinase 2
CC	corpus callosum
cCPu	central caudate-putamen
CFM	carbon fibre microelectrode
ChAT	choline acetyltransferase
ChI	cholinergic interneuron
ChR2	channelrhodopsin-2
CPu	caudate-putamen, dorsal striatum
CL	central-lateral nucleus of intralaminar thalamus
D1-5	dopamine (1-5) receptors
D-AP5	D-(2R)-amino-5-phosphonopentanoate
DA	dopamine
$[DA]_o$	extracellular evoked dopamine concentration
DAT	dopamine uptake transporter
DHβE	dihydro-β-erythroidine
dlCPu	dorsolateral caudate-putamen

dmCPu	dorsomedial caudate-putamen
dmidCPu	dorsomidline caudate-putamen
DMSO	dimethylsulphoxide
DREADDs	designer receptors exclusively activated by designer drugs
eYFP	enhanced yellow fluorescent protein
DV	dorsal-ventral
E	embryonic day
eGFP	enhanced green fluorescent protein
FCV	fast-scan cyclic voltammetry
EM	electron microscopy
eNpHR	halorhodopsin
GABARs	gamma-aminobutyric acid receptors
GPe	globus pallidus external segment
GPi	globus pallidus internal segment
GYKI25466	4-(8-methyl-9H-1,3-dioxolo[4,5-h][2,3]benzodiazepin-5-yl)-benzenamine hydrochloride
HPLC	high performance liquid chromatography
iGluRs	ionotropic glutamate receptors
IT	intratelencephalic corticostriatal projection
LED	light emitting diode
M1-5	muscarinic (1-5) receptors
mAChRs	muscarinic acetylcholine receptors
MCPG	(S)-α-methyl-4-carboxyphenylglycine
mGluRs	metabotropic glutamate receptors
LDT	laterodorsal tegmental nucleus of brainstem
ML	medial-lateral
MPTP	1-methyl-4-phenyl-1, 2, 5, 6-tetrahydropyrine
MSNs	medium spiny neurons
NA	noradrenalin
NAc	nucleus accumbens, ventral striatum
nAChRs	nicotinic acetylcholine receptors
NGS	normal goat serum

NMDARs	N-methyl-D-aspartate receptors
Oxo-M	Oxotremorine-M
PBS	phosphate buffered saline
PBS-Tx	phosphate buffered saline containing 0.3% Triton X-100
PD	Parkinson's disease
Pf	parafascicular nucleus of intralaminar thalamus
PFA	paraformaldehyde
Pr	release probability
PPN	pedunculopontine nucleus of brainstem
PT	pyramidal tract corticostriatal projection
SEM	standard error of the mean
SNARE	soluble NSF attachment protein receptor
SNc	substantia nigra pars compacta
SNr	substantia nigra pars reticulata
STN	subthalamic nucleus
TANs	tonically active neurons
TH	tyrosine hydroxylase
VGCCs	voltage-gated calcium channels
VTA	ventral tegmental area
WT	wild type
Snca -/-	mouse α-synuclein knockout mice
SNCA OVX	mice overexpressing human wild-type α-synuclein on mouse α-synuclein null background
Synapsin 3 -/-	synapsin 3 knockout mice
TTX	tetrodotoxin
VGLUT1	vesicular glutamate transporter 1
VGLUT2	vesicular glutamate transporter 2
vlCPu	ventrolateral caudate-putamen
vmCPu	ventromedial caudate-putamen

1. General Introduction

1.1 Introduction overview

This chapter aims to provide a summary of the research concerned with understanding the functional interplay between two major basal ganglia (BG) neuromodulators, dopamine (DA) and acetylcholine (ACh). It begins with an overview of the BG anatomy and function, which outlines the major constituent parts of this circuit. Subsequently the functional roles of striatal dopaminergic and cholinergic neurotransmission are discussed and related to behavioural data and pathology.

1.2 The structure and function of the basal ganglia

1.2.1 Functional role of the basal ganglia circuits

The BG are a collection of interconnected nuclei, predominantly of subcortical origin, forming an extensive information processing network involved in a variety of functions. Research to date provides evidence for the BG involvement in practically all aspects of behaviour. The BG facilitate novel task performance based on integrative processing of information currently available in the environment which is necessary for action selection. The BG are also indispensable for using previously overlearned, and therefore automatically performed, behavioural strategies in habitual contexts. The previously held assumptions of BG roles being exclusive to motor performance have now been challenged (Doyon et al., 2009). A wealth of functional data suggest that these circuits also mediate cognitive operations, including selection and execution of cognitive programs, as well as reward-related and probabilistic learning (Packard and Knowlton, 2002; Grahn et al., 2009).

The BG networks are crucial for motor control, planning and motivation (Graybiel et al., 1994; Albin et al., 1995), context-dependent action selection (Nicola, 2007; Cisek and Kalaska, 2010), cognition (Middleton and Strick, 2000), reward-related and habit learning (Knowlton et al., 1996; Schultz, 2006; Yin and Knowlton, 2006), and addiction (Gerdeman et al., 2003; Everitt and Robbins, 2005). Further, BG dysfunctions are involved in a number of neurological conditions, including Parkinson's disease, Tourette's syndrome, attention deficit hyperactivity disorder, obsessive-compulsive disorder, Huntington's disease and schizophrenia. A comprehensive understanding of any single component of this constellation of behaviours is already challenging. Yet, understanding how a network is built to mediate such a variety of functions adds another level of complexity to building working models of the BG. To set a context for a better understanding of the functional underpinnings these behaviours share, the BG anatomical organization is examined next.

1.2.2 Anatomical organization of the basal ganglia: circuit components

Anatomical evidence encompassing data from synaptic to circuit level analyses demonstrate unsurpassed complexity of the BG architecture. Individual BG nuclei, either directly or indirectly interconnected with every other part of the BG, form open and re-entrant processing circuits (Joel and Weiner, 1994), determining the direction and speed of information flow through the network. These multiple operational loops, mediating parallel and sequential information processing, unite the individual BG components to enable adaptive behaviour.

From the input BG nuclei, striatum, or caudate-putamen (CPu), and subthalamic nucleus (STN), information relayed by cortical and thalamic afferents is conveyed to the

output nuclei, substantia nigra pars reticulata (SNr) and globus pallidus internal segment (GPi) (entopeduncular nucleus in rodents), either directly or via relay stations in STN and globus pallidus external segment (GPe). The output BG nuclei then influence behaviour via their projections to thalamus, and hence to cortex, and subcortical pathways, including afferents and/or collaterals to superior colliculus, reticular formation, pedunculopontine nucleus (PPN) and habenula (Figure 1.1). Circuit diagrams summarizing the BG anatomical organization provide an overview of its basic structure. Inclusion of all the functionally relevant components, however, renders these diagrams too complex to be useful. Therefore, for this summary I will focus on the fundamental constituents only.

Conceptually, open processing loops enable adaptive behavioural control by the BG via integration of information across different domains. For example, cortical area that receives the final BG output originating from the pallidum and transmitted via the thalamus can be different from the one that provided afferent signal to the CPu/STN in the first place. This could happen when motor circuits are modified by information from sensory or limbic BG loops, and *vice versa*. Re-entrant computational loops are crucial for control over unwanted interference and maintain segregated processing across functionally distinct territories, such as limbic, associative, sensory, and motor. This division is based on the cortical input origin (e.g. somatosensory, prefrontal, cingulated, amygdala), the striatal territory involved in afferent signal processing (e.g. dorsal CPu, ventral CPu), the pallidal output target (e.g. GPi, SNr, ventral pallidum) and finally the thalamic territory receiving the finalized message (e.g. ventral lateral, ventral anterior, mediodorsal, intralaminar nuclei) (Redgrave et al., 2011). Based on the same organizational principles, these functionally distinct circuits are deemed to perform

similar processing on information from different origins (Voorn et al., 2004). In theory, such organization enables the BG to use common currency for action selection across functionally distinct domains.

Computational models of the BG suggest that it could function as a central behavioural selection mechanism by adopting winner-takes-all strategy to perform program selection based on the relative saliency of the incoming signals (Gurney et al., 2001). This strategy is expected to perform equally well regardless of the total number of competing programs (Stewart et al., 2010), ensuring a stable performance across conditions with small and large number of relevant and competing cues. Thus, having a common denominator for decision-making based on saliency attribution, while still maintaining functional segregation between distinct information processing domains, the BG architecture supports the most advantageous design for a system which generates adaptive behaviour.

1.2.3 Direct and indirect basal ganglia pathways

The BG ability to conduct the orchestra of behavioural selection is critically dependent on the functional and anatomical subdivision of these circuits into direct and indirect pathways, which respectively facilitate and inhibit execution of behavioural programs (Albin et al., 1989; DeLong, 1990; Mink, 1996). The direct pathway medium spiny neurons (MSNs), expressing D1 DA receptors, substance P and dynorphin, enable direct information flow from the CPu to GPi/SNr, while the indirect pathway D2-positive and enkephalin-expressing MSNs transmit messages from the CPu to GPi/SNr via GPe and STN (Gerfen et al., 1990; Smith et al., 1998; Bolam et al., 2000; Gerfen and Surmeier, 2011). Using an intricate balance of glutamate and GABA transmission at the major

input-output junctions of the BG, the direct and indirect pathways regulate disinhibition of their respective targets in ventral thalamus resulting in performance of a selected action (Chevalier and Deniau, 1990)

The exact roles of the direct and indirect pathways in program selection remain the subject of further investigation and debate. Current models postulate that the direct and indirect pathway activation is crucial for behavioural performance, including movement execution, reinforcement learning and drug sensitization (Hikida et al., 2010; Kravitz et al., 2010, 2012; Ferguson et al., 2011; Freeze et al., 2013). The proposed implementation strategies differ markedly, however. Some suggest that direct pathway facilitates command execution, indirect pathway inhibits competing representations, and a pathway with the highest overall activity wins this competition (Mink, 2003; Kravitz et al., 2010; Freeze et al., 2013). Others argue that the timing of signal arrival to the final output targets in the SNr/GPi determines performance (Chan et al., 2005; Brown, 2007). Yet, the latest data demonstrate concurrent and equal activation of direct and indirect pathways in self-guided behaviours *in vivo,* showing that inactivity of the animal corresponds to a silent period in activity of both pathways (Cui et al., 2013). These findings are consistent with another study reporting cooperativity between the two BG projections in voluntary movement, as both D1 and D2 MSNs show motor-related activation, which is positively modulated by reward expectation (Isomura et al., 2013).

Nonetheless, it remains unknown how selection of a single behavioural program occurs even if both the direct and indirect pathways contribute to this process concurrently. Data point to the timing of signal arrival and a brief reset of the beta-band

frequency throughout the BG as a correlate of cue utilization for behavioural performance (Leventhal et al., 2012). Thus, synchronized direct and indirect pathway activity elicited by salient events may transiently stabilize the BG networks to ensure uninterrupted performance of a selected program. Consequently, abnormal beta-band synchronization in Parkinson's patients may impair performance due to over-stabilized network activity, or could persistently engage STN loops halting behavioural output (Leventhal et al., 2012; Shimamoto et al., 2013). The latter interpretation is consistent with the data showing that hyperdirect pathway, cortical-STN-pallidal projection that bypasses striatum (cortex → STN), can intercept striatal messages to the output BG nuclei: by reversing the direct pathway inhibition of SNr, hyperdirect pathway can activate SNr neurons to re-start behavioural selection process (Schmidt et al., 2013). Further research is required to unequivocally determine the processes underlying action selection by the direct and indirect pathways. Given the data on the hyperdirect pathway messages racing to intercept signal arrival to the BG output nuclei, it is likely the relative timing of action potential (AP) discharge by D1 and D2 MSN populations is the key to this BG function.

1.2.4 Striatum as the primary input region of the basal ganglia

1.2.4.1 Local computational circuitry

The direct and indirect pathway distinction first emerges in the CPu, where cortical and thalamic projections, the primary sources of afferent inputs to the BG, target D1 and D2 MSNs (Somogyi et al., 1981; Hersch et al., 1995; Lanciego et al., 2004; Castle et al., 2005). These afferents form an equal number of synaptic contacts with both MSN types (Doig et al., 2010). For the BG the CPu is one of the primary input

stations (for the purpose of this introduction the role of STN as a BG input station is acknowledged, but not discussed), where MSNs integrate messages from their glutamatergic afferents, and by signalling to their output targets generate adaptive behaviour.

MSNs are the primary striatal workforce, accounting for 80-98% of the total cell count (Kemp and Powell, 1971a, 1971b; Somogyi et al., 1981; Graveland and DiFiglia, 1985; Dubé et al., 1988; Smith and Bolam, 1990; Sadikot et al., 1992; Bolam et al., 2000). Compared to MSNs projecting outside the CPu, striatal interneurons constitute a minority, comprising between 2-15% of the total neuronal population depending on species. Among these, nitric oxide synthase-, parvalbumin-, calretinin-, neuropeptide Y- or somatostatin-expressing GABAergic interneurons form extensive feed-forward and feed-back inhibitory circuits via direct cortical innervation or recurrent connections with other striatal neurons (Takagi et al., 1983; Cowan et al., 1990; Bennett and Bolam, 1993; Kawaguchi, 1993; Smith et al., 1998; Bolam et al., 2000; Ramanathan et al., 2002; English et al., 2011; Fino and Venance, 2011; Ibáñez-Sandoval et al., 2011; Sharott et al., 2012). These GABA interneuron circuits have a wide-reaching functional impact on striatal information processing as they regulate the overall excitability of the direct and indirect pathway MSNs and other interneurons (Sullivan et al., 2008; Brown et al., 2012). Therefore, GABAergic interneurons play a significant role in striatal function, including modulation of online processing of the incoming synaptic messages and induction of long-term plasticity. A different type of interneuron, expressing choline acetyltransferase (ChAT), is also an important component of striatal computational circuits (Kawaguchi, 1992). The anatomy and role of ChAT-positive interneurons are discussed in more detail in the subsequent paragraphs (Section 1.5).

1.2.4.2 Corticostriatal projections

Practically the entire cortical mantle sends topographically organized projections to the CPu in all species (Kemp and Powell, 1970; Jones et al., 1977; Tanaka, 1987; McGeorge and Faull, 1989; Wictorin and Rklund, 1989; Berendse et al., 1992; McFarland and Haber, 2000; Cheatwood et al., 2003; Parent and Parent, 2006; Schilman et al., 2008). These corticostriatal afferents originate from cortical pyramidal neurons predominantly found in layer III, and deep and superficial parts of layer V, and form two distinct projections. The pyramidal tract (PT) corticostriatal projection, in addition to innervating ipsilateral CPu, also sends collaterals to the brainstem, while intratelencephalic (IT) neurons project to both ipsilateral and contralateral CPu, with no collaterals outside the telencephalon (Reiner et al., 2010). Interestingly, striatal innervation density observed following targeting deep cortical layers for anterograde anatomical tracing is more widespread than from the more superficial layers. The majority of corticostriatal fibres penetrate the external capsule and directly enter striatal neuropil. However, fibres originating from layers V and VI tend to join the external capsule and only emerge near their striatal target area.

Early anatomical studies reported IT and PT corticostriatal projections display significant variability in the size of their synaptic varicosities, with IT terminals measuring approximately half the size of PT terminals. By inferring that the terminal diameter could reliably identify afferents' origin, researchers suggested that PT projections target indirect, while IT projections preferentially contact direct pathway MSNs (Wright et al., 1999, 2001; Reiner et al., 2003; Lei et al., 2004). A recent study ensuring accurate separation of these overlapping striatal projections using viral transduction, suggested that apparent preferential innervation of direct versus indirect pathway MSNs by IT and

PT projections may not hold true when examined using physiology. Specifically, both IT and PT corticostriatal projections formed functional synaptic connections with D1 and D2 MSNs (Kress et al., 2013). Further, IT projections had similar connection strength with both direct and indirect pathway MSNs, while currents recorded following selective PT afferents stimulation were twice as big in D1 MSNs (Kress et al., 2013). Thus, using optogenetic approach with paired recordings from two MSN classes simultaneously, the Surmeier group showed that the differences between PT and IT projections in conduction velocity, measured as a function of EPSP rise time, observed with electrical stimulation disappear with targeted optical activation. In contrast, the differences in synaptic strength, measured as a function of EPSP amplitude, become more apparent.

1.2.4.3 Thalamostriatal projections

The second major afferent pathway supporting information traffic through the CPu originates in thalamus. As corticostriatal afferents, thalamic projections to the CPu are highly topographically organized, displaying prominent medial-to-lateral and anterior-to-posterior innervation gradients (Schwab et al., 1977; Erro et al., 1999; Smith et al., 2009; Pan et al., 2010; Galvan and Smith, 2011). The total number of striatal terminals staining for vesicular glutamate transporters VGLUT1 and VGLUT2, markers of cortical and thalamic projections respectively (Fremeau et al., 2004b; Raju et al., 2006, 2008), is similar in rodents (Lacey et al., 2005), although in primate CPu occurrence of VGLUT1 terminals is twice as prevalent as VGLUT2 terminals (Raju et al., 2008). Yet, unlike the whole of cortical mantle, only certain thalamic nuclei provide significantly large and robust striatal innervation. Specifically, the midline and intralaminar nuclei of the thalamus form the major thalamostriatal projection pathway, with some contribution from other sub-regions including ventrolateral, mediodorsal, lateral and

anterior thalamic nuclei (Jones and Leavitt, 1974; Cornwall and Phillipson, 1988; Berendse and Groenewegen, 1990; Giménez-Amaya et al., 1995; Sidibé and Smith, 1999; McFarland and Haber, 2000; Van der Werf et al., 2002; Pinto et al., 2003; Cheatwood et al., 2005; Parent and Parent, 2005; Lacey et al., 2007; Kamishina et al., 2008; Kato et al., 2011). The regional specificity of thalamic innervation likely reflects participation of distinct functional modules necessary for rapid and efficient information extraction, processing and transfer from subcortical circuits to the CPu. In contrast, practically ubiquitous cortical innervation demonstrates that recurrent connections supporting higher order processing may rely on dynamic participation of multiple processing units.

1.2.4.4 Tagging the input origin for differential information processing

As the primary point of contact between the BG and its afferents, striatal circuits may selectively utilize information with different origin 'tags' (e.g. based on the timing of signal arrival or the somatodendritic location of synaptic inputs). It is likely that cortical and thalamic afferents provide distinct messages that support behavioural performance in different, yet complementary ways. The distinction can be glimpsed from the following data: a dramatic increase in corticostriatal contacts is observed in SNc lesioned rats with L-DOPA-induced dyskinesia, while the number of thalamic projections remains unaltered (Zhang et al., 2013). These data suggest that remodelling of cortical, not thalamic synapses is responsible for this pathological state, although, unlike rat models, human Parkinson's patients also frequently present with thalamic lesions. The textbook rule of thumb for the BG anatomy also suggests that direct-indirect pathway distinction is a hallmark of striatal architecture, while new data argue that functional segregation can already be observed at cortical level. In particular, motor and sensory-limbic regions seem to preferentially innervate indirect and direct pathways respectively, compared to

thalamic projections which show no selectivity for D1 over D2 MSN targets (Wall et al., 2013).

The functional significance of this arrangement remains unknown, but suggests a possibility of different information types carried by cortical afferents being given precedence for processing in direct versus indirect BG pathways. Further, data showing that D1 MSNs are less excitable compared to D2 MSNs, predominantly due to their dendritic arbour architecture with D2 MSNs having significantly smaller dendritic trees (Gertler et al., 2008), suggest that differential weighting may be given to the afferent messages routinely. This hypothesis is further supported by observations that D2 MSNs fire higher number of APs at similar current intensities as D1 MSNs (Kreitzer and Malenka, 2007), and D2 MSNs generally having lower AP threshold (Cepeda et al., 2008). Thus, the overall impact of any afferent message on its way to the BG output nuclei would be determined by two major factors: 1) the intrinsic properties of the recipient MSNs which equally affect all afferents with a similar synaptic contact architecture, and 2) intrinsic properties of the afferents, including preferential contact with a particular neuronal population, conduction velocity and the mode of information transfer, including release probability and synaptic plasticity.

Modulatory dopaminergic innervation from the midbrain substantia nigra pars compacta (SNc) and ventral tegmental area (VTA) converges with cortical and thalamic terminals at striatal level (Moss and Bolam, 2008). The midbrain DA projections shape network excitability and output of the BG circuits via interaction with local striatal interneurons, projection MSNs and their afferents (Nicola et al., 2000; Bamford et al., 2004; Calabresi et al., 2007; Surmeier et al., 2007; Day et al., 2008). In particular, DA

governs integration of multiple afferent signals by MSNs (Horvitz, 2002; Surmeier et al., 2007; Gerfen and Surmeier, 2011). The anatomy and functional role of the midbrain DA projections are discussed in more detail in the subsequent sections (Section 1.3).

1.2.4.5 Striatal subregions and their behavioural functionality

The CPu is a highly heterogeneous nucleus not only because of its varied cell type composition and abundant innervation from diverse brain structures. Striatal subregions also have a functional gradient in terms of anatomy, biochemistry and behavioural output (Voorn et al. 2004). Dorsal striatal regions are commonly associated with sensorimotor functions, while ventral regions are thought of as limbic territories.

The DA innervation to dorsal striatum originates from the SNc, while VTA projections target more ventral regions, including the nucleus accumbens (NAc), forming an inverse medio-lateral projection gradient (Björklund and Lindvall, 1984; Gerfen et al., 1987b; Nelson et al., 1996; Haber et al., 2000; McFarland and Haber, 2000). The afferents from motor and sensory cortices preferentially innervate dorsal CPu, while prefrontal, cingulate, amygdala and hippocampal projections are more prominent in ventral striatum (Veening et al., 1980; Parent et al., 1983; Berendse et al., 1992; Brog et al., 1993; McFarland and Haber, 2000; Cheatwood et al., 2003; Reep et al., 2003; Schilman et al., 2008). In summary, dorsolateral CPu (dlCPu) receives inputs from the primary and secondary sensory and motor cortices, and its DA innervation originates from the SNc ventral tier. Dorsomedial CPu (dmCPu) is innervated by afferents from the medial prefrontal cortex and SNc dorsal tier. In ventral CPu, NAc core receives prominent input from the basolateral amygdala and ventral prefrontal cortex, while its DA projections originate from the lateral VTA. NAc shell, in turn, receives cortical input

from the orbitofrontal cortex and DA projection comes from the medial VTA. Likewise, for thalamostriatal projections the general rule is for the regions involved in processing of visceral/limbic information, such as paraventricular and medial posterior nuclei, to project to ventromedial striatum, while more posterior and lateral intralaminar nuclei predominantly conveying motor information target dorsolateral striatum (Parent et al., 1983; Van der Werf et al., 2002; Alloway et al., 2014). The heterogeneity in anatomical organization of the afferent inputs corresponds to distinct functional roles these striatal subregions play in behaviour.

Experiments manipulating the connectivity state between corticostriatal and thalamostriatal networks demonstrated that a close interaction between the CPu and its afferents is required for intact behavioural performance. For example, unperturbed information flow between the dlCPu and infralimbic cortical circuits underlies acquisition of habitual behaviours (Smith and Graybiel, 2013), while intact connectivity between parafascicular nucleus (Pf) and dmCPu are critical to adaptive performance in goal-directed paradigms following contingency change (Bradfield et al., 2013). Plenty of data also demonstrate that functional disruption of distinct striatal regions is detrimental to specific behavioural outcome measures, presenting a good case for double dissociation between stimulus-response (habitual) and action-outcome (goal-directed) learning and behavioural performance mediated by dlCPu and dmCPu, respectively.

Interference with the dlCPu function is detrimental to formation of new habits and performance of already acquired habitual behaviours. For example, rodents no longer display habitual behavioural performance following dlCPu lesions, reverting to goal directed actions sensitive to outcome devaluation, and also fail to form new habits

(Yin et al., 2004, 2006; Quinn et al., 2013). Further, performance of complex motor sequences, characteristic of habitual behaviour, and operant task learning reliably elicit increased neuronal activity in the dlCPu (Aldridge et al., 2004; Kimchi et al., 2009). In humans, habit formation was also linked to increased dlCPu activity, observed following cue presentation after extensive overtraining (Tricomi et al., 2009). The dmCPu lesions, in contrast, impair goal-directed performance and lead to reversal to habitual behaviours, also curtailing acquisition of new action-outcome contingencies (Yin et al., 2005a, 2005b). The Balleine group elegantly addressed double-dissociation between dlCPu and dmCPu roles in habitual and goal directed behaviours. By selective disruption of extracellular signal-related kinase activity researchers showed that dlCPu is crucial in sensorimotor-based learning, while dmCPu is required for acquisition of action-outcome associations and performance of goal directed behaviours (Shiflett et al., 2010). Finally, ventral striatum, NAc in particular, is long accepted to mediate basic reward-related learning based on Pavlovian conditioning paradigms (Everitt et al., 1991; Day et al., 2006, 2007). Together, these data demonstrate that regional specificity in striatal anatomy and function has prominent correlates in animal behaviour.

1.2.5 The role of neuromodulators in basal ganglia functions

The BG functions are also critically dependent on modulatory neurotransmitter systems. In particular, DA and ACh play a prominent role in facilitating normal information flow through the BG, especially at striatal level. Collectively these neuromodulators regulate the excitation balance between direct and indirect BG pathways, control induction of plasticity between local striatal circuits and their afferents, and mediate some of the pathological changes following BG dysregulation in disease (Mercuri et al., 1985; Calabresi et al., 1993, 2000a, 2000b; Levine et al., 1996;

Centonze et al., 1999, 2001; Reynolds and Wickens, 2002; Zhou et al., 2003). This dependence is further evidenced by dramatic changes in BG-related behaviours in human patients with Parkinson's disease, 6-OHDA-lesioned rodents and MPTP-treated primates. It is also illustrated by disorders of addiction whereby drugs capable of interfering with dopaminergic neurotransmission cause abnormal habit learning and thus substance dependence. Furthermore, increased DA transmission is hypothesised to underlie schizophrenia, psychotic episodes, and in some cases of Tourette's syndrome could also produce behavioural hyperactivity, increased stereotypy and reduced control over motor inhibition (e.g. tics). The data on ACh role in BG function suggest that this neuromodulator also plays a substantial role in controlling normal BG output. Although for the cholinergic system the evidence is more circumstantial, mostly related to ACh regulation of DA transmission and intrinsic excitability of direct and indirect pathway MSNs. The functional and anatomical organization of these striatal neuromodulatory systems, as well as their reciprocal interactions and the overall impact on the BG circuitry, are discussed next.

1.3 Midbrain dopaminergic neurons

1.3.1 Anatomical organization of the SNc and VTA: ontogeny and connectivity

The developmental origin of some 45 000 dopaminergic SNc and VTA neurons in rodents (German and Manaye, 1993), can be traced using [3H]-thymidine injections in pregnant dams, with subsequent co-localization of this marker with tyrosine hydroxylase (TH) staining. These studies show that the SNc DA neurons are born before the VTA neurons, around embryonic day 11 (E11) (Bayer et al., 1995). Originating from a

common neuroepithelial source, midbrain DA neurons found in the dorsolateral regions differentiate earlier than those from the ventromedial tier (Altman and Bayer, 1981; Bayer et al., 1995). A whole host of transcription and neurotrophic factors is involved in the process of lineage induction, commitment and subsequent differentiation and survival of the midbrain DA neurons (Smits et al., 2006). These complex signalling cascades comprise multiple interdependent components intricately regulated along the time and concentration axis, but they are still incompletely understood. It is well established, however, that soon after DA neurons are born, they extend their processes dorsally and then rostrally, forming the medial forebrain bundle upon their exit from the midbrain on the way to their striatal and cortical targets (Voorn et al., 1988; Nakamura et al., 2000; Gates et al., 2004).

During early postnatal development dopaminergic innervation of striatum is not homogenous: patch compartment receives first dopaminergic projections, while matrix compartment is innervated by later developing dopamine neurons (Gerfen et al., 1987a; van der Kooy and Fishell, 1987). In adult animals these regions can only be distinguished by neurochemical markers, such as calbindin staining for matrix (Gerfen et al., 1985), and mu opioid receptors staining for patch compartment (Herkenham and Pert, 1981). Distinct sets of dopamine neurons provide differential input to patch and matrix regions with VTA and SNc dorsal tier favouring striatal matrix, while SNc ventral tier projections target striatal patch (Gerfen et al., 1987b). Such anatomical organization is present across species and found in rodent, cat and primate (Gerfen et al., 1985; Jimenez-Castellanos and Graybiel, 1987; Langer and Graybiel, 1989). A more recent study labelling dopamine neuron axonal arbour in its entirety actually showed that both dorsal

and ventral tier SNc neurons could target both patch and matrix compartments, although any given neuron favours only one territory (Matsuda et al., 2009).

Midbrain efferents from area A9, corresponding to the SNc, project almost exclusively to dorsal CPu forming nigrostriatal DA projection pathway; while projections from A8 and A10 VTA regions form mesolimbocortical pathway, innervating ventral CPu, cortical and subcortical limbic areas, including prefrontal and cingulate cortices, septum, basal forebrain and amygdala (Fallon and Moore, 1978; Gerfen et al., 1987b; Fallon, 1988; Gasbarri et al., 1994; Del-Fava et al., 2007). These SNc and VTA projections travel to the forebrain via the medial forebrain bundle (Haber et al., 2000), and upon exit from this tight axonal bundle near their target areas form extensive axonal arborisations. These dopaminergic axonal arbours densely innervate all striatal sub-territories constituting approximately 10% of all synaptic contacts (Groves et al., 1994), with an average nearest neighbour distance of just 1.2 μm between individual axons (Arbuthnott and Wickens, 2007). The architecture of dopaminergic terminals in the striatum is described in more detail in the subsequent sections (Section 1.3.3).

Early anatomical studies examining afferent projections to the midbrain DA neurons using anterograde and retrograde tracer injections suggested afferents to both SNc and VTA neurons display convergent innervation. The majority of midbrain afferent inputs were found to originate from cortical and subcortical structures, including limbic cortex, amygdala, hippocampus, ventral pallidum and striatum (Zahm et al., 2011). In contrast, a recent study employing trans-synaptic rabies virus tracing approach showed SNc and VTA have a divergent profile of monosynaptic afferent connections. Specifically, SNc afferents were dominated by projections from sensorimotor cortex, superior

colliculus and STN, while VTA predominantly received hypothalamic and dorsal raphe innervation, and both SNc and VTA were densely innervated by striatopallidal projections (Watabe-Uchida et al., 2012). These contrasting results are likely to stem from the methodologies employed. Tracer studies, in general, are limited due to possible tracer uptake by damaged and intact fibres of passage that form no actual synaptic connections in the regions where they are detected. Using rabies virus that can cross one synaptic junction enables detection of afferent connections which actually form functional contacts with the anatomical structure of interest. For connectivity mapping using viral transduction, however, limiting factors are the extent of virus spread and possible off target effects.

Overall, the big picture of the afferent midbrain DA neuron innervation is the following. Circuits which the SNc and VTA send efferents to also reciprocally innervate these midbrain regions, forming pallidum-midbrain projecting network (Hattori et al., 1975). Thus, the internal organization of the BG truly adheres to the rule of closed-loop circuits, which has important implications for its behavioural output. The other SNc afferent projection extensively innervating this region and having profound influence on SNc output is the innervation from brainstem PPN (Clarke et al., 1987; Lokwan et al., 1999). The VTA role in reward-related, visceral/limbic and subjective decision bias processing (Stopper and Floresco, 2014), is broadly supported by afferents from periaquedactal grey, locus coeruleus and ventral and dorsomedial medulla, and lateral habenula complex, respectively (Mejías-Aponte et al., 2009; Omelchenko and Sesack, 2010; Bernard and Veh, 2012). Finally, there is some evidence for species differences in the density and extent of prefrontal cortical innervation of the midbrain between rodents and primates. In mouse extensive prefrontal afferents selectively target GABA

mesoaccumbens projecting and DA mesocortical projecting neurons (Carr and Sesack, 2000). In contrast, primates generally have a small number of sparsely distributed fibres innervating SNc and VTA (Frankle et al., 2006).

1.3.2 Cell type composition of the SNc and VTA neuronal populations

Electron microscopy (EM) studies of the tissue following tracer injections in SNc/VTA enable to determine the sites of synaptic contact that midbrain projections make with their post-synaptic neurons. These data revealed that the anatomical sites of the midbrain afferent terminals did not always co-localize with TH staining. Thus, in addition to heterogeneity in the afferent and efferent connections, SNc and VTA are also characterized by heterogeneous cell type composition. While the majority of the midbrain neurons from these regions, commonly referred to as DA neurons, are indeed dopaminergic, expressing markers for TH, vesicular monoamine transported 2 and dopamine uptake transporter (DAT) (Perrone-Capano et al., 1996; Pickel et al., 2002; Li et al., 2013), there are subsets of cells which are non-dopaminergic (Swanson, 1982).

To date, neurons expressing GABA (Steffensen et al., 1998; Carr and Sesack, 2000) or glutamate (Yamaguchi et al., 2007; Dobi et al., 2010) have been identified within the VTA, as well as the SNc (Nair-Roberts et al., 2008; Yamaguchi et al., 2013). As a population, these non-dopaminergic midbrain neurons also give rise to long axonal projections innervating the same targets as the DA neurons. These non-dopaminergic cells also form synaptic contacts with local midbrain DA neurons. Furthermore, the early studies demonstrating co-expression of VGLUT2 and DA neuron markers in the midbrain (Kawano et al., 2006), are now supported by functional evidence. New data present a case for co-release of DA and other neurotransmitters taking place from SNc and VTA

neurons both *in vivo* and *in vitro* (Chuhma et al., 2004). Specifically, targeting of genetically defined DA neuronal populations for selective activation with light using optogenetics showed that DA neurons are capable of co-releasing glutamate (Stuber et al., 2010; Tecuapetla et al., 2010; Hnasko et al., 2012; Adrover et al., 2014; Chuhma et al., 2014), GABA (Tritsch et al., 2012, 2014; Nelson et al., 2014b), and yet unidentified neurotransmitter which excites striatal ChIs (Straub et al., 2014). The functional significance of this transmitter co-release arrangement remains the subject of intense debate. Some groups suggest that glutamate co-transmission could aid DA packaging and storage (Hnasko et al., 2010), as is the case with glutamate-acetylcholine co-packaging in ChIs (Nelson et al., 2014a). Others argue that no glutamate transporters co-localize with DA axon terminals in the CPu in adult rodents (Moss et al., 2011), suggesting lack of classical pre-synaptic machinery for glutamate handling. Thus, it is possible that glutamate co-transmission from the midbrain DA neurons depends on the neurodevelopmental stage.

The case of GABA and DA co-transmission is even more controversial. A study showing that GABA is not synthesized *de novo* by DA neurons, but is taken up from the CPu terminals (Tritsch et al., 2014), offered a plausible mechanism for DA and GABA co-localization at dopaminergic terminals. Yet, the functional role this mechanism could fulfil remains the subject of speculation. Researchers have suggested that DA-GABA co-release could be necessary for rapid inhibition of striatal output neurons (Nelson et al., 2014b), possibly via shunting the response to excitatory cortical and thalamic inputs (Tritsch et al., 2014), or for mediating feed-forward inhibition (Tritsch et al., 2012). This mechanism could facilitate filtering of the afferent inputs to the striatal MSNs of cortical and thalamic origin, ensuring only the strongest signals elicited by the most salient cues

are transmitted. Another and not mutually exclusive possibility is that regulation of BG circuits by SNc and VTA happens via a multitude of signalling cascades employing different neurotransmitter systems and their respective anatomical organizations. Such an arrangement would enable semi-independent regulation of distinct receptor classes on different temporal and spatial scales. For example, GABA transmission mediated by point-to-point synaptic mechanisms and DA volume transmission could affect striatal output acting at distinct neuronal subtypes in partially overlapping anatomical regions. This conjecture is further supported by the data showing distinct release profiles of DA and GABA from dual transmitter neuronal cell cultures. In this experimental paradigm, GABA is released in single rapid quantal events as measured by electrophysiology, while amperometry reveals 'prolonged' asynchronous release of DA vesicles (Borisovska et al., 2013).

1.3.3 Architecture of dopaminergic circuits in somatodendritic and axon terminal regions

At the midbrain level, SNc and VTA DA neurons are known to have particularly long and modestly branched dendrites extending in multiple directions depending on the tier. Dorsal tier neurons extend their processes longitudinally along the rostro-caudal and medial-lateral axis, while ventral tier neurons are particularly likely to extend their dendritic branches ventrally into the SNr (Henny et al., 2012). At the axon terminal level in the CPu, midbrain DA neurons undergo massive expansion of their total arbour volume. The axonal arbour of a single rat DA neuron can occupy up to 6% of the total striatal volume (Matsuda et al., 2009), forming a colossal number of synaptic contacts on the order of 150 000 per neuron (Oorschot, 1996; Roberts et al., 2002), although some estimates reach 400 000 per single SNc neuron innervating CPu territories (Arbuthnott

and Wickens, 2007). On average, DA axonal varicosities form a synapse every 10-20 μm^3 (Descarries et al., 1996; Matsuda et al., 2009; Threlfell and Cragg, 2011). In comparison to the grand total size of their dendritic and axonal arbour, the cell body of a DA neuron constitutes less than 1% of its total volume (Matsuda et al., 2009; Henny et al., 2012).

Extensive innervation of striatal territories by DA projections ensures that all striatal microstructures are positioned within 1 µm of a DA releasing site (Moss and Bolam, 2008). The average intersynaptic distance between neighbouring DA axons is around 3.5 µm (Cragg and Rice, 2004). This dopaminergic architecture ensures that all synaptic transmission events, especially those between local striatal circuits and their glutamatergic afferents, are in a position to be modulated by DA. EM data also show that the majority of putative DA release sites in the CPu lack post-synaptic density specialization (Descarries et al., 1996; Descarries and Mechawar, 2000), suggesting DA transmission mostly occurs outside the confinements of a synaptic cleft. The fact that DA uptake transporters and the majority of DA receptors are predominantly found extrasynaptically (Nirenberg et al., 1996, 1997; Pickel, 2000; Rice et al., 2011), also indicates that the architecture of striatal dopaminergic innervation is conducive to volume transmission. Similarly, at the midbrain level very few dendro-dendritic synapses are present (Wilson et al., 1977; Groves and Linder, 1983), while DA receptors on the DA neuron plasma membranes and afferent inputs, as well as DAT are localized extrasynaptically (Sesack et al., 1994; Yung et al., 1995; Nirenberg et al., 1996). Therefore, dopaminergic transmission in both axon terminal regions and somatodendritic areas is likely a subject to volume transmission (Cragg and Rice, 2004). This hypothesis is supported by the data demonstrating DA spillover from the synapse

both in the CPu and midbrain, where it can be recorded with electrochemical detection techniques (Cragg and Rice, 2004; Rice and Cragg, 2008; Cragg et al., 2011).

1.3.2 Dopamine neuron physiology and its relevance to behaviour

Mesostriatal DA neurons typically display two characteristic firing modes *in vivo*: low frequency tonic discharge and high frequency burst firing. In tonic mode, midbrain DA neurons fire single APs at frequencies up to 10 Hz, while in burst firing mode DA neurons fire groups of 3-5 APs at frequencies of up to 30-60 Hz (Grace and Bunney, 1984a, 1984b; Hyland et al., 2002; Floresco et al., 2003; Jeong et al., 2012). Burst firing mode of DA neurons is frequently characterized as phasic activity, and thought to encode salient events, including prediction-related information about rewards and reward delivery (Schultz et al., 1993; Schultz, 1998; Morris et al., 2004; Matsumoto and Hikosaka, 2009), aversive events (Brischoux et al., 2009), and possibly stress (Anstrom and Woodward, 2005). Recent data also suggest the existence of a third transmission mode, extended phasic firing, present during behaviours directed towards distant goals. Researchers suggest that this mode of DA signalling could be responsible for sustained motivational drive (Howe et al., 2013).

Correlation analyses of tonic and phasic DA neuron firing modes with amperometry recordings of striatal DA release demonstrate that distinct DA transmission modes are associated with each firing mode of the parent cell bodies. In particular, tonic DA neuron firing results in uniform monoamine concentrations throughout the CPu, while phasic firing can elicit temporally and spatially heterogeneous DA concentration profiles (Venton et al., 2003). Thus, transient burst firing of midbrain DA neurons is expected to produce a different state of network coupling between DA

transmission and its downstream effectors than their tonic discharge. Computational modelling of experimental data also agrees on phasic burst firing of DA neurons carrying the largest amount of information to their post-synaptic targets, while tonic firing patterns correspondingly generate a truly stochastic output structure (Jeong et al., 2012). Consequently, it can be argued that phasic burst firing of DA neurons carries the largest amount of meaningful information that can be utilized in shaping behavioural output in a manner that differentially engages distinct subdivisions of the BG circuitry, depending on the primary striatal recipient territory.

The behavioural relevance of striatal DA signals finds extensive support in the literature, both as a teaching signal in reinforcement learning and motivating signal for working towards obtaining a reward. As predicted by Rescorla-Wagner learning model, the amplitude of responses conveying a teaching signal should decrease with learning. A similar behaviour is characteristic of DA neuron firing, where electrophysiology recordings consistently show a decrease in DA neuron firing once reward prediction error is absent, i.e. learning function has reached asymptote (Hollerman and Schultz, 1998). Further, attenuation of DA signal is observed following extended training as animals acquire complete knowledge of the temporal structure of a task and fully anticipate reward-predictive stimuli (Clark et al., 2013). Some researchers, however, suggest that an alternative explanation of established contingency leading to decreased attention to conditioned stimulus or even response suppression by conditioned stimulus cannot be excluded (Holmes and Fam, 2013). Amphetamine challenge data also demonstrate that strict temporal coupling of striatal DA signal with reward predictive cues is essential for learning (Daberkow et al., 2013). Yet, striatal DA signalling is also

extensively involved in motivational aspects of behaviour (Robbins and Everitt, 1996; Berridge and Robinson, 1998).

A working model of how motivational and learning aspects of dopaminergic signalling fit together suggest that tonic DA participates in motivational coding, as DA tone manipulations globally affect response rates, while phasic increases in DA neuron activity provide the actual prediction error signal (Niv, 2007). This model provides a plausible account of how behavioural performance is combined across motivation and learning domains supported by DA signalling. It was further extended by Morita and Kawaguchi (2013) who put forward a closed-circuit model to incorporate the upstream circuits affected by DA. Authors suggest that computations performed by intracortical and corticostriatal loops are differentially modulated by DA acting at D1 and D2 receptors on MSNs. Therefore, motivation and learning are supported by indirect pathway encoding the value of the previous action (template), while the direct pathway provides the information about the current value (comparator) upon which action is performed (Morita et al., 2013). By matching the template and comparator values, DA system identifies the discrepancies, providing motivational and teaching signals.

In order to identify and isolate the necessary and sufficient components for translation of DA neuron signalling into behavioural output, correlation data must be supported by direct manipulations of the midbrain circuits. With the advent of optogenetic approaches, this has been made possible. Now there is data showing that mimicking reward prediction error by transient selective activation of DA neurons concurrent with reward delivery leads to cue-elicited reward-seeking behaviour in blocked learning paradigm (Steinberg et al., 2013). These data indicate that animals have

learned the association between a new predictor and reward delivery even though under normal circumstances previously formed associations would prevent new learning. Activation of the VTA DA neurons following nose poke in reward magazine was also sufficient to drive operant responses in the absence of reward delivery (Kim et al., 2012), further demonstrating the causal role of DA signals in driving reward-seeking behaviours.

1.4 Mechanisms underlying dopamine release

The significance of DA signalling for the BG networks lies not only in its critical role in mediating normal circuit function and reward-related learning dependent on the firing mode of the midbrain DA neurons, but also the associated DA release events occurring in two distinct BG compartments, the midbrain and striatum. Both somatodendritic and axonal dopamine release depend on the firing rate and pattern of the midbrain DA neurons, which oscillate between low-frequency tonic firing and short high frequency burst activity already described. Mechanisms regulating somatodendritic and axonal DA release are explained next.

1.4.1 Midbrain somatodendritic and striatal axon terminal dopamine release

Neurotransmitter release events require Ca^{2+} entry through voltage-gated calcium channels (VGCCs) to prime assembly of the vesicle fusion machinery. DA release in both the somatodendritic compartment and at the axon terminal level have been shown to be Ca^{2+}-dependent (Rice et al., 1994, 1997; Cragg and Greenfield, 1997; Chen and Rice, 2001; Ford et al., 2010). Some studies, however, find that Ca^{2+}-dependence of somatodendritic DA release is substantially lower than the axonal DA release in CPu

under similar experimental conditions (Hoffman and Gerhardt, 1999; Chen and Rice, 2001; Chen et al., 2006), suggesting minimal Ca^{2+} entry may be required for somatodendritic release. There are several possible reasons for these contradicting results. Firstly, species differences between guinea pig and rat/mouse could explain this discrepancy, especially given that cadmium and VGCCs blockers were previously shown to inhibit somatodendritic release in rat/mouse slices (Herdon and Nahorski, 1989; Jaffe et al., 1998; Phillips and Stamford, 2000). Secondly, prolonged pulse trains for driving somatodendritic release events can also evoke release of other transmitters, including GABA, glutamate, ACh, which can dynamically alter DA release via feedforward and feedback mechanisms (Rice et al., 2011). Lastly, KCl application for driving release events may collapse normal ionic gradients that regulate vesicle fusion, thus limiting detectability of Ca^{2+} involvement in DA release. Moreover, Ca^{2+} entry is important not only for regulation of DA release, but also for homeostatic events which regulate tonic and burst firing of DA neurons by altering responsiveness of DA neurons to their glutamatergic inputs (Kim et al., 2013). Overall, blockade of the VGCCs and application of Ca^{2+}-free perfusion media decrease the amplitude of or completely abolish DA release events, although may do so to a different extent within the somatodendritic versus axon terminal regions, depending on the stimulation protocol and species. Another factor which accounts for the strong Ca^{2+} dependence of axonal DA release compared to somatodendritic compartment is the compound dependence of both DA and ACh release on Ca^{2+}, which constitute two lots of 4^{th} power dependence on Ca^{2+} entry for quantal release (Rice et al., 2011).

The assumption that both terminal and somatodendritic DA release events are supported by vesicle fusion is controversial, however. Data suggest that vesicle fusion

events in the SNc are rare (Wilson et al., 1977). Moreover, vesicle density in the midbrain is low, while DA axon terminals in the CPu are densely packed with readily identifiable vesicles (Wilson et al., 1977; Groves and Linder, 1983; Nirenberg et al., 1996, 1997). Consequently, some researchers suggest that somatodendritic DA release is not supported by classical vesicle fusion processes but rather reversal of DAT, which may explain its limited dependence on Ca^{2+} entry in some species. Further, somatodendritic DA storage is suggested to take place at the endoplasmic reticulum (Mercer et al., 1979; Wassef et al., 1981). Yet, the bulk of data show that for both axonal and dendritic DA release are dependent on both AP propagation and calcium as evoked DA events are abolished by sodium channel blocker tetrodotoxin (TTX) and in Ca^{2+}-free solutions or following application of VGCCs blockers (Rice et al., 1994, 1997; Cragg and Greenfield, 1997; Chen and Rice, 2001; Ford et al., 2010). Furthermore, somatodendritic DA release is not prevented by DAT inhibitors which would be expected to prevent DAT reversal as an alternative mechanism of release to vesicular exocytosis (Cragg et al., 1997a; Hoffman et al., 1998; Chen and Rice, 2001). Moreover, VTA DA release, evoked by *in vivo* stimulation of the medial forebrain bundle, shows an increase in signal amplitude with DAT blockade and is depleted by continuous stimulation lasting 5 seconds and longer (Kita et al., 2009). Therefore, fundamentally similar release mechanisms probably regulate DA release in both neuronal compartments, even though conventional vesicle fusion processes in the somatodendritic regions may not support all evoked DA events, contrary to spontaneous DA release (Fortin et al., 2006). It is also possible that differences in the mechanisms regulating exocytosis of DA-containing vesicles from dendrites versus axon terminal compartments is determined by fine-tuned regulation processes that are species-specific.

Release events in the somatodendritic and axon terminal regions do differ in terms of the extracellular DA concentrations and the timecourse of DA signal. Generally, release levels are substantially higher in CPu and NAc, while VTA and SNc show more modest evoked extracellular DA concentrations (Cragg and Greenfield, 1997; Cragg et al., 1997a; Rice et al., 1997; Ford et al., 2010). Even in the midbrain itself evoked DA amplitudes follow a gradient from VTA to medial SNc to lateral SNc, with the highest extracellular DA concentrations on the order of 1 μM observed in the latter (Rice et al., 1997). The exact reason for this regional heterogeneity in DA release still remains unknown. Although it is likely to be the function of vesicle loading as well as the relative density of the release sites, and the larger extracellular volume fraction in the midbrain compared to the CPu (Rice and Nicholson, 1991; Cragg et al., 2001). Another possibility is the termination of DA signal by D2 autoreceptors which differ between somatodendritic and axon terminal compartments, having significantly weaker influence on limiting evoked DA release in the midbrain (Cragg and Greenfield, 1997). In summary, the main factors contributing to prolonged timecourse of DA transients in the midbrain compared to the CPu would be the level of DAT expression/activity, the size of the extracellular volume fraction, which lead to delayed DA signal termination in SNc and VTA due to limited DA uptake and increased diffusion, respectively, and reduced D2 autoreceptor control (Cragg et al., 1997b, 2001; Chen and Rice, 2001; Rice and Cragg, 2008; Ford et al., 2010). Importantly, both somatodendritic and axon terminal release events can be frequency- or pulse number-dependent (Rice et al., 1997; Rice and Cragg, 2004; Zhang and Sulzer, 2004; Fortin et al., 2006; John et al., 2006; Kita et al., 2009). This suggests that the firing activity of the midbrain DA neurons is dynamically translated in release events that may reflect the degree of DA neuron excitation. However, DA transmission

in striatum is extensively regulated by local striatal factors, including the cholinergic system, which controls dynamic gating of DA release probability and also drives local striatal DA release, as outlined in the next sections (Section 1.6).

1.4.2 Factors regulating regional variability of striatal dopamine release

The timecourse and amplitude of evoked DA transients in striatum can vary significantly between different regions. Availability and absolute concentrations of evoked extracellular DA ($[DA]_o$) in the CPu and NAc are strongly governed by factors regulating striatal DA release, such as autoinhibition of DA release by D2 receptors, and DAT-mediated uptake of $[DA]_o$. For example, with single pulse stimulation, the timecourse of evoked DA signal reaching its peak and subsequently being terminated by DAT is similar between different striatal territories. However, in the presence of D2 receptor antagonist, with pulse train stimulation lasting 1000 ms or longer, the maximal response is reached within 500 ms in dorsal CPu, whilst in the NAc extracellular DA levels continue to rise for the whole stimulus duration. While initial release probability, which is tightly regulated by ACh and is higher in CPu than NAc, contributes to this difference, the primary players are likely to be inhibition of DA release by D2 receptors and availability of DA transporters (Cragg and Greenfield, 1997; Cragg et al., 2000, 2002).

Striatal DAT expression follows dorsolateral to ventromedial gradient with significantly higher expression and activity levels of DAT in the dlCPu, corresponding to the sensorimotor striatal territory (Cragg et al., 2000, 2002; Voorn et al., 2004). Consistent with DAT expression gradient, DA signal termination upon its extracellular release happens faster in the dlCPu, than in the ventromedial CPu (vmCPu) or NAc. Similar to the ventral striatum, limited uptake substantially hinders the rate of DA

clearance following exocytotic events in the SNc and VTA, although in the midbrain this process is also significantly affected by diffusion (Cragg et al., 1997b, 2001; Chen and Rice, 2001; Rice and Cragg, 2008; Ford et al., 2010).

D2 receptor-dependent regulation of DA release via autoinhibition also shows regional specificity. It is likely to be another important factor which determines the shape of extracellularly recorded evoked DA transients. D2 autoreceptors on DA neurons suppress DA release in the SNc (Cragg and Greenfield, 1997) and striatum (Phillips et al., 2002; Moquin and Michael, 2009), whilst VTA seemingly lacks D2 autoreceptor regulation (Cragg and Greenfield, 1997; Kita et al., 2009). Further, in CPu post-synaptic D2 receptors on MSNs also have an inhibitory effect on DA release (Anzalone et al., 2012). Thus, the distinct timecourse of evoked DA release observed in different midbrain and striatal territories likely incorporates feedback signal provided by D2 receptors.

Regional variability of DA release regulation by D2 receptor-mediated feedback and possibly DAT expression gradient, at least in the CPu and NAc, has been taken by some researchers to mean that distinct DA release micro domains exist. Arguably, these distinct micro domains present with different DA release dynamics in the experiments where the same tissue and electrodes are used for the monoamine recordings with fast-scan cyclic voltammetry (FCV) (Moquin and Michael, 2009, 2011; Mitch Taylor et al., 2012; Shu et al., 2013; Taylor et al., 2013). These claims are not unequivocally accepted, given the inherently stochastic nature of neurotransmitter release in any given system. Moreover, the fact that FCV recordings which sample DA release from a population of transmitter releasing sites may not converge on the same population within any one striatal region all of the time also undermines the micro domain hypothesis. It is

possible, however, that such micro domains indeed exist, providing an additional axis for the fine-tuned regulation of the local computational circuitry by DA. In addition, to highlight the behavioural relevance of D2-mediated inhibition of DA release, at least for the somatodendritic compartment, mice lacking D2 receptors in the midbrain DA neurons present with enhanced DA synthesis and release which leads to hyperlocomotion, enhanced motivation and cocaine hypersensitivity (Bello et al., 2011).

The auto regulation of release by the DA system itself plays a prominent role in supporting normal functioning of the BG circuits. Nonetheless, all the data collected to date suggest that these internal control systems are routinely overridden by ACh axis, both in CPu and NAc (Threlfell and Cragg, 2011). Therefore, striatal cholinergic system and its close interactions with striatal dopaminergic innervation, in particular the regulation of DA neurotransmission at the axon terminal level, are discussed next.

1.5 Striatal cholinergic interneurons

1.5.1 Anatomy and functional characteristics of the striatal cholinergic interneurons

The birth date of striatal cholinergic interneurons (ChIs) in the embryonic development cycle is close to the time when the midbrain DA neurons are generated. Specifically, tissue graft transplants from the foetal rodent brain suggest that ChIs are born in the medial ganglionic eminence around E12.5 (Olsson et al., 1998). These ChI precursors then migrate tangentially from the progenitor zone to the CPu, where they differentiate into local striatal interneurons (Marin et al., 2000). ChIs are the resident striatal ChAT-positive interneurons, with fusiform- or polygonal-shaped giant cell body

(20-50 μm) and aspiny dendrites, which are tonically active, maintaining one of the highest cholinergic marker levels in the whole brain (Hoover et al., 1978; Smith and Bolam, 1990; Wilson et al., 1990; Kawaguchi, 1992, 1993; Bolam et al., 2000). Given that ChIs constitute roughly ~1-5% of the total number of striatal neurons, depending on the species, their functional impact is staggering and is broadly supported by their extensive dendritic and axonal arbours innervating large striatal territories (Kemp and Powell, 1971a; Bolam et al., 1984; Phelps et al., 1985). The lower percentage of ChIs is generally found in rodents, while primates are reported to have higher cell count of ChIs relative to the total striatal neurons, as previously reported for other striatal interneuron types (Wu and Parent, 2000). The architecture of dendritic and axonal arborisations of ChIs enables them to create densely interconnected networks which extensively communicate to regulate population activity either directly (Drukarch et al., 1990) or via recruitment of fast-spiking GABAergic interneurons (Sullivan et al., 2008). The functional significance of the networks built by the striatal ChIs is further supported by data from the human brain. In the caudate and putamen regions with fewer ChIs, cells are larger in size, suggesting an increase in size may be required to compensate for the lack of higher ChI density (Bernácer et al., 2007).

The total number of axonal varicosities formed by a single ChI can total up to 500 000, with a 10 μm radius sphere of striatal neuropil containing on average 400 cholinergic axon terminals (Contant et al., 1996; Descarries and Mechawar, 2000; Threlfell and Cragg, 2011). Although the size of a single ChI in the entirety of its dendritic and axonal arbour has not been formally quantified, rough estimates suggest that the total volume of striatal tissue occupied by DA terminals is on the same order as the tissue volume taken up by cholinergic processes. The immunohistochemical markers for

these neurotransmitter systems overlap substantially (Zhou et al., 2001). Extensive arborisation of ChI processes are also closely interposed with the dopaminergic axonal lattice (Contant et al., 1996; Descarries and Mechawar, 2000). Moreover, similar to striatal dopaminergic transmission, there is evidence that ACh, a classic point-to-point transmitter in the peripheral nervous system and at the neuromuscular junction, could employ volume transmission in the central nervous system. Specifically, there is a significant mismatch between the location of ACh release sites and their respective post-synaptic ACh receptors, as well as low incidence of synaptic specializations on cholinergic structures (Wainer et al., 1984; Houser, 1990; Hill et al., 1993; Mrzljak et al., 1993; Umbriaco et al., 1994; Descarries et al., 1997; Arroyo-Jim nez et al., 1999; Mechawar et al., 2002; Kawai et al., 2007). Together, data suggest that the architecture of the cholinergic and dopaminergic circuits is conducive to their close interaction both with each other and other components of striatal computational circuitry. This hypothesis finds extensive support in the literature with data showing that reciprocal interactions between ACh and DA are critical to normal striatal function (Bertorelli et al., 1992; Di Chiara et al., 1994; Calabresi et al., 2000b, 2007; Rakovska et al., 2003; Rice and Cragg, 2004; Zhang and Sulzer, 2004; Bonsi et al., 2011).

ChIs, also termed tonically active interneurons (TANs), have been shown to display tonic firing both *in vivo* and *in vitro* (Wilson et al., 1990; Kawaguchi, 1993; Aosaki et al., 1994b; Bennett and Wilson, 1998, 1999; Zhou et al., 2002). Tonic AP firing in striatal ChIs happens independent of their synaptic inputs and is regulated by intrinsic pace-making mechanisms (Bennett and Wilson, 1998; Bennett et al., 2000). Previously believed to be the sole source of striatal cholinergic innervation (Woolf, 1991; Contant et al., 1996), ChIs maintain consistently high ACh levels in the striatum. The ACh signal is

terminated through hydrolysis of ACh into choline and acetic acid by acetylcholinesterase (AChE), although ACh degradation rate is expected to differ between patch and matrix compartments due to variable AChE activity levels (Graybiel and Ragsdale, 1978; Messamore, 1993). The latest anatomical data further suggest that the brainstem innervation could be another significant source of striatal ACh. Specifically, cholinergic afferents from rostral and caudal PPN territories and laterodorsal tegmental nucleus (LDT), provide relatively sparse, but robust and topographically organized innervation of all striatal subregions (Dautan et al., 2014). The functional significance of this newly described projection is currently the subject of an intense study effort, and some of the relevant data will be discussed in Chapter 4.

1.5.2 Behavioural relevance of cholinergic interneuron activity: encoding of novel/unexpected events and learning

Striatal ChIs encode behaviourally salient events, including occurrence of novel/unexpected and/or motivationally relevant events, as well as contextual information about action performance (Graybiel et al., 1994; Calabresi et al., 2000b; Apicella, 2002, 2007; Kimura et al., 2003). Some researchers even suggest that dorsally- and ventrally-located putative ChIs encode different aspects of task performance, with the former conveying motor and the latter transmitting task-related information (Yarom and Cohen, 2011). Although the causal evidence from studies which directly manipulate ChI activity to measure behavioural outcomes is currently lacking, the type of afferent inputs that ChIs receive from their cortical, but most significantly thalamic afferents, argues that transient activation of ChIs could convey alerting response to behaviourally significant cues (Sadikot et al., 1992; Pisani et al., 2000; Matsumoto et al., 2001; Van der

Werf et al., 2002; Reynolds and Wickens, 2004; Lacey et al., 2007; Ding et al., 2010; Doig et al., 2014).

The unique feature of ChI participation in behaviour is that they transiently alter their tonic activity in response to behaviourally relevant, alerting or unexpected cues even prior to conditioning. With repeated cue presentation TANs show habituation and the amplitude of their responses diminishes. Yet, ChIs also acquire characteristic burst-pause firing pattern following conditioning, which is thought to be the main correlate of ChI involvement in learning (Aosaki et al., 1994b; Schulz et al., 2011). Acquisition of this response pattern could happen via entrainment of ChI activity to cue or reward related information by synchronized cortical or thalamic inputs (Reynolds and Wickens, 2004), perhaps with the added contribution of long-latency cortically driven excitation to aid rebound ChI spiking (Schulz and Reynolds, 2013). This feature of the ChIs makes them a significant player in the field of adaptive behavioural control. However, as the data presented in the next section argue, it is not ACh alone that makes conditioning paradigms work.

1.5.3 Coordinated processing of behaviourally significant events by dopaminergic and striatal cholinergic systems

The behavioural relevance of interactions between DA neurons and ChIs can be glimpsed from the studies showing coincident firing of the two neuron classes recorded in SNc and CPu, respectively, in conditioning paradigms. Specifically, midbrain DA neurons and striatal ChIs show temporally coincident responses to reward-related events in probabilistic instrumental conditioning task (Morris et al., 2004). The Bergman group show that the intrinsic activity patterns of ChIs and DA neurons during task

performance change in opposing direction, with DA neurons showing a phasic increase in their spiking activity, while ChIs pause their ongoing tonic firing in a temporally coincident manner (Morris et al., 2004). Authors interpret the data of single unit activity during cue presentation, response execution and reward delivery anticipation as DA neurons encoding information about the reward, while ChI responses keeping circuit timing. This conclusion emerged from observation that ChI activity did not encode reward, but instead ChI responses correlated with reward omission, suggesting the cholinergic system kept track of when the outcome was to occur. Further, in light of data showing that ChI pauses enable an increase in the amplitude of striatal DA signals by mechanisms described in the following section (Cragg and Rice, 2004; Rice and Cragg, 2004; Zhang and Sulzer, 2004), it is plausible to argue that ChIs could set the time during which DA signals are processed most efficiently to govern behavioural performance. A later study from the same group also showed coincident albeit opposite responses of DA neurons and ChIs in a classical conditioning task with rewarding and aversive events, demonstrating that both neuronal populations were more strongly modulated by rewards (Joshua et al., 2008). The authors again interpret their data as indicating that DA neurons encode the cue and outcome delivery, while ChIs encode the outcome delivery and omission. Computational modelling of these data also suggests complementary encoding of salient events by striatal ACh and DA transmission (Tan and Bullock, 2008).

The observation that the two transmitter systems encode different task parameters during execution of a given behavioural episode coincides with interpretation of adaptive coding supported by close interactions between ACh and DA. The question, however, is what information the two systems provide, and one explanation is that while DA signals supply the prediction error signal, ChIs set the

temporal frame for when the information provided by dopaminergic system is to be considered. This hypothesis is supported by the data showing dynamic gating of DA release by ACh, which is discussed in the next section. Importantly, gating of DA signals by ChIs doesn't just support the timing idea, but also suggests direct shaping of DA signal by ACh transmission. Further, it has been shown in the literature that pauses in ChIs acquired with learning are dependent on DA (Aosaki et al., 1994a), and that interference with either DA or ACh transmission significantly impairs reward-related procedural learning and even produces neglect-like symptoms (Ljungberg and Ungerstedt, 1976; Knowlton et al., 1996; Matsumoto et al., 1999; Kitabatake et al., 2003). Together, these data suggest that close interactions between striatal ACh and DA axes on anatomical and functional levels support complementary encoding that is necessary for adaptive behaviour.

1.6 Interaction between striatal cholinergic and dopaminergic systems at the synaptic level in driving dopamine release events

Close examination of data from behavioural studies is necessary for understanding the context in which ACh-DA interactions happen, and explaining the behavioural relevance of striatal signalling cascades supported by ACh and DA release. It is also necessary to understand the mechanisms governing those interactions. This section will expand on the processes governing interdependence of ACh and DA transmission in regulating striatal DA release.

1.6.1 The antagonistic balance hypothesis

The early conceptual framework for understanding ACh-DA interactions was that the two neurotransmitter systems operated in an antagonistic balance. Several lines of evidence supported this case. Firstly, data from Parkinson's studies provided perhaps the most dramatic demonstration of this effect with administration of drugs which inhibit ACh (e.g. atropine) or increase DA (e.g. L-DOPA) to the patients alleviating motor and some cognitive symptoms and producing similar therapeutic outcomes (Pisani et al., 2003; Calabresi et al., 2006; Bonsi et al., 2011; Smith et al., 2012b). Secondly, a wealth of data from physiology studies show that at the post-synaptic neuron level DA and ACh release/application have the opposing effects on both the intrinsic excitability of striatal MSNs and plasticity induction between the striatal circuitry and its glutamatergic afferents (Calabresi et al., 2000b, 2007; Reynolds and Wickens, 2002; Centonze et al., 2003; Wang et al., 2006, 2013; Fino and Venance, 2010). Finally, there is data suggesting that DA release can inhibit or reduce the rate of ChI firing by activating D2 receptors and potentiating slow hyperpolarisation currents, which in turn inhibit ACh release (DeBoer and Abercrombie, 1996; DeBoer et al., 1996; Pisani et al., 2000; Maurice et al., 2004; Reynolds et al., 2004; Deng et al., 2007; Sanchez et al., 2011b). On the flip side, the data regarding ACh release either inhibiting or potentiating DA release had until recently been highly inconsistent. While some researchers showed that ACh exercises tonic inhibitory influence on DA release (Kudernatsch and Sutor, 1994), others found both increases and decreases in the amplitude of evoked DA transients following manipulation of the cholinergic axis. Recently, an explanation for these data has emerged from this lab, with the idea of dynamic gating of DA release probability by ACh.

1.6.2 Dynamic frequency-dependent gating of striatal dopamine release by acetylcholine

A basic feature of any transmitter-releasing synapse is the release probability (Pr) that characterizes this synapse. The Pr is a product of multiple interdependent but random factors due to stochastic nature of the transmitter release events, and in the case of dopaminergic system, the function of extracellular ACh levels. Data collected by our group and others suggest that the cholinergic system operates a gain control mechanism on striatal DA release: by increasing the release probability of the first spiking event and introducing a short-term depression for the subsequent APs arriving in close succession (Schmitz et al., 2002; Cragg, 2003), via two distinct acetylcholine receptor types. Specifically, nicotinic ACh receptors (nAChRs) residing on DA axon terminals and muscarinic ACh autoreceptors (mAChRs) on ChIs have been shown to dynamically gate DA release in a frequency-dependent manner (Zhou et al., 2001; Rice and Cragg, 2004; Zhang and Sulzer, 2004; Exley et al., 2008; Threlfell et al., 2010; Cohen et al., 2012).

The functional implications are at least two-fold. Firstly, when nAChRs are briefly activated by ACh, electrical stimulation of DA axons *in vitro* results in DA release events that vary very little with stimulation frequency or pulse number. Thus, activation of nAChRs effectively clamps Pr at the dopaminergic synapse/release site to a single high value, boosting release for individual action potentials or low frequencies, and reducing the gain during successive action potentials in a high frequency burst. Thus, short-term depression of Pr at short interpulse intervals limits the amount of DA released (Abeliovich et al., 2000; Cragg, 2003; Montague et al., 2004). However, when nAChR

effects are removed either by receptor desensitization via inhibition of AChE activity leading to increased extracellular ACh or via application of nicotine, or blocked by application of nAChR antagonists, the picture of release changes dramatically: low frequency or single pulse stimulations now evoke significantly lower DA levels than high frequency bursts (Rice and Cragg, 2004; Zhang and Sulzer, 2004). Under these circumstances, the activity of DA neurons can be dynamically translated into the release events where extracellular DA concentrations, i.e. signal amplitude, can reflect the rate of input activity or stimulation strength. The same principles apply to manipulation of cholinergic transmission by interfering with mAChR function: activating mAChRs effectively shuts down spiking activity in ChIs via autoinhibition and by reducing extracellular ACh levels decreases cholinergic tone at nAChRs, which no longer exercise their control on DA Pr (Threlfell et al., 2010).

Different subtypes of nAChRs and mAChRs are known to mediate the influence of the cholinergic system on DA transmission in dorsal and ventral striatum (Threlfell and Cragg, 2011). For the purpose of this introduction I focus on nicotinic receptor expression on dopaminergic terminals and muscarinic receptor expression on cholinergic neurons, because other striatal cell types also express diverse combinations of these receptors. Striatally-projecting dopaminergic neurons express a diverse array of α (α3-7) and β (β2-4) nAChR subunits, which form homomeric or heteromeric pentamers consisting of different subunit combinations (Picciotto et al., 1998; Champtiaux et al., 2003; Salminen et al., 2004; Exley et al., 2008, 2011, 2012; Gotti et al., 2010). The α3 subunit, however, is not present in rodent, but is found in primate striatum (Gotti et al., 2005; Quik et al., 2005). All nAChRs on striatal DA axon terminals putatively contain β2

subunit (Champtiaux et al., 2003; Salminen et al., 2004), while expression of α4, α5 and α6 subunits is thought to vary between different striatal territories. In particular, α4α5β2-containing subtypes of nAChR are predominantly found and govern dopaminergic transmission in the CPu, while in the NAc dopaminergic transmission is regulated by α4α6β2β3-containing subtypes of nAChR (Drenan et al., 2010; Exley et al., 2011, 2012).

In contrast to the ligand-gated nAChRs which form a channel pore in the cellular membrane to exercise their action, mAChRs are G-protein-coupled. Five different mAChR subtypes M_1-M_5 are divided into two large families according to their down-stream effector coupling, M_1-like (M_1, M_2, M_5) and M_2-like (M_2, M_4). In striatum predominantly M_1, M_2 and M_4 mAChR subtypes are found (Zhang et al., 2002b; Zhou et al., 2003). ChIs in particular express and are extensively modulated by M_2 and M_4 mAChRs (Yan and Surmeier, 1996; Alcantara et al., 2001; Ding et al., 2006). Pharmacologically, subtype-specific ligands for mAChRs are lacking. Thus, mouse receptor-specific knockout models only recently began to elucidate differential involvement of mAChR subtypes in striatal function. For example, experiments measuring potassium-stimulated ^{3}H-ACh release in mice lacking either M_2 or M_4 receptors suggested that autoinhibition of striatal ACh release is predominantly mediated via M_4 mAChRs (Zhang et al., 2002a). Preparations for those experiments, however, lacked regional information as the whole striata from the single receptor knockout mouse brains were processed. Thus, more recently, both M_2 and M_4 receptors have been shown to regulate ACh release in dorsal striatum, whilst in NAc core and shell M_4 mAChRs dominate (Threlfell et al., 2010). These observations suggest that predominance of M_4 versus combined M_2-M_4 mAChRs signalling in striatum is strongly

influenced by the dorso-ventral divide. These data present another example of region- or domain-specific control over striatal function and in particular fine-tuning of ACh-DA interactions. Nonetheless, advancements in the field of optogenetics showed that the dynamic gating hypothesis was still oversimplified, and in fact that under the right conditions activation of the cholinergic system can directly drive DA release.

1.6.3 Direct drive of striatal dopamine release by cholinergic interneurons

Direct axon-axonic interaction for driving DA release by ACh were uncovered by recent investigations coupling FCV with optogenetics (Cachope et al., 2012; Threlfell et al., 2012). This newly identified mechanism bypasses the need for activation of the parent cell bodies residing in the SNc and VTA in driving terminal DA release in the CPu and NAc. This body of work revealed that interactions between ChIs and DA go beyond the modulatory gate-keeping that governs contrast enhancement between tonic and phasic DA signals during ChI pauses (Cragg, 2006). In fact, ChIs can also directly drive striatal DA release, by activating nAChRs on DA axon terminals and triggering local DA release events both in dorsal and ventral striatum (Cachope et al., 2012; Threlfell et al., 2012). This ACh-evoked drive of striatal DA release is present both *in vivo* and *in vitro*, and was shown using two different mouse models. Our group used knock-in ChAT-Cre mouse line in which a floxed viral vector for selective light activation of ChIs was stereotaxically injected (Threlfell et al., 2012). The Cheer group used a bacterial artificial chromosome (BAC) model constitutively expressing an optogenetic construct in ChAT-positive neurons (Cachope et al., 2012). A later study, however, found increased vesicular acetylcholine transporter copy number expression in this line and consequently

an increased cholinergic tone (Kolisnyk et al., 2013). However, the fact that the locally mediated ACh-evoked DA signalling was present across different recording and stimulation conditions, and in different mouse models suggests that this is a robust phenomenon. The main body of work presented in this thesis focuses on exploring and characterizing candidate networks that could engage and regulate this local drive of striatal DA release.

Understanding which afferent inputs trigger ChI-evoked DA signalling in striatum would also provide a major scientific advance. A direct drive of DA release by ACh indicates that the local cholinergic control of striatal DA transmission goes beyond the dynamic gating of DA release in response to spiking activity of the midbrain DA neurons, and instead can directly mediate DA release events. The staggering implication of this finding is that the information encoded by ChIs, and possibly their long-range afferent inputs synchronizing ChI activity, might also be translated into striatal DA signals. Under these circumstances, striatal DA transmission could reflect not only parameters encoding reward-prediction error or related states conveyed by the phasic burst firing of the midbrain DA neurons. It could also incorporate signalling from other systems, such as thalamostriatal or corticostriatal projections, which can provide attentional and/or contextual information, creating an expectation set for aiding task performance.

1.6.4 Other mechanisms regulating axonal dopamine release

Regulation of axonal DA release by the cholinergic system is best put in perspective by comparing it to other mechanisms that locally regulate striatal DA release. While ACh-DA interactions happen on a millisecond time scale and are mediated

by direct interaction between the two systems, other regulatory intermediaries acting on different time scales and involving diverse secondary signalling cascades also exist.

The most simple example is that of DA release suppression by glutamate acting at metabotropic glutamate receptors (mGluRs) on DA axon terminals, mGluR I subtype in particular (Paquet and Smith, 2003; Zhang and Sulzer, 2003). Activation of mGluR I is unlikely to happen routinely under experimental conditions employing short stimulation protocols. Yet, prolonged depolarization of multiple circuits, including glutamatergic, as is the case with long pulse train electrical stimulations, is likely to drive glutamate 'spillover' leading to DA release inhibition via SK channel activation (Zhang and Sulzer, 2003). Similarly, only long pulse train stimulations reveal the involvement of ionotropic glutamate (AMPA) and GABA ($GABA_A$) receptors in regulation of striatal DA release, with application of their respective antagonists leading to activation and inhibition of evoked $[DA]_o$ respectively (Avshalumov et al., 2003, 2008). These interactions happen on a much longer time scale than can be revealed by a single pulse or short high frequency burst protocols, and involve an intermediary. In this case, it is the MSNs, which are also activated by local electrical stimulation (Kita, 1996) and express AMPA and $GABA_A$ receptors (Bernard and Bolam, 1998; Chen et al., 1998; Fujiyama et al., 2000). The data show that activated MSNs stimulate production and release of H_2O_2, which serves as a secondary messenger in regulation of striatal DA release by glutamatergic and GABAergic transmission with long stimulation protocols (Avshalumov et al., 2003, 2008; Patel et al., 2011). These interactions are predominantly found in dorsal striatum, while local regulation of dopaminergic signalling in the ventral striatum presents an even more complex picture.

Data on regulation of DA release in the NAc core and shell reveal extensive involvement of cannabinoid receptors. Systemic administration of CB1 receptor agonist suppresses the evoked DA release, simultaneously increasing the frequency and amplitude of spontaneously occurring DA events *in vivo* (Cheer et al., 2004, 2007). Administration of δ-opioid and μ-opioid receptor agonists suppresses DA release evoked by single pulse and enhances release by intermediate stimulation frequencies via modulation of ChI activity, while κ-opioid receptor agonist uniformly inhibits DA release across all stimulation frequencies independently of ChIs (Svingos et al., 2001a, 2001b; Britt and McGehee, 2008). Finally, nitric oxide supplied by the local striatal nitric oxide synthase-positive interneurons can directly regulate DA release in activity dependent manner, similar to when nAChR activity is suppressed (Hartung et al., 2011).

Together, these data demonstrate that striatal DA release is also subject to multiple regulatory mechanisms outside the cholinergic axis and dopaminergic autoregulation. These mechanisms involve multiple signalling cascades and yet again emphasize the complexity of functional and anatomical organization of the BG, particularly in regulation of striatal DA transmission. While gating of evoked DA by the above processes happens on a longer time scale than ACh-dependent regulation of DA release and release probability, and is secondary to ACh-DA interactions, it is important to be aware of these effects. Furthermore, paradigms which employ electrical stimulation are most likely to drive those secondary gating mechanisms by concurrent stimulation of multiple circuits releasing a multitude of neurotransmitters and neuromodulators, especially if long stimulation protocols (<1000 ms) are used.

1.7 Studying basal ganglia circuit components with optogenetics

The combined use of optogenetics and FCV enabled our group and others to explore whether synchronous activation of a population of striatal ChIs can directly drive local DA release. This experimental question could not be addressed using electrical stimulation, as such an approach would also activate the DA axis directly. In this section, I explore the working principles of optogenetics, and how this technique could be used to answer fundamental questions about locally evoked striatal DA neurotransmission.

1.7.1 Driving neural circuit activity with light

The use of conventional stimulation methods, such as electrical stimulation, has shortcomings for investigating how isolated circuits function. Although electrical stimulation is temporally precise, it is non-specific in the cell types that it depolarizes in the vicinity of the stimulating electrode. Thus, it cannot be used to activate a specific pathway or cell type. Investigations into the roles of specific circuits therefore require use of cocktails of receptor antagonists for known interfering transmitters, while other unknown substances that might also be released in response to stimulation cannot be controlled for. Consequently, insights from electrical stimulation approaches are limited. The recent introduction of optogenetics has overcome this major shortcoming. Optogenetics enables study of the functions of defined circuits and cells with a specificity that has previously been unattainable. In the context of the work presented in this thesis, optogenetic stimulation of corticostriatal and thalamostriatal afferents significantly advanced our ability to explore the contribution made by each circuit in driving ChI-evoked DA release. It also enabled us to examine the role of specific thalamic subregion, which with electrical stimulation approach would be impossible.

In overview, optogenetics is an optical stimulation technique whereby light-sensitive ion channels, such as channelrhodopsin-2 (ChR2), or ion pumps, such as halorhodopsin-3 (eNpHR 3.0) or archaerhodopsin-3 (Arch 3.0), are expressed in a population of genetically identifiable cells to allow their activity to be controlled with light. Depending on the type of opsin chosen, neuronal circuits targeted for optogenetic stimulation can be either depolarized or hyperpolarized with light of appropriate wavelength and intensity. Specifically, ChR2 is a light-sensitive algal cation channel (Nagel et al., 2003), that can be expressed in mammalian neurons making them amenable to depolarization with 473 nm blue light with high temporal precision (Boyden et al., 2005; Gradinaru et al., 2007). Further, in neurons where ChR2 is expressed at high levels in axons and terminals, terminal arbours can be directly excited by light even in the absence of intact connection with their parent cell body (Petreanu et al., 2007). eNpHR 3.0 is an inward chloride ion pump, which following light activation increases the intracellular concentration of Cl^- leading to neuronal hyperpolarization, and has been successfully used to inhibit neuronal activity and manipulate behaviour in rodents (Han and Boyden, 2007; Royer et al., 2010; Britt et al., 2012; Mattis et al., 2012; Smith et al., 2012a; Smith and Graybiel, 2013). Arch 3.0 is another light-activatable ion pump, which pumps H^+ out into the extracellular space to achieve hyperpolarization, and has been successfully applied for neuronal response inhibition and behavioural manipulation in mouse (Chow et al., 2010; Beltramo et al., 2013; Znamenskiy and Zador, 2013). Both of these hyperpolarizing tools have red-shifted light activation response in the yellow-green spectra around 560 nm, although they can also be activated by blue light.

Overall, optogenetic methods achieve sophisticated control over the activity of specific neural circuits and genetically defined neuronal populations, including activation

and inhibition, using cell-type specific expression of depolarizing and hyperpolarizing opsins. To date, this has been achieved primarily through the use of transgenic rodent driver lines expressing *Cre*-recombinase under the control of a neuron-type-specific promoter, combined with injections of floxed viral constructs, whereby opsins are expressed in a neuron-type-specific manner. This is the approach that was also adopted for the work presented here and it is described next using the example of ChR2. An alternative method for expression of optogenetic constructs if not using *Cre*-LoxP system, is by using cell-type specific promoters (e.g. Thy 1) in vectors driving opsin expression. This way optogenetics can be used in wild-type animals, but this approach lacks the specificity offered by the *Cre*-LoxP system.

1.7.2 Expressing opsin constructs in cell type-specific manner

The *Cre*-LoxP optogenetic approach enables cell type-specific expression of ChR2 using viral vector delivery of doubly-floxed inverted open reading frame constructs carrying the gene sequence from algae *Chlamydomonas reinhardtii* that encodes the light-activated cation channel (Boyden et al., 2005; Zhang et al., 2006; Cardin et al., 2009, 2010; Tsai et al., 2009). Such constructs use a strong general promoter (e.g. EF-1α) to drive ChR2 expression as due to the low single channel conductance, high levels of cell surface expression are required for successful activation of neurons with light (Lin, 2011; Yizhar et al., 2011). These construct are usually packaged in replication-deficient viral vectors, for example adeno-associated virus (AAV), which offer extensive spatial spread and high transduction levels (Taymans et al., 2007; Cardin et al., 2009).

The *Cre*-loxP system is ideal for selective optogenetic control of genetically-defined neuronal networks owing to the ready availability of transgenic mouse lines

expressing *Cre*-recombinase under numerous cell-type specific promoters using knock-in or BAC technology (Gong et al., 2007; Tsai et al., 2009; Madisen et al., 2010; Taniguchi et al., 2011; Zhao et al., 2011). *Cre*-recombinase expressing rat lines are also emerging (Weber et al., 2011; Witten et al., 2011; Schönig et al., 2012). Thus, it is possible to virally deliver opsins to a specific brain region using stereotaxic surgery. Only the *Cre*-positive cells in the target area will activate ChR2 expression by selective recombination of the loxP sites in the construct resulting in inversion of the transcription frame and subsequent expression of ChR2 driven by the strong ubiquitous promoter. For my optogenetic work, I used different mouse Cre lines and targeted stereotaxic injections of AAV-packaged floxed vectors to drive opsin expression in selected neuronal populations, described in more detail in Chapter 2.

1.7.3 Choosing vectors for targeted opsin expression

Currently available data on AAV vectors suggest that different serotypes may have differential 'preferences' for a cell type that they predominantly transduce (Rabinowitz et al., 2002; Broekman et al., 2006; Korecka et al., 2011; Sanchez et al., 2011a; Hutson et al., 2012). This factor is important when choosing a vector, as preferential transduction of a particular cell type could mean that low expression levels are achieved in the cell population of interest if 'wrong' construct is used. Preferential transduction with higher expression levels in a related pathway may also confound results where experimentally unrelated co-activation masks the signals from the main pathway of interest. To address these concerns in the work presented in this thesis, AAV5-packaged ChR2 construct was employed as it has better reported transduction efficiency and spread (Burger et al., 2004; Paterna et al., 2004; Taymans et al., 2007;

Markakis et al., 2010), as well as previously reported success in activating projections to ChIs originating from caudal intralaminar thalamus (Threlfell et al., 2012).

Another critical issue in vector choice that emerged from the experiments targeting corticostriatal and thalamostriatal projections with AAV5-packaged ChR2 was that the direction of vector trafficking from the injection site could differ between AAV serotypes. Very few publications to date explicitly distinguish between retrograde and anterograde trafficking of AAV-packaged injectable ChR2 constructs. There is now sufficient evidence, however, to suggest that different AAV serotypes used for opsin packaging differentially employ axonal transport in rodents and primates (Ciesielska et al., 2011; Masamizu et al., 2011). For example, AAV serotype 2 is transported only anterogradely, while AAV serotype 6 has the capacity for preferential retrograde transport (Salegio et al., 2012). In the work presented here, I have encountered both retrograde and anterograde axonal transport for ChR2 packaged in AAV serotype 5 but not serotype 2, which is consistent with observations made by other groups (Paterna et al., 2004). These issues are discussed in more in Chapters 3 and 4.

1.7.4 LED versus laser for light activation of opsin-expressing neuronal populations

The choice between a laser and a light emitting diode (LED)-based system for optical activation depends on the type of stimulation required for the experiment. Use of a laser system offers focused spot illumination achievable by directing the light through the microscope optics via a fibre-optic cable. Depending on microscope objective magnification and the size of fibre-optic cable, a spot size as small as a few micrometres can be achieved. This set up offers advantages in targeting small volumes

of tissue, even though due to diffractive properties of the brain, light scattering may occur. For the work on ChI-evoked DA release using a focused laser beam of only 15 µm in diameter to activate ChR2-expressing ChIs, our group was able to establish that action potentials synchronised in only a few cells were required to directly drive striatal DA release (Threlfell et al., 2012). In contrast, the use of an LED system enables full-field illumination of the tissue under the microscope objective, although focused spot illumination can also be achieved to some degree with an LED using a pin-hole system, but for that purpose LED systems needs to be coupled to the microscope optics.

The amount of depolarization generated in a given cell by optical stimulation reflects the summation of photocurrents from all activated opsin channels, and is proportional to the light intensity at the target and the illuminated surface area. On a per cell basis, a diffuse light from an LED system having lower light intensity power, but able to cover larger illumination area, could have the same effect as high-intensity illumination from a highly focused laser beam on a smaller surface area. However, in practical terms, experiments run on LED and laser systems can be expected to depend on the geometry of the system under study, the expression pattern of opsin, the question addressed and the measured outcome. For example, when population activation with little spatial specificity is required, a full field LED approach would be suitable, whereas to study effects of activation of a single synapse/cell, a laser might be required. Work performed in our lab shows that both small spot laser illumination and full field LED illumination can be used interchangeably when studying a population-based response, i.e. locally evoked DA release, at least when directly driving population activity in striatal ChIs.

By contrast, when using ChR2 to activate thalamostriatal or corticostriatal terminals to depolarise ChIs and subsequently evoke DA release, we used the LED system. ChR2-expressing thalamic or cortical terminals which innervate individual ChIs are likely to be variable in number and patchy in expression pattern. In part, this happens due to variable transduction of parent neurons with ChR2. Therefore, the probability of driving ChI-evoked DA release by activation of thalamic/cortical afferents is lower than when directly driving a population of ChIs. Thus, focused spot-illumination of tissue with laser would be and was less successful than full-field illumination with LED in these experiments. Consequently, LED system was used to ensure that any ChR2-expressing fibres present in the field of view, which may happen to be in close proximity to or make synaptic contacts with sparsely distributed ChIs can be activated with blue 473 nm light to drive ACh-evoked DA release by depolarization of striatal ChIs via activation of their glutamatergic afferents of thalamic or cortical origin.

1.8 Parkinson's disease: α-synuclein and dopamine

In addition to exploring the circuits which support dopaminergic signalling in health, an important aspect of characterizing factors which regulate DA neurotransmission is related to understanding DA in disease. In this case, the primary focus of discussion will be Parkinson's disease (PD), as a mouse model of this human condition was also used for the work presented in this thesis to integrate aspects of DA and ACh interactions which are relevant to both health and diseased states.

1.8.1 Dopamine neuron degeneration in Parkinson's disease

PD is a neurodegenerative condition widely affecting aging populations, with the global prevalence of 1.8 per 100 of persons aged over 65 (de Rijk et al., 2000). PD is the

result of degeneration of a subset of dopaminergic neurons residing in the SNc (Yamada et al., 1990; Fearnley and Lees, 1991), which disrupts normal functioning of the BG. Specifically, degeneration of SNc neuromelanin-positive and calbindin-negative cells results in dopaminergic denervation of striatum (Hirsch et al., 1988; Kish et al., 1988; Scherman et al., 1989), and aberrant synaptic weighting of activity in this brain region (Calabresi et al., 1993). Consequently, in patients suffering from PD, a triad of motor symptoms encompassing bradykinesia, rigidity and resting tremor, and non-motor impairments become manifest.

The success of dopamine replacement therapies in alleviating movement impairments, at least during the early disease stages prior to the onset of secondary dyskinesias, suggests that dopaminergic deficits are central to the motor phenotype in PD (Smith et al., 2012b). Moreover, during the later disease stages patients begin to present with additional cognitive and neuropsychiatric impairments, indicative of dysfunction in other neural circuits (Dubois and Pillon, 1997). This observation underscores the importance of interactions between DA and other neurotransmitters in maintaining functional homeostasis. Mechanisms underlying the dysfunctional state of DA transmission in PD are still not established unequivocally.

1.8.2 *SNCA* gene involvement in Parkinson's disease

Genetic and genome-wide association studies point to the *SNCA* gene (encoding α-synuclein protein) involvement in both sporadic and familial PD (Satake et al., 2009; Simón-Sánchez et al., 2009). Identified point mutations (A53T, A30P and E46K) (Polymeropoulos et al., 1997; Krüger et al., 1998; Zarranz et al., 2004), as well as duplication and triplication of the *SNCA* locus (Polymeropoulos et al., 1997; Krüger et al.,

1998; Zarranz et al., 2004) are known to cause autosomal dominant PD. GWAS also support the involvement *SNCA* gene in sporadic cases (Venda et al., 2010).

Pathophysiology data from *SNCA* locus multiplication studies highlight a gene dosage effect. The *SNCA* gene triplication leads to earlier symptom onset, more severe disease progression with the added burden of dementia, compared to duplication (Fuchs et al., 2007). However, clinical variability in disease onset and advancement rates could reflect not only the gene dosage effects, but also point to different aetiological pathways determined by the site of action of aberrant quality/quantity of α-synuclein. For example, global overexpression of α-synuclein could undermine a multitude of neural systems and cell types, leading to generalized break down in normal cellular physiology, whilst 'restricted' point mutations could selectively affect SNc neurons due to yet unidentified vulnerability mechanism.

1.8.3 Aggregation of α-synuclein protein in Parkinson's disease

Lewy body pathology, present in most patients with idiopathic and familial PD, also attests to involvement of α-synuclein in disease-related processes. Lewy body pathology is characterized by cytoplasmic filamentous aggregates containing α-synuclein found in surviving dopaminergic cells and other neurons, and is one of the hallmark PD features (Baba et al., 1998; Spillantini et al., 1998). It remains undetermined whether α-synuclein aggregation is a neurotoxic event in itself, leading to neuronal dysfunction and subsequent apoptosis, or a way in which cells cope with a protein displaying abnormal properties. Given that post-translation modifications of α-synuclein, including phosphorylation (Fujiwara et al., 2002), oxidation (Hashimoto et al., 1999), or alterations in its normal turnover rate prime aggregate formation (Al-Mansoori et al., 2013), it is

possible that cellular quality control mechanisms attempt to sequester aberrant protein by forming fibrils.

Despite different rates of aggregate formation, both wild-type and mutant oligomeric α-synuclein species display neurotoxic properties, at least in a culture dish, and assemble basic building blocks for fibril formation (Lashuel et al., 2002; Kayed et al., 2003; Feng et al., 2010; van Rooijen et al., 2010; Giehm et al., 2011). Thus, it is hypothesised that high-order oligomeric α-synuclein species allow cells to lower toxicity incurred by pre-fibrillar structures, which can, for example, perforate neuronal lipid bilayer (Tsigelny et al., 2012) or disrupt mitochondrial membrane integrity (Nakamura et al., 2011). Several early studies suggested that up-regulation and aggregation of α-synuclein in response to neural insult may have neuroprotective effects (Bodner et al., 2006; Quilty et al., 2006). However, data emerging from *in vivo* rodent studies suggest that fibril formation could be the final common pathway for SNc neuronal death (Taschenberger et al., 2012).

In the face of contradictory findings from cell culture and animal model studies, in human disease it also remains controversial whether neurophysiological manifestations of PD are preceded or followed by α-synuclein aggregate formation, and what form those aggregates adopt initially. Post-mortem tissue samples predominantly from late-stage PD available for histology commonly present with α-synuclein fibrillar tangles, whilst oligomeric structures are no longer detectable. Further, TH staining of brains obtained from patients with Incidental Lewy Body Disease, presenting with Lewy body pathology but no PD, is reduced (Beach et al., 2008), signifying that aggregate formation is detrimental to SNc neurons. Yet, cell death could have occurred at an

earlier time point, therefore co-manifestation of Lewy body pathology with reduced TH staining does not address whether oligomeric or fibrillar species resulted in DA neuron degeneration.

Regardless of current technological limitations in establishing a direct causal link between α-synuclein fibrillation and SNc neuronal death, the above data suggest that disruption of normal α-synuclein function is detrimental. Specifically, overexpression or alterations in protein's constitutional biophysical properties, may result in a host of neurodegenerative conditions, including PD, dementia with Lewy bodies, multiple system atrophy and others (Campbell et al., 2001; Tong et al., 2010).

1.8.4 Mouse models for investigating early Parkinson's disease stages

To elucidate the involvement of α-synuclein in human PD, especially at pre-symptomatic and early disease stages, animal models, mainly rodents where α-synuclein expression was experimentally manipulated, are commonly employed. For example, several studies report progressive reduction in nigrostriatal dopamine transmission in models overexpressing human wild-type α-synuclein using vector-driven overexpression, including lentiviral- or AAV-packaged constructs (Kirik et al., 2002; Lo Bianco et al., 2002; Lundblad et al., 2012), or using heterologous gene promoters, such as Thy1 (Lam et al., 2011). Several mutant α-synuclein models presenting with dopaminergic deficits were also reported, and those were created using a mouse prion promoter for A53T variant overexpression (Gispert et al., 2003; Kurz et al., 2010; Platt et al., 2012) or BAC technology for A30P variant expression (Taylor et al., 2014). Transgenic approaches employing general promoters, however, only allow for a coarse manipulation of α-synuclein expression, and no wild-type α-synuclein model reported to date was created

using endogenous promoters/regulatory elements. The latter step is crucially important to ensure that the native expression profile of the *SNCA* gene is recapitulated, and to ascertain that no compensatory changes due to aberrant protein expression occurred. Viral overexpression, in contrast, exclusively produces acute models, where normal developmental regulation or even long-term presence of abnormally high protein levels is amiss.

A mouse model, overexpressing α-synuclein at levels relevant to human disease under the endogenous promoter on a mouse *SNCA* knock-out background, was created in Wade-Martins laboratory using BAC technology (Janezic et al., 2013). Further details on generation of this mouse model will be given in Chapter 5. This transgenic model expresses human wild type protein at 1.9 times the level of endogenous mouse α-synuclein, roughly corresponding to α-synuclein levels seen in patients with *SNCA* locus duplications (Janezic et al., 2013). The mouse is null for mouse α-synuclein to ensure that no interference form the endogenous gene undermines the integrity of experimental findings for overexpression of human protein. Thus, age and sex-matched littermates lacking mouse α-synuclein (*Snca -/-*) serve as controls for the α-synuclein overexpressing transgenic mice on mouse α-synuclein null background (*SNCA OVX*).

Previous work in this laboratory found release deficits in dorsal striatum of transgenic animals. Specifically, *SNCA OVX* mice presented with approximately 30% reduction in dopamine release from young adulthood throughout their lifespan (Janezic et al., 2013). Multidisciplinary characterization of the model further revealed that release deficits were present prior to SNc neuronal loss or manifestation of motor impairments. These observations support the notion that a dysfunctional state of

dopaminergic transmission caused by aberrant α-synuclein levels disrupts the system prior to the onset of neuronal loss. Further, biochemical assays and *in vivo* electrophysiology showed alterations in vesicle pool distributions and subsequent reduction in the firing rates of SNc neurons in aged animals (Janezic et al., 2013), suggesting that the process of disruption is gradual and happens across multiple cellular function domains.

The work on this mouse model of PD was further extended by research undertaken as part of this thesis work, with the main focus on functional interactions between dopaminergic and cholinergic systems. In particular, I wanted to address whether interference with ACh action on nAChRs or mAChRs would uncover any further DA release deficits which could be masked or compensated for by ACh, as discussed in Chapter 5.

1.9 Summary

An outline of the background literature necessary to provide context for the work presented in this thesis is presented in this chapter. The anatomy and function of the BG circuits are very complex, yet currently the field has accumulated enough data to begin elucidating the processes which govern function of the BG. The knowledge of anatomical structure is absolutely vital for understanding circuit connectivity and is indispensable for identifying the basic building blocks supporting adaptive behaviour. In turn, physiology and functional data help to explain how these components interact on the cellular and systems levels. The architecture of ACh and DA systems in striatum enables close interactions between the two neurotransmitters, and functional data unequivocally suggest that they interact in complex ways. ACh transmission in the CPu is

able both to dynamically gate the release probability from DA terminals, but also can directly drive DA release events via axo-axonic interactions. The behavioural significance of these processes is difficult to overestimate, and it is further emphasized by studies showing that both ACh and DA are involved in a wide variety of processes mediating learning and adaptive behaviour.

In this body of scholarly work I explore striatal afferent circuits which could support local ACh-evoked drive of DA release events. Specifically, the data presented in Chapters 3 and 4 examine and functionally characterize striatal afferent circuits capable of driving population activity in striatal ChIs and thus engage ACh-evoked striatal DA signalling. These chapters further explore some methodological issues arising from the use of optogenetics for mapping functional interactions of reciprocally connected networks with a third circuit. Chapter 4 also investigates use of alternative optogenetic tools, such as hyperpolarizing ion pumps, for manipulating population activity of striatal ChIs for driving ACh-evoked DA release and explores whether brainstem cholinergic afferents can contribute to or drive striatal DA. In Chapter 5 I explore the ACh-DA axis in a mouse model of Parkinson's disease, and further examine possible mechanisms underlying dopaminergic transmission deficits in the *SNCA OVX* line. Chapter 2 provides an overview of the methods and techniques used in the current work. Finally, Chapter 6 places all the presented data together in an attempt to synthesize a bigger picture of the BG function based on the past research and currently made experimental observations.

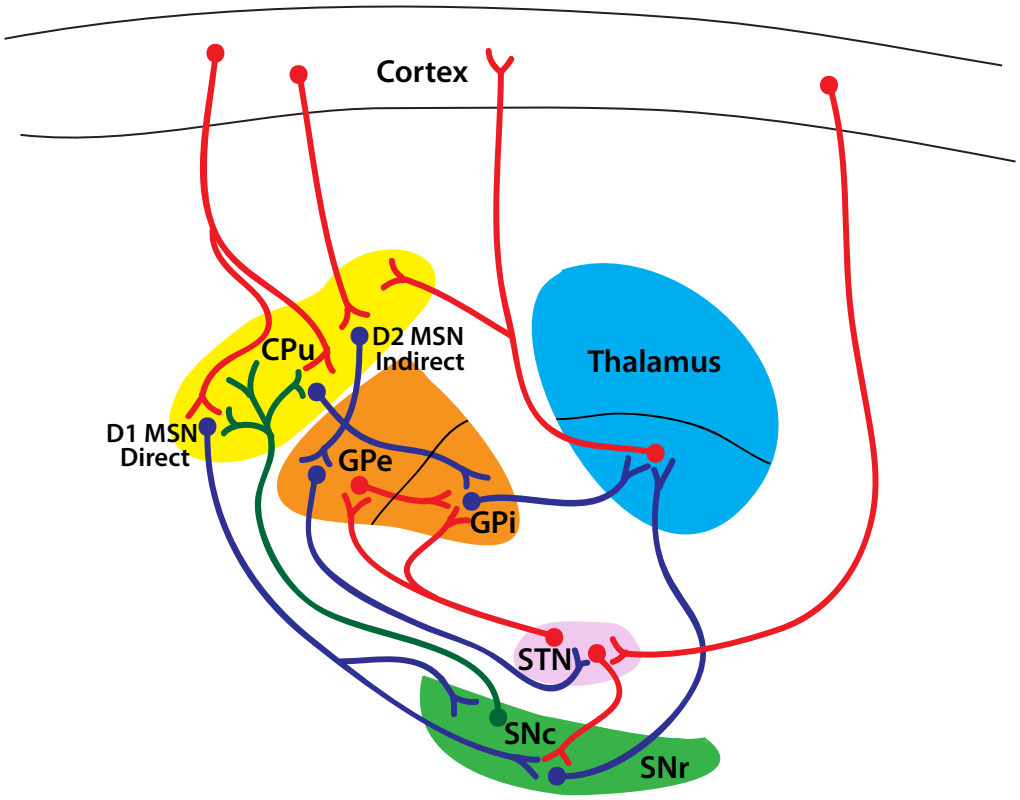

Figure 1.1 Simplified circuit diagram of the major components and pathways of the basal ganglia
This diagram shows the major projection pathways of the basal ganglia circuits and their respective input and output targets. Red connections are excitatory glutamatergic projections, blue connections are inhibitory GABAergic projections and green are modulatory dopaminergic innervation. Many connections are purposefully omitted for simplicity.

2. General Methods

2.1 Methods overview

Electrochemical detection of monoamine neurotransmitters and their metabolites exploits a well-known property of catecholamines (e.g. dopamine (DA), noradrenaline (NA)) and indoleamines (e.g. serotonin (5-HT)) to undergo oxidation. Electrochemical detection techniques, such as voltammetry, measure currents produced during redox, or electron exchange, reactions. During the process of oxidation electrons are lost from a compound being oxidised, whereas during reduction of a species electrons are gained. The redox current thus generated is proportional to the concentration of the chemical in the brain tissue or medium, and is recorded as the Faradaic current in voltammetry experiments. The exact concentration of the compound of interest can be subsequently deduced from a calibration value obtained by measuring current from a known concentration of the chemical of interest to determine current-concentration function. Electrochemical detection approaches, therefore, allow for an accurate quantification of electroactive neurotransmitter levels in the brain, both *in vivo* and *in vitro*, and can be used to study factors regulating monoamine neurotransmission. Work presented in this thesis employed a voltammetric approach to study the circuits which govern and the properties of striatal DA transmission.

2.2 Fast-scan cyclic voltammetry

2.2.1 Fast-scan cyclic voltammetry: background

The earliest voltammetry experiments performed by Ralph Adams' group at carbon paste electrodes *in vivo* served as a proof of principle for *in situ* DA detection, although recorded signals were contaminated by other electroactive species, such as

ascorbate (Kissinger et al., 1973). The large size of the carbon paste electrodes, reaching 150 – 300 μm in diameter, incurred significant tissue damage at implantation and required slow scan rates. Both of these parameters considerably limited spatial and temporal resolution that the original voltammetry techniques could offer.

The invention of carbon-fibre microelectrodes (CFMs), whereby diameter of the recording electrode was reduced to 7 – 10 μm (Gonon et al., 1978; Armstrong-James and Millar, 1979), curtailed high levels of mechanical damage incurred by electrode insertion in the brain tissue. Further, significantly smaller diameter of carbon fibre enabled use of shorter recording tip length for CFMs, thus lowering background charging currents and facilitating higher voltage scans rates. While the background current is directly proportional to the voltage scan rate, the Faradaic current is proportional to its square root (Bond, 1980). This means that in a typical CFM with the background current in the range of ~1 μA, detection of 1 μM of extracellular DA would generate oxidation current in the low nA range. Thus, high scan rates with large carbon paste electrodes could only be achieved by sacrificing data quality. Improvements introduced by invention of CFMs have substantially increased both temporal and spatial resolution of voltammetry approaches, leading to the emergence of fast-scan cyclic voltammetry (FCV). Concurrently, *in vitro* voltammetry applications introduced a more controlled physiological environment for electrochemical detection experiments, including greater precision of pharmacological manipulations in terms of time and concentration of drug applications, and anatomically precise localization of the electrode insertion sites (Rice et al., 1985; Kelly and Wightman, 1987).

FCV at CFMs is the current state-of-the-art technique for real-time monitoring of identifiable electroactive molecules, such as monoamines, with sub-second temporal and micrometer spatial resolution. This electrochemical detection approach is particularly suited to monitoring of neurotransmission, both evoked and spontaneous, as discrete release and uptake events can be resolved. Also, the small size of CFMs is appropriate for detecting transmitters with remarkable regional specificity, enabling sampling of release in discrete brain regions.

2.2.2 Fast-scan cyclic voltammetry compared to other electrochemical detection approaches

Several alternative electrochemical detection methods are also available, but none are currently able to surpass the advantages offered by FCV at CFMs in real-time monitoring of identifiable transmitter exocytosis. Whilst electrochemical detection approaches like amperometry or high-performance liquid chromatography (HPLC) with electrochemical detection may offer higher sensitivity, detecting lower levels of compounds of interest, or even detect several electroactive species simultaneously (e.g. microdialysis with HPLC with electrochemical detection), both techniques have disadvantages.

Currents recorded during amperometric events are directly proportional to the number of oxidized transmitter molecules. By employing continuous scan sweeps at a fixed potential amperometry provides higher electrode sensitivity due to better signal to noise ratio than FCV. As there are no timing limitations associated with sweep waveforms used in FCV, amperometry also offers higher temporal resolution as timing is only limited by electronics used for data acquisition (Michael and Wightman, 1999).

However, this greater temporal resolution comes with a price, as amperometry provides no information to allow identification of the detected compounds. In contrast, a characteristic FCV voltammogram is unique to each electroactive species and acts as a fingerprint for classification of chemicals that are being detected (Stamford, 1989; Zimmerman and Wightman, 1991). For example, in FCV measurements both DA and 5-HT have a similar oxidation potential occurring approximately at +630 mV, but display different reduction profiles with DA reducing at -250 mV and 5-HT having a dual reduction profile with peaks appearing at -20 mV and -670 mV (Figure 2.1). This holds true with the triangular scan waveform that our group routinely employs. It may not always be seen with other waveforms, especially if they do not include suitable potentials for registering oxidation and reduction processes happening at higher/lower voltages. Further, some compounds may have remarkably similar voltammograms, for example DA and NA (Figure 2.1). Thus, additional pharmacological and/or anatomical evidence is required to confirm the identity of the species, as for instance is the case with mixed DA and NA detection in the bed nucleus of stria terminalis.

Microdialysis is a sampling technique where transmitter molecules are recovered from the extracellular fluid removed from the brain by separation on a hollow fibre column filled with a sorbent using HPLC and subsequently presence of any electroactive species is quantified using electrochemical detection. While microdialysis with HPLC and electrochemical detection permit concurrent detection of several electroactive compounds at very low levels, FCV provides significantly better temporal and spatial resolution. FCV recording sweeps happen on the order of milliseconds (5 ms for our set up), whilst dialysate samples for HPLC are normally collected over minutes and hours, enabling detection of slow changes in transmitter release or basal neurochemical levels

only. The large size of microdialysis probes, ranging from ~ 250 µm to ~ 1 mm, on average disrupts tissue integrity up to ~ 1.5 mm away from the probe implantation site (Clapp-Lilly et al., 1999). Thus, microdialysis probes limit sampling to considerably larger areas than CFMs (~ 10 µm), which provide significantly better spatial resolution and ensure minimal tissue damage (Peters et al., 2004). Tissue trauma associated with microdialysis probe implantation, both during its insertion through the tissue and at the recording site, is also a significant shortcoming. In particular, tissue damage generally produces results that are different from what the true state of neurotransmission would be at an uninjured site (Yang and Michael, 2007). Further, in FCV experiments detection of electroactive compounds happens *in situ* and no specimens are removed, ensuring normal homeostatic processes remain unaltered.

2.2.3 Fast-scan cyclic voltammetry: principles of voltammetric detection of extracellular dopamine

The Faradaic current recorded with FCV provides a read-out of redox reactions happening at CFMs, arising from voltage scan sweeps encompassing the potentials known to oxidise the neurochemical of interest. For electrochemical detection of DA, voltage scan from negative to positive potential oxidises DA to dopamine-o-quinone, which is subsequently reduced back to DA during positive to negative phase of the scan (Figure 2.2a). The amount of current generated by DA redox reactions is proportional to its concentration in tissue, and thus the extracellular concentration of DA ($[DA]_o$) can be determined from a known calibration value.

The resulting cyclic voltammograms from these redox reactions also help to identify the detected species, as each compound has a characteristic signature of typical

oxidation and reduction potentials. Experimentally recorded voltammograms can be directly compared to voltammograms from electrode calibration with a fixed concentration of a given electrochemical compound, to ascertain neurochemical identity and consider whether there is any cross-contamination from other electroactive species. Importantly, because the transmitter being detected in the extracellular space comes from the direct vicinity of the recording CFM, FCV data suffers significantly less from signal distortion due to component diffusion away from the release sites (Wightman et al., 1988), as diffusion away from the recording electrode is equal to transmitter diffusion towards it.

2.2.4 Waveform scan for detection of $[DA]_o$

Electrochemical properties of the compound to be detected determine the shape of the voltage scan waveform. For the purposes of electrochemical detection of DA with FCV, a biphasic triangular waveform scan is commonly used. DA adsorption on the CFM surface during triangular scan waveform is relatively low, and is further limited by the electrode being switched out of circuit in between sweeps. Moreover, triangular waveform introduces fewer recording artefacts due to multiple switches in polarity (Threlfell and Cragg, 2007), yet allows for monitoring of the reduction potential signature to distinguish DA from neurotransmitters with similar oxidation profiles such as 5-HT.

Our laboratory uses triangular current scan waveform against Ag/AgCl reference electrode from -0.7 V to +1.3 V and back to -0.7 V. This scan range allows capturing the expected oxidation and reduction peaks for DA occurring at +630 mV and -250 mV, respectively (Figure 2.2b). The cyclic component of FCV approach comes from induction

and recording of both oxidation and reduction elements of the redox cycle. Return to the baseline zero current at the end of each scan facilitates maintenance of unperturbed electrochemical environment as it allows diffusion to replenish oxidized agents (Stamford et al., 1992). The negative phase of the scan which reduces oxidised DA also allows sampling of evoked DA release with minimal consumption, ensuring more accurate quantification of extracellular DA release and uptake compared to amperometry (Schönfuss et al., 2001; Venton et al., 2003).

The scan duration of 5 ms with return to baseline zero current lasting for another 120 ms enables sampling rate of 800 V/s during our FCV experiments. Thus, the entire scan lasting no longer than 5 ms during which scan wave goes 2 V up and 2 V down, approximates the duration of physiological neurotransmitter release events which happen on the order of milliseconds. In turn, scan frequency of 8 Hz enables accurate read-out of $[DA]_o$ in tissue every 125 ms. Other groups choose different scan waveforms, but variation in these setting will affect sensitivity, selectivity and temporal resolution of FCV measurements (Armstrong-James et al., 1980; Kennedy et al., 1992).

2.2.5 Carbon fibre microelectrodes for recording $[DA]_o$

First invented by Francois Gonon (Gonon et al., 1978, 1980) and Julian Millar (Armstrong-James and Millar, 1979; Armstrong-James et al., 1980), CFMs revolutionized voltammetry applications in neuroscience and enabled development of FCV in its current form. 7 µm in diameter, the size of commonly used CFMs exceed the size of synaptic cleft (~10 nm), but permits sampling of transmitter which escaped confines of the synapse. Thus, CFMs are well suited to monitoring volume transmission, including DA neurotransmission (Rice and Cragg, 2008). The length of a typical electrode (~50-120

µm) also ensures sampling from a population of DA releasing sites, rather than a single site. This could arguably provide a more representative estimate of neurotransmission properties within a given sampling region, primarily due to characteristic release heterogeneity within a single site and between different transmitter releasing sites. Consequently, population sampling supported by FCV at CFMs is expected to provide a more accurate estimate of the average or typical transmitter release state.

The small size of CFMs incurs little or no tissue damage both for *in vivo* experiments requiring electrode implantation and for *in vitro* sampling of release in acute slices. Further, unlike carbon paste electrodes, the active surface of a CFM is largely parallel to the tissue surface during insertions, and thus is less likely to be coated with tissue fragments which frequently render electrode unusable. Yet, electrode fouling with tissue fragments still happens with CFMs, and because it typically alters electrode properties, including electrode response time, we use CFMs only once and always calibrate them at the end of the experiment.

2.2.5.1 Carbon fibre microelectrode sensitivity and selectivity

A typical CFM has a fast response time, and hence is well suited to kinetic characterization of DA release events, including the time course of signal build-up during exocytotic release, and decay due to diffusion of $[DA]_o$ away from the CFM and $[DA]_o$ uptake by transporters. However, sensitivity of CFMs is limited, and therefore FCV at CFMs is most appropriate for monitoring evoked release events. In particular, recording of spontaneous neurotransmission may be difficult if extracellular neurotransmitter levels are below the detection threshold of a CFM. Thus, the reported lack of spontaneous striatal DA release *in vitro* may not be due to the actual absence of

transmitter release from dopaminergic terminals severed from their parent somas. Instead, spontaneous DA release events may occur, but the $[DA]_o$ could be below the detection threshold. Typical sensitivity of CFMs to DA used in the current work was on the order of 15-30 nA/μM as determined from CFMs calibration with a fixed DA concentration, and detection limits were ~ 100 nM as calculated based on 2 standard deviations above the noise level.

Signals recorded at CFMs in FCV experiments presented here were classified as DA by comparing the potentials for peak oxidation (+500-600 mV vs. Ag/AgCl) and reduction (-250 mV vs. Ag/AgCl) with currents recorded during calibration with 2 μM DA dissolved in experimental media, i.e. calibration voltammograms (Figure 2.3). The signature cyclic voltammograms allow for a reasonable certainty regarding the identity of detected DA. Nonetheless, there still exists a possibility of cross contamination from other electroactive substances, such as acids (e.g. ascorbic acid), DA metabolites (DOPAC) or other transmitters (5-HT and NA), especially for small or noisy signals. Therefore, double confirmation with anatomical (location) and pharmacological approaches (receptors, transporters, known modulators) is desirable, and was employed in present investigations where appropriate.

Another way to circumvent possible cross-contamination from related species in detecting the actual electroactive transmitter over its metabolic precursors is electrode pre-treatment, for example using Nafion coating (Gerhardt et al., 1984; Crespi et al., 1988; Kawagoe et al., 1992; Pihel et al., 1996). This step facilitates an increase in sensitivity of the CFMs to one electroactive component over others, for example 5-HT over 5-hydroxyindoleacetic acid and uric acid, and DA over ascorbic acid and

dihydroxyphenylacetic acid. This procedure, however, can also change electrode kinetics making it slow. Consequently, electrode pre-treatment is not widely employed for FCV. The latter is designed to measure events of very short duration, and therefore any kinetic alterations introduced by pre-treatment would be detrimental to detection of release events lasting only a few milliseconds.

Untreated CFMs themselves have differential sensitivity to various monoamines, with 2-fold greater sensitivity to DA over NA (Noga et al., 2004), and 3-10 fold greater sensitivity to 5-HT than DA (Cragg et al., 1997b). This characteristic of CFMs ensures that even in brain regions where several monoamine neurotransmitters are present, the intrinsic electrode sensitivity allows for preferential capture of one signal over another. For the data reported here, all FCV recordings were performed in striatum: a region with high density DA innervation, and relatively low contribution from 5-HT or NA projection fibres, as evidenced by successful DA detection in striatum both *in vivo* (Ewing et al., 1983; Millar et al., 1985; Stamford et al., 1985) and *in vitro* (Rice et al., 1985; Kelly and Wightman, 1987; Bull et al., 1990). In contrast to the relatively 'clean' profile of striatal DA innervation, cross-contamination from other electroactive neurotransmitters is more likely to occur in other regions such as SNc and VTA (Rice et al., 1994; Cragg et al., 1997b; Iravani and Kruk, 1997; Moukhles et al., 1997; John et al., 2006). For example, 5-HT and DA are present in the midbrain at comparable extracellular concentrations, meaning that careful examination of voltammograms and pharmacology are necessary to confirm identity of the detected species. The same cross-contamination challenge holds true of NA and DA co-presence in the bed nucleus of stria terminalis, VTA and subthalamic nucleus (Cragg et al., 1997a, 2004; Miles et al., 2002; Park et al., 2009), with the added complication of NA and DA having very similar voltammogram signatures. In

this case, inhibition of transmitter-specific transporters is vital for accurate classification of the detected species.

2.2.5.2 Carbon fibre microelectrode fabrication

All CFMs used in experiments presented in this thesis were made in-house, using epoxy-free carbon fibre 7 µm in diameter (Goodfellow Cambridge Ltd, UK). Single strands of carbon fibre were threaded through borosilicate glass capillary tubes (Harvard Apparatus, UK; outer diameter 2 mm, inner diameter 1.16 mm) immersed in acetone. This step was taken to facilitate insertion of a free-floating fibre strand inside the glass capillary, and remove any residual epoxy coating from the fibre surface. Once single fibre strand was inserted through the whole length of the capillary, the glass tube was removed from acetone, dried with filter paper and pulled on a vertical electrode puller at high heat setting (Narishige, Japan). Pulled capillaries formed two glass electrodes of equal length with carbon fibre remaining inside only one of the pulled pipettes. The latter was used for CFM production. Puller heat settings were adjusted so that a tight seal between glass capillary and carbon fibre was formed to ascertain good electrode quality (i.e. low noise levels), whilst the glass/fibre boundary was still visible under 100x microscope objective (10x eyepiece X 10x objective) to cut fibre of specific length.

The exposed end of the fibre was cut to a final tip length of ~ 100 µm with a scalpel blade, ensuring that the seal between carbon fibre and glass capillary remained intact. Then, a length of insulated wire was cleared of its plastic coating 5 mm from both ends, and treated with conductive silver paint at one end, which was subsequently inserted inside the glass capillary. Wire was fixed in place with cyanoacrylate glue. This wire made an electronic connection between the carbon fibre and the voltammeter.

Before use in an experiment, CFMs were allowed to charge in tissue for at least 30 min or until no more drift in full signal gain was observed and the recording baseline was steady. CFMs were inserted ~100 µm below the tissue surface at a 45° angle (Figure 2.4). This insertion depth was chosen to ensure that the entire exposed carbon fibre was embedded within the slice, while angled CFM positioning minimizes tissue damage. Each fabricated electrode was used once only, to prevent changes in electrode kinetics and sensitivity that may occur due to DA adsorption on the CFM surface with time and fouling of the electrode surface with tissue fragments, which by far is the most significant contributor to changes in electrode kinetics and sensitivity. At the end of each experiment, CFMs were calibrated with 2 µM DA dissolved in experimental media. This concentration of DA was chosen as one in the range of experimentally recorded $[DA]_o$ measurements and within the range where it is directly proportional to the current it generates (Figure 2.5).

2.2.6 Fast-scan cyclic voltammetry: recording equipment

The working (CFM), reference (Ag/AgCl) and auxiliary electrodes were connected via a headstage to Millar voltammeter (Julian Millar, Barts and the London School of Medicine and Dentistry), which served as a three-electrode potentiostat. The Millar voltammeter was connected to both an oscilloscope for continuous monitoring of the applied triangular waveform and background-subtracted Faradaic current, and data acquisition system (Digidata 1440A) coupled to a PC via an acquisition card for data recording and storage. This arrangement creates a sample-and-hold circuit, which provides background-subtracted voltammograms of the detected substance, in this case DA, that can be monitored in real time and the signal, or the change above background, can be amplified as necessary. Data were digitized at 50 kHz using Digidata 1440A

acquisition board and stored for off-line analysis. All signals from the CFMs were recorded using Whole Cell Program (WCP) (University of Strathclyde, Glasgow) or AxoScope 10.2 (Molecular Devices) software packages.

Stimuli for evoking DA release were generated out-of-phase with the voltammetric scans to prevent stimulus artefacts from clashing with DA currents, using a dual protocol stimulator pulse generator (Digitime DS3, UK) triggered by Millar voltammeter. Stimulation pulses varying in number and frequency were delivered either to an electrical stimulating electrode via a constant current isolated stimulator unit (FHC, USA) or to an LED system directly coupled to microscope objective via fluorescence arm. Stimuli were delivered out of phase with the voltammetric scans in one of the two different ways. Firstly, by blanking any stimuli delivered during a voltammetric sweep; this approach was employed for long stimulation protocols. Secondly, by introducing a fixed duration phase delay for the electronic timing circuit to offset stimulus onset clashing with the ongoing voltage scan. This method was employed for all routine experiments using short and intermediate stimulus durations. Delivering stimuli out of phase with FCV current scan is important for ensuring that stimulation artefacts, which are common in electrical stimulation protocols and frequently obscure real DA peaks, do not distort recorded electrochemical currents.

2.2.7 Fast-scan cyclic voltammetry *in vitro*

Although FCV was initially developed as an *in vivo* method and is widely used for monitoring monoamines in intact brain (Stamford et al., 1992; Park et al., 2011; Takmakov et al., 2011), there are several advantages to using FCV in slice work.

Firstly, *in vitro* approach affords precise control over physiological environment during data acquisition. Thus, most physiological factors that significantly influence signal detection, such as ionic composition, temperature, oxygenation and pH levels of the media, can be readily adjusted to meet experimental demands. On the other hand, work in acute slices means that a non-physiological preparation is used, as the readily adjustable pH, temperature and salt content of superfusates are not native. Nonetheless slice recordings enable better control over concentrations of the applied drugs in addition to reducing interference from other transmitter systems. Control over drug concentrations is particularly difficult for *in vivo* recordings that rely on systemic administration of pharmacological agents as drug metabolism and pharmacokinetics frequently change drug concentration, making it difficult to determine the final drug dose at the site of interest. Likewise, contribution from different neurotransmitter systems makes it difficult to unpick the circuits involved due to intact connectivity and inability to precisely control the concentration of the applied receptor agonists/antagonists which may show selectivity only at certain concentrations.

Secondly, visually guided electrode placement *in vitro* using known anatomical landmarks ensures precise targeting of the CFM towards the intended recording site. In contrast, stereotaxic coordinates, which only offer rough approximations for localization of the site of interest, guide *in vivo* electrode placements. Therefore, actual electrode location for *in vivo* experiments can only be confirmed post-hoc, and electrode misplacement is a relatively frequent occurrence, meaning the animal use is often greater. Also, *in vitro* recordings allow multiple electrode placements and therefore data collections from multiple recording sites during the same experiment is possible. In this configuration FCV approach can also be combined with other techniques for which

visualization is beneficial, such as electrophysiology (Stamford et al., 1993), or crucial, such as calcium imaging.

Finally, *in vitro* preparations facilitate the study of isolated circuits due to simplified connectivity profile of the slice. A number of afferent and efferent projection pathways present in an intact brain are severed, reducing the barrage of incoming and outgoing synaptic messages. Yet, basic local circuitry composed of different neuron and interneuron types, glia cells and modulatory transmitters remains intact. Conversely, removing interference from large-scale afferent projections and feedback loops could change the rules that govern interactions between neurotransmitters and their regulatory elements, and in particular obscure the contribution from other circuit elements that may be absent in a slice preparation. Consequently, some observations may not be strictly physiological and require cautious extrapolation to *in vivo* context.

2.3 Preparation of acute slices for monitoring striatal $[DA]_o$ *in vitro*

2.3.1 Animals

All animal procedures were approved by the Ethical Review Committee of the University of Oxford, and performed under the authority of a UK Home Office Project Licence in accordance with the Animals (Scientific Procedures) Act 1986 (amended 2012).

For the experimental work reported here, mouse (*mus musculus*) was the species of choice for several reasons. Firstly, as a mammalian species, mouse models enable the study of systems closely related to human, with particularly high homology for phylogenetically conserved pathways. Secondly, a plethora of previous voltammetry

experiments used mouse models. The current results, therefore, can be directly compared with other studies, given the background strain used was the same. Thirdly, across all mammalian species currently used in scientific research, understanding of and ability to manipulate mouse genome is the most advanced. Numerous transgenic lines carrying tailor-made genetically encoded changes, such as carrying specific transgenes to model human disease, or expressing proteins in cell-specific manner, such as *Cre*-mouse driver lines, are readily available off-the-shelf. Finally, work with mouse models enables the use of lower order mammalian species compared to rat or primate, yet the species which can directly inform work in other mammals. Experiments presented here, used several different mouse lines bred on pure C57Bl6/J background.

Wild type (WT) C57Bl6/J mice (Charles River) were chosen for routine experiments requiring control WT data and for pilot experiments in Chapter 3. For the work characterizing a mouse model of Parkinson's disease in Chapter 5, mice expressing high levels of human wild type α-synuclein on a mouse α-synuclein knockout background (*SNCA OVX*) and α-synuclein knockout littermate controls (*Snca -/-*) were used (Janezic et al., 2013). These studies were further extended by using Synapsin 3 knockout mice (Feng et al., 2002; Kile et al., 2010) on WT (*Synapsin 3 -/-*) or mouse α-synuclein null (*Synapsin 3 -/- Snca -/-*) background.

For optogenetic experiments in Chapters 3 and 4, several *Cre*-driver lines were employed, including CaMK2a-Cre, ChAT-Cre and DAT-Cre lines on C57Bl6/J background. The *Cre*-driver lines were employed for opsin transduction using *Cre*-loxP system, which restricts transgene expression to neuronal populations expressing *Cre*-recombinase following floxed vector injections. Transgenic mouse lines used in this work selectively

expressed *Cre*-recombinase protein in neurons positive for Ca^{2+} calmodulin-dependent kinase II (CaMK2), choline acetyltransferase (ChAT) or dopamine transporter (DAT), respectively. The transgenic Cre mice were bred locally from homozygote for ChAT-internal ribosome entry site (IRES)-Cre, DAT-IRES-Cre, or CaMK2-Cre obtained from Jackson Laboratories (B6.129S6-*Chat*$^{tm1(cre)Lowl}$/J, stock 006410; B6.SJL-*Slc6a3*$^{tm1.1(cre)Bkmn}$/J, stock 006660; B6.Cg-Tg(CaMK2a-Cre)T29-1Stl/J, stock 005359). For generation of heterozygous lines, predominantly employed for the work described here, male homozygous *Cre*-expressing transgenic males were crossed with WT C57Bl6/J females. For optogenetic experiments exploring the role of cholinergic brainstem afferents in driving ACh-evoked striatal DA release in Chapter 4, ChAT-Cre rats were also used (Witten et al., 2011; Dautan et al., 2014).

All mouse and rat lines were maintained on a 12h light/dark cycle with *ad libitum* access to food and water.

2.3.2 Preparation and maintenance of acute brain slices for FCV

Mice were sacrificed by cervical dislocation or overdose of isoflurane anaesthesia and decapitated. Rats were deeply anaesthetised with isoflurane and decapitated. Brains were quickly removed from the skulls and placed in ice-cold oxygenated aCSF. Acute 300 µm-thick coronal slices were cut on a vibratome (Leica VT1200S) with tissue submerged in ice-cold continuously oxygenated solution. Coronal slices, containing caudate-putamen (CPu) and nucleus accumbens (NAc) (+1.5 mm to +0.5 mm from bregma in mouse, Paxinos and Franklin, 2008), were collected for experiments. For a subset of experiments where electrical stimulation of corticostriatal fibres was employed, acute 300 µm-thick slices containing CPu and NAc were cut in sagittal plane.

Once cut, sections were incubated at room temperature for one hour. Then, individual slices were transferred to a recording chamber superfused continuously (2 ml/min) with oxygenated aCSF at 32°C. Slices were allowed to equilibrate for at least 30 min in the recording chamber, whilst the CFM was charging in tissue. This incubation time is determined by ascorbate and DOPAC degradation, which happens after 30 min of slice incubation in a superfused bath (Schenk et al., 1983; Rice et al., 1994). Therefore, pre-experimental incubation in the recording chamber eliminates the potential for cross-contamination of DA signals from these compounds. Further, 30 min equilibration time allows slice physiology to adjust to different temperature and ionic composition of the superfusate and for the CFM to charge.

For all optogenetic experiments, slices were cut in high Mg2+ solution containing in mM: 85 NaCl, 25 NaHCO3, 2.5 KCl, 1.25 NaH2PO4, 0.5 CaCl2, 7 MgCl2, 10 glucose, 75 sucrose, and maintained in aCSF containing in mM: 130 NaCl, 25 NaHCO3, 2.5 KCl, 1.25 NaH2PO4, 2 CaCl2, 2 MgCl2, 10 glucose. For all other FCV experiments, for slice cutting and maintenance, HEPES-buffered aCSF was used containing in mM: 120 NaCl, 5 KCl, 20 NaHCO3, 6.7 HEPES acid, 3.3 HEPES salt, 2 CaCl2, 2 MgSO4, 1.2 KH2PO4, 10 glucose, and bath perfusion media was bicarbonate-buffered aCSF containing in mM: 124 NaCl, 3.7 KCl, 26 NaHCO3, 2.4 CaCl2, 1.3 MgSO4, 1.3 KH2PO4, 10 glucose.

2.4 Fast-scan cyclic voltammetry data acquisition and processing

2.4.1 Data acquisition

After slices were transferred to the recording chamber superfused with oxygenated aCSF at 32°C and allowed to equilibrate for 30 min, FCV recordings were

performed in different sites of interest in striatum. The choice of sampling regions is explained in more detail in each individual results chapter. Light or electrical stimulations were delivered every 2.5 min. The choice of stimulation protocols is also explained in individual results chapters. Electrically or light evoked DA transients were recorded before/during/after drug application or just sampled in different release sites.

2.4.2 Data processing and statistical analyses

All the data were acquired and processed using AxoScope 10.2 (Molecular Devices) or Whole Cell Program (WCP, University of Strathclyde, Glasgow, UK) software packages. Data were then pre-processed and analysed using custom written Excel macros scripts (Prof S. Cragg & Dr K. Jennings). Subsequently, these data sets were plotted and analysed statistically using GraphPad Prism 6.0 software. The details of the statistical analyses employed are provided in individual results chapters.

2.4.3 Drugs

D-(2R)-amino-5-phosphonopentanoate (D-AP5), 4-(8-methyl-9H-1,3-dioxolo[4,5-h][2,3]benzodiazepin-5-yl)-benzenamine hydrochloride (GYKI 52466 hydrochloride), KN-62, bicuculine, saclofen, (S)-α-methyl-4-carboxyphenylglycine (MCPG) and Oxotremorine-M (Oxo-M) were purchased from Tocris Bioscience or Ascent Scientific. Cocaine, dihydro-β-erythroidine (DHβE) and all other chemicals were purchased from Sigma-Aldrich.

All solutions were prepared using distilled and de-ionized water. Drugs were dissolved in distilled and de-ionized water, aqueous alkali (MCPG), acid (GYKI 52466 hydrochloride) or dimethylsulphoxide (DMSO) (L-741,626; KN-62) to make stock aliquots at 1000-10000 × final concentrations and stored at -20°C. The drug stocks were diluted

to the final concentration in oxygenated aCSF from frozen aliquots immediately before use and were bath applied. None of the drugs at the concentrations used altered electrode sensitivity.

2.5 Stimulating striatal dopamine release *in vitro*

Striatal DA innervation originates from the midbrain neurons residing in the SNc and VTA (Nelson et al., 1996). Both of these neuronal populations are tonically active and exhibit transient increases in their firing rate, hypothesized to encode reward prediction error (Schultz, 1998; Matsumoto and Hikosaka, 2009). Despite their tonic activity *in vivo* which translates into spontaneous release events both in the midbrain and in the CPu (O'Neill et al., 1982), *in vitro* striatal dopaminergic axon terminals severed from their parent somas under normal drug-free physiological conditions show no spontaneous DA release events (Rice et al., 2011). It is possible that spontaneous release events from severed DA terminals do occur, but if so, they remain below the CFM detection threshold. Therefore, *in vitro* recording of DA release with FCV at CFMs in acute slices requires active stimulation of striatal dopaminergic axon terminals. There are several approaches currently available for evoking striatal DA release.

2.5.1 Electrical stimulation

Electrical microstimulation has been classically used for evoking striatal DA release *in vitro*. The basic working principle behind this approach is that direct or alternating current pulses of fixed duration are delivered to the tip of a stimulating electrode positioned in close contact with tissue surface. This current is of small amplitude (mA scale) and short duration (ms scale), and is used for direct excitation of cellular membranes, most likely via direct depolarization, in the vicinity of the electrode

tip. Such discrete stimulation events directly activate striatal DA terminals, and DA release transients can be recorded in response to each of the delivered stimulations at 2.5 min intervals for up to 9 hours (Bull et al., 1990). One advantage of this approach is that no additional preparations are required for such experiments, unlike with light-activation of ChR2 expressing neurons/terminals as will be described in the next section, which require transgenic animals and/or surgery. Therefore, electrical stimulation approach can be readily used with any tissue. Further, the technique itself is well characterized and understood.

Local electrical stimulation, however, depolarizes all membranes in the vicinity of the stimulating electrode, and thus can offer no selective activation of a single cell type or projection pathway. Further, passive current spread, radiating up to 2 mm away from stimulating electrode tip (Tehovnik et al., 2006), introduces the possibility of compromising quality of site-sampling experiments where only the first read-out of released DA is used for quantitative evaluation of release levels. For example, in the site sampling experiments performed in the *SNCA OVX* and *Snca -/-* lines (Chapter 5). The likelihood of stimulating more than one nuclei or projection pathway, especially in small brains such as mouse, also introduces serious confounds into the experiments where stimulation specificity is required. This certainly was the case with the experiments using distal electrical stimulation of corticostriatal projections in WT slices (Chapter 3).

For the experiments described here, electrical current stimulation was delivered via a bipolar concentric Pt/Ir electrode with 25 µm tip diameter, using constant current stimulus isolation unit (FHC, USA). The stimulating Pt/Ir electrode was positioned on the slice surface, 100 µm away from the recording CFM, unless otherwise stated (Figure 2.6).

It was always positioned first, to avoid disturbing tissue around the CFM due to impact from Pt/Ir electrode movement. Pulse duration was 200 µs, and peri-maximal current amplitude used in all experiments employing electrical stimulation was 0.6 mA. Electrical stimuli were delivered at 2.5 min intervals to enable sustainable DA release for the entire duration of the experiment.

2.5.2 Optogenetic stimulation

The recent emergence of optogenetics has circumvented some confounds associated with electrical stimulation. This technique was described in more detail in Chapter 1. Briefly, the basic working principle behind optogenetics is that opsin channels, such as ChR2, expressed on the cellular membranes, directly transduce light energy used to activate them into membrane potential changes by changing their conformation and forming cation-permeable channel pore. This tool has been widely used for depolarizing single neurons and circuits. Alternatively, membrane expression of hyperpolarizing tools, such as eNpHR 3.0, an inward chloride pump, or Arch 3.0, an outward proton pump, enables silencing of neuronal activity. These ion pumps upon light activation directly move one ion per photon of light across the cellular membrane (Geibel et al., 2001; Seki et al., 2007). Thus, opsins behave as light-activatable non-selective ion channels, or light-activatable ion-selective pumps. Cells targeted to express such opsins become amenable to control of their activity with light, both at the level of the soma and axon terminals. Optical stimulation approaches employing optogenetics offer an advantage in enabling selective activation of genetically defined cell populations, and thereby facilitate functional isolation of a particular circuit. For the series of experiments described here, optogenetic approach enabled preferential

activation of thalamostriatal or corticostriatal terminals, either of which are difficult to target selectively with electrical stimulation.

For the main body of work presented here, ChR2 was the opsin of choice for inducing direct membrane depolarization with blue 473 nm light. To selectively target ChR2 expression to a subset of cortical or thalamic neurons in a CaMK2a-Cre driver line with stereotaxic viral vector injections *Cre*-loxP system was used. A doubly-floxed inverted open reading frame construct under strong general promoter (EF-1α) carrying a gene sequence from *Chlamydomonas reinhardtii* for light-activatable cation channel ChR2 was used (pAAV-EF1α-D10-hChR2(H134R)EYFP-WPRE-pA) (Boyden et al., 2005; Zhang et al., 2006; Tsai et al., 2009) (Figure 2.7). The H134R point mutation introduced into the native ChR2 genetic sequence increases light sensitivity and decreases channel desensitization leading to the overall increase in evoked photocurrents, but at the expense of slower channel closing kinetics than wild-type ChR2 (Lin, 2011). In this experimental paradigm, ChR2 expression occurs selectively in neurons expressing *Cre*-recombinase, where *Cre*-mediated inversion of ChR2 sequence into correct orientation allows transcription of ChR2 by ubiquitous EF-1α promoter. The ChR2 construct was packaged into AAV vectors, and serotypes 2 and 5 were chosen for these experiments (Cardin et al., 2009; Tsai et al., 2009; Kravitz et al., 2010; Lin, 2011). Typical viral titers were ~10^{12} IU ml^{-1}, and injection volumes were 400 nl per site, unless specified otherwise.

For a subset of experiments in ChAT-Cre mouse driver line, hyperpolarizing light-activatable tools were employed. AAV2-packaged eYFP-tagged eNpHR 3.0 vector from Karl Deisseroth where viral DNA included the loxP-flanked sequence for eNpHR3.0 from

Natronomonas pharaonis driven by the human elongation factor 1a promoter (*EEF1A1*) was injected in CPu in ChAT-Cre line (Raimondo et al., 2012). AAV5-packaged eGFP-tagged Arch 3.0 construct from Ed Boyden driving Arch 3.0 from *Halorubrum sodomense* expression in loxP-dependent manner under CAG promoter was also used (rAAV5-Arch-FLEX-GFP) for CPu injections in a different group of ChAT-Cre mice. For these vectors, *Cre*-mediated floxed-site excision and inversion of transgene sequence into correct orientation allows transcription of the opsin protein by the associated promoter sequence in striatal ChIs selectively. Typical viral titers were ~10^{12} IU ml^{-1}, and injection volumes were 800 nl per site with all mice injected bilaterally. These light-activatable ion pumps have red-shifted response spectra and were stimulated with 560 nm yellow LED.

ChR2 vectors were purchased from Gene Therapy Centre Virus Vector Core, University of North Carolina from Karl Deisseroth. eNpHR 3.0 vector was a gift from Dr Tommas Ellender (Ackerman group) and Arch 3.0 vector was a gift from James Cooke (King group).

2.5.3 Stereotaxic surgery for optogenetic experiments

Stereotaxic injections of *Cre*-inducible recombinant AAV-packaged vectors containing gene sequence for ChR2, eNpHR 3.0 or Arch 3.0 were performed on homozygous and heterozygous CaMK2a-Cre mice (21-40d), and heterozygous DAT-Cre mice (30-45d) and ChAT-Cre mice (30-45d).

Animals were anaesthetised with isoflurane (2% w/o) and placed in stereotaxic frame (WPI), with head securely positioned in between ear bars, and shaved. The shaved area was cleaned with antimicrobial agent (HiBi scrub, 1:3 dilution in dH_2O), and sterile environment was established with autoclaved surgical drape. After injection of a local

anaesthetic (Marcaine, 1:3 dilution in sterile saline), an incision in the skin was made with a scalpel blade. Bilateral burr hole craniotomies were made over the target injection sites using small hand drill. With 2.5 µl Hamilton syringe microinjector with a 33-gauge needle 400-800 nl of the viral vector were pressure injected in each hemisphere. Unless otherwise stated, all injections were performed bilaterally. In our hands, using a 33-gauge needle for stereotaxic injections conferred the advantage of more precise targeting of the injection sites based on given coordinates compared to glass pipettes, even though needle incurs more collateral tissue damage in the process insertion and removal. The virus was injected at 300 nl/min flow rate, followed by 10 min delay before needle retraction to decrease backflow of vector up the injection tract and reduce non-specific transduction. Finally, wound was closed with surgical suture, and after administration of subcutaneous doses of post-operative analgesic (Metacam, 1:4 dilution in sterile saline) and sterile saline mice were allowed to recover in a Thermacage unit (Bioservices, UK). All surgical procedures were performed aseptically.

All bregma coordinates were taken from adult mouse brain atlas (Paxinos and Franklin, 2008). AAV5 ChR2 and AAV2 ChR2 vector injections in CaMK2a-Cre mouse line were selectively targeted to the motor cortex, areas M1 (ML 1.7 mm, AP +1.3 mm, DV 1.0 mm from bregma) (Figure 2.8a), or Pf nucleus of the caudal intralaminar thalamus (ML 0.8 mm, AP -2.3 mm, DV 3.5 mm) (Figure 2.8b). Two distinct groups of animals received cortical and thalamic injections. For a subset of experiments employing AAV2-based ChR2 construct, dual bilateral thalamus + cortex injections were performed. The expression time allowed was between 4-14 weeks to ensure sufficient levels of opsin expression, consistent with previously published observations (Zhang et al., 2010; Yizhar et al., 2011; Ellender et al., 2013).

For anatomical localization of the AAV5- and AAV2-packaged ChR2 constructs following their transportation from the injection site, injections targeted to the central CPu under cortical M1 area (1.5 mm ML, +0.5 mm AP, 3.2 mm DV from bregma) were performed in the DAT-Cre mice (Figure 2.8c). 400 nl of AAV-packaged ChR2 construct were injected per hemisphere, all mice were injected bilaterally. 4-6 weeks later brains from the injected DAT-Cre mice were processed for immunohistochemistry.

For the experiments where hyperpolarizing optogenetic tools were used to examine direct inhibition of ChI population activity for driving ACh-evoked DA release following a 'pause', 800 nl of AAV-packaged Arch 3.0 or eNpHR 3.0 construct were injected per hemisphere in the central CPu (1.5 mm ML, +0.5 mm AP, 3.2 mm DV from bregma) of adult ChAT-Cre mice. All animals received bilateral injections, 6-11 weeks were allowed for opsin expression.

2.5.4 Light-activation of opsin-expressing neurons and terminals

ChR2-expressing cortical or thalamic terminals in striatum, visualised by eYFP fused to the ChR2 sequence, were activated using 473 nm LED system (OptoLED, CAIRN). The LED was directly coupled to the microscope objective via a fibre optic coupled to the fluorescence arm. The LED system provided full-field illumination of the striatum, activating all ChR2-expressing somas and terminal fibres in the field of view (Figure 2.9). This illumination area constitutes a region 2.2 mm in diameter for a X10 immersion objective used in this work. TTL-driven light pulses (2 ms wide) were delivered at 2.5 min intervals and generated out-of-phase with voltammetric scans to prevent possible interference from photovoltaic currents.

473 nm light pulses were delivered with the LED stimulation current value set to 7.0. This corresponded to the light power read-out of 62.9 mW by the Thor Labs power meter (PM-160) at the microscope objective, thus producing 28.6 mW/mm^2 light power density output. Light stimulation power was not adjusted on experiment-to-experiment basis, as eYFP signal intensity, and therefore putative ChR2 expression levels, observed following cortical and thalamic injections with AAV5 ChR2 4 weeks post-injection were consistently high. Current value of 7.0 was also chosen as it reliably evoked large amplitude DA events sustainable over time, while decreasing light current to lower values led to a sharp drop off in release levels, and increasing current resulted in events which 'oscillated' between larger and smaller evoked $[DA]_o$. For AAV2 experiments stimulation power was also set to the maximum current output value of 7, chosen to maximize the chances of finding light-evoked DA release in case insufficient terminal depolarization was due to low stimulation intensity. It was also the maximal current value at which LED power box could accurately deliver pulse trains of more than 20 pulses without overloading, resulting in premature termination of light stimuli delivery.

Expression of eNpHR 3.0 and Arch 3.0 in striatal ChIs was visualized by eYFP and eGFP tags, respectively. For light activation of the hyperpolarizing ion pumps 560 nm yellow light LED system was used (OptoLED, CAIRN). The LED stimulation box current value was set between 5.0-7.0, which corresponded to the light power read-out at the objective of 23.4-30.8 mW by the Thor Labs power meter (PM-160). This light power at the objective translated to 10.6-14.0 mW/mm^2 power density. The power output was adjusted between lower and higher current values to prevent the LED from overloading during stimuli delivery lasting longer than 30 pulses or requiring pulse width of 10 ms.

2.6 Immunohistochemistry for optogenetic experiments

2.6.1 Histological analyses: cortical injection localization

Localization of the cortical injection sites was done with the help of polystyrene fluorescent spheres (Invitrogen). 5-20 nl of these red fluorospheres were injected in addition to the AAV-packaged ChR2 construct in a subset of experiments. 300 µm slices used for FCV experimental recordings were subsequently fixed in paraformaldehyde (PFA) fixative for at least 24 h and maximum of 48 h at 4°C (0.1M PBS with 4% PFA and 0.2% saturated picric acid, pH 7.2-7.4, Somogyi and Takagi, 1982). For fixation, slices were held between filter paper to ensure that they were flat for microscopy. Following fixation, tissue was washed in PBS (5x5 min), mounted on gel-coated microscope slides and coverslipped using hard set Vectashield mounting medium (Vector Laboratories). Location of fluorescent beads and eYFP expression was visualized using a fluorescence microscope Olympus BX41 (Olympus medical) coupled to Q-Click cooled monochrome CCD camera using Q-capturePro 7.0 software. For fluorescence microscopy imaging work no additional staining was required either for visualization of eYFP-tagged ChR2-transduced cells and processes or red fluorescent spheres, as signal intensity in both channels was high.

2.6.2 Histological analyses: thalamic injection site localization

Following striatal slice preparation from Pf-injected CaMK2a-Cre mice, the remaining brain blocks containing thalamus were fixed in 4% PFA and 0.2% saturated picric acid (pH 7.2-7.4), and stored at 4°C. After at least 72 h in fixative, these blocks were washed in PBS (5x5 min) and re-sectioned at 50 µm or 100 µm on a vibrating microtome (VT1000S, Leica Microsystems).

50 µm thick sections containing caudal intralaminar thalamus were further processed to delineate Pf boundaries from its neighbouring nuclei as previously described in Ellender et al. (2013) using immunostaining for cerebellin-1 (Kusnoor et al., 2010). Sections were washed in PBS (5x5 min) and heat-treated at 80°C for 30 min in sodium citrate buffer (10 mM, pH 5.95). After heat-treatment, vials were allowed to cool down to room temperature and sections were again washed in PBS (5x5 min). Slices were then blocked with 20% normal goat serum (NGS) (Jackson ImmunoResearch Laboratories Inc.) in 0.3% Triton-X-100 PBS (PBS-Tx) on a shaker at room temperature for 60 min.

Then sections were incubated in the primary antibody, 1:2500 rabbit polyclonal α- cerebellin-1 (Prof J. Morgan, St. Jude Children's Research Hospital) with 1% NGS in PBS-Tx overnight at 4°, and washed 5x5 min in PBS. The secondary antibody was a 1:500 dilution of goat α-rabbit-DyLight 594 fluorophore (Jackson ImmunoResearch Laboratories Inc.) in PBS-Tx in which the sections were incubated for 2 hours at room temperature on a shaker. Thereafter, the sections were washed 5x5 min in PBS, mounted on gelled microscope slides and coverslipped with hard set mounting medium Vectashield (Vector Laboratories). Location of DyLight 594-tagged Pf neurons and eYFP expression in the ChR2-transduced cells and processes was visualized using a fluorescence microscope Olympus BX41 (Olympus medical) coupled to Q-Click cooled monochrome CCD camera using Q-capturePro 7.0 software. eYFP-expressing terminals and cells identified as ChR2-containing required no additional immunostaining for eYFP as high levels of fluorescence intensity in transduced fibres/ somas were present even in heat-treated fixed slices.

In a subset of surgeries, 5-20nl of red polystyrene fluorescent spheres (Invitrogen) were injected together with the ChR2 construct to mark the exact location of the Pf injection tracts. In this case, fixed thalamic brain blocks were re-sectioned at 100 μm, washed in PBS (5x5 min) and mounted with Vetashield (Vector Laboratories). For fluorescence microscopy imaging work no additional staining was required either for visualization of eYFP-tagged ChR2 or red fluorescent spheres. These sections were visualized using a fluorescence microscope Olympus BX41 (Olympus medical) coupled to Q-Click cooled monochrome CCD camera and Q-capturePro 7.0 software.

2.6.3 Histological analyses: confirmation of retrograde-anterograde axonal transport of AAV-packaged ChR2 vectors

Whole brains from the AAV5 ChR2 or AAV2 ChR2 CPu-injected DAT-Cre mice were fixed in 4% PFA for at least 72h after animals were transcardially perfused with PBS. Then brains were washed in PBS (5x5 min), and re-sectioned at 50 μm. Slices containing the CPu, SNc and VTA were collected for fluorescence microscopy. These sections were washed in PBS (5x5 min), mounted on gelled slides and coverslipped with hard set Vetashield mounting medium (Vector Laboratories). These mounted sections were then examined for eYFP fluorescence to determine the possibility of retrograde axonal transport of the AAV-packaged ChR2 constructs used in this work.

A subset of section was processed for TH immunostaining. Re-sectioned 50 μm slices were washed in PBS (5x5min), and then blocked with 10% NGS and 10% bovine serum albumin (BSA) in PBS-Tx for 30 min on a shaker at room temperature. Then sections were again washed in PBS (5x5min) and incubated overnight in 1% NGS, 1% BSA and 1:2000 dilution of primary rabbit anti-TH antibody (Sigma) in PBS-Tx at 4°C. After

overnight incubation sections were washed in PBS (5x5min) and incubated for 2 h on a shaker at room temperature with 1% NGS, 1% BSA and 1:2000 dilution of secondary DyLight 594 goat anti-rabbit antibody (Jackson ImmunoResearch Laboratories Inc.) in PBS-Tx. Subsequently, sections were washed, mounted on microscopy slides and coverslipped with Vectashield (Vector Laboratories).

Sections were visualized using a fluorescence microscope Olympus BX41 (Olympus medical) coupled to Q-Click cooled monochrome CCD camera and Q-capturePro 7.0 software. As before, no additional immunostaining was required for visualizing eYFP in the brains from DAT-Cre mice where the ChR2 construct was transported retrogradely from the CPu injection site to the midbrain.

2.6.4 Histological analyses: expression of eNpHR 3.0 and Arch 3.0 in striatum

To visualize expression of Arch 3.0 and eNpHR 3.0 constructs in striatal ChIs, 300 μm striatal coronal sections were fixed after being used for FCV recordings in PFA fixative for at least 24 h and maximum of 48 h at 4°C. For fixation, slices were held between filter paper to ensure that they were flat for microscopy. Following fixation, slices were washed in PBS (5x5 min), mounted on gelled slides using Vectashield (Vector Laboratories). Location of fluorescently tagged opsins in striatum and striatal ChIs was visualized using a fluorescence microscope Olympus BX41 (Olympus medical) coupled to Q-Click cooled monochrome CCD camera and Q-capturePro 7.0 software. No additional staining was required either for visualization of eGFP-tagged Arch 3.0 or eYFP-tagged eNpHR 3.0 due to high signal intensity.

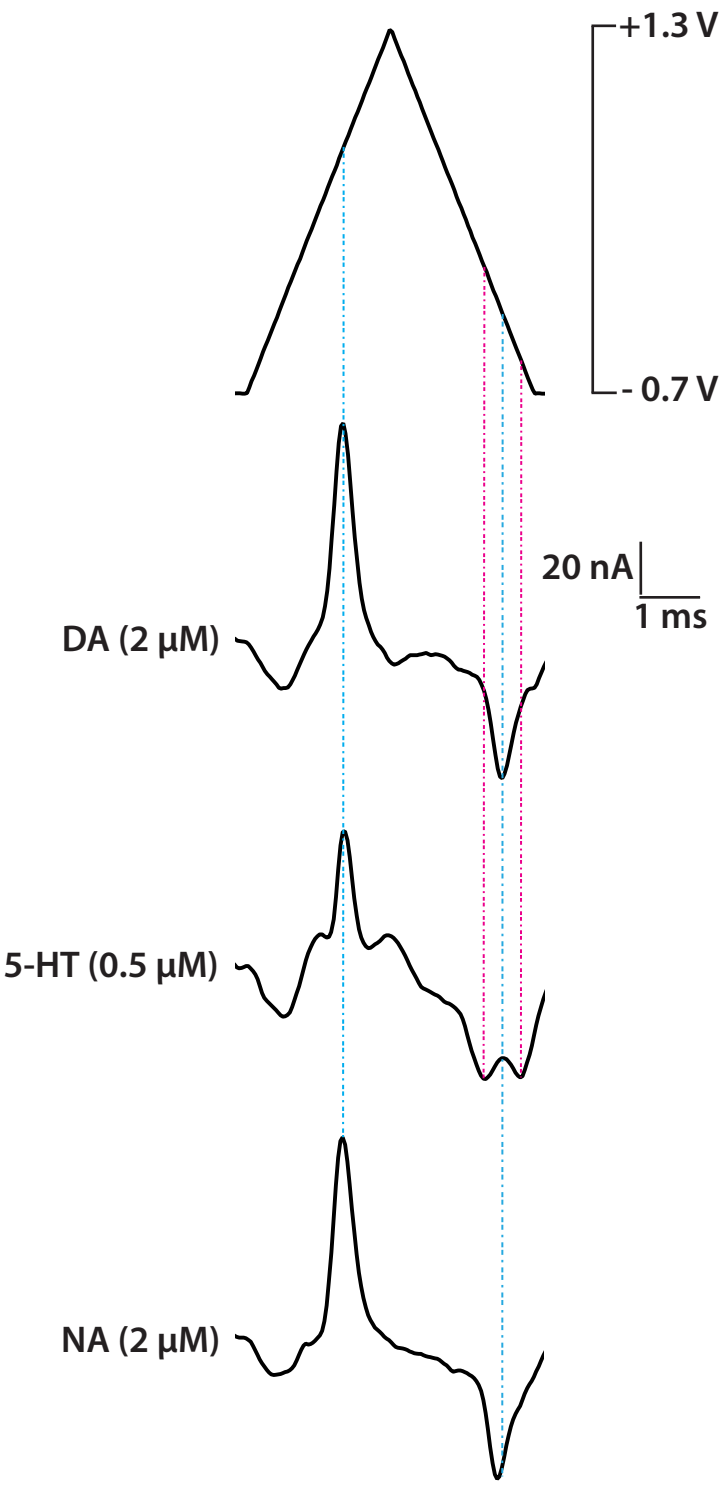

Figure 2.1 Triangular waveform and representative calibration voltammograms for dopamine, serotonin and noradrenalin
Waveform scan from -0.7 V to +1.3 V relative to Ag/AgCl reference electrode. Representative voltammograms from CFM calibration with 2 µM dopamine (DA), 0.5 µM serotonin (5-HT) and 2 µM noradrenalin (NA), showing characteristic oxidation peaks occuring at + 0.6 V and reduction peaks for DA and NA occuring at -0.25 V, while 5-HT has dual reduction profile with reduction peaks at -0.02 V and -0.67 V.

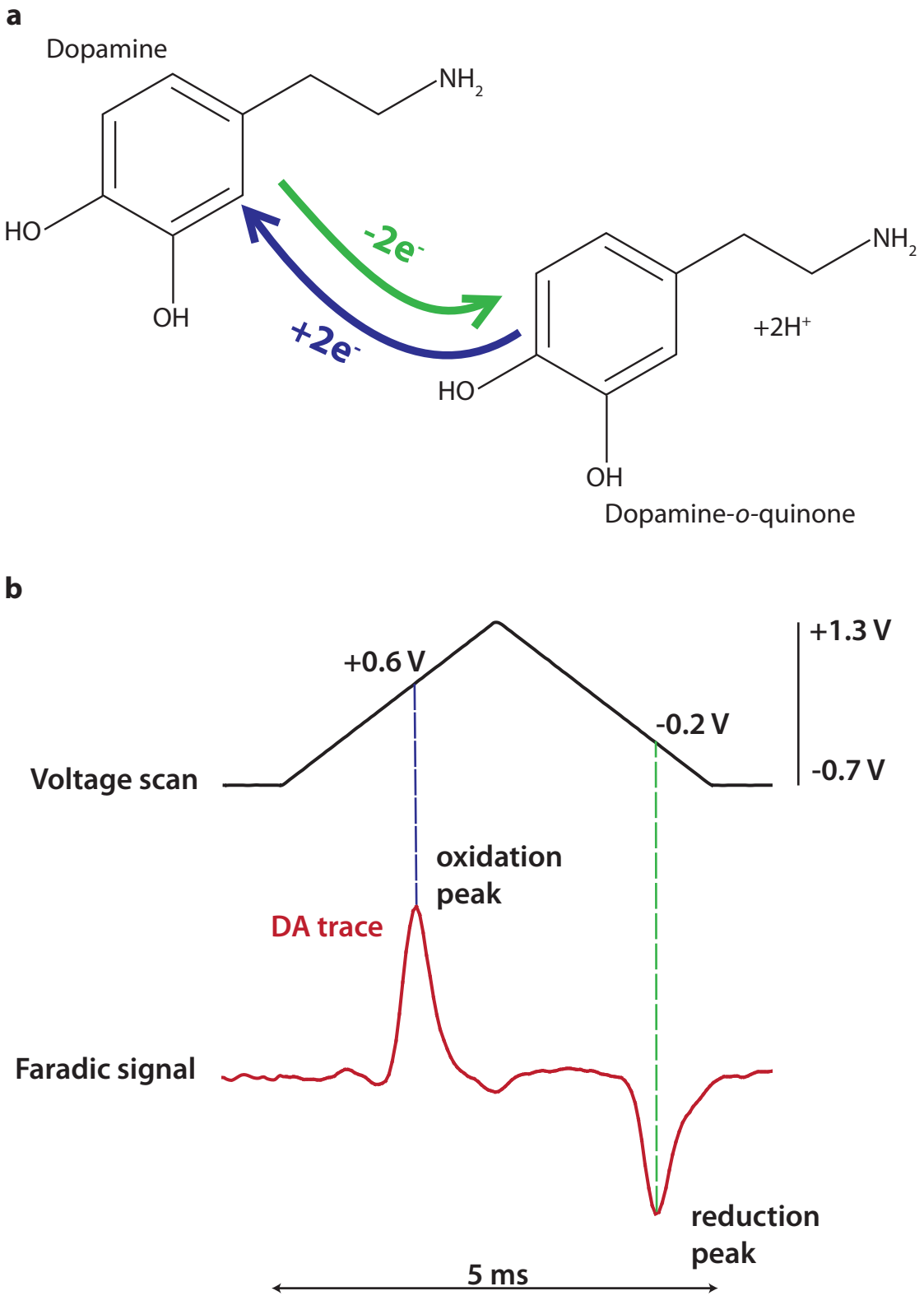

Figure 2.2 Oxidation of dopamine to dopamine-o-quinone generates Faradic current recorded at CFM with FCV

(a) During positive phase of the triangular waveform scan from -0.7 V to +1.3 V DA oxidises to DA-o-quinone, which is subsequently reduced back to DA during the negative phase of the scan from +1.3 V to -0.7 V, the whole process is lasting 5 ms. **(b)** The resulting Faradic current recoded with FCV at CFM produces DA voltammogram showing typical DA signature of oxidation peak occurring at +0.6 V and reduction peak at -0.2 V.

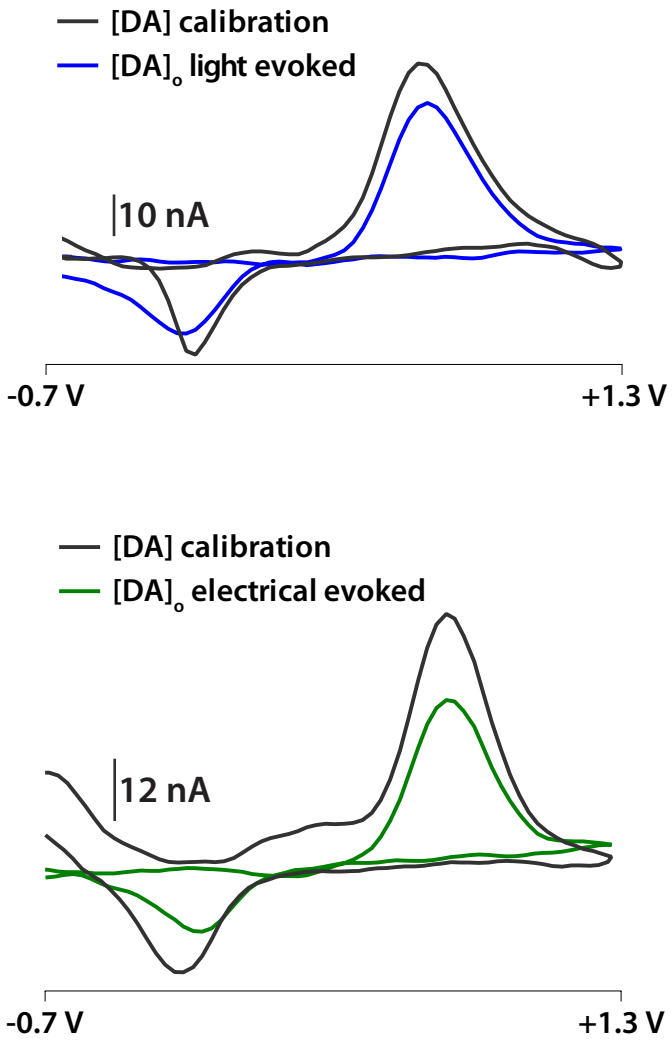

Figure 2.3 Representative cyclic voltammograms of $[DA]_o$ evoked with light or electrical current stimulation and respective [DA] calibration voltammograms for the same CFMs
Representative voltammograms from CFM calibration with 2 µM dopamine showing characteristic DA oxidation peak occurring at +0.6 V and reduction peak at -0.25 V. Light evoked $[DA]_o$ was recorded in CPu of CaMK2a-Cre mouse injected with AAV5 ChR2 vector in cortical area M1. Electrically evoked $[DA]_o$ was recorded in CPu of Snca -/- mouse.

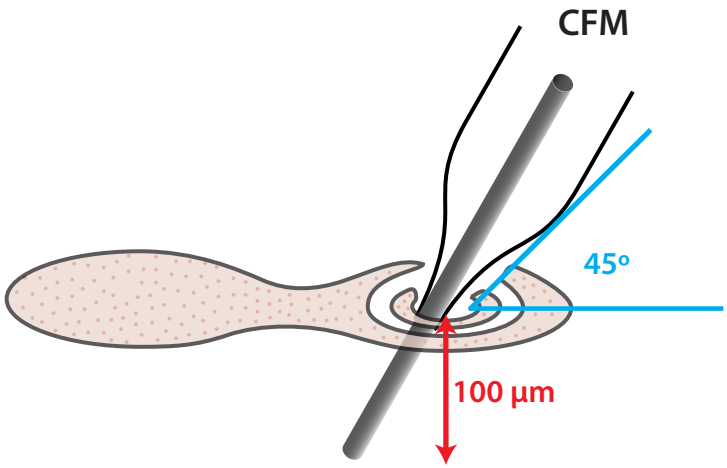

Figure 2.4 Positioning of the recording CFM for detection of evoked $[DA]_o$ in acute slices
A schematic showing positioning of the recording CFM, which is inserted up to 100 µm below the tissue surface at a 45° angle. Angled electrode positioning minimizes tissue damage incurred by electrode insertion, while 100 µm insertion depth ensures that the whole of the CFM tip is within the slice, detecting evoked $[DA]_o$ from a population of DA-releasing sites.

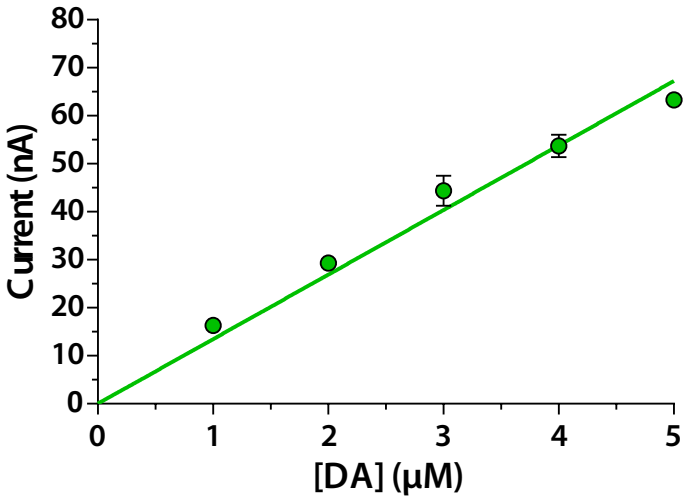

Figure 2.5 Linear relationship between dopamine concentration and oxidation current
Typical calibration graph illustrating the linear relationship between applied DA concentration and the resulting DA oxidation, or Faradaic, current measured with FCV at CFM. The resulting calibration factor for DA sensitivity at this electrode was 29.32 nA/µM in aCSF at 32°C, R^2=0.94 (n=3 calibrations).

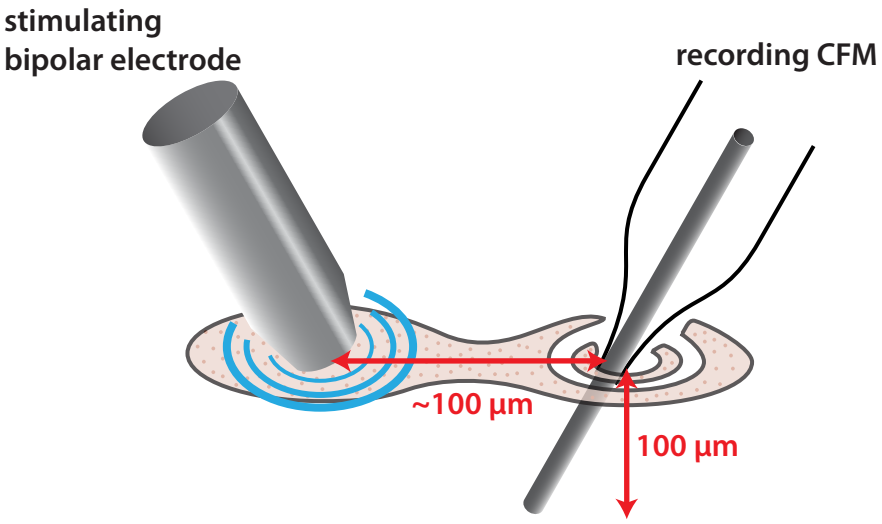

Figure 2.6 Positioning of bipolar stimulating electrode and CFM for recording of evoked $[DA]_o$ with FCV at CFM following local electrical stimulation
A schematic showing positioning of stimulating bipolar electrode for driving striatal DA release with electrical current stimulation. Typical pulse width was 2 ms and perimaximal current amplitude was 0.6 mA. The stimulating electrode is placed on the very surface of brain tissue to minimize mechanical damage from the electrode tip. The CFM is positioned ~100 µm away from the bipolar electrode and is inserted up to 100 µm below the tissue surface.

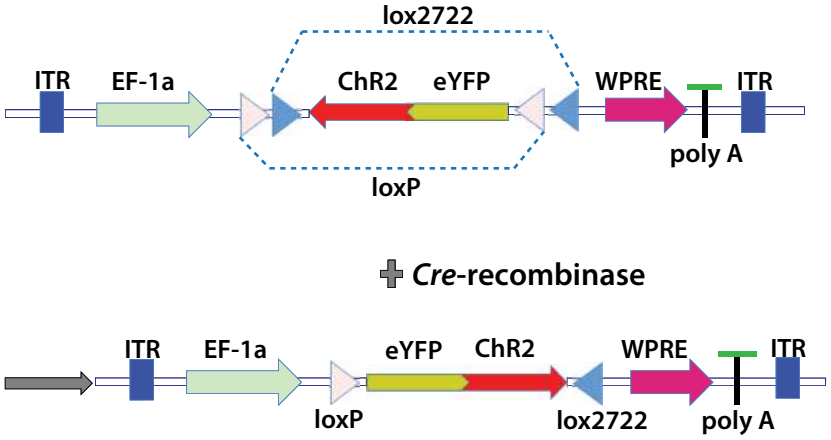

Figure 2.7 Channelrhodopsin-2 construct
The recombinant Cre-dependent vector carrying an inverted double-floxed gene sequence for channelrhodopsin-2 (ChR2) fused with enhanced yellow fluorescent protein (eYFP) under strong general promoter EF-1a. Cre-dependent excision of loxP sites inverts the construct in the correct orientation to enable transcription of ChR2 in neurons expressing Cre-recombinase.

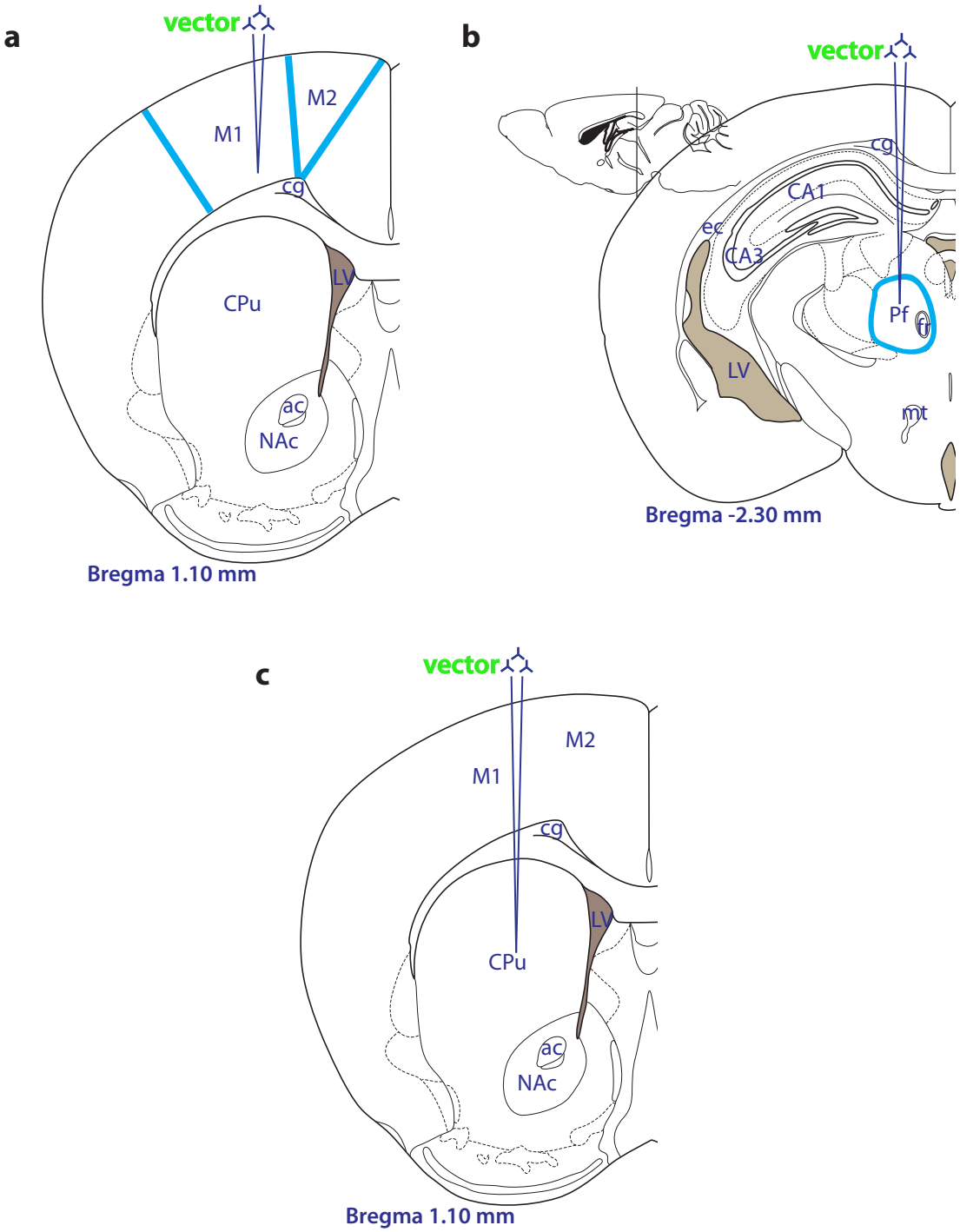

Figure 2.8 Targeting of viral vector injections to motor cortex, caudal intralaminar thalamus and striatum in Cre-mouse driver lines
Schematics of the mouse brain in coronal plane showing targeting of AAV-packaged floxed viral vector injections in mice expressing *Cre*-recombinase in genetically defined neuronal populations. Stereotaxic injections of AAV-packaged vectors carrying gene sequences for depolarizing and hyperpolarizing opsins were targeted to cortical area M1 **(a)**, caudal intralaminar thalamus Pf nucleus **(b)** or central striatum CPu **(c)**.

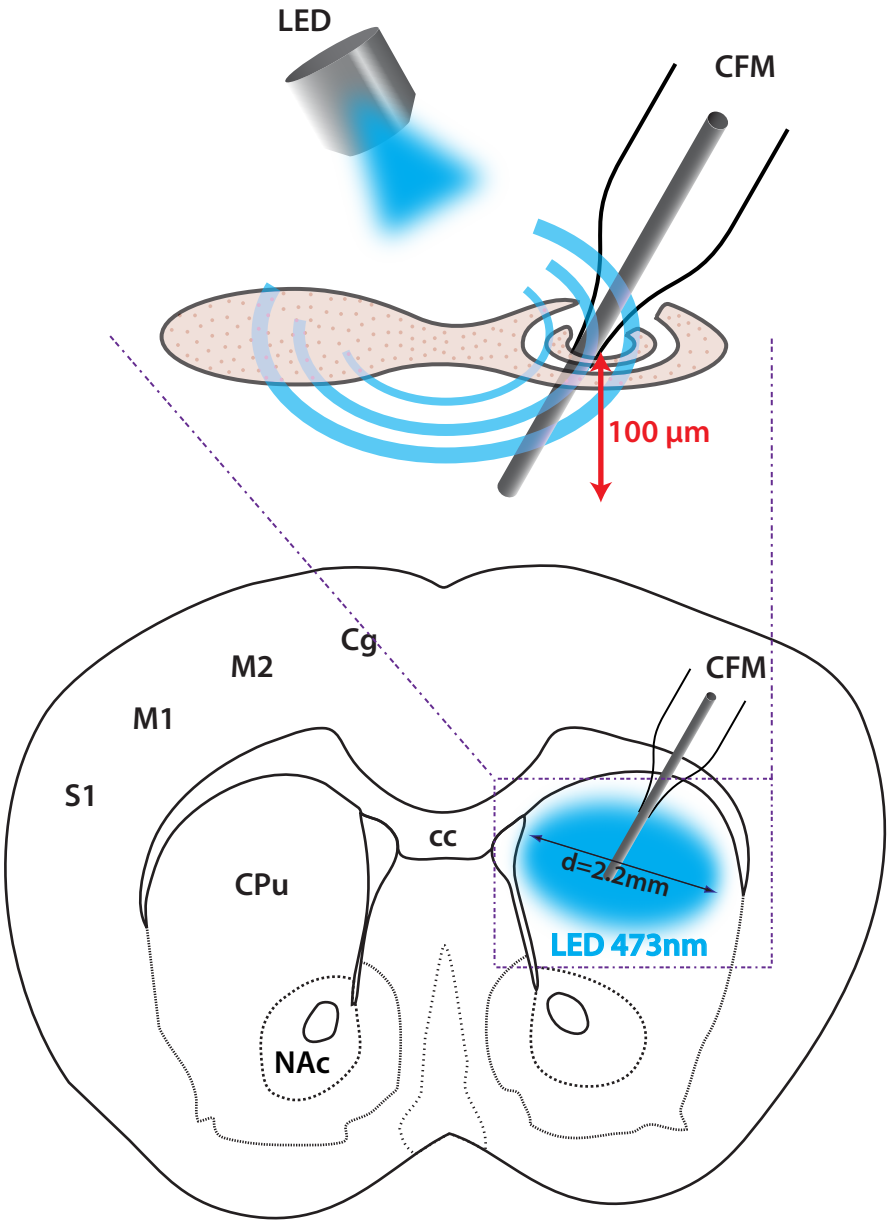

Figure 2.9 Full-field LED stimulation of opsin-transduced circuits for FCV recordings of light-evoked $[DA]_o$

A schematic showing set up for full field LED stimulation of opsin-transduced cell bodies and/or terminals in acute striatal slices in mice. 300 µm-thick coronal sections where opsin expression was confirmed by visualizing fluorescent tags were used for FCV at CFM recordings of light-evoked $[DA]_o$. Full-field LED stimulation covered an area 2.2 mm in diameter under x10 immersion objective. CFM was inserted in tissue 100 µm below the surface in the region where high fluorescence intensity was detected. This region and the CFM insertion site were centred in the field of view to ensure the centre of the light circle was aligned with the CFM position.

3. Acetylcholine-evoked striatal dopamine release: exploring circuits driving cholinergic interneuron activity with AAV5 ChR2

3.1 Introduction

3.1.1 Historical perspective: dynamic gating of dopamine release by acetylcholine

Historically, cross talk between ACh and DA was best encompassed by the dynamic gating hypothesis. It emerged from data showing that ACh release by striatal ChIs operates a local gain control mechanism on translation of DA neuron soma activity into release events at striatal dopaminergic axon terminals. Acting at nAChRs on DA axons and/or mAChRs on ChIs, ACh dynamically gates DA release probability (Pr), controlling the amplitude of striatal DA signals following SNc/VTA activation, or local electrical stimulation of striatal dopaminergic terminals (Rice and Cragg, 2004; Zhang and Sulzer, 2004; Exley et al., 2008; Threlfell et al., 2010; Cohen et al., 2012; Patel et al., 2012). Specifically, tonic activation of nAChRs by low extracellular ACh concentrations increases the initial Pr for single/first pulse stimulation, whilst triggering short-term depression during subsequent depolarisations arriving in close temporal proximity. This arrangement effectively creates a low pass filter on striatal DA signalling (Cragg, 2006). Functionally it translates in DA release events of similar amplitude regardless of stimulation frequency when nAChRs are active. Yet, when nAChRs are inactivated either by desensitization or receptor antagonism, ACh no longer governs DA Pr: evoked DA transients begin to display a frequency-dependent increase in amplitude. Similar effects are exercised by mAChRs, which by limiting ChIs firing remove ACh tone, an action that is equivalent to nAChRs inactivation (Threlfell et al., 2010).

3.1.2 State-of-the-art knowledge: acetylcholine drives striatal dopamine release

Data supporting the dynamic gating hypothesis was acquired using electrical stimulation. This approach enables discrete and temporally precise activation of striatal DA release, but lacks specificity in the cell types it depolarizes. Thus, it significantly limited the ability to dissect out the role played by striatal ChIs. In contrast, optogenetic probing of cellular/circuit function enables precise targeting of genetically-defined neuronal populations for light activation (Packer et al., 2013). Application of optogenetics for examining the role of ChIs in DA transmission revealed a mechanism for direct stimulation of striatal DA release by ChIs. Using a *Cre*-loxP system to selectively express ChR2 in striatal ChIs of ChAT-Cre mice with viral vector injections, our group showed that ACh released upon synchronous activation of a small ChI population directly drives DA release in dorsal striatum *in vitro*, acting at nAChRs on DA axon terminals (Threlfell et al., 2012). Joseph Cheer's group also showed that ChIs drive DA release in the NAc *in vivo*, although they employed a mouse model which constitutively expresses ChR2 in ChIs throughout the brain (Cachope et al., 2012).

Together, these elegantly performed studies provided the direct evidence for axo-axonic action of ACh on dopaminergic terminals driving striatal DA release. ACh-DA interactions most likely occur via volume transmission, and not classical axo-axonic synapses found in cerebral cortex (Tamás and Szabadics, 2004; Wang and Sun, 2012; Takács et al., 2014). This local drive of striatal DA events bypasses the need for parent cell body activation of SNc/VTA neurons, suggesting that in some circumstances striatal DA signalling may happen independently of midbrain activity. The drive of DA release by

the local striatal circuits highlights an additional level of fine-tuned ACh control over DA neurotransmission not previously considered.

3.1.3 Possible drivers of acetylcholine-evoked striatal dopamine release

Synchronized activity in a small population of ChIs is the crucial parameter for ACh-evoked drive of striatal DA release. No DA events follow current injections which trigger APs in single ChIs recorded in current clamp mode, yet a laser beam as small as 15 μm in diameter drives ACh-evoked DA release successfully (Threlfell et al., 2012). Given the extensive arborisations and the average neighbour distance of a few microns between processes of nearby ChIs, the laser beam likely depolarized a small ChI population by activating ChR2 on several neurons simultaneously.

The requirement for synchronized population activity may be rooted in the high levels of AChE activity in striatum (Calabresi et al., 2000a; Zhou et al., 2001; Bernácer et al., 2007). This enzyme rapidly catalyses the breakdown of extracellular ACh, and thus, if only one or two ChIs released ACh, may prevent a sufficient number of post-synaptic nAChRs from being activated for driving DA release. Further, as tonically active neurons (Wilson et al., 1990; Goldberg and Wilson, 2005; Goldberg and Reynolds, 2011), ChIs are likely to display de-synchronized population firing, generating high levels of background noise with 'random' ACh release events. Therefore, synchronized population activity may enable the DA system to distinguish noise from 'real' signal. Concurrently, ACh release supported by de-synchronized spiking of individual ChIs likely provides tonic occupancy of nAChRs on DA axons dynamically gating DA Pr. Whatever the reason for synchronicity to be the determinant of successful drive of striatal DA release by ACh, it needs to be supported by the cholinergic system architecture and physiology.

Widespread dendritic and axonal fields of neighbouring ChIs interdigitate and efficient re-current connections between local ChI networks are likely to aid synchronization of population activity (Bolam et al., 1984). Electrophysiology studies also suggest that ChIs function as a network. Cross-correlogram physiology data show that ChI pairs are coupled in their characteristic burst-pause-burst discharge (Morris et al., 2004; Graybiel, 2008), and abnormal levels of synchronous ChI discharges are recorded in pathological states (Raz et al., 1996). Together, these data suggest that the striatal cholinergic system could successfully employ synchronous population activity as the means of conveying task-relevant information to its downstream targets, DA axons.

Afferent projections can also aid generation of synchronous activity in ChI networks by ensuring decoding and integration of correlated inputs by multiple recipient cells. Thus, it is necessary to determine the extended neuronal circuits capable of driving this local ChI-evoked DA signalling cascade. Moreover, the state of synchrony induced by optogenetic stimulation of ChIs may have limited correlates *in vivo*, as this stimulation approach enables rapid and direct depolarization of ChR2-expressing neurons by induction of cation flow though the channels that ChR2 forms in the neuronal membranes upon light-induced conformational change in its pore structure.

The work presented in this thesis aimed to explore the circuits capable of driving ChI-evoked DA release pursuing two main objectives. Firstly, showing that this local DA signalling cascade is physiologically relevant and can potentially be engaged *in vivo*. Secondly, exploring functional characteristics of the extended circuits capable of recruiting ACh-evoked drive of striatal DA. I examined afferents to striatal ChIs known to be strong physiological drivers of ChI activity *in vivo* and *in vitro*. By probing whether ChI

population activity can be engaged via stimulation of their afferent inputs, hence removing the activation site one set of synaptic connections away from the primary driver mechanism, I aimed to demonstrate that ChI-evoked DA signalling is physiologically relevant. In particular, I explored whether driving afferent circuits with stimulation rates known to be present in behavioural conditions and/or brain states that readily engage striatal computational circuits, such as events signalling arousal, can also drive local striatal DA release, putatively via population activity in ChIs. There is some evidence that thalamic projections are able to recruit ChI-evoked DA release (Threlfell et al., 2012). However, the possibility of other excitatory projections to ChIs driving ACh-evoked DA events, including those from sensorimotor cortex, has remained unexplored.

3.1.4 Thalamostriatal and corticostriatal projections as candidate drivers of acetylcholine-evoked striatal dopamine

Afferents capable of engaging synchronous ChI population activity should provide robust striatal innervation, as ChIs are a relatively rare cell type, constituting 1-2% of striatal neuron count in rodents. Both cortical and thalamic projections to CPu fulfil these criteria. The wealth of anatomical data on thalamostriatal afferents demonstrate that the centromedian-parafascicular complex of the caudal intralaminar thalamus provides densest CPu innervation (Berendse and Groenewegen, 1990; Van der Werf et al., 2002; Smith et al., 2004; Sadikot and Rymar, 2009). These data also show that afferents from the parafascicular nucleus (Pf) in particular target proximal and distal dendritic shafts and spines of striatal ChIs, forming asymmetric synaptic contacts on those structures (Lapper, 1992; Sadikot et al., 1992; Lacey et al., 2007; Doig et al., 2014). Functionally, these monosynaptic connections between the intralaminar thalamic

afferents and striatal ChIs modulate ChI firing rates both *in vivo* and *in vitro* (Consolo et al., 1996b; Matsumoto et al., 2001; Lacey et al., 2007; Ding et al., 2010; Schulz et al., 2011; Doig et al., 2014). They also contribute to synchronization of ChI firing in conditioning paradigms (Graybiel, 2008). These anatomy and physiology data are consistent with the observation that optogenetic activation of striatal Pf terminals can elicit ChI-evoked DA release (Threlfell et al., 2012).

By contrast, until recently, there was a lack of anatomical evidence for a direct innervation of striatal ChIs by cortical afferents. Frontoparietal cortical areas, sensorimotor regions in particular, densely innervate CPu in rodents (McGeorge and Faull, 1989; Berendse et al., 1992; Cheatwood et al., 2003, 2005; Reep et al., 2003; Kamishina et al., 2008; Schilman et al., 2008). Whether these projections also directly target striatal ChIs was unknown. Early studies either failed to identify cortical synaptic contacts on ChIs or suggested the existence of distal and sparse synapses (Meredith and Wouterlood, 1990; Lapper, 1992; Thomas et al., 2000; Alcantara et al., 2001). The latest data, however, demonstrate that cortical projections indeed synapse on distal and proximal dendrites of ChIs, albeit the number of synapses was estimated to be one third of those formed by thalamic afferents (Doig et al., 2014). These findings are consistent with electrophysiology data showing intact monosynaptic functional connectivity between cortex and ChIs, as cortical stimulations drive changes in ChIs firing rates *in vivo* and in *vitro* (Wilson et al., 1990; Consolo et al., 1996a; Pisani et al., 2000; Reynolds and Wickens, 2004; Ding et al., 2010; Doig et al., 2014). Together, these data suggest that corticostriatal afferents could also fulfil the task of driving ACh-evoked DA release by recruiting ChI population activity. This possibility remained unexplored until now.

Determining whether thalamic afferents are the sole input capable of driving ACh-evoked DA has important implications for understanding the role of this local dopaminergic signalling cascade in striatal function. Based on the type of information that Pf projections likely supply to striatal ChIs, thalamically-induced drive of DA release could create a preparatory or expectation set for contextually-embedded action performance by aiding activation of D1 MSNs (Hernández-López et al., 1997; Podda et al., 2010). In particular, this mechanism would support acquisition and execution of discriminatory-based learning (Kato et al., 2011). If cortical projections can also engage sufficient ChI synchronization to drive ACh-evoked DA, cortically-elicited DA events could provide a filter for active input selection via D2 receptor activation on corticostriatal terminals (Bamford et al., 2004). Specifically, cortical drive of DA release could enable feed-forward facilitation of highly active corticostriatal inputs, augmenting learning of situationally appropriate behaviours. The thalamic projections could also fulfil this role, but as a feedback mechanism. Hence, identifying afferent projections capable of driving ACh-evoked striatal DA is necessary for comprehending functional and behavioural significance of locally-mediated DA signalling.

3.1.5 Early studies of glutamate-evoked striatal dopamine release

Prior to the data showing striatal DA release following Pf afferents stimulation (Threlfell et al., 2012), the possibility of other glutamatergic projections to ChIs driving ACh-evoked DA events remained unexplored. There is some evidence, however, of glutamate transmission increasing extracellular DA levels, suggesting glutamate-dependent ACh-evoked DA drive could be an established phenomenon.

A number of studies from the early 1990s reported increased DA efflux in striatal synaptosomal preparations and *in vivo* microdialysis experiments upon glutamate

application (Chéramy et al., 1986; Leviel et al., 1990; Shimizu et al., 1990; Krebs et al., 1991; Lonart and Zigmond, 1991; Verma and Moghaddam, 1998). These observations have been subject to much controversy, given the lack of evidence for glutamate receptor localization to DA axon terminals (Moss et al., 2011). Some groups suggested that glutamate application could trigger DA release via DAT reversal (Lonart and Zigmond, 1991) or even exercise direct, activity-independent facilitatory and inhibitory effects on DA release (Roberts and Anderson, 1979; Leviel et al., 1990; Borland and Michael, 2004). The unequivocal evidence for the processes underlying these glutamate actions on DA release was lacking.

While these early experiments provide some evidence for direct modulation of DA release by glutamate, they were mostly based on HLPC analyses of dialysates collected over a long period *in vivo*. Consequently, these data do not accurately reflect moment-to-moment changes in extracellular DA levels or delineate the circuits involved. The Glowinski group in the 1970s showed that DA release could also be evoked by electrical stimulation of the cortex in cat, although authors concluded the recorded terminal DA release to be the result of direct SNc activation (Nieoullon et al., 1978). The above data, therefore, set a scene for our investigation of glutamate-dependent drive of striatal DA release. Unlike the past studies advocating direct glutamate effects on DA transmission, we suggest that the mechanism at play actually involves an intermediary in the face of resident ChIs.

3.1.6 Summary

The early studies of ACh-DA interactions in striatum put forward a number of working hypotheses for describing this relationship. The dynamic gating hypothesis of DA release by the cholinergic system stood its ground until the advancements in

research technology provided evidence for this conceptualization of ACh-DA relationship being oversimplified yet. Coupling of FCV with selective optogenetic activation of striatal ChIs uncovered an unprecedented level of cooperativity between ACh and DA, demonstrating that ChIs can evoke striatal DA release via nAChRs located on DA axon terminals. However, whether this local DA signalling cascade can be recruited physiologically to a large extent remained unexplored. The experiments described in this chapter aimed to examine the relative roles and functional characteristics of cortical and thalamic afferents to striatal ChIs in driving ACh-evoked DA release events.

3.1.7 Goals and aims of the current study

In this work we set out to investigate the recruitment of ACh-evoked DA release by two well-established physiological drivers of ChI activity, corticostriatal and thalamostriatal projections, originating from primary motor cortex and Pf nucleus of caudal intralaminar thalamus, respectively. These afferents were previously shown to increase the firing rate of tonically active ChIs *in vivo* and *in vitro*. Firstly, I employed electrical stimulation of corticostriatal afferents in sagittal slices for detection of evoked DA events. Secondly, I used selective optogenetic activation of cortical and Pf thalamic terminals in coronal striatal slices coupled with FCV recordings of light-evoked DA events. Experimental results showed that both M1 cortical and Pf thalamic projections are capable of driving striatal DA release, and ChIs play the gatekeeper role in mediating this glutamate-dependent drive of striatal DA signalling.

3.2 Methods

Methods used were as described in Chapter 2, unless otherwise stated here.

3.2.1 Animals

Adult (35-70d) male C57Bl6/J wild type (WT) mice were used for electrical stimulation experiments. Adult (21-40d) male and female homozygous and heterozygous CaMK2a-Cre mice (B6.Cg-Tg(CaMK2a-Cre)T29-1Stl/J, stock 005359) were used for optogenetic experiments. For anatomy experiments addressing anterograde versus retrograde axonal transport of the AAV5 vector, adult (30-45d) male heterozygous DAT-Cre mice (B6.SJL-*Slc6a3*$^{tm1.1(cre)Bkmn}$ /J, stock 006660) were used.

3.2.2 Optogenetic surgery

Stereotaxic injections of AAV5-packaged floxed ChR2 construct for optogenetic experiments were performed on CaMK2a-Cre mice (21-40d). 400 nl of the AAV5 ChR2 vector were pressure-injected per hemisphere bilaterally. 4-10 weeks were allowed for opsin transduction to ensure sufficiently high levels of ChR2 expression. For the corticostriatal afferents injections targeted primary motor cortex M1 (ML 1.7 mm, AP +1.3 mm, DV 1.0 mm from bregma) or somatosensory cortex M1/S1 (ML 2.6 mm, AP +0.5 mm, DV 2.1 mm from bregma). During the later stages, all injections targeted M1 exclusively. For the thalamostriatal afferents injections targeted the Pf nucleus (ML 0.7 mm, AP -2.3 mm, DV 3.5 mm from bregma).

For anatomical localization of the AAV5 ChR2 vector following its transportation from the injection site, DAT-Cre mice (30-45d) received injections targeting central CPu (1.5 mm ML, +0.5 mm AP, 3.2 mm DV from bregma). 400 nl of the ChR2 construct were

injected per hemisphere bilaterally. After 4-6 weeks incubation time, mice were transcardially perfused with PBS and their brains were fixed.

3.2.3 Slice preparation

Acute slices were prepared as described in Chapter 2. Brains from the WT mice for the electrical stimulation experiments were cut in sagittal plane starting from the midline. 4-5 consecutive sagittal slices containing CPu and NAc were collected for experimentation.

3.2.4 Stimulation protocols and experimental set up

To probe the role of corticostriatal afferents in driving ChI-evoked DA release, electrical stimulation of descending L5/6 fibres in WT sagittal sections was used. Coronal slices from AAV5 ChR2-injected CaMK2a-Cre mice were used in optogenetic experiments where cortical or thalamic striatal terminals were activated with blue light.

3.2.4.1 Distal electrical stimulation

The stimulating Pt/Ir electrode was first positioned in corpus callosum (CC), in sagittal slices preserving the integrity of ipsilateral and crossed corticostriatal projections. The working CFM was placed distally 450-500 μm away from the stimulating electrode in dorsal CPu. After the CC stimulation protocols were completed, the stimulating electrode was positioned for intrastriatal (CPu) stimulation, equidistantly from the CFM. For the control experiments designed to probe glutamate involvement in evoked DA events during intrastriatal distal stimulation, both the stimulating electrode and CFM were positioned in dorsal CPu 450-500 μm apart. Electrical current amplitude was adjusted between 0.8-2.0 mA to ensure evoked $[DA]_o$ were sufficiently large to be easily detected in control pre-drug recordings. A range of stimulation frequencies and

pulse number, including single pulses, paired pulses and pulse trains at 10-100 Hz were used.

3.2.4.2 Optogenetic stimulation

ChR2-expressing cortical and thalamic terminals were visualised by eYFP expression and DA release was sampled in areas with high fluorescence signal intensity. ChR2-expressing terminals were depolarized using a blue 473 nm LED. Light stimulation protocols were designed to reflect physiological firing frequencies of each of the afferent pathways observed *in vivo*. For thalamic projections single pulses and trains of 5 pulses at 10 Hz were used, for cortical afferents single pulses and trains of 10 pulses at 25 Hz were employed.

3.2.5 Fast-scan cyclic voltammetry

Striatal DA release following electrical stimulation of corticostriatal projections in sagittal sections, or light activation of ChR2-expressing cortical/thalamic terminals in coronal slices was monitored with FCV at CFMs as described in Chapter 2.

3.2.6 Immunohistochemistry and injection site localization

Immunohistochemical processing was carried out as described in Chapter 2.

100 μm thick Pf- and 300 μm thick M1-containing sections from the animals where 5-20nl of red polystyrene fluorescent spheres (Invitrogen) were injected together with the ChR2 construct were used for identification of the injection sites. 50 μm thick sections containing Pf were immunostained with α-cerebellin-1 antibody, the putative marker of Pf neurons (Kusnoor et al., 2010; Ellender et al., 2013). These sections were then used for co-localization of ChR2 with the secondary antibody conjugated to DyLight

594 fluorophore (Jackson ImmunoResearch Laboratories Inc.). 50 μm slices containing SNc and VTA from CPu-injected DAT-Cre mice were examined for eYFP signal to detect retrograde AAV5 ChR2 transport, and some of the sections were processed for immunostaining with TH antibody to show co-localization of TH-positive cells with eYFP-expressing fibres.

Visualization of ChR2-expressing cell bodies and processes in all Cre driver lines was possible without additional immunostaining due to high levels of eYFP signal intensity in heat-treated and unprocessed PFA-fixed sections.

3.2.7 Drugs

D-AP5, GYKI 52466 hydrochloride (GYKI), bicuculine, saclofen, Oxo-M and MCPG were purchased from Tocris Bioscience or Ascent Scientific. DHβE and all other chemicals were purchased from Sigma Aldrich. All solutions were prepared in distilled de-ionized water or aqueous acid (GYKI) to make stock aliquots at 1000-10000x final concentrations and stored at -20°C. Drug stocks were diluted in oxygenated aCSF from frozen aliquots immediately before use and were bath applied. None of the drugs altered electrode sensitivity at the concentrations used.

3.2.8 Data analyses

All data were recorded, pre-processed and analysed using Whole Cell Program (University of Strathclyde, Glasgow) or AxoScope 10.2 (Axon Laboratories) software packages and in-house Excel macros scripts (Prof S. Cragg & Dr K. Jennings). All statistical analyses and data plotting were performed using GraphPadPrism 6.0.

The data are expressed as mean ± standard error of the mean (SEM), where N is the number of animals and n is the total number of observations. Typically, 2-4 slices per animal were recorded from for optogenetic experiments, 1-3 slices per animal for electrical stimulation experiments. The minimum N for each experimental data set presented here is 3, unless otherwise stated. DA transients represent traces averaged across different experiments that employed the same experimental manipulation and are always normalized to their mean peak control value (single pulse or pulse train in pre-drug condition), unless the data are presented as raw extracellular DA concentrations in μM ($[DA]_o$). Mean evoked DA transients were calculated by averaging at least 4 traces from every recording site for each stimulation and/or drug application protocol. The averaged data were plotted and analysed statistically using comparison of the means and regression analyses. When raw data passed Shapiro-Wilk normality tests, parametric tests were used. The mean peak evoked DA values were used for statistical comparisons, unless otherwise stated.

3.3 Results

3.3.1 Electrical stimulation of corticostriatal afferents

To test whether corticostriatal afferents could drive ChI-evoked DA release electrical stimulation was used in exploratory studies. This approach presented a potential for straightforward experiments remotely activating corticostriatal afferents in WT tissue. However, this turned out to be not the case for several reasons outlined below. It was possible to detect striatal DA release with distal electrical stimulation of corticostriatal fibres (Figure 3.1b-f, 3.3b-f), although evoked DA transients were typically small, on the order of 0.4-0.7 μM. Thus, only 1 in 3 experiments had sufficiently high release levels to complete data acquisition following pharmacological manipulations.

Ionotropic glutamate AMPA (GYKI, 10 μM) and NMDA (D-AP5, 50 μM) receptor antagonists were used to delineate glutamate-dependent component in DA transients evoked by distal electrical stimulation of corticostriatal afferents in CC (Figure 3.1a). D-AP5 and GYKI application on average reduced peak evoked $[DA]_o$ to 38% of control across all stimulation protocols (Figure 3.1b-f). iGluR antagonists decreased evoked DA release independently of stimulation frequency. Two-way ANOVA showed the main effect of drug application ($F(1,136)=476.0$, $p<0.0001$), and post-hoc Bonferroni t-tests revealed that for every stimulation protocol peak evoked $[DA]_o$ was significantly decreased with iGluR antagonism ($p<0.0001$) (Figure 3.1g). However, progressive decline in evoked $[DA]_o$ over time likely exaggerated the observed drug effects (Figure 3.1h), because no steady baseline could be achieved in control prior to drug administration. To investigate whether decrease in evoked $[DA]_o$ was due to tissue quality decline, the stimulating electrode was moved and positioned for remote intrastriatal (CPu)

stimulation (Figure 3.1a). Distal CPu stimulation in iGluR block evoked DA transients with larger amplitude compared to distal CC stimulation in drug-free conditions (Figure 3.1b-f), thus revealing a significant passive current component in evoked $[DA]_o$. The implications are two-fold. Firstly, a decrease in evoked $[DA]_o$ following iGluR antagonism was not purely due to decline in slice quality. Secondly, the CC itself can limit electrical current spread to distal sites where the CFMs were positioned, possibly due to higher impedance of myelinated fibre tracts.

Further experiments explored glutamate contribution to evoked DA events with distal CPu stimulation (Figure 3.2a). Application of AMPA (GYKI, 10 μM) and NMDA (D-AP5, 50 μM) receptor antagonists on average decreased peak evoked $[DA]_o$ to 80% of control (Figure 3.2b-f). The reduction in evoked $[DA]_o$ was small but significant and two-way ANOVA revealed the main effect of iGluR antagonism ($F(1,133)=29.14$, $p<0.0001$). Post-hoc Bonferroni comparisons, however, showed that only for single pulse and 5 pulses at 10 Hz stimulation protocols reduction in evoked $[DA]_o$ was statistically significant ($p<0.05$) (Figure 3.2g). In contrast to distal CC stimulation experiments, evoked $[DA]_o$ with distal CPu stimulation was relatively stable over time, both during baseline pre-drug recordings and following iGluR block (Figure 3.2h). However, evoked $[DA]_o$ with distal CPu stimulation protocol was also generally higher, on the order of 1.0-1.2 μM. Thus, approximately 60% reduction in evoked $[DA]_o$ following iGluR antagonism with CC stimulation and 20% decrease with CPu stimulation suggested that glutamate-dependent component of CC-evoked DA events could account for up to 40%. These data were initially suggestive of a glutamate-dependent component in DA release events following distal electrical stimulation of corticostriatal fibres in CC.

I next examined whether corticostriatal DA events were mediated via ChIs. The hypothesis tested was that striatal ChIs following their activation by corticostriatal glutamatergic afferents drive DA release via nAChRs. If DA release following activation of corticostriatal projections happens via ChIs, application of nAChR antagonist would abolish DA events evoked with distal CC stimulation (Figure 3.3a). The DA events evoked with distal CPu stimulation (Figure 3.3a), however, would be spared, as intrastriatal electrical currents also directly depolarize dopaminergic terminals. Application of nAChR antagonist (DHβE, 1 μM) reduced electrically evoked $[DA]_o$ to 11% of control with CC and 16% of control with CPu stimulation (Figure 3.3b-f). The mean peak $[DA]_o$ evoked in the presence of nAChR antagonist with CC and CPu stimulation was significantly decreased in a frequency-sensitive manner. Two-way ANOVA revealed the main effect of drug application ($F(1,89)=9.73$, $p=0.0024$) and stimulation frequency ($F(4,89)=7.52$, $p<0.0001$). Thus, evoked $[DA]_o$ following CC and CPu distal electrical stimulation in the presence of DHβE was frequency sensitive (Figure 3.3g). However, across all stimulation frequencies mean peak evoked $[DA]_o$ in the presence of DHβE was not significantly different between CC and CPu stimulation protocols ($F(2,12)=0.60$, $p<0.0001$, one-way ANOVA, post-hoc Tukey tests $p>0.05$; Figure 3.3h). Frequency sensitivity of DA events evoked with distal electrical stimulation was similar to frequency-sensitive DA transients evoked with local electrical stimulation of DA axons following nAChR blockade. These data strongly suggested that passive current spread directly depolarizing DA terminals was a significant contributing factor to $[DA]_o$ evoked with CC and CPu distal electrical stimulations. Further, under these circumstances passive current could also be driving corticostriatal and other glutamatergic inputs during distal CPu stimulation.

Together, the above data suggest that with distal electrical stimulation there could be no certainty regarding which afferent fibres or local circuits are being activated. Most likely due to passive current effects DA axons, striatal ChIs as well as local and afferent glutamatergic circuits were stimulated at once. In this case, it is impossible to discern the contribution of each individual component. While comparison of the data from distal CC and distal CPu stimulation following iGluR blockade suggested some glutamate-dependence of evoked $[DA]_o$, due to passive current spread and site rundown only a minor proportion of DA evoked stemmed from corticostriatal pathway activation. Consequently, the role of corticostriatal afferents to ChIs in driving ACh-evoked DA release could not be assessed using distal electrical stimulation. Therefore, optogenetic approach was adopted for all subsequent experiments.

3.3.2 Optogenetic activation of cortical and thalamic afferents to striatal cholinergic interneurons

The advantage of optogenetic approaches lies in the ability to selectively activate terminals of cortical or thalamic origin at striatal level. With electrical stimulation it is virtually impossible to examine contributions from a specific thalamic nuclei group (Ellender et al., 2013). Even distinguishing between cortical and thalamic afferents in CPu is challenging, requiring preparation of parahorizontal slices with distal stimulation of the afferent fibre bundles (Ding et al., 2008, 2010; Goldberg and Reynolds, 2011; Ibáñez-Sandoval et al., 2011; Goldberg et al., 2012). In contrast, optogenetic approaches enable direct and selective light activation of ChR2-expressing cortical or thalamic striatal terminals. Hence, I used CaMK2a-Cre driver line, expressing *Cre*-recombinase in most excitatory cortical and thalamic neurons (Benson et al., 1992; Liu and Jones, 1996,

1997), to targeted ChR2 expression to M1 and Pf neurons using AAV5 ChR2 vector injections.

3.3.3 AAV5 ChR2 transduction of the target cortical and thalamic areas

I first aimed to confirm that cortical and thalamic regions of interest (Figure 3.4a) were successfully targeted during stereotaxic surgery using fluorescence microscopy. High intensity eYFP signal in striatum following cortical (Figure 3.4b) or thalamic (Figure 3.4c) injections showed that ChR2 was successfully trafficked to the axon terminals from the transfected parent cell bodies at the injection sites 5-6 weeks post-surgery. Injections of the AAV5 ChR2 vector into either M1 or Pf also yielded robust transduction of the local neuropil in cortex (Figure 3.4d,f) and caudal intralaminar thalamus (Figure 3.4e,g). Importantly, higher-resolution confocal microscopy images are necessary to unequivocally show ChR2 expression in striatal terminals and parent cell bodies residing in M1 or Pf. Due to high signal intensity, no additional staining was required for visualizing eYFP fluorescence in fixed tissue. In a subset of surgeries red fluorescent spheres (Invitrogen) were injected together with the viral construct to aid injection tract localization. The needle tract labelling with red fluorospheres further confirmed that both cortical M1 (Figure 3.4f) and thalamic Pf (Figure 3.4g) injections were targeted successfully. Specifically, M1 needle tracts span the depth of cortical mantle without extending below the corpus callosum, while the fluorescent beads for Pf injections are largely localised to structures above the Pf nucleus with the end of the labelled tract extending to the dorsal aspect of Pf. Such an arrangement is expected for this labelling technique because fluorescent beads label the injection tract rather than injection site per se, since fluorospheres are injected last and are most likely to be drawn back up the injection tract during needle retraction.

Cerebellin-1 staining was used to determine the extent to which ChR2-transduced neurons in the caudal intralaminar thalamus were localized to Pf nucleus, for which cerebellin-1 is a selective marker (Kusnoor et al., 2010; Ellender et al., 2013). These data showed that while eYFP-positive processes could be detected in the thalamic neuropil in the direct vicinity of the cerebellin-1-labelled cell bodies, no perfect overlap between the green and red fluorescence channels was found (Figure 3.4h,i). Thus, whilst some eYFP-positive somas and processes were also cerebellin-1-positive, eYFP-positive processes were not exclusively restricted to this area.

3.3.4 Light-evoked dopamine release events occur throughout striatum, but the signal is not ubiquitous

The AAV5 ChR2-injected animals were used from 4 weeks post-surgery. No eYFP signal was detectable in the CPu of M1- or Pf-injected CaMK2a-Cre mice taken for experimentation at 2 weeks; while from 4 weeks onwards ubiquitous eYFP signal throughout striatal neuropil was readily visible (Figure 3.4b,c). CFMs were always positioned in areas with high fluorescence intensity. Light-evoked DA transients were successfully recorded throughout dorsal and ventral striatum following optical stimulation of ChR2-expressing glutamatergic terminals originating from cortex or thalamus. For both projections pathways, light-evoked DA events were of similar amplitude, with typically observed DA concentrations on the order of 1-1.5 μM. There was no significant difference between the mean peak evoked $[DA]_o$ following M1 or Pf afferents stimulation (Mann-Whitney U=10,948, n_1=139, n_2=165, p=0.497, two-tailed; Figure 3.5a). Typical cyclic voltammograms from AAV5 ChR2 experiments in Pf- and M1-injected CaMK2a-Cre mice also show that the detected species following light

stimulation of ChR2-transduced striatal glutamatergic afferents were indeed DA (Figure 3.5b).

The light-evoked DA signals were not ubiquitous, however. In some regions despite high eYFP signal intensity no DA transients could be evoked/detected, while recordings from a neighbouring and equally bright site (within 500-2000 μm) yielded robust light-evoked DA events. The fact that light-evoked DA release is not uniform and scattered in a way that is not directly correlated with eYFP, and thus ChR2 expression, suggests that there is an intermediary involved. Specifically, as DA events are not always found in the regions where the glutamate terminals are, it is likely that a confluence of several factors determines the occurrence of light-evoked DA release. In this case, as illustrated in Sections 3.3.5 and 3.3.6, it is both the presence of ChR2-expressing cortical/thalamic glutamatergic inputs and their down-stream ChI targets.

No formal quantification of ChI density/number near the eYFP-positive terminals was attempted. However, a number of sections, where DA events were recorded from and where no detectable light-evoked DA was elicited, were processed to label ChIs with ChAT antibody. This exploratory microscopy showed that in approximate regions where light stimulation of ChR2-transduced glutamatergic afferents readily evoked DA, several ChIs were present, usually in groups of 2-3 neurons in close spatial proximity. In contrast, in slices where no DA was detected, or even near the 'unsuccessful' sites from a DA-releasing section, no ChIs or single neurons were found. Because the recording sites were not labelled and these estimates are approximate, no data is shown. However, these observations support the argument that di-synaptic drive of striatal DA release requires co-localization of glutamate-releasing afferents and striatal ChIs.

3.3.5 Cortical and thalamic afferents drive AP-dependent dopamine release via engagement of different ionotropic glutamate receptors

First, bath perfusion of voltage-gated sodium channel blocker tetrodotoxin (TTX, 1 μM) confirmed that light-evoked DA release was dependent on APs for both thalamic (Mann-Whitney U=0, $n_1=n_2=8$, p=0.0002, two-tailed; Figure 3.5c) and cortical (Mann-Whitney U=0, $n_1=24$, $n_2=8$, p<0.0001, two-tailed; Figure 3.5d) experimental groups.

To confirm glutamate-dependence of the light-evoked DA events selective NMDA (D-AP5, 50 μM) and AMPA (GYKI, 10 μM) receptor antagonists were applied sequentially. The non-parametric alternative to one-way ANOVA analyses revealed that D-AP5 and GYKI application significantly decreased the amplitude of thalamically-evoked (H(3)=40.68, p<0.0001, Kruskal-Wallis test; Figure 3.5e), and cortically-evoked (H(3)=41.32, p<0.0001, Kruskal-Wallis test; Figure 3.5f) DA transients. Post-hoc comparisons showed that D-AP5 significantly decreased evoked $[DA]_o$ for thalamic afferents stimulation (p<0.01), while cortically-evoked DA release remained unchanged (p>0.05). Subsequent application of GYKI significantly decreased evoked $[DA]_o$ in both experimental groups, abolishing light-evoked $[DA]_o$ following both thalamic (p<0.001) and cortical (p<0.0001) afferents stimulation. These data show that light-evoked DA events following optical stimulation of ChR2-expressing thalamic striatal terminals were dependent on glutamate acting at post-synaptic NMDA and AMPA receptors, while cortical afferents preferentially recruited AMPA receptors. In pilot experiments, application of AMPA antagonist alone (GYKI, 10 μM) also abolished light-evoked DA release for both thalamus (Mann-Whitney U=0, $n_1=n_2=12$, p<0.0001, two-tailed; Figure 3.5g) and cortex (Mann-Whitney U=0, $n_1=n_2=4$, p=0.029, two-tailed; Figure 3.5h).

3.3.6 Striatal cholinergic interneurons are the gatekeepers of glutamate-dependent striatal dopamine release

I next examined the cholinergic axis involvement in glutamate-dependent DA events. The working hypothesis was that striatal glutamatergic afferents by recruiting ChI population activity drive DA release by stimulating axo-axonic acetylcholine-mediated interactions between dopaminergic terminals and ChIs. Application of nAChR antagonist (DHβE, 1 μM) abolished light-evoked DA release following activation both thalamic (Mann-Whitney U=0, n_1=11, n_2=12, p<0.0001, two-tailed; Figure 3.6a) and cortical (Mann-Whitney U=0, n_1=n_2=20, p<0.0001, two-tailed; Figure 3.6b) striatal afferents. mAChR agonist (Oxo-M, 10 μM), which autoinhibits AP firing by ChIs arresting release of ACh, also eliminated light-evoked DA transients following activation of thalamic (Mann-Whitney U=0, n_1=n_2=12, p<0.0001, two-tailed; Figure 3.6c) and cortical (Mann-Whitney U=0, n_1=n_2=16, p<0.0001, two-tailed; Figure 3.6d) projections. These data show that light-evoked DA events following stimulation of ChR2-transduced cortical or thalamic striatal terminals were ACh-dependent, not evoked directly by glutamate acting at iGluRs on DA axons. When the cholinergic axis was removed by antagonism of nAChRs or following mAChR activation, light-evoked DA events were abolished, demonstrating ChIs are the primary gatekeepers of glutamate-dependent drive of local striatal DA release by corticostriatal and thalamostriatal inputs.

3.3.7 The role of mGluRs and GABARs in regulating glutamate-dependent acetylcholine-evoked dopamine events

Previous research showed that GABAergic transmission aids synchronization of ChI firing (Sullivan et al., 2008), while mGluRs can inhibit DA release *in vitro* (Zhang and

Sulzer, 2003), and stimulate/inhibit DA release in an activity-dependent manner *in vivo* (Verma and Moghaddam, 1998), and modulate ChI activity (Pisani et al., 2001, 2002; Bell et al., 2002; Bonsi et al., 2005). Therefore, I next examined whether GABARs and mGluRs were involved in regulation of di-synaptic circuit for local striatal DA release between glutamatergic afferents and ChIs.

Application of broad-spectrum mGluR antagonist (MCPG, 200 μM) revealed no mGluR involvement in light-evoked DA release events following stimulation of thalamic (Mann-Whitney U=54, $n_1=n_2=12$, p=0.314, two-tailed; Figure 3.6e) or cortical (Mann-Whitney U=140, $n_1=n_2=20$, p=0.107, two-tailed; Figure 3.6f) striatal afferents. Likewise, combined application of $GABA_A$ (bicuculine, 10 μM) and $GABA_B$ (saclofen, 50 μM) receptor antagonists demonstrated no GABAR effects on thalamically-evoked (Mann-Whitney U=66, $n_1=n_2=12$, p=0.743, two-tailed; Figure 3.6g) or cortically-evoked (Mann-Whitney U=272, $n_1=n_2=24$, p=0.747, two-tailed; Figure 3.6h) DA transients. Thus, mGluRs and GABARs did not significantly affect glutamate-dependent ChI-evoked drive of striatal DA release, at least under the current experimental conditions. However, broad-spectrum antagonists could cancel pre- and post-synaptic effects leading to no net change in evoked DA release, and thus these data should be interpreted with caution.

Overall, following light-activation of ChR2-expressing striatal terminals of Pf origin, blockade of Na^+ channels, NMDARs, AMPARs, nAChRs and activation of mAChRs significantly decreased evoked $[DA]_o$, while antagonism of mGluRs and GABARs had no significant effect on the light-evoked DA release events (Figure 3.7a). For optical stimulation of ChR2-transduced M1 striatal terminals, antagonism of Na^+ channels, AMPARs, nAChRs and activation of mAChRs significantly decreased evoked $[DA]_o$, while

antagonism of NMDARs, mGluRs and GABARs had no significant effect on the light-evoked DA release events (Figure 3.7b).

3.3.8 Glutamate-dependent cholinergic interneuron-evoked dopamine release is frequency insensitive

I next investigated whether frequency insensitivity of ChI-evoked DA events reported previously (Threlfell et al., 2012), holds true for DA release evoked by driving afferent circuits removed one synapse away from the primary driver mechanism. Frequency sensitivity is a fundamental characteristic of the dopaminergic system, enabling the BG to compute learning signals based on the discrepancy between anticipated and actual DA signal amplitudes. In striatum, frequency-dependent DA signal gain is normally clamped by nAChRs, but in the absence of ACh influence evoked $[DA]_o$ shows frequency-dependent increase in amplitude (Rice and Cragg, 2004; Zhang and Sulzer, 2004). In agreement with this, optogenetically-induced synchronization of ChI activity results in frequency-insensitive DA events, despite individual ChIs following optical stimulation trains of various frequencies and durations (Threlfell et al., 2012). The working hypothesis was that as ACh-signalling is the actual driver of glutamate-dependent DA events, preferential activation of cortical or thalamic striatal terminals would drive DA events whose amplitude conveys no frequency information.

Mean peak evoked $[DA]_o$ following single pulses or light trains of 5 pulses at 5, 10, 25 and 40 Hz were not significantly different from each other following thalamostriatal (one-way ANOVA, $F(4,55)=0.63$, $p=0.642$, $R^2=0.044$; Figure 3.8a,c) or corticostriatal (one-way ANOVA, $F(4,55)=1.38$, $p=0.254$, $R^2=0.091$; Figure 3.8b,d) afferents stimulation. Therefore, DA release events evoked via these axes are also

frequency insensitive, like ChI-evoked DA events following direct activation of ChIs in ChAT-Cre driver line.

3.3.9 Dopamine re-release profile is different following activation of cortical versus thalamic synapses on striatal cholinergic interneurons

I also aimed to explore the timecourse of light-evoked DA release recovery. The timecourse of DA re-release following initial activation of DA axons by ChIs is an important parameter. It determines how quickly the system recovers from the first ACh-evoked release event for translating the subsequent synaptic activity into DA transients. Thus, if frequency information is not conveyed by the ACh-evoked DA events, speculatively due to high rate of nAChRs desensitization that makes them refractory for a short time, upon termination of the refractory state cholinergic system re-calibrates and is ready to drive another DA release event. Consequently, neurotransmitter re-release dynamics largely determines the efficiency with which the incoming cortical or thalamic signals can drive glutamate-dependent ChI-evoked DA release with repetitive stimulation.

For these experiments, DA re-release events were recorded at variable intervals (between 1-5 s) following the delivery of the initial optogenetic stimulation. Glutamate-dependent ChI-evoked DA release showed slower recovery rate and lower amplitude of re-release events following activation of thalamic (Figure 3.9a,d) compared to cortical afferents (Figure 3.9b,d) ($F(1,6)=51.65$, $p=0.0004$). 3 seconds after the initial light pulse the amplitude of cortically-evoked DA events recovered to 30% of control, while for thalamic projections recovery was 12%. The mean peak evoked $[DA]_o$ following the first light pulse delivery was not significantly different between Pf- and M1-injected animals

(Mann-Whitney U=1,469, n_1=56, n_2=63, p=0.117, two-tailed; Figure 3.9c), suggesting that same vesicle pools likely contributed to the light-evoked DA release events in both experimental groups.

3.3.10 Combined retrograde and anterograde transport of AAV5 ChR2

The AAV5 ChR2 vector was used in the current work as it has better transduction efficiency (Burger et al., 2004; Paterna et al., 2004; Taymans et al., 2007; Markakis et al., 2010), and previously reported success in driving Pf-striatal projections to ChIs (Threlfell et al., 2012). However, there is evidence that AAV5 could be transported retrogradely (Burger et al., 2004; Paterna et al., 2004; Diester et al., 2011). In these experiments, retrograde transport presents a complication: in the CaMK2a-Cre line both cortical and thalamic neurons express *Cre*-recombinase and these regions are reciprocally connected. Consequently, retrograde transport of AAV5 ChR2 vector could lead to concurrent transduction of both corticostriatal and thalamostriatal afferents with ChR2.

Cortical eYFP expression following thalamic injections and *vice versa* could not conclusively verify retrograde transport. Both corticostriatal and thalamostriatal afferents have collaterals in thalamus and cortex, respectively. Consequently, even anterograde-only transport would generate eYFP signal in the other region. Therefore, I examined somatic eYFP expression, as AAV-based vectors cannot cross synapses and the only way for the resident cortical/thalamic neurons to express eYFP following injections to the other target region would be via retrograde AAV5 ChR2 transport. In this case, however, eYFP fluorescence intensity was so high, as to preclude distinguishing between terminals and fibres of passage and resident cell bodies.

Therefore, to test whether the AAV5 ChR2 vector is transported retrogradely I used DAT-Cre mouse line. DAT-Cre mice (N=2) were injected with AAV5-packaged ChR2 construct in central CPu, and eYFP fluorescence in SNc/VTA was examined 4-6 weeks post surgery. As evidenced by robust eYFP expression in the local cell bodies and processes, striatal AAV5 ChR2 injections yielded ubiquitous transduction of the SNc/VTA regions (Figure 3.10a-d). Further, eYFP-positive processes co-localized with TH-labelled cell bodies, indicating that retrograde transport and transduction happened in DA neurons (Figure 3.10e). Thus, AAV5 construct was subject to retrograde axonal transport in the DAT-Cre line. This suggests the AAV5 ChR2 is also likely to be transported in a combined retrograde-anterograde fashion in the CaMK2a-Cre line, potentially enabling cross-activation of M1 and Pf striatal terminals.

Careful examination of the data presented in sections 3.3.5 and 3.3.9, however, points to differential contribution of thalamostriatal and corticostriatal inputs to driving striatal ACh-evoked DA release. Therefore, preferential, if not selective, activation of each afferent projection could be achieved with AAV5 ChR2 in CaMK2a-Cre driver line. Further, direct stimulation of nigrostriatal afferents did not contribute to DA transients recorded in the AAV5 ChR2 experiments. Firstly, I confirmed that cortical injections never extend beneath the corpus callosum by labelling typical injections tracts for M1 experiments. Secondly, in control experiments where CaMK2a-Cre mice received CPu injections AAV5 ChR2 vector no light evoked DA events could be detected (N=3) (no data shown).

3.4 Discussion

In the work presented in this chapter I aimed to explore the relative roles of cortical (M1) and thalamic (Pf) afferents to ChIs in driving glutamate-dependent ACh-evoked striatal DA release. These data are indispensable for showing physiological relevance of the axo-axonic interactions between ACh and DA, and exploring context in which locally-mediated drive of striatal DA release may happen *in vivo*.

At first, electrical stimulation of corticostriatal afferents was used to examine the role of corticostriatal afferents in WT tissue. Close scrutiny of the data from CC and CPu distal stimulation experiments following application of iGluR and nAChR antagonists revealed passive current spread was a significant contributing factor to electrically-evoked DA events. Hence, electrical stimulation activated not only the projection of interest, but via passive current spread all the local cell types and afferents, including DA terminals, ChIs and other sources of striatal glutamate. Consequently, in these experiments the contribution from pathway-specific activation could not be discerned from all other components activated at the same time. Presence of frequency-sensitive evoked $[DA]_o$ following nAChR blockade with CC stimulation, in particular, suggested that direct electrical depolarization of striatal DA axons also contributed to evoked DA release in this experimental paradigm.

The observed current spread boundaries are consistent with previous estimates of electrical field spreading up to 2 mm from a point stimulation source (Tehovnik et al., 2006). In this case, non-selective electrical depolarization could also drive glutamate release from cells other than striatally-projecting cortical pyramidal neurons, including glutamate co-release by ChIs (Guzman et al., 2011; Higley et al., 2011) or even astrocytes

(Ormel et al., 2012; Morales et al., 2013). Yet, application of iGluR antagonists would not distinguish the contribution from afferent versus local circuits. Further, due to the small size of DA transients evoked via distal CC stimulation, site rundown characterized by progressive decline in evoked $[DA]_o$ was an issue and rendered data from 2 out of every 3 experiments unusable. Together, these observations showed that electrical stimulation could not be used to address the experimental question at hand.

Next, the roles of cortical and thalamic projections to striatal ChIs in driving ACh-evoked DA release were examined using optogenetics. For this purpose, CaMK2a-Cre mice were stereotaxically injected with AAV5-packaged *Cre*-dependent ChR2 construct in either cortex (M1) or caudal intralaminar thalamus (Pf). At least 4 weeks post-surgery, light-evoked DA events following optical stimulation of ChR2-transduced cortical or thalamic striatal terminals were monitored in acute coronal slices with FCV at CFMs.

The needle-tract localization with fluorescent spheres showed ChR2 construct injections were accurately targeted to M1 and Pf regions. ChR2 transduction generated strong eYFP signal 2 weeks post-surgery at the injection sites, while striatal terminals showed robust eYFP fluorescence from 4 weeks post-surgery. The overlap between selective Pf neuron marker cerebellin-1 (Kusnoor et al., 2010; Ellender et al., 2013) and eYFP expression was minimal, however. This finding has several explanations. Firstly, brains processed with cerebellin-1 immunostaining protocol came from animals injected 4-12 weeks prior to being used for experiments. Previous studies employing AAV-based constructs found that with time ChR2 is trafficked to axons and terminals, while somatic protein expression falls. Thus, little overlap in eYFP and cerebellin-1 labelling may signify that most of the protein was trafficked outside the somatic region, with little ChR2 still

remaining in the nucleus, not the lack of Pf ChR2 transduction per se. This conclusion is further supported by the needle tract data showing Pf injections were targeted at the correct rostro-caudal, medial-lateral and dorso-ventral level, using fasciculus retroflexus as a landmark. Secondly, eYFP-positive processes could be detected in areas outside the Pf nucleus, based on both cerebellin-1 staining and mouse brain atlas (Paxinos and Franklin, 2008). High eYFP signal intensity precluded identification of ChR2-transduced structures as either passing fibres or local cell bodies. Consequently, the possibility that other intralaminar thalamic nuclei were also transduced with AAV5 ChR2 cannot be excluded. However, Pf nucleus is the main intralaminar thalamic structure densely innervating distal and proximal dendritic processes of striatal ChIs (Lapper, 1992; Sadikot et al., 1992; Lacey et al., 2007; Doig et al., 2014). Thus, even if other intralaminar nuclei came to express ChR2 by injection mistargeting and/or excessive spread of ChR2 aided by AAV5-packaged vector, their contribution to ChI-evoked DA release events is unlikely.

The AAV5 ChR2 vector was chosen on the basis of its previously reported success (Threlfell et al., 2012) and high transduction efficiency (Burger et al., 2004; Paterna et al., 2004; Taymans et al., 2007; Markakis et al., 2010). The latter was necessary to ensure a large enough population of striatally-projecting cortical or thalamic neurons expressed ChR2, and hence maximize the chances of driving light-evoked DA events. Yet, even with extensive ChR2 transduction of corticostriatal and thalamostriatal terminals evidenced by high eYFP signal intensity throughout striatum, DA events were found to be not uniform and scattered in a way that did not correlate directly with ChR2 expression. This suggested a confluence of ChI presence and sufficient density of glutamatergic afferent fibres were required for driving ACh-evoked striatal DA via activation of corticostriatal and thalamostriatal inputs to ChIs.

Light activation of ChR2-expressing cortical and thalamic terminals evoked DA release, revealing both striatal afferents were able to stimulate this locally-mediated dopaminergic signalling. As evidenced by inhibition of light-evoked DA events with sodium channel blocker, both corticostriatal and thalamostriatal afferents required APs for driving striatal DA release. Although whether APs were fired only by ChIs following their activation by cortical or thalamic afferents, or additionally required back-propagated AP firing in DA axon terminals currently remains undetermined. The possibility of back-propagated axonal spiking in DA neurons could be investigated either directly by patch-clamp recording from DA axons, or indirectly by expression of DREADDs in the SNc dopaminergic neurons and subsequent application of clozapine-N-oxide during the FCV experiments. Both of these manipulations, however, were beyond the scope of the currently presented work.

The main difference between cortical and thalamic projections in driving striatal DA release emerged from comparison of the post-synaptic iGluR profiles. Specifically, corticostriatal projections predominantly relied on activation of AMPA receptors, while thalamostriatal projections engaged both NMDARs and AMPARs. Following confirmation of glutamate-dependence of the light-evoked DA events, ChI involvement was probed pharmacologically by altering the outcome of ACh transmission by blocking nAChRs on DA axons or activating mAChRs on ChIs. Both manipulations abolished light-evoked DA release, even though glutamatergic transmission at corticostriatal and thalamostriatal synapses on ChIs remained intact. These data underscore the role of ChIs as the principal gatekeepers of glutamate-dependent drive of striatal DA release by cortical and thalamic projections. Thus, in the absence of functional nAChRs which could bind ACh released upon synchronous activation of a small ChI population, or following inhibition of ACh

release by mAChR activation, optogenetically induced glutamate release from cortical and thalamic terminals was no longer sufficient or able to drive striatal DA release. These data are consistent with and further reinforce previously published observations regarding the primary role of nAChRs in driving locally-evoked striatal DA release, including early synaptosomal data showing Ca^{2+}-dependent activation of DA release via pre-synaptic nAChR action (Giorguieff et al., 1977; Cachope et al., 2012; Threlfell et al., 2012). Further, current data for the first time conclusively show that glutamate can indeed drive striatal DA, but the mechanism at play involves an intermediary in the face of resident ChIs.

Successful drive of ACh-evoked DA release with optogenetic activation of ChI afferents removed one set of synapses away from the primary driver mechanism, namely activation of nAChRs on DA axons, underscores the physiological relevance of this locally-mediated DA signalling. Stimulation of cortical and thalamic projections, previously shown to exercise powerful effects on ChI activity both *in vivo* and *in vitro* (Wilson et al., 1990; Consolo et al., 1996a, 1996b; Pisani et al., 2000; Matsumoto et al., 2001; Reynolds and Wickens, 2004; Lacey et al., 2007; Ding et al., 2010; Schulz et al., 2011; Doig et al., 2014), effectively recruited ChI population activity for driving ACh-evoked DA, thus providing first-hand evidence that this mechanism can be recruited physiologically. In particular, direct depolarization of ChIs by light activation following cell type specific expression of *Cre*-dependent ChR2 in ChAT-Cre mice or using constitutively expressed ChR2 in a BAC ChAT-ChR2 mouse line arguably could induce artificial synchrony in striatal cholinergic networks. Given the rapid timecourse of ChR2-induced depolarization, and the fact that it happens in multiple cellular domains simultaneously, synchronicity achieved with ChR2 may have limited correlates *in vivo*.

Therefore, recruiting ChIs afferents to drive ACh-evoked striatal DA release provides a possible way of addressing physiological relevance of this locally-mediated DA signalling, as synaptic transmission at two junction points between afferents-ChIs and ChIs-DA axons would have some failures, mimicking a more physiological activation state.

Regardless of stimulation frequency glutamate-dependent ACh-evoked DA transients had similar amplitudes. Yet, ChIs were previously reported to faithfully follow a variety of stimulation frequencies with antidromic stimulation *in vivo*, at least for thalamic afferents (Doig et al., 2014), as well as during direct optogenetic depolarisations *in vitro* (Threlfell et al., 2012). Thus, the question remains regarding where the main rate-limiting component that restricts frequency sensitivity is placed. The data, showing that no frequency sensitivity is observed even with direct depolarization of ChIs which successfully follow high-frequency pulse trains themselves (Threlfell et al., 2012), suggest that lack of frequency sensitivity of both cortically- and thalamically-triggered DA events is determined by factors downstream of striatal cholinergic signalling. Further, flat frequency response of ACh-evoked DA events across different recruitment paradigms (i.e. direct via ChIs and di-synaptic via glutamatergic inputs to ChIs) suggests it could be a rule for locally evoked DA, whereby DA release *per se*, rather than the relative signal amplitudes convey all the necessary information to the local computational circuits.

The primary rate-limiting factor in faithful transfer of frequency sensitivity could be rapid desensitization of nAChRs. This property may render nAChRs ineffective in relaying frequency information to their downstream targets, DA axons. It is also possible, given the evidence for nAChRs regulating DA release probability at short latencies, that

changes in release probability are a contributing factor. Arguably, local drive of DA release is therefore not required to convey information normally relayed by the varying amplitudes of evoked DA signals. Consequently, ChI-evoked DA release likely provides a different read-out for striatal circuits sensitive to DA level changes compared to SNc/VTA activity-dependent DA release events. It may perhaps be an all-or-nothing 'digital' DA signal which gets the circuit ticking along. Although, some subtle alterations of ACh-evoked DA release by AChE, which is differentially active between striatal matrix and patch compartments (Graybiel and Ragsdale, 1978; Mink, 1996), may be present. Further, the lack of GABAR and mGluR modulation of glutamate-dependent ACh-evoked DA release argues that extrinsic feed-forward and feedback circuits, normally playing a significant role in striatal function at a single cell level, are discounted in a population-dependent DA signalling. Consequently, locally generated DA transients, being insensitive to primary modulators, such as GABA or mGluR signalling, or stimulation frequency, could support information transfer irrespective of surrounding environment, with a view that this mechanism could facilitate stable information processing across different conditions.

Predominant recruitment of AMPARs by corticostriatal projections on ChIs, compared to contribution from both NMDARs and AMPARs at thalamic-ChI synapses is consistent with iGluR composition previously reported for cortical and thalamic contacts on striatal MSNs (Consolo et al., 1996a; Smeal et al., 2008; Ellender et al., 2013), although others report the opposite association (Ding et al., 2008). The latter could stem from recruitment of different subsets of afferent projections. Common association seen in MSNs and ChIs between the afferent sources and the post-synaptic iGluR composition argue that different receptor subtypes provide functionally relevant information. For

example, variable NMDA/AMPA receptor contributions could facilitate recognition of the signal origin, or set different baselines for plasticity induction at cortical versus thalamic synapses (Ellender et al., 2013). Although glutamate affinity for NMDARs is hundred-fold higher than for AMPARs, the latter have faster response kinetics and thus are responsible for the fast EPSP rising phase. Distinct iGluR compositions also suggest that cortical and thalamic afferents may employ different strategies for recruiting ChI population activity and ensuring response synchronicity.

In particular, differential contribution from AMPA and NMDA receptors at cortical versus thalamic synapses on ChIs would set different temporal frames for recruiting synchronous population spiking. Protracted NMDA current kinetics by slow gating which broadens spike integration time (Götz et al., 1997; Gasparini et al., 2004), would facilitate signal summation by setting a long temporal window for collating synaptic messages arriving within a 'critical period'. Thus, discrete messages carried by individual Pf neurons, which may not arrive in perfect synchronization but in close temporal proximity due to characteristic low-frequency burst discharges of Pf neurons (Lacey et al., 2007), would succeed in recruiting synchronous population response in ChIs. Thus, 'extended' temporal summation of the incoming messages supported by NMDA currents would enable Pf neurons to recruit ChIs with high fidelity.

In contrast, AMPA receptors faithfully broadcast synaptic messages at high frequency with little temporal summation, showing fast gating and desensitization (Götz et al., 1997). Thus, the temporal window for cortical inputs summation would be narrow, yet with spiking activity of striatally-projecting cortical neurons occurring as barrages of highly coincident synaptic inputs (Agmon and Connors, 1989; Helmchen et al., 1999),

predominant reliance on AMPA signalling would enable cortex to also recruit synchronized population activity in ChIs. The long membrane time constant of ChIs would enable some input summation at cortical synapses (Ding et al., 2010), yet this temporal frame would be much shorter than thalamic. Thus, whether in driving glutamate-dependent ACh-evoked DA release ChIs are adapted to detecting highly coincident inputs which dramatically change their firing frequency synchronizing population activity, or whether synchronization is achieved via integration of the incoming synaptic messages over time, the answer depends on the afferent pathway.

The different timecourse of DA release recovery with repetitive stimulation could also reflect the distinct integration properties of corticostriatal and thalamostriatal synaptic contacts with ChIs supported by variable NMDA and AMPA receptor composition. Light-evoked DA events following activation of cortical afferents had more pronounced recovery with faster re-release and larger event amplitude, while thalamic projections showed slower recovery timecourse with subsequent events of smaller amplitude. Although recovery of pre-synaptic ACh release and post-synaptic nAChR re-activation are important, those parameters are not expected to differ significantly between the two afferent pathways, unless distinct sub-populations of ChIs are recruited by thalamic versus cortical projections. Assuming that no distinct cortically- and thalamically-innervated ChI populations exist, there are three explanations for the distinct re-release profiles. These are by no means mutually exclusive, and are determined by synaptic transmission properties between ChIs and their afferents.

Firstly, temporal summation supported by NMDA currents at thalamic synapses on ChIs could drive extended sub-threshold depolarisations in the post-synaptic neurons

which continuously 'tickle' nAChRs on DA axons, rendering Pf afferents less successful at driving re-release at short inter-stimulus intervals once the first release event was generated. In contrast, predominance of AMPA currents at corticostriatal contacts with ChIs would avoid this by providing little temporal integration, and thus once the first DA event is generated, the system promptly re-calibrates to drive subsequent release events. Secondly, given predominant reliance of cortical afferents on AMPARs and thalamic projections recruiting both NMDARs and AMPARs, driving successive DA release events by cortex requires recovery of 2 receptors (AMPARs+nAChRs), while thalamic projections require 3 (AMPARs+NMDARs+nAChRs). Consequently, delayed DA re-release for the Pf terminals may reflect the time taken by all 3 receptors to exit from a refractory state. Thirdly, low release probability of cortical synapses compared to thalamic (Fremeau et al., 2004a, 2004b; Ding et al., 2008), would make the latter more refractory following a release event, while the former as population would recover quicker. Together, these explanations are consistent with better release recovery supported by cortical afferents compared to thalamic.

Further, following a train of five pulses delivered at 40 Hz ChIs were mostly shown to respond to the first pulse with cortical and each pulse with thalamic stimulation *in vivo* (Doig et al., 2014). These physiology data provide a context for a better understanding of significantly better recovery of DA re-release for cortical compared to thalamic afferents. While ChIs are continuously responding to Pf stimulation, only the first 'complete' signal will succeed in driving DA release, beyond which point strong nAChR desensitization and subsequent refractoriness will transiently arrest glutamate-dependent ACh-evoked DA release. For cortical afferents, in contrast, the first and only transmitted message is successful in triggering DA transients, while the

subsequent lack of ChI responses facilitates nAChR recovery, which are then ready for the next barrage of synaptic inputs. These observations further suggest that cortical and thalamic projections may not only employ different strategies for recruiting synchronized population activity in striatal ChIs, but also facilitate processing of diverse signal parameters.

However, retrograde axonal transport of the AAV5 ChR2 vector introduces confounds into the current optogenetic paradigm. Due to combined retrograde-anterograde axonal transport of the AAV5 ChR2 in the CaMK2a-Cre driver line where both cortical and thalamic neurons express *Cre*-recombinase, and further as the two regions are reciprocally connected, injections targeted to a single pathway could inadvertently lead to concurrent transduction of the other. The distinction in iGluR profiles between the data from M1 and Pf injected animals is critical to addressing possible co-activation of cortical and thalamic afferents with the AAV5 ChR2 vector. An identical response profile to iGluR antagonism would suggest 100% overlap in activation of cortical versus thalamic striatal terminals in M1- or Pf-injected mice, arguing that neither pathway could be activated selectively. The current data, however, suggest that despite bi-directional axonal transport of AAV5 ChR2, each of the two projections could be preferentially engaged. Of course, the percentage contribution from each respective pathway still remains unknown.

Anatomical data provide further support for the above conclusion. From the literature it follows that anatomical organization of intralaminar thalamic neurons innervating striatum is distinct from cortically projecting neurons. Caudal intralaminar thalamus, Pf nucleus in particular, preferentially innervate striatum with a few sparse

collaterals terminating in cortex, although this anatomical segregation is less evident in rodents than primates (Jones and Leavitt, 1974; Macchi et al., 1984; Sadikot et al., 1992; Parent and Parent, 2005; Galvan and Smith, 2011). By contrast, rostral intralaminar nuclei and intralaminar nuclei outside the centromedian-parafascicular complex, including central-lateral nucleus (CL), predominantly innervate cortex with less robust striatal projections and most striatal fibres displaying *en passant* morphology (Royce, 1983; Macchi et al., 1984; Deschenes et al., 1996; Deschênes et al., 1996; Smith et al., 2004, 2009). Thus, striatal and cortical projections originating from intralaminar thalamus are distinct. Hence, transduction of Pf nucleus, the most well established driver of ChI activity (Meredith and Wouterlood, 1990; Lapper, 1992; Thomas et al., 2000; Doig et al., 2014), following M1-targeted injections of AAV5 ChR2 would be limited due to sparseness of Pf cortical projections. Yet, cortical transduction following Pf injections could be more pronounced, as cortex robustly innervates most thalamic structures, and virus spread facilitated by AAV5 ChR2 not only ensured robust Pf transduction, but also some eYFP-positive fibres could also be found more anteriorly in CL. Consequently, bi-directionally transported AAV5 ChR2 vector probably conferred some selectivity in transduction of cortical versus thalamic afferents to striatal ChIs in CaMK2a-Cre mice due to anatomical architecture of caudal intralaminar thalamic projections innervating cortex and striatum. This conclusion is further supported by my data revealing distinct NMDA and AMPA receptor-dependence and release recovery profiles of light-evoked DA release events between Pf- and M1-injected CaMK2a-Cre mice.

3.5 Summary

In this work with the AAV5-packaged ChR2 construct for preferential optogenetic activation of corticostriatal versus thalamostriatal afferents, I demonstrate that both afferent inputs can be glutamatergic drivers of ChI-evoked striatal DA release. Specifically, I show that ChR2-transduced M1 and Pf striatal terminals were capable of recruiting ChIs for driving ACh-evoked DA release, putatively via synchronous activation of ChI population spiking. However, corticostriatal and thalamostriatal circuits operated using different complement of post-synaptic iGluRs, and showed distinct release recovery profiles, suggesting that despite confounding effects of bi-directional axonal transport of AAV5 ChR2, some pathway selectivity was achieved. I also demonstrate that ChIs play the role of gatekeepers in mediating cortical and thalamic drive of local striatal DA signalling, as application of nAChR antagonist or mAChR agonist, which effectively arrest cholinergic transmission, abolish light-evoked DA release following optical stimulation of ChR2-transduced glutamatergic afferents. These data further provide an explanation for glutamate-evoked DA release observed in earlier studies by conclusively showing the mechanism at play involves resident ChIs.

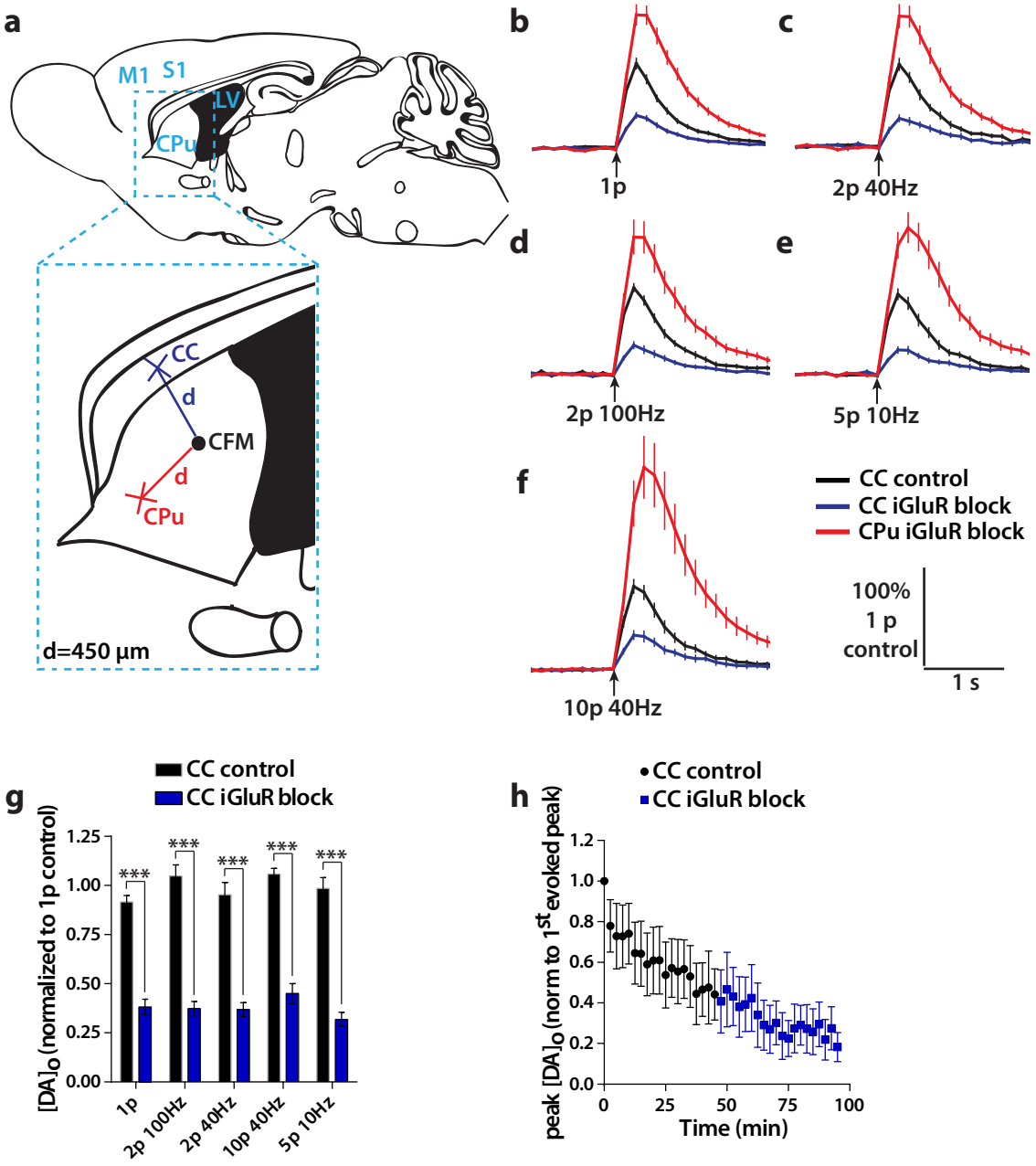

Figure 3.1 Distal electrical stimulation of corticostriatal afferents revealed a significant decrease in evoked $[DA]_o$ following iGluR block, but data are compromised by progressive decline in $[DA]_o$ **(a)** A schematic showing recording set up for distal electrical stimulation of corticostriatal afferents in corpus callosum (CC) and intrastriatal (CPu) stimulation with bipolar stimulating electrode and CFM positioned d=450 µm apart. **(b,c,d,e,f)** Mean $[DA]_o$ ± SEM versus time evoked in dorsal striatum of 2-3 months old WT mice following CC and CPu distal electrical stimulation using a range of frequencies (10 Hz, 40 Hz and 100 Hz) and pulse number (1 p, 2 p, 5 p and 10 p). All data are normalized to CC control 1 p release. iGluR antagonists for NMDA (D-AP5, 50 µM) and AMPA (GYKI, 10 µM) receptors on average reduced evoked $[DA]_o$ by 61.8% across all stimulation protocols. Equidistant CPu stimulation in iGluR block was used to control for tissue viability and showed large passive current spread component, evoking higher $[DA]_o$ than control. **(g)** Mean peak evoked $[DA]_o$ ± SEM versus stimulation protocol arranged in the order of increasing stimulus duration, summary of the data from (b,c,d,e, f). Across all stimulation protocols application of iGluR antagonists significantly reduced peak evoked $[DA]_o$ (Two-way ANOVA, *post-hoc* Bonferroni t-tests, ***p<0.001). **(h)** Mean peak $[DA]_o$ ± SEM versus time, normalized to the peak value of the first evoked transient show that with distal CC stimulation the data were compromised by site decline, characterized by progressive decrease in evoked $[DA]_o$ over time in a given recording site.

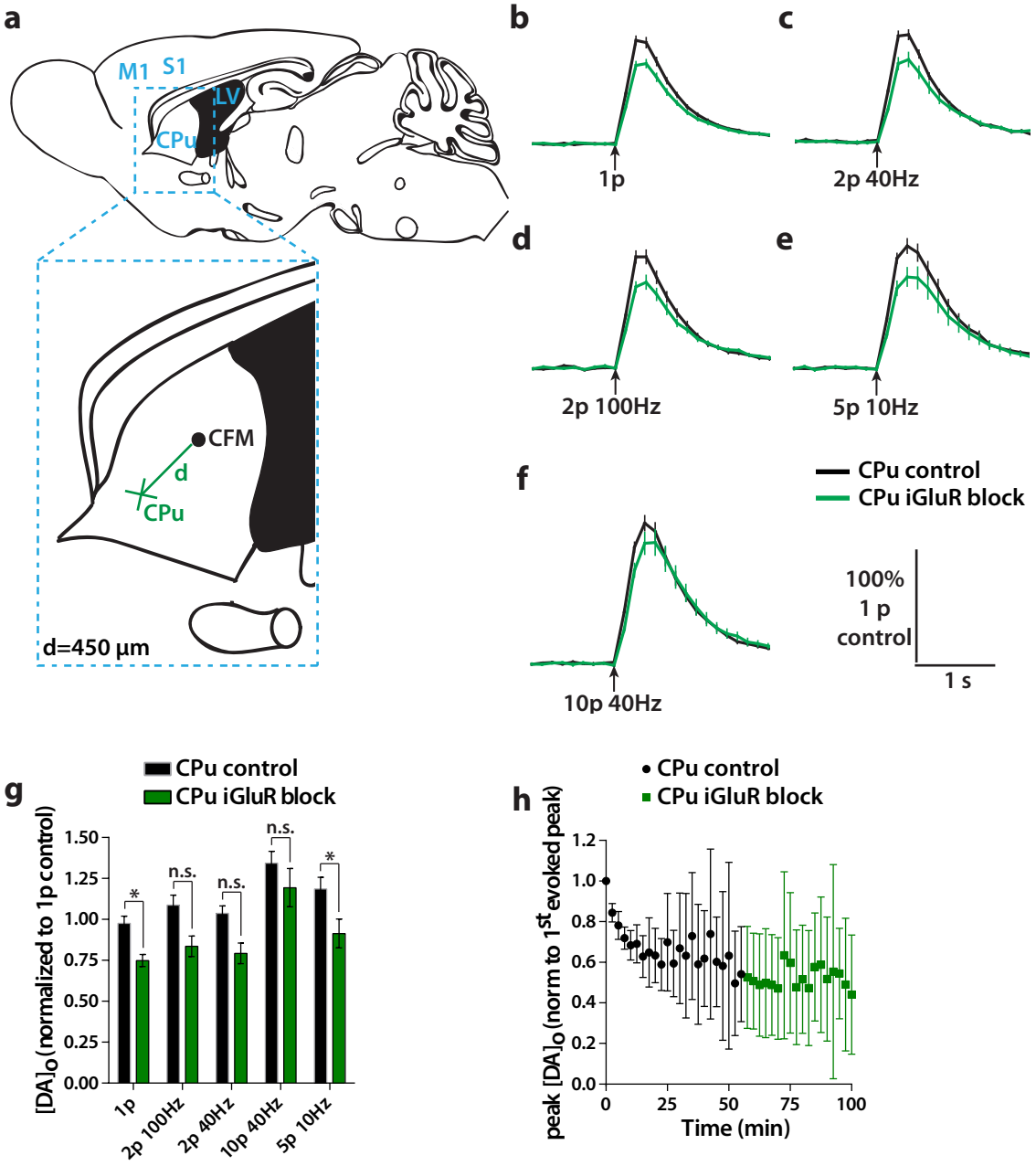

Figure 3.2 Distal intrastriatal electrical stimulation revealed small effect of iGluR antagonism on evoked $[DA]_o$ with distal CPu stimulation protocol

(a) A schematic showing the arrangement for distal intrastriatal (CPu) electrical stimulation with stimulating electrode and CFM positioned d=450 µm apart. **(b,c,d,e,f)** Mean $[DA]_o$ ± SEM versus time evoked in dorsal striatum of 2-3 months old WT mice following CPu distal electrical stimulation using a range of frequencies (10 Hz, 40 Hz and 100 Hz) and pulse number (1 p, 2 p, 5 p and 10 p). All data are normalized to CPu control 1p release. Data show that application of iGluR antagonists for NMDA (D-AP5, 50 µM) and AMPA (GYKI, 10 µM) receptors on average reduced evoked $[DA]_o$ release by 23% across all stimulation protocols, but for the 10p 40 Hz stimulation evoked $[DA]_o$ release decreased by 11%. **(g)** Mean peak evoked $[DA]_o$ ± SEM versus stimulus arranged in the order of increasing stimulus duration, summary of the data from (b,c,d,e, f). Statistical analyses on the mean peak $[DA]_o$ ± SEM data showed that for 1 p and 5 p at 10 Hz stimulation protocols application of D-AP5 and GYKI iGluR antagonists significantly reduced evoked $[DA]_o$ (Two-way ANOVA, *post-hoc* Bonferroni t-tests, *p<0.05). **(h)** Mean peak $[DA]_o$ ± SEM versus time, normalized to the peak value of the first evoked transient show that with distal CPu stimulation evoked DA levels were relatively stable across the whole experiment duration.

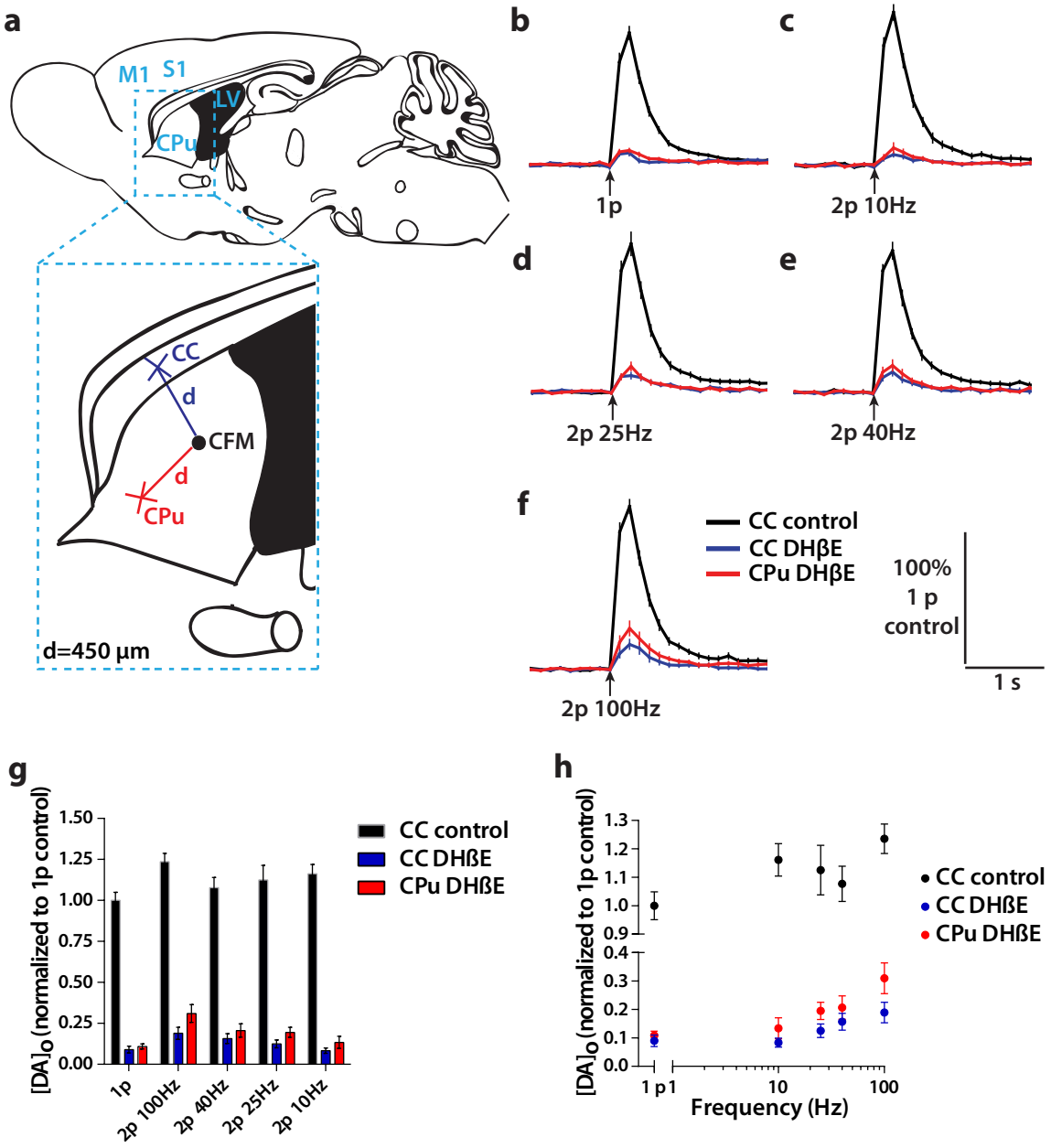

Figure 3.3 Distal electrical stimulation of corticostriatal afferents evoked $[DA]_o$ by passive current directly activating DA axons, as evoked $[DA]_o$ in the presence of nAChR antagonist with CC distal electrical stimulation was still present and showed frequency-sensitivity

(a) A schematic showing set up for distal electrical stimulation of corticostriatal afferents in corpus callosum (CC) and intrastriatal (CPu) stimulation, with stimulating electrode and CFM positioned d=450 µm apart. **(b,c,d,e,f)** Mean $[DA]_o$ ± SEM versus time evoked in dorsal striatum of 2-3 months old WT mice following CC and CPu distal electrical stimulation with single pulses or paired pulses at 10Hz, 25Hz, 40 Hz and 100Hz. All data are normalized to CC control 1 p release. nAChR antagonist (DHßE,1 µM) on average reduced peak evoked $[DA]_o$ to11% of control for CC stimulation and 16% of control for CPu stimulation. Presence of evoked $[DA]_o$ following distal CC stimulation during nAChR blockade shows that passive current spread contributed to evoked $[DA]_o$. **(g)** Mean peak $[DA]_o$ ± SEM versus stimulus arranged in the order of increasing stimulus duration, summarizing data in (b,c,d,e,f). Following DHßE application, $[DA]_o$ evoked with distal CC and CPu stimulation was significantly affected by stimulation frequency (Two-way ANOVA, ***p<0.001). **(h)** Mean peak $[DA]_o$ ± SEM versus stimulation frequency evoked with distal CC and CPu stimulation in the presence of DHßE was not significantly different between CC and CPu stimulation condition (One-way ANOVA, Tukey post-hocs, p>0.05). Frequency-sensitive evoked $[DA]_o$ which is similar for both CC and CPu stimulation protocols demonstrates that passive current spread was a significant contributing factor to evoked $[DA]_o$.

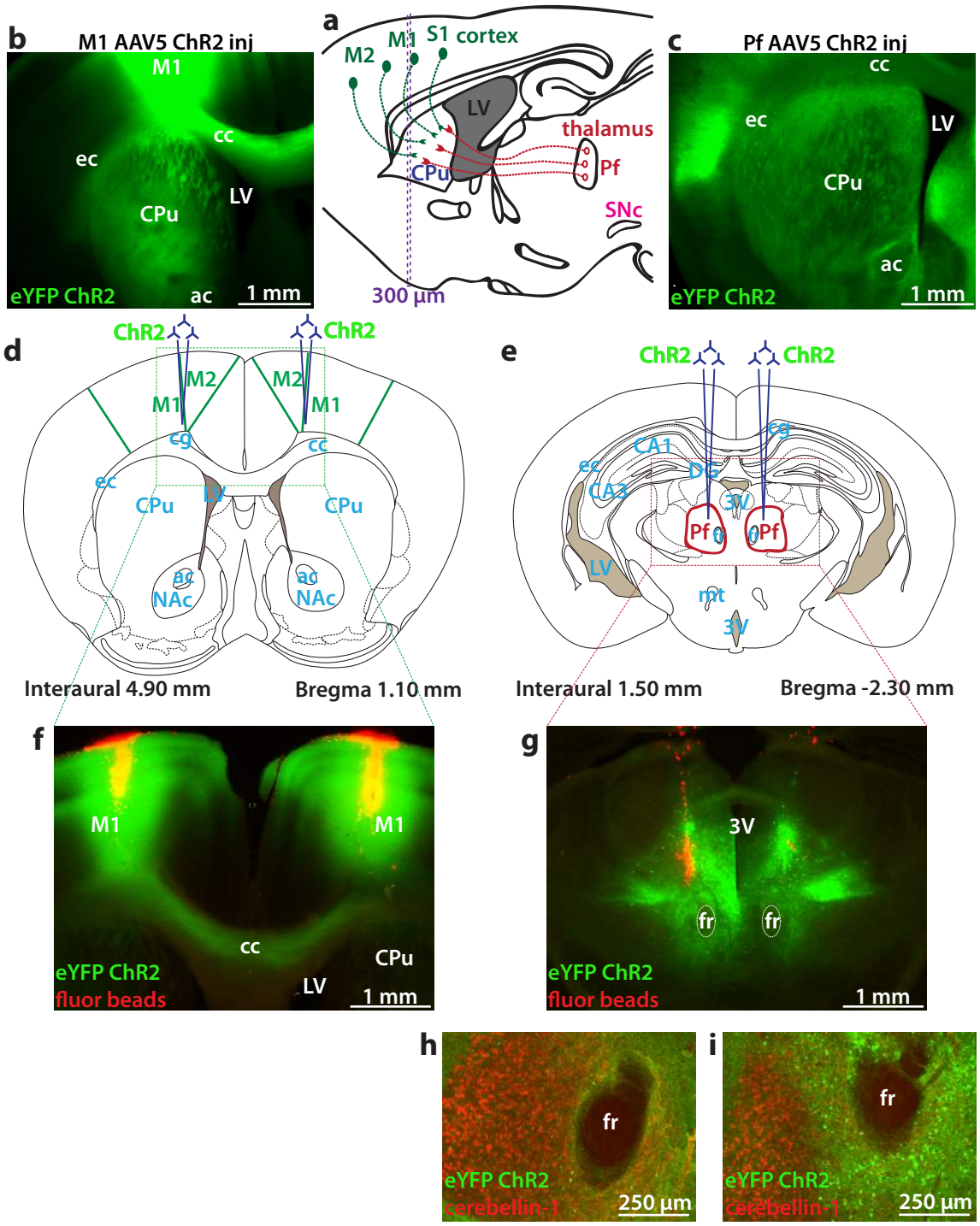

Figure 3.4 Afferent projections to striatum from cortex and thalamus: targeting AAV5 ChR2 vector injections to M1 and Pf and corresponding striatal eYFP ChR2 expression
(a) A schematic of mouse brain in sagittal plane showing afferent projections from M1 and Pf innervating CPu. **(b,c)** 300 µm-thick coronal slices show the pattern of striatal eYFP-tagged ChR2 expression 5-6 weeks following bilateral M1 **(b)** or Pf **(c)** injections of AAV5 ChR2 at 400 nl per site. **(d,e)** Schematic drawings of coronal sections through mouse brain showing targeting of M1 **(d)** and Pf **(e)** injections. **(f,g)** Fluorescence microscopy images localizing cortical **(f)** and thalamic **(g)** injection tracts in 300 µm- and 100 µm-thick sections, respectively, following injections of red polystyrene fluorospheres together with the AAV5 ChR2 vector. M1 injections **(f)** were sucessfully targeted to cortex only, injection tracts never extend below the corpus callosum (cc). Pf injections **(g)** were sucessfully targeted to Pf nucleus using fasciculus retroflexus (fr) as anatomical landmark. Both M1 **(f)** and Pf **(g)** groups show robust eYFP expression at the injection sites. **(h,i)** Immunofluorescence localization of eYFP ChR2 expression in caudal intralaminar thalamus following Pf injections with cerebellin-1 marker of Pf neurons.

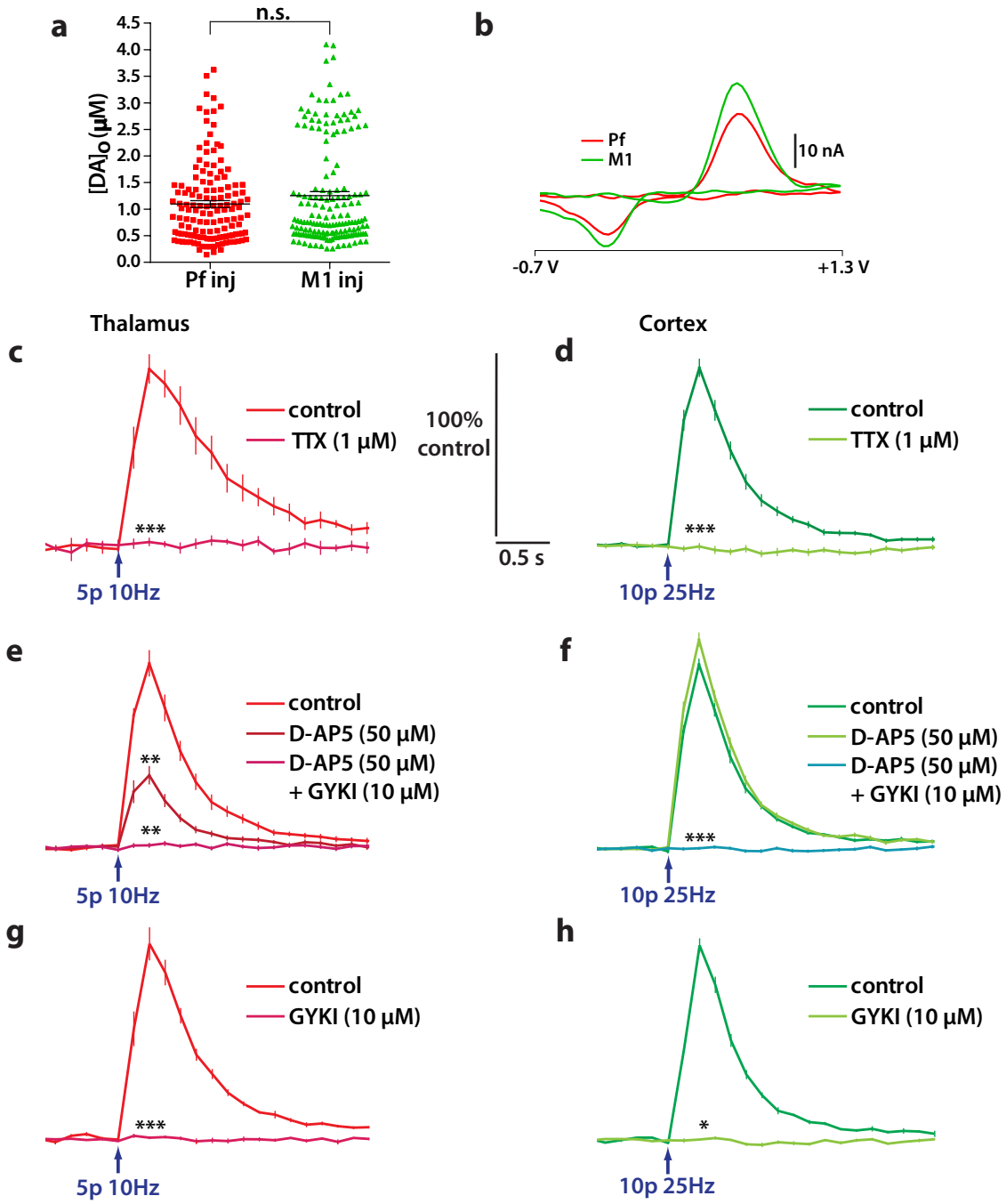

Figure 3.5 Light-evoked $[DA]_o$ following activation of ChR2-expressing Pf or M1 terminals in striatum required action potentials and recruited different complement of NMDARs and AMPARs
(a) Peak evoked $[DA]_o$ following light activation of ChR2-expressing Pf or M1 terminals in striatum of AAV5 ChR2-injected CaMK2a-Cre mice (N=12 per group). Error bars are SEM. Mean peak $[DA]_o$ was not significantly different between Pf and M1 (Mann-Whitney, $p>0.05$). **(b)** Cyclic voltammograms show the detected species following Pf or M1 inputs stimulation was DA. **(c,d)** Mean $[DA]_o$±SEM versus time evoked by activation of Pf (N=2) **(c)** or M1(N=2) **(d)** striatal terminals in control and following application of Na^+ channel blocker (TTX, 1 µM). TTX abolished light-evoked $[DA]_o$ (Mann-Whitney, ***$p<0.001$) in Pf **(c)** and M1**(d)** groups. **(e,f)** Mean $[DA]_o$±SEM versus time evoked by activation of Pf **(e)** or M1 **(f)** striatal terminals in control and following sequential application NMDARs (D-AP5, 50 µM) and AMPARs (GYKI, 10 µM) antagonists. D-AP5 significantly reduced evoked $[DA]_o$ in Pf -njected animals to 40% of control, and subsequent application of GYKI abolished light-evoked $[DA]_o$ (Kruskal-Wallis, post-hocs **$p<0.01$)**(e)**. In M1 group D-AP5 had no effect, while GYKI abolished light-evoked $[DA]_o$ (Kruskal-Wallis, post-hocs ***$p<0.001$) **(f)**. **(g,h)** Mean $[DA]_o$±SEM versus time evoked by activation of Pf **(g)** or M1 (N=1) **(h)** afferents in control and following application of AMPA receptor antagonist (GYKI, 10 µM) alone. GYKI abolished light-evoked $[DA]_o$ (Mann-Whitney, ***$p<0.001$) for both Pf **(g)** and M1 **(h)** groups.

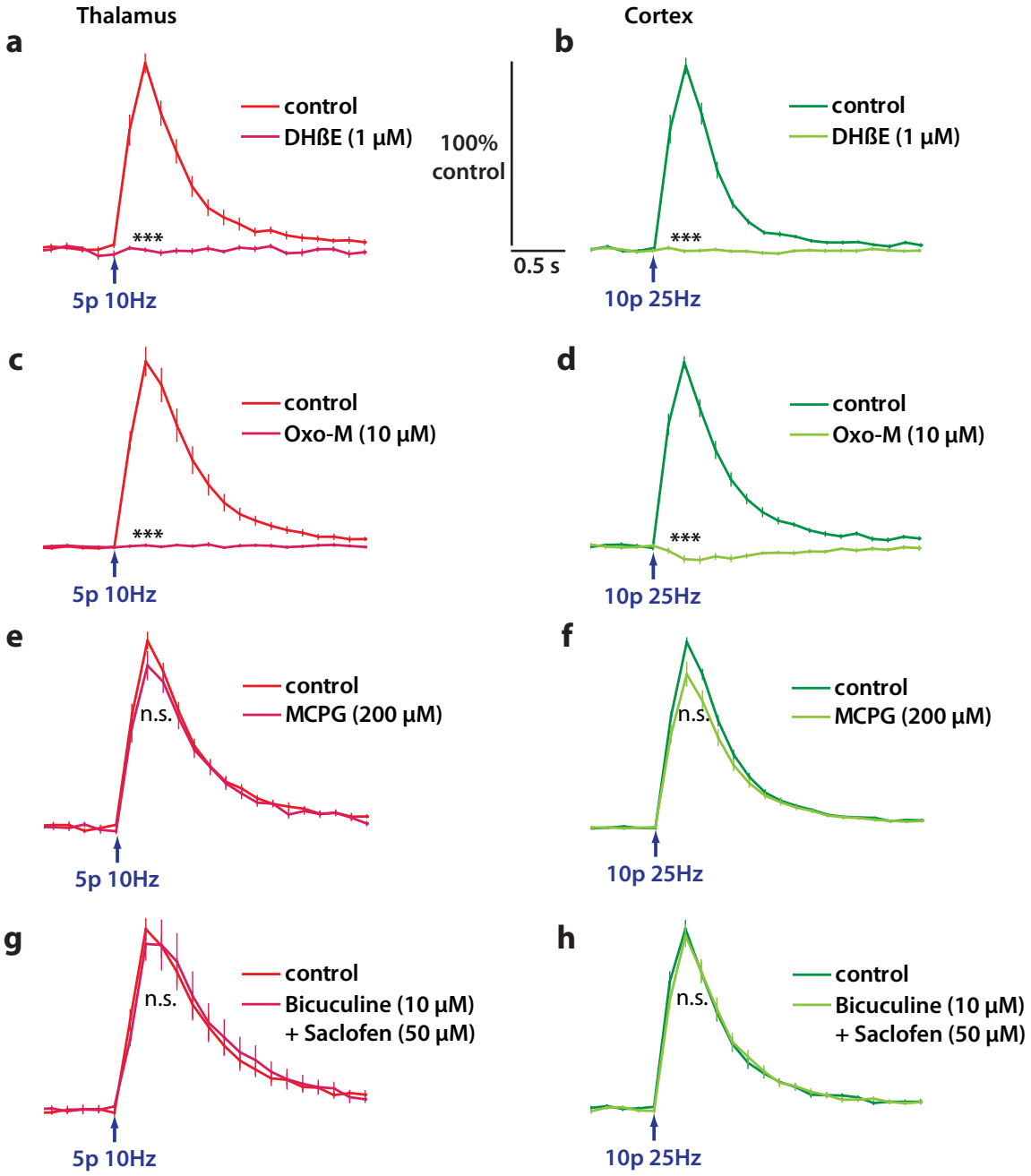

Figure 3.6 Glutamate-dependent $[DA]_o$ events following optical stimulation of ChR2-expressing Pf or M1 striatal terminals were mediated by cholinergic transmission, and were not affected by metabotropic glutamate or $GABA_A$/$GABA_B$ receptors

(a,b) Mean $[DA]_o$±SEM versus time evoked by activation of Pf **(a)** and M1 **(b)** striatal terminals in control and following application of nicotinic receptor antagonist (DHßE, 1 µM). Arresting cholinergic transmission at nAChRs, DHßE abolished light-evoked $[DA]_o$ (Mann-Whitney, ***p<0.001) for both Pf **(a)** and M1 **(b)** groups. **(c,d)** Mean $[DA]_o$±SEM versus time evoked by activation of Pf **(c)** and M1 **(d)** striatal terminals in control and following application of muscarinic receptor agonist (Oxo-M, 10 µM). Autoinhibiting ChI firing, Oxo-M abolished light-evoked $[DA]_o$ (Mann-Whitney, ***p<0.001) for both Pf **(c)** and M1 **(d)** groups. **(e,f)** Mean $[DA]_o$±SEM versus time evoked by activation of Pf **(e)** and M1 **(f)** striatal terminals in control and following application of broad-spectrum metabotropic glutamate receptor antagonist (MCPG, 200 µM). MCPG had no significant effect on light-evoked $[DA]_o$ events (Mann-Whitney, p>0.05) for both Pf **(e)** and M1**(f)** groups. **(g,h)** Mean $[DA]_o$±SEM versus time evoked by activation of Pf **(g)** and M1 **(h)** striatal terminals in control and following application of $GABA_A$ (Bicuculine, 10 µM) and $GABA_B$ (Saclofen, 50 µM) receptor antagonists . Arrest of GABAergic transmission had no significant effect on light-evoked $[DA]_o$ events (Mann-Whitney, p>0.05) for both Pf **(g)** and M1**(h)** groups.

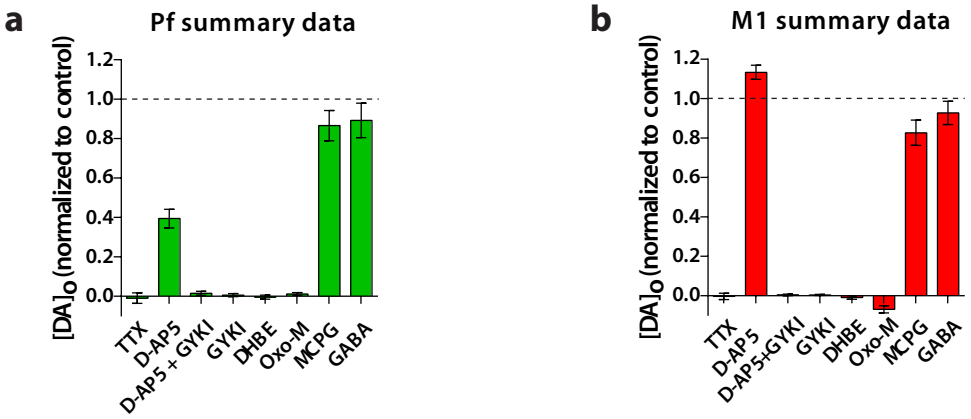

Figure 3.7 Summary of the data for the light-evoked $[DA]_o$ recorded following optical stimulation of ChR2-expressing Pf or M1 striatal terminals
(a,b) Mean peak $[DA]_o$±SEM evoked with light activation of ChR2-expressing Pf **(a)** or M1 **(b)** striatal terminals in CaMK2a-Cre mice after AAV5 ChR2 vector injections. **(a)** For Pf-injected animals, application of TTX, sequential application of D-AP5 and GYKI, GYKI alone, DHßE and Oxo-M significantly reduced or abolished light-evoked DA release events. GABA antagonists and MCPG had no effect. **(b)** In M1-injected animals application of TTX, GYKI, DHßE and Oxo-M abolished light-evoked $[DA]_o$ events, while D-AP5, GABA antagonists and MCPG had no effect.

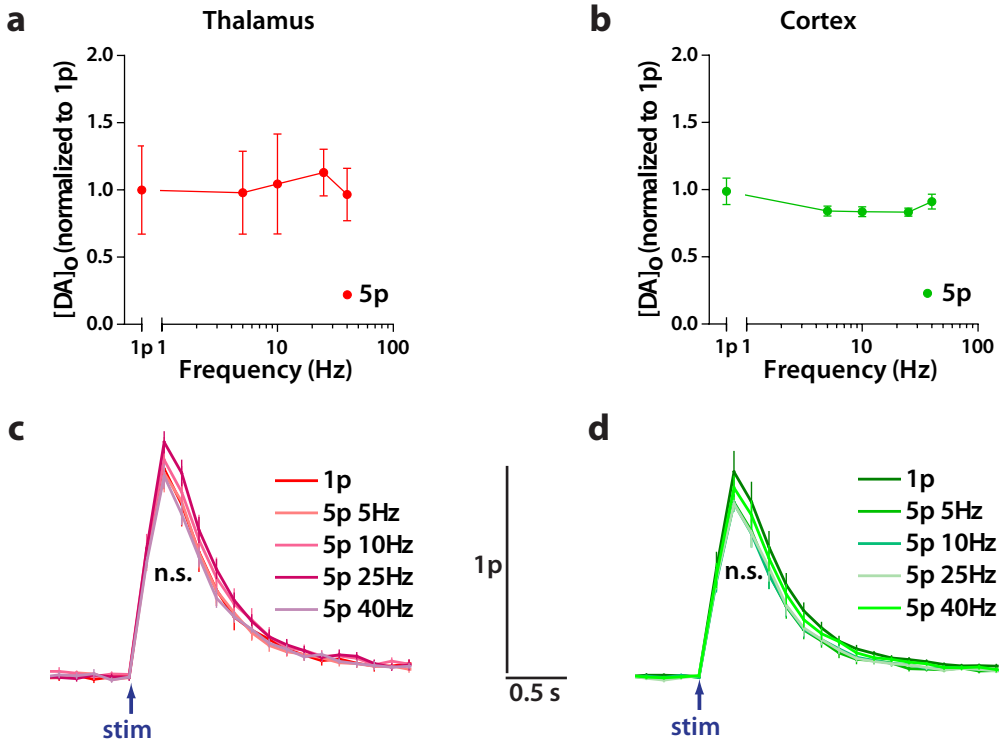

Figure 3.8 Light-evoked $[DA]_o$ events following optical stimulation of ChR2-expressing Pf or M1 striatal terminals are insensitive to stimulation frequency
(a,b) Mean peak evoked $[DA]_o$±SEM versus stimulation frequency evoked by optical activation of ChR2-expressing Pf **(a)** or M1 **(b)** striatal terminals. Single light pulses and pulse trains of 5 pulses at 5, 10, 25 and 40 Hz were used. Data are normalized to single pulse (1 p) peak evoked $[DA]_o$. **(c,d)** Mean $[DA]_o$±SEM versus time evoked by activation of Pf **(c)** and M1 **(d)** striatal afferents in with single pulses and pulse trains of 5 pulses at a range of stimulation frequencies (5-40Hz). Light-evoked $[DA]_o$ events following stimulation of thalamic Pf **(c)** or cortical M1 **(d)** inputs were frequency insensitive, producing evoked $[DA]_o$ events of similar amplitude regardless of stimulation protocol (one-way ANOVA, $p>0.05$).

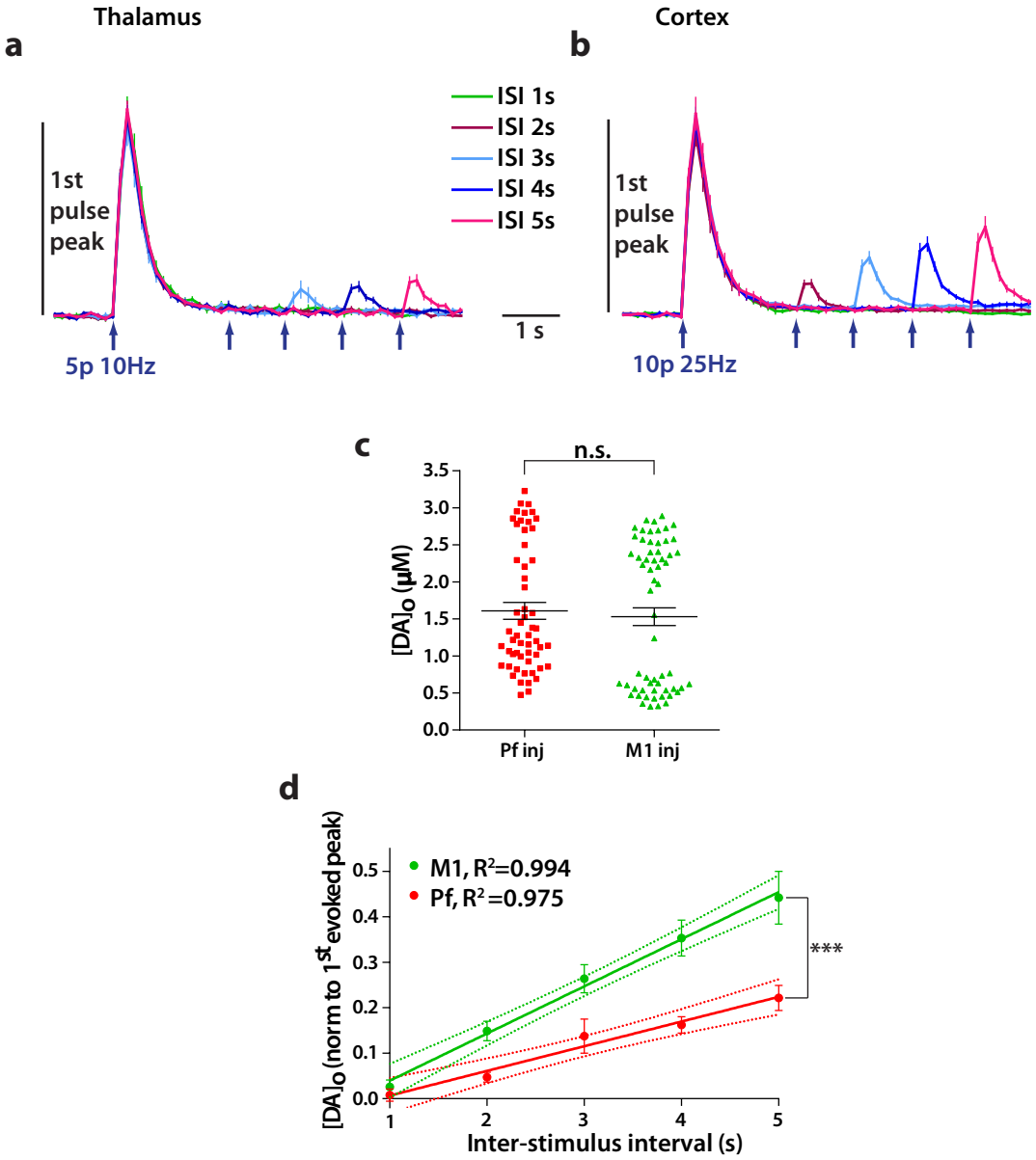

Figure 3.9 Light-evoked striatal $[DA]_o$ following optical stimulation of ChR2-expressing Pf or M1 striatal terminals show distinct release recovery profiles, with cortically-evoked DA events showing faster recovery timecourse and larger amplitude of re-release events
(a,b) Mean $[DA]_o$±SEM versus time evoked by optical activation of ChR2-expressing Pf **(a)** or M1 **(b)** striatal afferents at variable intervals (1-5 s) following the delivery of initial light stimulus. These data show faster and more pronounced recovery of light-evoked DA release upon subsequent stimulation for cortical compared to thalamic afferents. **(c)** Peak $[DA]_o$ evoked by initial light activation of Pf or M1 terminals in striatum were similar for both experimental groups (Mann-Whitney, $p>0.05$). **(d)** The mean peak $[DA]_o$±SEM between 1 -5 seconds after the first light stimulation delivery recovered significantly faster for M1-injected compared to Pf-injected CaMK2a-Cre mice (***$p<0.001$).

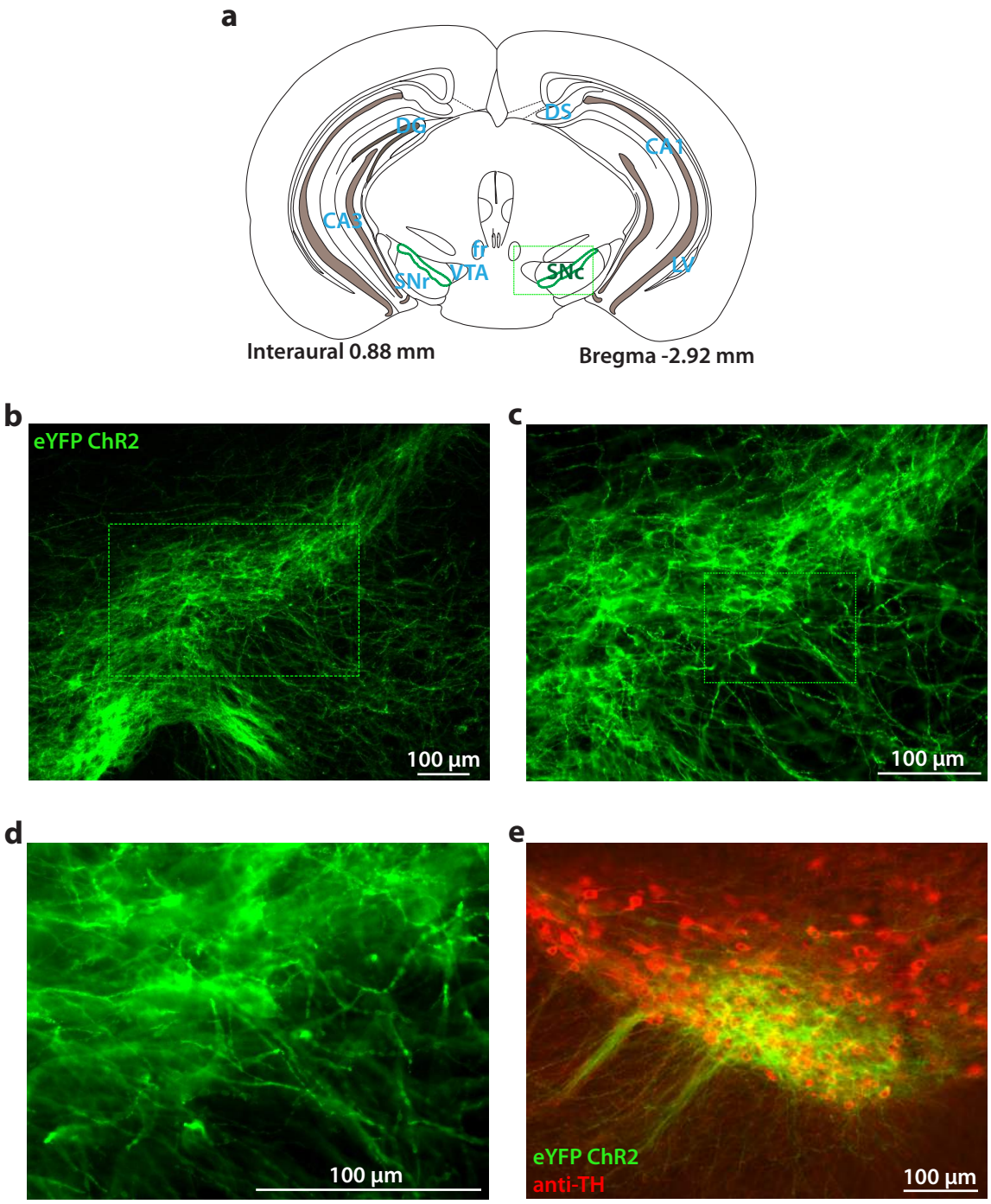

Figure 3.10 AAV5 ChR2 is retrogradely transported from striatal injection sites to the midbrain in DAT-Cre driver line

(a) A schematic of mouse brain in coronal plane showing localization of the midbrain SNc and VTA regions. **(b,c,d)** Fluorescence microscopy images of the midbrain SNc and VTA regions expressing eYFP-tagged ChR2 in 50 µm-thick sections from DAT-cre mice injected with the AAV5 ChR2 vector in striatum 4-6 weeks prior. Images taken at 10x **(b)**, 20x **(c)** and 40x **(d)** magnification show robust eYFP ChR2 expression in local midbrain neuropil, both dendritic arbours and cell bodies, following retrograde axonal transport of AAV5-packaged ChR2 construct from CPu injection sites. **(e)** Co-localization of eYFP-positive fibres transduced following retrograde axonal transport of AAV5 ChR2 vector from CPu to SNc with TH-positive DA neurons in the midbrain.

4. Exploring circuits driving acetylcholine-evoked striatal dopamine with AAV2 ChR2, hyperpolarizing opsins and brainstem cholinergic system.

4.1 Introduction

The work presented in this chapter explored different approaches to activating candidate circuits for driving ACh-evoked striatal DA release. This way I aimed both to address some of the shortcomings identified in the previous chapter and to expand the repertoire of tools that may be useful for understanding physiological relevance of the locally-mediated striatal DA signalling. I used AAV2-packaged Cre-dependent ChR2 construct to circumvent the confounds associated with retrograde axonal transport of AAV5 ChR2 vector in CaMK2a-Cre driver line (Section 4.3.2). I also explored whether hyperpolarizing optogenetic tools could be used for driving ACh-evoked DA events via rebound activity in ChIs following optogenetically-induced pause (Section 4.3.3). Finally, I examined whether a recently identified cholinergic brainstem innervation of striatum in rodent could drive or contribute to ACh-dependent DA release (Section 4.3.4).

4.1.1 Driving cholinergic interneuron population activity by activation of their glutamatergic afferents with AAV5 ChR2

Chapter 3 presented the data exploring whether cortical and thalamic afferents to ChIs can drive ACh-evoked striatal DA release. These experiments used AAV5 ChR2 vector injections in CaMK2a-Cre mouse driver line, demonstrating both thalamostriatal and corticostriatal projections can drive glutamate-dependent ACh-evoked DA events. However, I determined that AAV5 ChR2 vector was subject to combined anterograde and retrograde axonal transport from the primary injection site. Bi-directional axonal transport presents a serious challenge in establishing the relative contribution of cortical versus thalamic afferents to the light-evoked DA release events in CaMK2a-Cre mice.

CaMK2a-Cre is a relatively non-specific driver line where practically all glutamatergic cortical and thalamic neurons express *Cre*-recombinase (Benson et al., 1992; Liu and Jones, 1996, 1997). Although the reported CaMK2 mRNA levels in intralaminar and midline thalamic nuclei are low (Benson et al., 1991; Smith, 2007), earlier studies successfully activated striatal afferents originating from caudal intralaminar thalamus in CaMK2a-Cre mice using optogenetics (Ellender et al., 2011, 2013; Threlfell et al., 2012). Thus, the CaMK2a-Cre driver line was chosen for examining the relative roles of cortical and thalamic afferents in driving ChI-evoked DA release. This way, both projections could be targeted for ChR2 expression in the same mouse line, reducing confounds associated with differential expression of *Cre*-recombinase between the compared regions. By minimizing injections volumes to 400 nl I aimed to limit 'non-specific' ChR2 transduction outside the primary region of interest, either M1 or Pf. Yet, for a bi-directionally transported vector this strategy would not limit ChR2 expression outside the target injection site due to retrograde axonal transport of AAV5 ChR2.

Both cortex and thalamus, in particular frontal/sensorimotor cortex and intralaminar thalamus, are reciprocally connected (Jones and Leavitt, 1974; Royce, 1983; Carretta et al., 1996; Parent and Parent, 2005; Beatty et al., 2009; Minamimoto et al., 2009; Sadikot and Rymar, 2009; Galvan and Smith, 2011). Therefore, use of bi-directionally transported vector in the CaMK2a-Cre line may result in combined transduction of corticostriatal and thalamostriatal afferents when projection-specific ChR2 expression was intended. Consequently, although the AAV5 data demonstrate that both cortex and thalamus can drive ACh-evoked DA events, putatively by recruiting ChI population activity, whether the two pathways can do so independently of each other remains undetermined.

4.1.2 AAV5 ChR2 experiments cannot discern the contribution of M1 versus Pf afferents to driving cholinergic interneuron-evoked dopamine

Preferential innervation of striatal rather than cortical territories by neurons from caudal intralaminar thalamus (Jones and Leavitt, 1974; Macchi et al., 1984; Sadikot et al., 1992; Parent and Parent, 2005; Galvan and Smith, 2011) suggests that some specificity in ChR2-transduction of M1 versus Pf afferents could be achieved with AAV5 ChR2 injections in the CaMK2a-Cre line. Further, the data showing that Pf-evoked DA events were mediated by both NMDA and AMPA receptors and showed poorer recovery of release, compared to M1-evoked DA which was only mediated by AMPA receptors and showed faster recovery of release, support this conclusion. Yet, the relationship between combined versus independent activation of corticostriatal and thalamostriatal afferents to ChIs in driving ACh-evoked DA release cannot be quantified from the AAV5 ChR2 data.

I further explored the possibility of independently driving corticostriatal or thalamostriatal afferents using AAV2 ChR2 vector (Section 4.3.2). Previous reports suggest AAV2 ChR2 can only be transported anterogradely (Paterna et al., 2004; Ciesielska et al., 2011; Salegio et al., 2012), although the extent of viral spread and transduction efficiency is lower than for AAV5 ChR2 (Davidson et al., 2000; Paterna et al., 2004; Taymans et al., 2007; Aschauer et al., 2013). AAV2 ChR2 was also successfully employed to drive MSN activity with activation of corticostriatal afferents or projections from individual intralaminar thalamic nuclei (Ellender et al., 2011, 2013). In theory, AAV2 ChR2 vector confers greater transduction specificity due to exclusively anterograde mode of axonal transport, and should enable selective activation of M1 or Pf afferents to

ChIs in CaMK2a-Cre mice. The more limited ChR2 transduction of AAV2, which is expected to infect smaller neuronal population than AAV5, was a secondary consideration.

4.1.3 Packaging of AAV-based vectors and their transport

It is currently not well understood why different AAV serotypes differ in their ability to traffic and rates of infection. However, research shows that these recombinant replication-deficient parvoviruses use different binding partners for cell attachment and entry. Specifically, AAV2 was shown to transduce neurons via proteoglycan molecules using integrins and fibroblast growth factors as co-receptors (Summerford and Samulski, 1998; Qing et al., 1999; Summerford et al., 1999). In contrast, AAV5 constructs bind sialic acid and use platelet-derived growth factors for cell entry (Walters et al., 2001; Di Pasquale et al., 2003). These molecules, known as cell surface receptors, have different distribution in the neuropil and, therefore, could facilitate preferential binding and cell infection by certain AAV serotypes.

Further, once the cell entry phase is complete, viral DNA is not subject to passive diffusion. Rather it is actively transported to the site of transcription and replication, and following synthesis and assembly viral components are trafficked back to the cellular membrane (Sodeik, 2000). Data on which molecular motors different AAV serotypes employ is absent. It is feasible that trafficking to the nucleus and away from the nucleus are the two points where the difference between AAV2 exclusively anterograde and AAV5 bi-directional transport emerge. Yet, it remains unclear how viral DNA, which was already stripped of its serotype-specific capsid upon cell entry, can be selectively bound by retrograde and anterograde cellular motors. For the purpose of this work, however,

the important factor is the outcome of intracellular transport, even though the mechanisms underlying it remain poorly understood. To examine the roles of Pf and M1 afferents to striatal ChIs in driving glutamate-dependent ACh-evoked DA release independently of the other projection, I switched to using anterogradely transported AAV2 ChR2 vector.

4.1.4 Alternative tools for probing physiological relevance of acetylcholine-evoked striatal dopamine release: hyperpolarizing opsins

Another way to probe physiological relevance of ACh-evoked DA release is to monitor whether DA release events can be detected upon ChI rebound spiking. Thus, rather than using excitatory inputs for driving synchronous ChI activity, I explored an alternative approach of driving a pause in ChIs and examining whether DA release event could follow, consistent with 'rebound' spiking. The characteristic pause response that ChIs acquire in conditioning paradigms (Kimura et al., 1984; Aosaki et al., 1994b, 1995; Graybiel et al., 1994; Apicella, 2002; Morris et al., 2004), or display following activation of their glutamatergic afferents from cortex or thalamus (Matsumoto et al., 2001; Ding et al., 2010; Sharott et al., 2012; Doig et al., 2014), is often followed by a rebound excitation. While it remains unclear whether rebound excitation is the product of intrinsic membrane properties of ChIs (Wilson, 2005), manifestation of a separate long latency excitatory drive (Schulz and Reynolds, 2013) or is triggered by yet unidentified transmitter co-release from dopaminergic terminals (Straub et al., 2014), rebound ChI spiking could also be a possible mechanism for driving ACh-evoked DA release. In particular, rebound spiking in ChI populations following a pause is often time-locked and thus could result in a synchronous activation of ChIs leading to ACh-evoked DA release.

ChIs, or tonically active neurons (TANs), were previously shown to be spontaneously active in slices (Jiang and North, 1991; Bennett and Wilson, 1999). Further, in a small sample of ChIs recorded in acute slices prepared in the same way as for the current optogenetic FCV experiments, 40% of neurons also showed spontaneous action potential firing (data not shown). These cells have depolarized membrane potential of around -60 mV, and with injection of hyperpolarizing current frequently show rebound spiking upon termination of the negative current injection. The Tepper group also reported that following optogenetic hyperpolarization inhibiting AP firing, ChIs show rebound spiking and that released ACh is able to drive di-synaptic GABAergic inhibition of MSNs (English et al., 2011). I, therefore, hypothesized that light-induced inhibition of genetically-defined ChIs in ChAT-Cre mouse driver line following striatal injections of hyperpolarizing opsin constructs could be used for driving DA release events upon ChI rebound excitation.

The two most-widely used optical silencing tools are the light-activatable chloride pump Halorhodopsin (eNpHR 3.0, *Natronomonas pharaonis*) which moves Cl^- ions inside the cell (Han and Boyden, 2007; Zhang et al., 2007), and the proton pump Archaerhodopsin (Arch 3.0, *Halorubrum sodomense*) which moves H^+ out of the cell (Chow et al., 2010; Mattis et al., 2012). eNpHR 3.0 and Arch 3.0 generate hyperpolarizing currents which silence neuronal activity by moving one negatively/ positively charged ion inwardly/outwardly across the cellular membrane per photon of light (Geibel et al., 2001; Seki et al., 2007). Although rebound excitation following hyperpolarization of ChIs with eNpHR 3.0 was reported previously (English et al., 2011), this Cl^- pump was also shown to change $GABA_A$ reversal potential due to intracellular Cl^- accumulation for stimulations longer than 500 ms, leading to sign reversal for inhibitory

neurotransmission (Raimondo et al., 2012). Further, direct comparison of Arch 3.0 and eNpHR 3.0 previously showed that the former generates larger and more stable photocurrents (Mattis et al., 2012). Thus, Arch 3.0 could be better suited to probing activity for which the read out is a population-based response (i.e. DA release evoked by ChI population activity). In my experimental work I therefore used both constructs separately: Arch 3.0 as a control tool for intracellular Cl^- accumulation which generates larger photocurrents, and eNpHR 3.0 as a tool previously shown to successfully hyperpolarize and drive rebound spiking in striatal ChIs.

Tonic activity in striatal ChIs in acute slices is highly dependent on bath temperatures (32-34°C) and relatively high KCl levels (at least 2.5 mM) (Surmeier, personal communication). These criteria were incorporated in experimental design. Yet, while inhibition of tonic firing could result in rebound ChI activity driving ACh-evoked DA release, optogenetic hyperpolarization is still not equivalent to intracellular negative current injection. Specifically, in non-neuronal systems Cl^- and H^+ pumps were reported to achieve hyperpolarization of -150 mV and beyond (Geibel et al., 2001; Seki et al., 2007). For neuronal systems, however, because no decrease in input resistance is generated and only a single ion is moved per photo cycle, very high light intensities are required to generate 'true' hyperpolarization. I therefore explored whether Arch 3.0 and eNpHR 3.0 constructs could be used as suitable tools for optogenetic inhibition of ChIs and could generate ACh-evoked DA events (Section 4.3.3).

4.1.5 Alternative cholinergic pathways for driving acetylcholine-evoked striatal dopamine release in rodents

Although striatal ChIs are conventionally thought to be the sole source of striatal ACh (Bolam et al., 1984; Phelps et al., 1985; Phelps and Vaughn, 1986), the most recent anatomical evidence suggests otherwise. In particular, cholinergic brainstem was shown to also innervate rodent striatum. Pedunculopontine (PPN) and laterodorsal tegmental (LDT) nuclei send topographically organized projections to dorsal and ventral striatum, forming predominantly asymmetric synapses with dendritic spines and shafts of various post-synaptic structures (Dautan et al., 2014). Using ChAT-Cre rat, the Mena-Segovia group showed that cholinergic brainstem axons in particular give rise to frequent varicosities which form synaptic connections with striatal neurons, either following straight paths or giving rise to tortuous arborisations. The above anatomical data suggest that cholinergic innervation from rostral PPN and LDT, targeting dlCPu and dmCPu/NAc respectively, could provide an alternative source of striatal ACh. These brainstem afferents, therefore, could potentially contribute to ACh-evoked DA release observed in ChAT-Cre mice (Threlfell et al., 2012), since cholinergic brainstem projection would also expresses *Cre*-recombinase and bi-directionally transported AAV5 ChR2 vector used in the study could therefore also transduce PPN/LDT striatal afferents.

Cholinergic brainstem projections have four major relay stations for regulating the overall BG output as practically every element of BG circuitry is connected either directly or indirectly with PPN and LDT (Steriade et al., 1988; Bolam et al., 1991; Bevan and Bolam, 1995; Mena-Segovia et al., 2005, 2008; Omelchenko and Sesack, 2005; Parent and Descarries, 2008). In particular, brainstem cholinergic projections affect

information processing before it reaches the output BG targets via inputs to SNr and GPi. Targeting STN and GPe, brainstem cholinergic afferents influence hyperdirect and indirect pathways, while via projections to the intralaminar/midline thalamic nuclei they could ultimately affect striatal ChI activity. Finally, via projections to SNc and VTA brainstem cholinergic system directly regulates DA neuron activity and DA release in somatodendritic and terminal regions. Thus, PPN and LDT afferents in addition to possible influence on DA release via thalamic projections synchronizing ChI activity, or via direct control of SNc/VTA activity, could also drive striatal ACh-evoked DA events by releasing ACh themselves or directly activating striatal ChIs. Consistently, in behavioural paradigms these brainstem neurons transiently increase their firing rate in response to salient sensory stimuli (Pan and Hyland, 2005). PPN neurons also display activity consistent with encoding of the magnitude of expected and received rewards, possibly providing a substrate for midbrain representation of reward prediction error (Okada et al., 2009). Together, these data suggest that brainstem cholinergic pathway innervating CPu could be a constituent part of the local cholinergic control of striatal DA release.

To investigate the role of PPN and LDT projections in driving striatal ACh-evoked DA release, I collaborated with the Mena-Segovia group, who provided ChAT-Cre rats (Witten et al., 2011; Dautan et al., 2014) that received AAV2 ChR2 injections either in the brainstem (PPN/LDT) or the CPu. To examine whether cholinergic brainstem could drive striatal ACh-evoked DA release, I monitored light-evoked DA release following activation of ChR2-expressing cholinergic brainstem afferents (Section 4.3.4).

4.1.6 Summary

The work presented in this chapter is methods-oriented and explored possible approaches for studying mechanisms behind ACh-evoked striatal DA release using optogenetics. I examined whether glutamate-dependent drive of ACh-evoked striatal DA release was possible with independent activation of cortical or thalamic afferents to ChIs using AAV2 ChR2 vector. These experiments included a number of variations to address arising experimental issues and aimed to determine if either pathway in isolation is able to recruit population response of striatal ChIs to drive ACh-evoked DA release. Taking the advantage of ChIs being tonically active *in vitro* and previous studies showing successful induction of rebound spiking in ChIs with optogenetic hyperpolarization, I explored whether it was possible to evoke DA release following inhibition of ChI activity with hyperpolarizing ion pumps Arch 3.0 and eNpHR 3.0. Finally, in collaboration with the Mena-Segovia group, I examined whether an alternative cholinergic pathway to rodent striatum of brainstem origin could drive or contribute to ACh-evoked striatal DA release in rat. These experiments further established that ChI-evoked DA release was not a species artefact, as light-evoked DA events following ChR2 transduction of striatal ChIs were successfully recorded in ChAT-Cre rat.

4.2 Methods

4.2.1 Animals

Adult (21-40d) male and female homozygous and heterozygous CaMK2a-Cre (*B6.Cg-Tg(CaMK2a-Cre)T29-1Stl/J,* stock 005359) mice were used for probing the roles of corticostriatal and thalamostriatal projections to ChIs. For control experiments confirming AAV2 ChR2 functionality and for striatal injections of hyperpolarizing opsins Arch 3.0 and eNpHR 3.0, adult (30-45d) heterozygous male ChAT-Cre (B6.129S6-*Chat*$^{tm1(cre)Lowl}$/J, stock 006410) mice were used. For anatomical experiments confirming exclusively anterograde transport of AAV2 ChR2 vector, adult (30-45d) male heterozygous DAT-Cre (*B6.SJL-Slc6a3tm1.1(cre)Bkmn /J*, stock 006660) mice were used.

AAV2 ChR2-injected ChAT-Cre rats (Witten et al., 2011; Dautan et al., 2014) were supplied by the Mena-Segovia group and were used for probing the role of the brainstem cholinergic projections (PPN/LDT) to CPu in driving striatal ACh-evoked DA.

4.2.2 Optogenetic surgery

The DAT-Cre mice received bilateral striatal injections of AAV2-packaged floxed ChR2 construct targeted to the central CPu (1.5 mm ML, +0.5 mm AP, 3.2 mm DV from bregma). 400 nl of AAV2 ChR2 were pressure injected per hemisphere. After 4-6 weeks incubation time, mice were transcardially perfused with PBS, their brains were fixed in PFA and processed for fluorescence microscopy.

CaMK2a-Cre mice received bilateral AAV2 ChR2 injections targeted either to the primary motor cortex M1 (ML 1.7 mm, AP +1.3 mm, DV 1.0 mm from bregma) or caudal intralaminar thalamus Pf nucleus (ML 0.7 mm, AP -2.3 mm, DV 3.5 mm from bregma). To

replicate experiments performed with AAV5 ChR2, the first batch of mice received 400 nl injection volumes. Failing to detect light-evoked release events, injections targets/volumes were manipulated. The next batch received dual bilateral injections whereby both M1 and Pf were injected in the same animal with 400 nl of AAV2 ChR2 per site. Another group of mice received large injections volumes at either M1 or Pf with 800 nl of AAV2 ChR2 injected per hemisphere. 4-14 weeks were allowed for ChR2 transduction.

The ChAT-Cre driver line was always injected in the central CPu (1.5 mm ML, +0.5 mm AP, 3.2 mm DV from bregma). To confirm that AAV2 ChR2 vector was functional, 400 nl of AAV2 ChR2 were pressure injected per hemisphere and animals were used 4 weeks later. To explore whether optogenetic inhibition of ChIs by hyperpolarizing opsins could drive ACh-evoked DA release, 800 nl of either Arch 3.0 (AAV5-packaged eGFP-fused Arch 3.0) or eNpHR 3.0 (AAV2-packaged eYFP-fused eNpHR 3.0) were injected per hemisphere bilaterally. Two different groups of animals were used for eNpHR 3.0 and Arch 3.0 experiments. These mice were used 6-11 weeks post-surgery.

4.2.3 Slice preparation

Slices were prepared for optogenetic experiments as described in Chapter 2.

4.2.4 Optogenetic stimulation

4.2.4.1 Depolarizing ChR2 stimulation with blue light

ChR2-expressing cortical and/or thalamic terminals in CaMK2a-Cre mice or ChR2-transduced ChIs in ChAT-Cre mice were visualized by eYFP. In ChR2-injected rats striatal

ChIs or striatal brainstem terminals were also visualized by eYFP. Light-evoked DA release was sampled in eYFP-positive areas using 473 nm LED as described in Chapter 2.

For activation of thalamic projections trains of 5 pulses at 10 Hz were used, for cortical afferents trains of 10 pulses at 25 Hz were employed. For the experiments from dual bilateral injections (M1+Pf) stimulation protocols delivering 5 pulses at 10 Hz or 10, 20 or 30 pulses at 25 Hz were used. For direct stimulation of ChR2-expressing ChIs in both ChAT-Cre mice and ChAT-Cre rat single 2 ms-wide light pulses were used.

In brainstem injected ChAT-Cre rats, for activation of ChR2-transduced cholinergic afferents from PPN and LDT I used a range of protocols, varying pulse width between 2-10 ms, and delivering pulse trains of variable pulse number (5-25 pulses) and frequency (5-25 Hz).

4.2.4.2 Hyperpolarizing Arch 3.0 and eNpHR 3.0 stimulation with yellow light

Striatal expression of Arch 3.0 and eNpHR 3.0 was visualized with eGFP and eYFP tags, respectively. These hyperpolarizing opsins have red-shifted activation spectra, 520-560 nm for Arch 3.0 and 560-590 nm for eNpHR 3.0. Therefore, 560 nm yellow LED was used for light activation of hyperpolarizing tools as described in Chapter 2. Because the light power of 560 nm LED system was weaker than 473 nm LED and activation spectra for red-shifted opsins and ChR2 generally overlap, I also used 473 nm LED to activate Arch 3.0 and eNpHR 3.0. Blue light pulse trains were either delivered alone to stimulate these light-activatable ion pumps or following the delivery of yellow light pulse train to facilitate their recovery from photo-inactivation. ChIs expressing Arch 3.0 or eNpHR 3.0 were inactivated using stimulation frequency of either 25 Hz or 40 Hz. I varied pulse number to manipulate stimuli duration, using 10, 20, 40, 80, 120 or 200 pulse trains to

try to mimic typical ChI pause duration and achieve sufficiently long-hyperpolarization to enable rebound excitation.

For all optogenetic experiments presented in this chapter where only negative data were collected, electrical stimulation was used as a positive control of tissue quality, i.e. to determine that the lack of light-evoked DA release was not due to lack of evoked DA per se. Electrical stimuli were delivered as described in Chapter 2.

4.2.5 Fast-scan cyclic voltammetry

Striatal DA release following light activation of ChR2-expressing cortical/thalamic terminals, striatal ChIs or brainstem cholinergic terminals, and optogenetic inhibition of ChIs was monitored with FCV at CFMs as described in Chapter 2.

4.2.6 Immunohistochemistry

Immunohistochemical processing was carried out as described in Chapter 2.

100 μm thick Pf- and 300 μm thick M1-containing sections from CaMK2a-Cre mice were used for localization of ChR2 transduction at the injection sites and in striatum. 50 μm thick slices containing the SNc and VTA from DAT-Cre mice were used to examine retrograde AAV2 ChR2 transport.

To visualize expression of Arch 3.0 and eNpHR 3.0 constructs in striatal ChIs, 300 μm striatal coronal sections were fixed after FCV recordings in 4% PFA for at least 24h at 4°C. Then slices were washed in PBS (5x5 min), mounted on gelled slides, coverslipped using Vectashield (Vector Laboratories) and examined with fluorescent microscope. No additional staining was required either for visualization of eGFP-tagged Arch 3.0 or eYFP-tagged eNpHR 3.0 due to high signal intensity.

4.2.7 Drugs

Bicuculine, saclofen, Oxo-M and L-741,626 were purchased from Tocris Bioscience or Ascent Scientific. Cocaine, DHβE and all other chemicals were purchased from Sigma Aldrich. All solutions were prepared in distilled de-ionized water or DMSO (L-741,626) to make stock aliquots at 1000-10000x final concentrations and stored at -20°C. Drug stocks were diluted in oxygenated aCSF from frozen aliquots immediately before use and were bath applied. None of the drugs altered electrode sensitivity at the concentrations used.

4.2.8 Data analyses

All data was recorded, pre-processed and analyzed using WCP (University of Strathclyde, Glasgow) or AxoScope 10.2 (Axon Laboratories) software packages and in-house Excel macros scripts (Prof S. Cragg and Dr K. Jennings). All statistical analyses and data plotting were performed using GraphPadPrism 6.0.

Data are expressed as mean ± standard error of the mean (SEM) unless the data are presented as raw extracellular DA concentrations in μM ($[DA]_o$), where N is the number of animals. DA transients represent at least three averaged traces recorded at the same site in control and following experimental manipulation. The averaged data were plotted and analyzed statistically using comparison of the means and regression analyses. When raw data passed Shapiro-Wilk normality tests, parametric tests were used, otherwise non-parametric alternatives were employed. The mean peak evoked DA values were used for statistical comparisons, unless otherwise stated.

4.3 Results

4.3.1 AAV2 ChR2 is not transported retrogradely

AAV2 ChR2, based on previous reports of its exclusively anterograde transport (Paterna et al., 2004; Ciesielska et al., 2011; Salegio et al., 2012), was used to examine selective contribution of cortical or thalamic afferents to driving ChI-evoked striatal DA release. To confirm that AAV2 vector was not subject to retrograde transport I injected DAT-Cre mice in striatum and examined eYFP fluorescence in SNc/VTA 4-6 weeks post-surgery. The AAV2 ChR2 striatal injections in the DAT-Cre line had no associated eYFP fluorescence in either striatum or midbrain (N=2). Therefore, AAV2 ChR2 vector is not transported retrogradely and is well suited for the purposes of this study.

4.3.2 AAV2 ChR2 transduced striatal terminals of cortical or thalamic origin, but yielded no light-evoked dopamine release events

I next confirmed that AAV2 ChR2 transduced neurons in the target regions in the CaMK2a-Cre line with fluorescence microscopy. Following bilateral AAV2 ChR2 injections at 400 nl (Figure 4.1a), neuropil at the injection sites in either M1 (Figure 4.1b) or Pf (Figure 4.1d) expressed ChR2 as evidenced by eYFP signal. In striatum following M1 (Figure 4.1b) or Pf (Figure 4.1c) injections eYFP expression was detectable at least 4 weeks post-surgery. However, transduction levels, judged by eYFP signal intensity, were lower with AAV2 vector compared to AAV5, as expected from previous reports (Davidson et al., 2000; Paterna et al., 2004; Taymans et al., 2007; Aschauer et al., 2013). Specifically, AAV2 ChR2 transduction at the injection sites in M1 and Pf consistently produced robust eYFP signal, while at the striatal terminal level eYFP fluorescence was

sparse and weak. Unlike AAV5 ChR2 transduction resulting in uniformly high eYFP expression throughout most of striatum, the spatial distribution for AAV2 ChR2 was more restricted, with dense eYFP-positive plexuses in some areas and also areas of very low/absent eYFP signal when examined under x10 immersion objective in live tissue. Importantly, for further quantification of transduction efficiency by AAV5- and AAV2-packaged ChR2 constructs of cortical/thalamic neurons and their respective terminals in striatum higher-resolution microscopy images are needed. For example, establishing the proportion of eYFP co-localization with selective markers of cortical and thalamic terminals, VGLUT1 and VGLUT2, respectively, would enable a better comparison of the efficacy and selectivity of the AAV viral vectors.

4.3.2.1 Small volume injections of AAV2 ChR2 in either M1 or Pf led to sparse terminal transduction and evoked no dopamine release

To examine drive of ACh-evoked DA release following selective activation of cortical or thalamic afferents to ChIs, I replicated AAV5 paradigm bilaterally injecting CaMK2a-Cre mice with 400 nl of AAV2 ChR2 in either M1 (N=5) or Pf (N=5). 4-8 weeks post-surgery AAV2 ChR2 striatal expression was sparse and spatially restricted for both experimental groups. eYFP fluorescence signal intensity in striatal slices from AAV2 ChR2 injected animals (Figure 4.1b,c) was evidently weaker than after AAV5 ChR2 injections (Figure 4.1g,h). Light-evoked DA release was sampled throughout dorsal and ventral striatum in eYFP-positive areas; at least 4 slices were recorded from in each animal.

Two sampling strategies were alternated: either changing position of the CFM on every stimulation delivered at 2.5 min intervals, or staying at a given site for 3-8 stimulations. This approach enables sampling of evoked DA release from a large number

of striatal sites. Yet, in case light-evoked DA release is intermittent, staying in one recording site for several consecutive stimulations enables detection of DA events that may come and go. With either sampling strategy in both M1 or Pf injected CaMK2a-Cre mice no light-evoked DA release events were detected. To control for CFM quality and tissue viability, i.e. that the electrode could detect DA and that DA terminals were intact and could release neurotransmitter, single pulse electrical stimulations were also used. Electrical stimuli reliably evoked DA release in the recording sites where light evoked DA events could not be detected (Figure 4.1e). In case light-evoked DA events were below the CFM detection threshold, the DAT inhibitor (cocaine, 5 μM) was bath-applied to amplify DA signals. This manipulation increased the amplitude and duration of electrically evoked DA events (Figure 4.1f), but no light-evoked DA release was detected.

Tissue from one mouse in each experimental group was also used for experimentation on a 473 nm diode laser system (DL-473, Rapp Optoelectronic; 60 μm laser spot, 40 mW/mm^2 at specimen). This step was taken to control for LED providing insufficient light power for activation of sparsely expressed AAV2 ChR2. No light-evoked DA events were detected on the laser set up either. These negative data prompted me to explore whether the lack of light-evoked DA could be due to requirement for combined activation of cortical and thalamic afferents.

4.3.2.2 Dual bilateral injections of AAV2 ChR2 transduced both cortical and thalamic afferent pathways, but triggered no light-evoked dopamine release

To address whether combined pathway activation is required for successful engagement of ChI population activity to drive DA release, CaMK2a-Cre mice received dual bilateral injections (M1+Pf) of AAV2 ChR2 at 400 nl per site (total 1.6 μl). From

previous AAV2 ChR2 experiments I noted that eYFP fluorescence intensity was higher at 8 weeks post-injection, compared to 4 weeks. Thus, animals with dual bilateral injections were used for experimentation at least 6 weeks post-surgery (N=7). The striatal eYFP signal in CaMK2a-Cre mice with dual bilateral injections (Figure 4.2a) was brighter than for single site injected animals (Figure 4.1b,c), and ChR2 transduction in both M1 (Figure 4.2a) and Pf (Figure 4.2b) target regions was robust. Yet, striatal eYFP expression pattern was still sparse and patchy, mostly confined to dorsal regions.

Light-evoked DA release was sampled in eYFP-positive areas using previously described sampling strategies, and at least 4 slices were recorded from in each animal. Blue light LED stimulations were alternated between 5 pulses at 10 Hz and 10 pulses at 25 Hz, the stimuli protocols that successfully evoked DA in AAV5 ChR2 experiments. Failing to detect light-evoked DA, pulse number was increased to extend duration of the light stimulation train (20 or 30 pulses at 25 Hz), but no light-evoked DA transients were detected. In theory, however, dual site AAV2 ChR2 injections most closely replicate conditions of AAV5 ChR2 experiments. Electrical stimulation controls performed separately or delivered 8 s after light-stimulation train produced large amplitude electrically evoked DA transients (Figure 4.2c). The lack of light-evoked $[DA]_o$ in CaMK2a-Cre mice who received dual bilateral injections of AAV2 ChR2 led us to hypothesize that insufficient terminal transduction could fail to recruit ChI population activity to drive light-evoked DA release events.

4.3.2.3 Large volume injections of AAV2 ChR2 construct increased terminal transduction, but no dopamine release events were evoked

To address insufficient terminal transduction CaMK2a-Cre mice received doubled volume injections of AAV2 ChR2 at 800 nl in either M1 (Figure 4.2d) or Pf (Figure 4.2f) which increased eYFP fluorescence levels at the injection sites, but for Pf group eYFP signal intensity at striatal terminals was still low (Figure 4.2e). Incubation time was also extended with animals used 8-14 weeks post-surgery. In these M1 (N=3) or Pf (N=3) AAV2 ChR2-injected animals when no light-evoked DA events were detected, the following manipulations were performed.

First, to amplify possible sub-threshold light-evoked DA signals the DAT inhibitor (cocaine, 5 μM) was bath-applied. DA release sampling in the presence of cocaine revealed no light-evoked DA transients. Next, I examined whether I could detect changes in electrically evoked DA following potential sub-threshold ACh events triggered by light activation of ChR2-expressing excitatory inputs. Specifically, even if no light-evoked DA events occurred, putatively reflecting lack of synchronous ChI population activity, sub-threshold ACh release insufficient for driving DA could have consequences on subsequent ACh-modulated DA release. Thus, it is expected that a prior ACh release event triggered by light stimulation will change ensuing electrically evoked DA release. I therefore examined whether evoked DA events following single pulse or high frequency burst (4 p at 100 Hz) electrical stimulation were modulated by light pulse train delivered 500 ms or 1 s prior, consistent with desensitization of nAChRs following preceding ACh release. In this case, $[DA]_o$ evoked by 4 pulses at 100 Hz electrical stimulation would be amplified, while single pulse evoked $[DA]_o$ would decline, increasing the high frequency burst to single pulse ratio.

Single pulse and high frequency burst electrically evoked DA transients were recorded in dorsal CPu of M1-injected mouse (N=1) with and without prior blue light activation of ChR2-expressing corticostriatal afferents. Two-way ANOVA showed that across all stimulation protocols mean peak evoked $[DA]_o$ was not significantly different ($F(3,9)=1.68$, $p=0.2411$; Figure 4.3a,b). Further, there was no change in the ratio of $[DA]_o$ evoked by 4 pulses at 100 Hz stimulation to that evoked by 1 pulse (4p:1p ratio) between electrical stimulations delivered with and without preceding blue light pulse train ($t=0.74$, $df=6$, $p=0.4859$; two-tailed, unpaired t-test; Figure 4.3c).

For the Pf injected animal (N=1), electrically evoked $[DA]_o$ recorded in dorsal CPu was significantly different between the four stimulation protocols as revealed by two-way ANOVA ($F(3,6)=37.71$, $p=0.0003$; Figure 4.3d,e), but post-hoc Bonferroni t-tests were not significant ($p>0.05$). Further, preceding light-activation of ChR2-expressing Pf terminals did not significantly alter the 4p:1p ratio of electrically evoked DA transients ($t=0.77$, $df=4$; $p=0.4843$, two-way, unpaired t-test; Figure 4.3f). Thus, in these pilot experiments electrically evoked $[DA]_o$ was not modulated by light activation of ChR2-transduced afferents to striatal ChIs, suggesting lack of sub-threshold ACh release events.

4.3.2.4 ChAT-Cre positive control for AAV2 functionality – direct activation of cholinergic interneurons reliably drives light-evoked dopamine events

To test whether the AAV2 ChR2 vector was functional, direct activation of striatal ChIs was attempted following bilateral striatal injections of AAV2 ChR2 at 400 nl in ChAT-Cre mice (N=2). In these animals robust eYFP expression with high fluorescence intensity throughout dorsal and ventral striatum was present 4 weeks post-injections. At x40

times magnification eYFP was easily detectable in the cell bodies and processes of individual striatal ChIs in live tissue. Light-evoked DA transients were successfully recorded following single pulse blue light stimulations (2 ms) and in multiple striatal regions in dorsal and central CPu (Figure 4.4). Recordings were obtained from at least 2 slices in each mouse. These data conclusively demonstrate that the AAV2 ChR2 vector was functional. No further experiments with AAV2 ChR2 were conducted.

4.3.3 Hyperpolarizing optogenetic tools drive no dopamine release events

Application of hyperpolarizing Arch 3.0 and eNpHR 3.0 opsins has never been reported previously for monitoring of a population-based response. Earlier work successfully employed eNpHR 3.0 to measure the response to hyperpolarization-induced rebound spiking of ChIs in single post-synaptic MSNs with patch-clamp electrophysiology (English et al., 2011). However, monitoring the result of ChI population activity with FCV is fundamentally different from monitoring single cell response, as ACh-evoked DA release would rely on synchronized rebound activity in a small number of ChIs (Threlfell et al., 2012). Here I examined whether DA release events can be detected following optogenetic inhibition of striatal ChIs with hyperpolarizing opsins. In this case, ACh-evoked DA events would be indicative of synchronized rebound spiking in a population of striatal ChIs.

AAV5-packaged Arch 3.0 (N=3) or AAV2-packaged eNpHR 3.0 (N=2) vector injections at 800 nl targeted central CPu in ChAT-Cre mice (Figure 4.5a). At 6 weeks striatal Arch 3.0 expression (visualized by eGFP fluorescence) was sparse. At 10 weeks eGFP signal intensity was higher, the overall Arch 3.0 transduction throughout striatum

was denser and more robust, with eGFP expression readily identifiable in individual ChIs (Figure 4.5b). In eNpHR 3.0-injected mice eYFP-positive ChI cell bodies and processes were easily identifiable throughout CPu, mostly in dorso-central areas, both at 6 weeks and 11 weeks. The overall eYFP fluorescence intensity was high, with more focal/dense eYFP expression in some regions (Figure 4.5c).

Arch 3.0 and eNpHR 3.0 were activated with yellow 560 nm LED. To increase the probability of sufficiently long hyperpolarization driving population rebound spiking in striatal ChIs and to mimic the duration of ChI pauses observed *in vivo*, light trains of 40, 80, 120, 200 or 300 pulses at 25 or 40 Hz were used. The same protocols were repeated with 473 nm LED. In a subset of experiments, 473 nm and 560 nm LED stimulations also were combined as previous reports suggested blue light facilitates recovery from photo-desensitization for Arch 3.0 and eNpHR 3.0 (Mattis et al., 2012). For this blue light pulse train was delivered first, followed by the yellow light pulse train 1-5 seconds later, or *vice versa*. None of the above manipulations, however, were successful in driving light-evoked DA release in Arch 3.0- and eNpHR 3.0-injected ChAT-Cre mice.

To control for tissue and CFM quality electrical stimulation was used, producing robust DA signal in multiple recording sites in dorsal striatum (Figure 4.5d,g). Next, as previously described in Section 4.3.2.3, I used electrical and electrical combined with light stimulation protocols to examine whether sub-threshold ACh events occurred following light inhibition of ChIs that were insufficient to drive DA release *per se*, but could briefly turn off nAChRs and thus change electrically evoked $[DA]_o$ following 1 pulse or 4 pulses at 100 Hz stimulation. Light pulse trains were delivered 200 ms or 500 ms prior to electrical stimulus onset.

Single pulse and high frequency burst electrically evoked DA transients were recorded in dorsal CPu of Arch 3.0-injected ChAT-Cre mouse (N=1) with and without prior light inhibition of Arch 3.0-expressing ChIs. To eliminate any confounding effects of di-synaptic GABA release events limiting ChI activity, $GABA_A$ (bicuculine, 10 μM) and $GABA_B$ (saclofen, 50 μM) antagonists were bath-applied throughout this experiment. Electrically evoked $[DA]_o$ was significantly different across the four stimulation protocols as revealed by two-way ANOVA ($F(3,12)=9.48$, $p=0.0017$; Figure 4.5d,e), but post-hoc Bonferroni t-tests were not significant ($p>0.05$). Further, the 4p:1p ratio of electrically evoked $[DA]_o$ with and without preceding light inhibition of Arch 3.0-transduced ChIs in ChAT-Cre mouse in complete GABA block was not significantly different ($t=0.09$, $df=6$, $p=0.9306$; two-tailed unpaired t-test; Figure 4.5f).

For the eNpHR 3.0-injected ChAT-Cre mouse (N=1), electrically evoked $[DA]_o$ recorded in dorsal CPu following single pulse and high frequency burst stimulation with and without preceding light stimuli was significantly different across the four stimulation protocols as revealed by two-way ANOVA ($F(3,9)=27.79$, $p<0.0001$; Figure 4.5g,h), but post-hoc Bonferroni t-tests were not significant ($p>0.05$). There also was no change in the 4p:1p ratio between electrically evoked $[DA]_o$ with and without preceding light inhibition of eNpHR3.0-transduced striatal ChIs ($t=0.68$, $df=6$, $p=0.5172$, two-way, unpaired t-test; Figure 4.5i). In these pilot experiments lack of modulation of electrically evoked $[DA]_o$ following optogenetically-induced inhibition of striatal ChIs selectively expressing either Arch 3.0 or eNpHR 3.0 hyperpolarizing opsins suggests no sub-threshold ACh release events, indicative of synchronous rebound spiking, occurred.

As the lack of light-evoked DA release with Arch 3.0 and eNpHR 3.0 could be due to any rebound spiking of ChIs being insufficiently synchronized, I also attempted to get ChIs to be more synchronous in their activity patterns. For this I delivered alternating blue immediately followed by yellow light pulse trains (100 pulses at 100 Hz), repeated 10 times. This manipulation did not drive light-evoked DA events either. Overall, no light-evoked DA release was detected following yellow, blue or combined yellow/blue light stimulation of striatal ChIs expressing Arch 3.0 or eNpHR 3.0. These data suggest that hyperpolarizing ion pumps may not provide optimal hyperpolarization levels for driving synchronized rebound spiking in a population of striatal ChIs for ACh-evoked DA release. Although the initial plan for these experiments was examining DA release with FCV and companion firing properties of ChIs with electrophysiology, for the lack of DA events we did not then identify effects of optogenetic hyperpolarization on synchrony of firing in cell physiology experiments.

4.3.4 Striatal cholinergic brainstem afferents do not drive acetylcholine-evoked striatal dopamine release

Next I examined whether cholinergic projections from PPN and LDT could drive or contribute to ACh-evoked striatal DA release. For these experiments species were changed from mouse to rat. ChAT-Cre rats, unilaterally injected in the brainstem PPN or LDT nuclei with AAV2 ChR2 construct by the Mena-Segovia lab (Dautan et al., 2014), were used for FCV experiments. As previously observed in mice, terminal transduction 2 weeks post-injection for long-range brainstem afferents was absent (N=1). Therefore, all animals were used for experimentation at least 4 weeks post-surgery.

4.3.4.1 Direct activation of striatal cholinergic interneurons drives light-evoked dopamine release in AAV2 ChR2-injected ChAT-Cre rat

The brainstem experiments required a positive control to discard the possibility of species differences in ACh-evoked drive of striatal DA release and to confirm AAV2 ChR2 functionality in ChAT-Cre rat driver line. The control experiment used CPu-injected ChAT-Cre rat (N=1), where robust ChR2 transduction of striatal ChIs was confirmed by uniform and ubiquitously high eYFP signal throughout CPu and NAc. The pattern of ChR2 expression was similar to CPu-injected ChAT-Cre mice. Light-evoked DA release events were successfully triggered with single pulse and 4 pulses at 25 Hz light stimuli and in different striatal sub-regions (Figure 4.6a). These light-evoked DA events were of large amplitude and were easily detected without DA signal amplification.

Brief pulsed bath-application of nAChR antagonist (DHβE, 1 μM) lasting 2 min abolished light-evoked DA transients (Mann-Whitney U=0, $n_1=n_2=4$, p=0.0286, two-tailed; Figure 4.6b,c). Upon DHβE washout the amplitude of the light-evoked DA events returned to the pre-drug baseline (Figure 4.6d). To further confirm cholinergic origin of the detected DA events, mAChR agonist (Oxo-M, 10 μM) was bath-applied following washout of nAChR antagonist. This manipulation also abolished light-evoked DA release in ChAT-Cre rat (Mann-Whitney U=0, $n_1=n_2=4$, p=0.0286, two-tailed; Figure 4.6d,e). Using single pulse and light train stimuli of 4 pulses at 5, 10, 25 and 40 Hz I show that light-evoked ACh-dependent DA release events in ChAT-Cre rat are insensitive to stimulation frequency, evoking similar $[DA]_o$ regardless of stimulation protocol, as revealed by one-way ANOVA (F(4,15)=0.1, p=0.9805; Figure 4.6f,g). Bath-application of the DAT inhibitor (cocaine, 5 μM) showed the detected light-evoked release events were DA (in addition to cyclic voltammogram), as the amplitude and duration of the light-

evoked transients increased and this change was statistically significant (Wilcoxon W=1260, N=51, p<0.0001; Figure 4.6h).

4.3.4.2 Activation of ChR2-transduced cholinergic brainstem afferents does not drive or contribute to acetylcholine-evoked striatal dopamine release

In LDT-injected animals (N=3), where anatomical studies previously described brainstem terminal innervation in NAc and dmCPu, no or very few sparse and thin axonal segments were detected using fluorescence imaging in live striatum. Sampling of light-evoked DA in the unlabelled 'typical' innervation sites revealed no release events. Inability to visualize eYFP-transduced brainstem afferents in live 300 μm sections presented the main experimental challenge. When acute sections were mounted on microscopy slides with fluorescence-amplifying mounting media Vectashield (Vector Laboratories) and coverslipped, very thin and sparse, but detectable eYFP-positive axonal segments were found in the slices where no live fluorescence signal was visible. The signal intensity was very low, however. Low signal-to-noise ratio effectively prohibited detection of fluorescence signal in live tissue due to light scattering and less 'flat' slice architecture. I tested this by examining live tissue using optics on different microscope set ups, with both LED or mercury lamp for visualizing eYFP. In all cases striatum appeared devoid of eYFP fluorescence. In LDT-injected ChAT-Cre rats detectable eYFP signal could only be found in septum of live slices.

For the rostral PPN-injected animals (N=3), sparse eYFP-expressing terminals were detectable in dorsal striatum, dlCPu in particular. The area of detectable fluorescence signal was very patchy and restricted. In these experiments no light-evoked DA events were detected, and therefore the DAT inhibitor (cocaine, 5 μM) was bath-

applied to amplify DA signals that could be below CFM detection threshold. However, this manipulation did not uncover light-evoked DA release. Light-evoked DA transients were initially sampled in response to 25 pulses at 25 Hz or 10/20 pulses at 40 Hz light stimulation trains (pulse width 2 ms). Electrophysiology work from the Mena-Segovia group showed that 10 Hz pulse trains with wide pulses were most efficient in driving optogenetically-evoked activity in post-synaptic neurons following stimulation of brainstem afferents. Thus, I incorporated 5 pulses at 10 Hz stimulation protocol, extending pulse widths to 10 ms.

When adjustments in stimulation parameters and application of the DAT inhibitor revealed no light-evoked DA events across multiple sampling sites, I examined possible changes in electrically evoked $[DA]_o$ following single pulse and high frequency burst stimulation with and without prior blue-light activation of ChR2-expressing brainstem afferents from rostral PPN. Light pulse trains were delivered 500 ms or 1 s prior to electrical stimuli. Electrically evoked $[DA]_o$ following 1 pulse and 4 pulses at 100 Hz stimulations was recorded in dorsal CPu of rostral PPN injected rat (N=1), two slices were recorded from in the same animal. Evoked $[DA]_o$ was not significantly different across the four stimulation protocols as revealed by two-way ANOVA ($F(3,24)=0.25$, $p=0.8630$; Figure 4.7a,b). Further, the 4p:1p ratio of electrically evoked $[DA]_o$ was not significantly different as the result of preceding light pulse train delivery ($t=0.11$, $df=14$, $p=0.9173$; two–tailed, unpaired t-test; Figure 4.7c). Therefore, no detectable sub-threshold ACh release events took place following light stimulation of ChR2-expressing brainstem cholinergic terminals in striatum.

Another way to explore presence of sub-threshold cholinergic events is by examining current sensitivity of electrically evoked $[DA]_o$. Therefore, I examined whether electrically-evoked $[DA]_o$ recorded in dorsal CPu of rostral PPN injected animal (N=1) was potentiated when electrical and light stimuli were delivered concurrently. For both light and electrical stimulation protocols I used 2 ms wide single pulses. Because undetectable DA events could limit further DA release via D2 auto- and heteroreceptors, in these experiment I used D2 antagonist (L-741,626, 1 μM). The power output for the LED was kept constant at the maximum current setting. The electrical current amplitude was adjusted to 20% and 80% of the maximal current response (in this case, 0.3 mA and 0.7 mA). One-way ANOVA showed a significant difference between the stimulation conditions ($F(3,12)=95.59$, $p<0.0001$; Figure 4.7d), and post-hoc Bonferroni t-tests revealed a highly significant difference between 0.3 mA and 0.7 mA electrical stimulation protocols ($p<0.0001$). However, no significant difference between electrical and light+electrical stimulation protocols was present within a given current group ($p>0.05$). Thus, the amplitude of electrically evoked DA transients did not change as a result of concurrent light stimulation of ChR2-transduced cholinergic brainstem afferents at either low or high electrical current, suggesting that light stimulation did not potentiate/inhibit electrically evoked DA release. From these data it follows that brainstem cholinergic projections do not drive or contribute to ACh-evoked striatal DA release, at least under the current experimental conditions.

4.4 Discussion

The data presented in this chapter describe the search for alternative approaches to examining the circuits capable of driving ACh-evoked striatal DA release in mouse and rat. I used the AAV2 ChR2 vector to address the confounds associated with bi-directional axonal transport of the AAV5 ChR2 vector in the CaMK2a-Cre driver line. Exclusively anterograde transport of AAV2 ChR2 should have enabled examination of independent contributions of corticostriatal versus thalamostriatal projections to driving glutamate-dependent ACh-evoked DA release. However, no light-evoked DA events could be detected in experiments using AAV2 ChR2-injected CaMK2a-Cre mice.

The overall eYFP fluorescence intensity at striatal axon terminal level with AAV2 ChR2 was weaker and sparser compared to eYFP signal observed following AAV5 ChR2 injections, as reported previously (Davidson et al., 2000; Paterna et al., 2004; Taymans et al., 2007; Aschauer et al., 2013). The AAV2 ChR2 terminal transduction following both cortical and thalamic injections was lower and more spatially restricted than previously seen with the AAV5 vector, suggesting it was determined by intrinsic properties of the AAV2 vector. Hypothesizing the lack of light-evoked DA events was due to necessity for combined activation of cortical and thalamic afferents, as could be the case with AAV5 ChR2 experiments, I performed dual bilateral injections of AAV2 ChR2 into both M1 and Pf in the same animal. This manipulation increased striatal eYFP fluorescence intensity, putatively reflecting higher levels of ChR2 transduction and/or increase in the number of ChR2-expressing terminals, although the area of high eYFP signal remained fairly restricted and ‘patchy’. Sampling of DA release in striatal regions with the highest eYFP signal intensity revealed no light-evoked DA events or modulation of electrically evoked

$[DA]_o$ by light activation of ChR2-transduced excitatory inputs to ChIs. Next I doubled the injection volumes in an attempt to equalize the extent of virus spread between the AAV2- and AAV5-packaged vectors. Virus incubation was also extended to at least 8 weeks, as I consistently saw progressive increase in fluorescence intensity during the first two months following AAV2 ChR2 injections. These manipulations, however, did not result in light-evoked DA events.

The implications of the negative data for these experiments are difficult to evaluate, as a number of different explanations is valid. The lack of light-evoked DA release could be due to sub-optimal performance of the AAV2 ChR2 vector in the CaMK2a-Cre driver line and/or inability of thalamostriatal and corticostriatal circuits to drive glutamate-dependent ACh-evoked DA release independently of each other. Given the robustness of light-evoked DA events observed with AAV5 ChR2, it is improbable that striatal glutamatergic afferents are unable to engage ChI population activity for driving ACh-dependent DA events. Instead, due to limited spread of the AAV2-packaged ChR2 vector, terminal transduction could be low/insufficient for engaging synchronous spiking activity in an adequately large population of striatal ChIs.

Single site and dual site AAV2 ChR2 injections at small and large volumes may transduce only small populations of striatally-projecting cortical or/and thalamic neurons, which in turn failed to recruit population response from a sufficiently large number of striatal ChIs to drive ACh-evoked DA release. Yet, it is difficult to unequivocally establish the reason for low transduction efficiency. It could be the result of more restricted spatial spread or generally lower infection rates of the AAV2 ChR2 vector. It is also possible that AAV2 ChR2 trafficking to terminals, once parent cell bodies

at the injection site took up the virus, is slower or less efficient than for the AAV5 vector. Successful drive of light-evoked DA events in CPu-injected ChAT-Cre mice and rats hints that impaired AAV2 ChR2 trafficking could be a problem for distal terminal transduction. However, in the ChAT-Cre experiments the site of ChR2 action is located directly on the cholinergic axis, and thus no failures of synaptic transmission leading to reduced efficiency in recruiting population activity of striatal ChIs complicate experimental results.

It is also possible that the AAV2 ChR2 vector is not suited to this experimental paradigm, especially if co-activation of cortical and thalamic glutamatergic synapses on striatal ChIs is necessary and sufficient for driving glutamate-dependent ACh-evoked striatal DA release. While dual site injections of AAV2 ChR2 transduced both cortical and thalamic striatally-projecting neurons in the same animal, populations innervating non-overlapping striatal territories could express ChR2. Specifically, although I targeted both M1 and Pf in an attempt to replicate AAV5 ChR2 experiments, the end result could have been opsin transduction of neurons projecting to distinct striatal regions. Thus, no actual spatial overlap between cortical and thalamic ChI afferents was present whereby a truly 'combined' activation state could not be achieved. Together, these data cannot conclusively show whether sub-optimal experimental parameters, such as insufficient terminal transduction, produced current negative results, or whether cortical and striatal glutamatergic afferents are only capable of driving ACh-evoked DA release co-operatively.

To directly compare the data from these experiments addressing the confounding effects of possible cortical and thalamic co-activation with the data from

AAV5 experiments, I changed viral vector for ChR2 transduction while Cre-driver line remained the same. The current results, however, suggest the AAV5 ChR2 vector should be used in future work, but in a more specific driver line. If the main difference between the AAV2 and AAV5 experiments is the way in which these vectors transduce their Cre-expressing neuronal targets, control over the mechanisms regulating transduction, which are still incompletely understood, is not possible. Therefore, it is more straightforward to control the site of transduction by using a more specific Cre-driver line. Generation and use of better Cre-driver lines would significantly advance examination of selective and independent contribution of cortical versus thalamic projections to striatal ChIs in driving di-synaptically evoked ACh-dependent DA events. Specifically, cerebellin-1-Cre line, not previously reported, would enable selective targeting of intralaminar thalamic nucleus Pf for ChR2 transduction. Further, GENSAT stocks have two Cre-driver lines which could also benefit this line of inquiry: Tg(A830010M20Rik-cre)KJ227Gsat/Mmucd line expressing Cre-recombinase in deep cortical layers, and Tg(Cnnm2-cre)KD18Gsat/Mmucd strain with more ubiquitous cortical, but little thalamic Cre expression. The concern yet again is whether these more 'restricted' Cre-driver lines will limit ChR2 transduction to insufficiently large populations of cortical or thalamic neurons for driving synchronized population activity in their downstream ChI targets.

For the experiments where hyperpolarizing ion pumps Arch 3.0 and eNpHR 3.0 were used to monitor whether ACh-evoked DA release occurred following optical inhibition of striatal ChIs also only negative data were collected. These data suggest that either any rebound spiking was absent, or that temporal synchronization of rebound action potential firing across a small population of ChIs was lacking. These experiments

dramatically demonstrate the difference between monitoring single cell responses with electrophysiology, and monitoring population activity-dependent DA events with FCV. The relative inefficiency of the Arch 3.0 and eNpHR 3.0 tools in truly hyperpolarizing neurons, contrary to their ubiquitously reported success with inhibition of evoked and/or pacemaker activity (Mattis et al., 2012; Raimondo et al., 2012; Tsunematsu et al., 2013; Nagode et al., 2014), could explain the failure of these hyperpolarizing ion pumps to drive ACh-evoked DA release. In particular, if the achieved membrane hyperpolarization were small, ChIs could simply return to their normal tonic pattern of activity upon termination of the inhibitory optical stimulation which paused their AP firing, rather than display synchronized rebound spiking. Alternatively, I may not have established optimal experimental conditions for ChI rebound spiking-activated DA events.

The most recent reports on engineering of ChR2 ion channels to be selectively permeable to Cl^- (Berndt et al., 2014; Wietek et al., 2014) highlight that more efficient tools for neuronal hyperpolarization are becoming available. This chloride-selective configuration of ChR2 enables flow of multiple Cl^- per photon of light through the open channel pore, unlike the ion pumps actively transporting a single ion per photon of light. Future experimental work could examine rebound spiking-activated DA release using hyperpolarizing variants of opsin channels, which would generate significantly larger and more stable currents at lower light stimulation intensities. Thus, chloride-selective ChR2 variant would provide a better tool for achieving true membrane hyperpolarization, comparable to negative current injection in patch-clamp configuration, in neurons which actively maintain their resting membrane potential (Wilson, 2005).

Finally, the work on ChAT-Cre rats, provided by the Mena-Segovia group, enabled us to establish that ACh-evoked drive of local striatal DA release is not an artefact of species or transgenic mouse use. I replicated the earlier ChAT-Cre mouse findings in ChAT-Cre rat (Threlfell et al., 2012), where striatal ChIs were transduced with ChR2 using AAV2-packaged vector. Specifically, light-evoked DA transients mediated by cholinergic transmission were evoked with single pulse blue light stimulations, and were abolished following blockade of nAChRs or arrest of cholinergic transmission following activation mAChRs. Application of DAT inhibitor amplified the light-evoked signal, demonstrating that the recorded traces were indeed DA, and frequency insensitivity of ACh-evoked DA release events was replicated in ChAT-Cre rat. These data provided a positive control for the brainstem cholinergic projection experiments, demonstrating functional viability of the AAV2 ChR2 vector in ChAT-Cre rat, and further showing that the lack of light-evoked DA release events is not the result of species differences in ACh-evoked drive of DA release.

In contrast, from the data acquired to date it appears that the brainstem cholinergic projections to rodent striatum do not drive or contribute to ACh-evoked striatal DA release. If PPN/LDT afferents were shown to drive ACh-evoked DA release, the next step would be to determine whether these DA events are evoked directly by ACh released from the PPN/LDT axon terminals, or indirectly via brainstem recruitment of the local ChI activity. Further, given the cholinergic nature of the brainstem projection to striatum, it was possible that light-evoked DA release events in ChAT-Cre mice injected in CPu with the bi-directionally transported AAV5 ChR2 vector were also partly dependent on co-activation of brainstem cholinergic afferents. The current data, therefore, have very important implications for the previously reported experiments,

demonstrating the recorded DA transients in ChAT-Cre mice expressing ChR2 in striatal ChIs following viral vector injections were purely the product of local striatal cholinergic transmission (Threlfell et al., 2012). In functional terms, these results underscore the discrepancy between the anatomy and predicted function of a projection pathway. However, while brainstem cholinergic afferents could not be engaged to drive ACh-evoked striatal DA release, the characteristic firing patterns of the parent cell bodies in behavioural paradigms (Pan and Hyland, 2005; Okada et al., 2009) suggest that these cholinergic afferents may convey important information to striatal computational circuits by means other than direct regulation of local DA release events by cholinergic transmission.

4.5 Summary

The data presented in this chapter highlight the difficulties associated with finding alternative tools for studying candidate circuits regulating striatal ACh-evoked DA release with optogenetics. In this case, the primary challenge lies in interpretation of the negative results because there can be no certainty as to whether the lack of light-evoked DA release events is the result of an imperfect experimental paradigm, or whether the circuits under study genuinely do not regulate the function of interest. To delineate the two explanations more data, including electrophysiology, are required.

Overall, I suggest that the AAV2 ChR2 vector due to limited transduction efficiency is not suited to studying the role of cortical and thalamic striatal glutamatergic afferents in driving DA release via recruitment of ChI population activity. As an alternative research strategy I propose that the AAV5 ChR2 vector should be used in future work, but in a more specialized Cre-driver line. I also show that hyperpolarizing

ion pumps are not the best tools for studying rebound activity-dependent DA events, and rather the newly emerging chloride-selective modifications of ChR2 should be trialled. Finally, with the ChAT-Cre rats I replicate the presence of ACh-evoked striatal DA release events following light activation of ChR2-transduced striatal ChIs in different rodent species, but show that the brainstem cholinergic projections are unlikely to contribute to ACh-dependent striatal DA release.

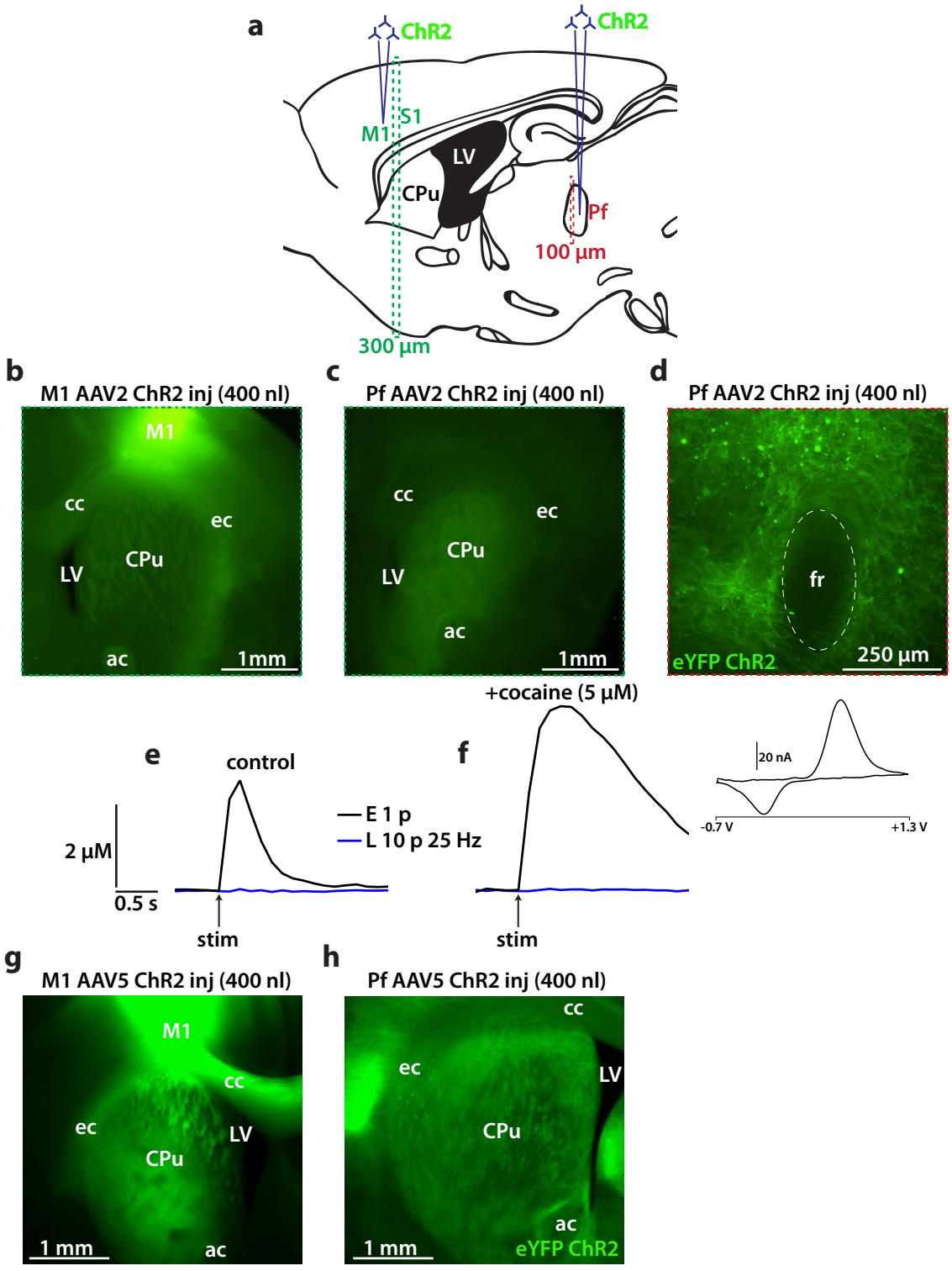

Figure 4.1 AAV2 ChR2 injections in CamK2a-Cre mice successfully transduced M1 and Pf target regions, with eYFP fluorescence also detectable in striatal neuropil

(a) A schematic of mouse brain in sagittal plane showing targeting of ChR2 injections to M1 or/and Pf, and plane through which associated 300 µM-thick CPu/M1 or 100 µM-thick Pf sections were taken. **(b)** eYFP expression after small volume injections of AAV2 ChR2 at 400 nl in M1 at the cortical injection site and in CPu neuropil. **(c)** Striatal eYFP fluorescence after small volume injections of AAV2 ChR2 at 400 nl in Pf and **(d)** associated ChR2 transduction at the injection site in Pf. **(e,f)** Typical DA transients recorded in striatum following single pulse electrical (E) or light pulse train (L) stimulation in AAV2 ChR2-injected mice in control **(e)** and with DAT blockade (cocaine,5 µM) **(f)** showing evoked $[DA]_o$ was only present following electrical, and not light stimulation. Compared to AAV2, injections of AAV5 ChR2 in either M1 **(g)** or Pf **(h)** at 400 nl previously resulted in higher eYFP fluorescence signal throughout striatum.

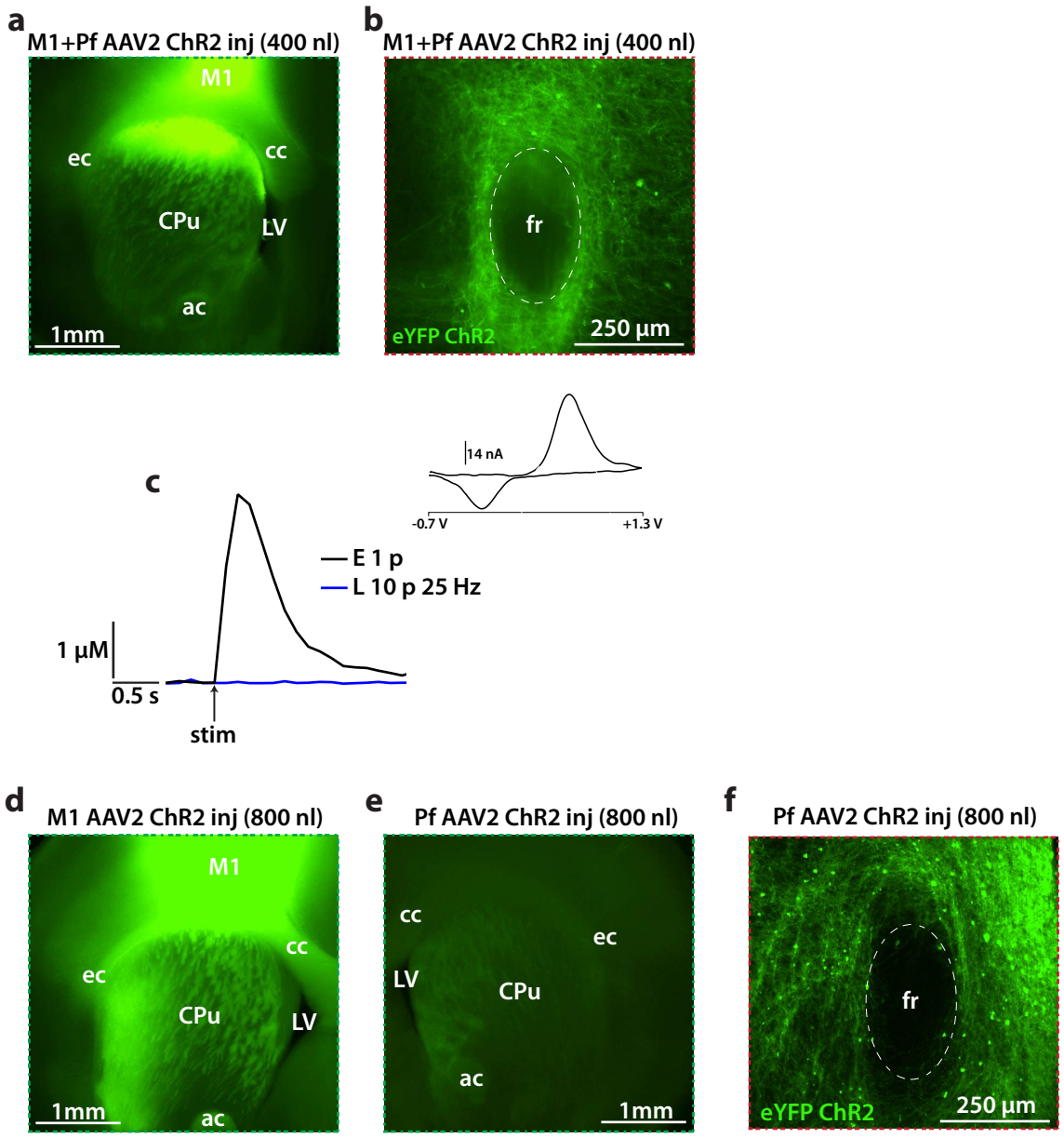

Figure 4.2 Dual bilateral and large volume AAV2 ChR2 injections in CamK2a-Cre mice increased eYFP fluorescence intensity at in striatal neuropil, but expression pattern was still less intense and differently distributed compared to AAV5 ChR2

(a) M1 and striatal eYFP expression following small volume dual bilateral injections of AAV2 ChR2 at 400 nl simultaneously targeting M1 and Pf regions in the same animal, and **(b)** associated ChR2 transduction at the Pf injection site. Targeting both corticostriatal and thalamostriatal afferents with AAV2 ChR2 increased the associated eYFP signal intensity in CPu. The fluorescence pattern was still different to AAV5 ChR2 (Figure 4.1g,h), with most signal confined to dorsal CPu and other striatal territories only showing sparse eYFP expression. **(c)** Typical DA transients recorded following single pulse electrical (E) and light pulse train (L) stimulation of ChR2-expressing cortical and thalamic terminals in CPu of CaMK2a-Cre mice after dual bilateral injections of AAV2 ChR2 at 400 nl per site in M1+Pf. Evoked $[DA]_o$ was only present following electrical, and not light stimulation. **(d)** eYFP expression following large volume injections of AAV2 ChR2 at 800 nl in M1 at the cortical injection site and in CPu neuropil. **(e)** Striatal eYFP fluorescence following large volume injections of AAV2 ChR2 at 800 nl in Pf and **(f)** associated ChR2 transduction at the injection site in Pf.

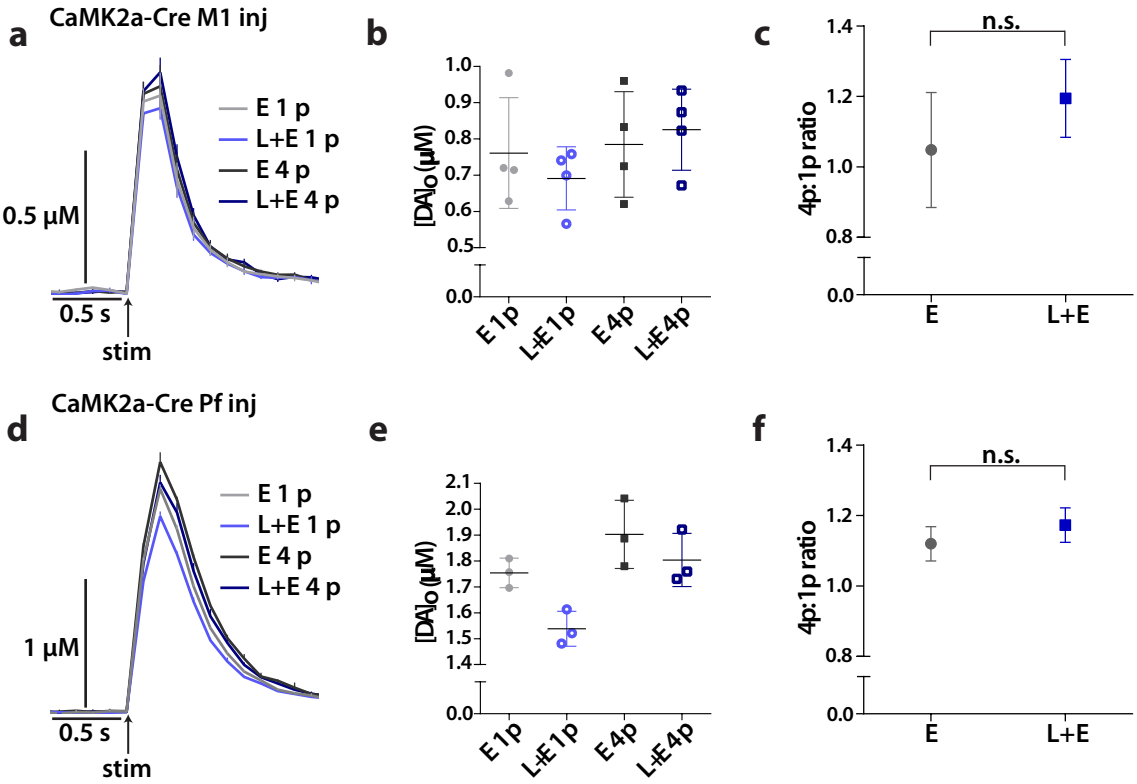

Figure 4.3 Light-activation of ChR2-expressing cortical or thalamic striatal terminals in AAV2 ChR2 injected CaMK2a-Cre mice did not alter the 4p:1p ratio of electrically evoked $[DA]_o$
(a,d) Mean $[DA]_o$ ± SEM versus time evoked by single pulse (1 p) and high frequency burst (4 p at 100 Hz) electrical stimulation (E) with and without prior light (L) activation of ChR2-expressing terminals in CamK2a-Cre mice injected with AAV2 ChR2 at 800 nl. DA release was recorded in dorsal CPu of M1-injected mouse **(a)** (N=1) or Pf-injected mouse **(d)** (N=1). **(b,e)** Peak $[DA]_o$ of individual DA transients evoked with different stimulation protocols in dorsal CPu of M1-injected **(b)** or Pf-injected **(e)** mice. Error bars are SEM. Regardless of stimulation protocol for M1 animal evoked $[DA]_o$ was not significantly different (Two-way ANOVA, $p>0.05$). In Pf animal evoked $[DA]_o$ was significantly different between stimulation protocols, but post-hoc Bonferroni t-tests were not significant (Two-way ANOVA, ***$p<0.001$). **(c,f)** Ratio of $[DA]_o$ evoked by 4 p electrical stimulation to that evoked by 1 p electrical stimulation (4p:1p ratio) with and without light-activation of ChR2-expressing M1 **(c)** or Pf **(f)** striatal terminals 500 ms or 1 s prior to electrical stimulus delivery was not significantly different ($p>0.05$; unpaired t-test), suggesting lack of sub-threshold ACh release events.

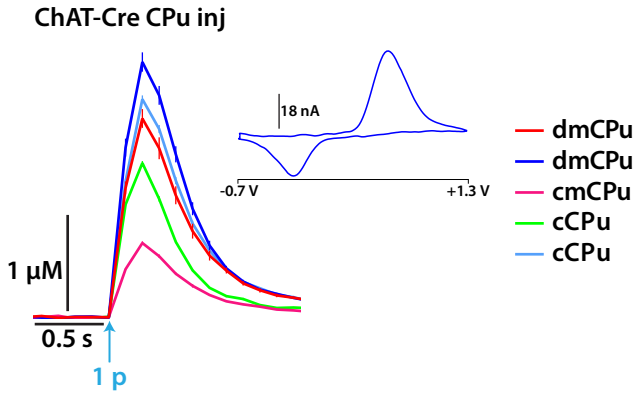

Figure 4.4 AAV2 ChR2 vector was functional as light-evoked $[DA]_o$ was successfully recorded in multiple sites throughout dorsal striatum in ChAT-Cre mice following CPu injections
Mean $[DA]_o$ ± SEM versus time evoked by single light pulses (2 ms) recorded in multiple sampling sites throughout dorsal striatum in dorsomedial (dmCPu), centromedial (cmCPu) and central (cCPu) sites in ChAT-Cre mice (N=2) injected with AAV2 ChR2 at 400 nl in CPu. Thus, AAV2 ChR2 vector was functional.

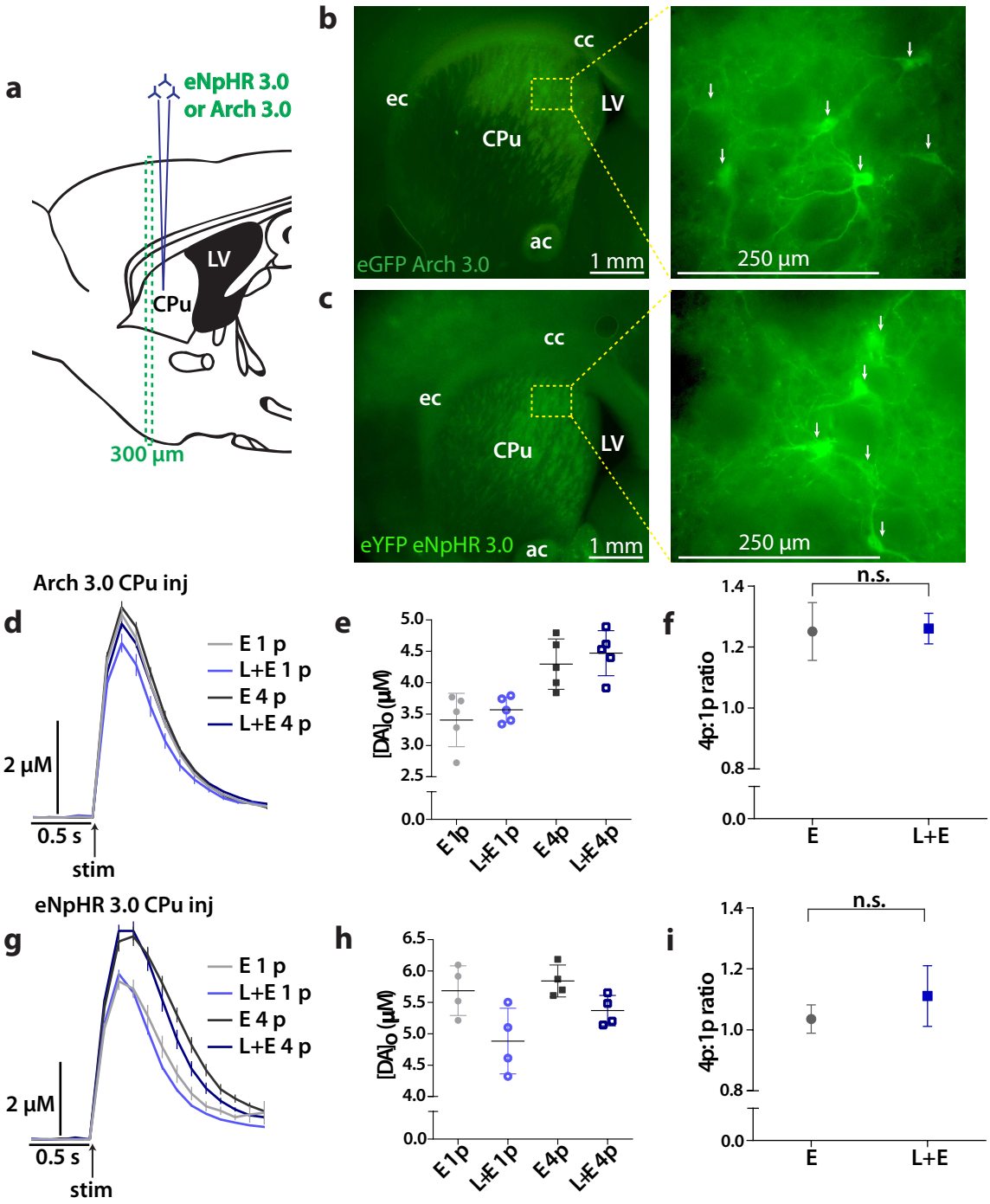

Figure 4.5 Arch 3.0 and eNpHR 3.0 opsins successfully transduce striatal ChIs in ChAT-Cre line, but do not drive light-evoked DA events or change the 4p:1p ratio of electrically evoked $[DA]_o$
(a) A schematic of mouse brain in sagittal plane showing targeting of Arch 3.0 or eNpHR 3.0 injections to cCPu in ChAT-Cre mice. **(b,c)** eGFP or eYFP expression in CPu following bilateral injections of Arch 3.0 **(b)** or eNpHR 3.0 **(c)** at 800 nl per site showing opsin expression throughout striatum and in individual ChI cell bodies and processes. **(d,g)** Mean $[DA]_o$ ± SEM versus time evoked by 1 pulse or 4 pulses at 100 Hz electrical (E) stimulation with and without preceding light (L) inhibition of ChIs. $[DA]_o$ were recorded in dorsal CPu of Arch-injected mouse in complete GABA block (bicuculine, 10 µM; saclofen, 50 µM)**(d)** (N=1) or in drug-free conditions in eNpHR-injected mouse **(g)** (N=1). **(e,h)** Peak $[DA]_o$ of individual DA transients evoked with different stimulation protocols in dorsal CPu of Arch **(e)** or eNpHR **(h)** injected ChAT-Cre mice. Error bars are SEM. Evoked $[DA]_o$ was significantly different between different stimulation protocols (Two-way ANOVA, **p<0.01), but post-hoc Bonferroni t-tests were not significant. **(f,i)** The ratio of $[DA]_o$ evoked by 4 p electrical stimulation to that evoked by 1 p electrical stimulation with and without light-inhibition of Arch- **(f)** or eNpHR-expressing **(i)** ChIs 200 or 500 ms prior to electrical stimulus delivery was not significantly different (p>0.05; unpaired t-test).

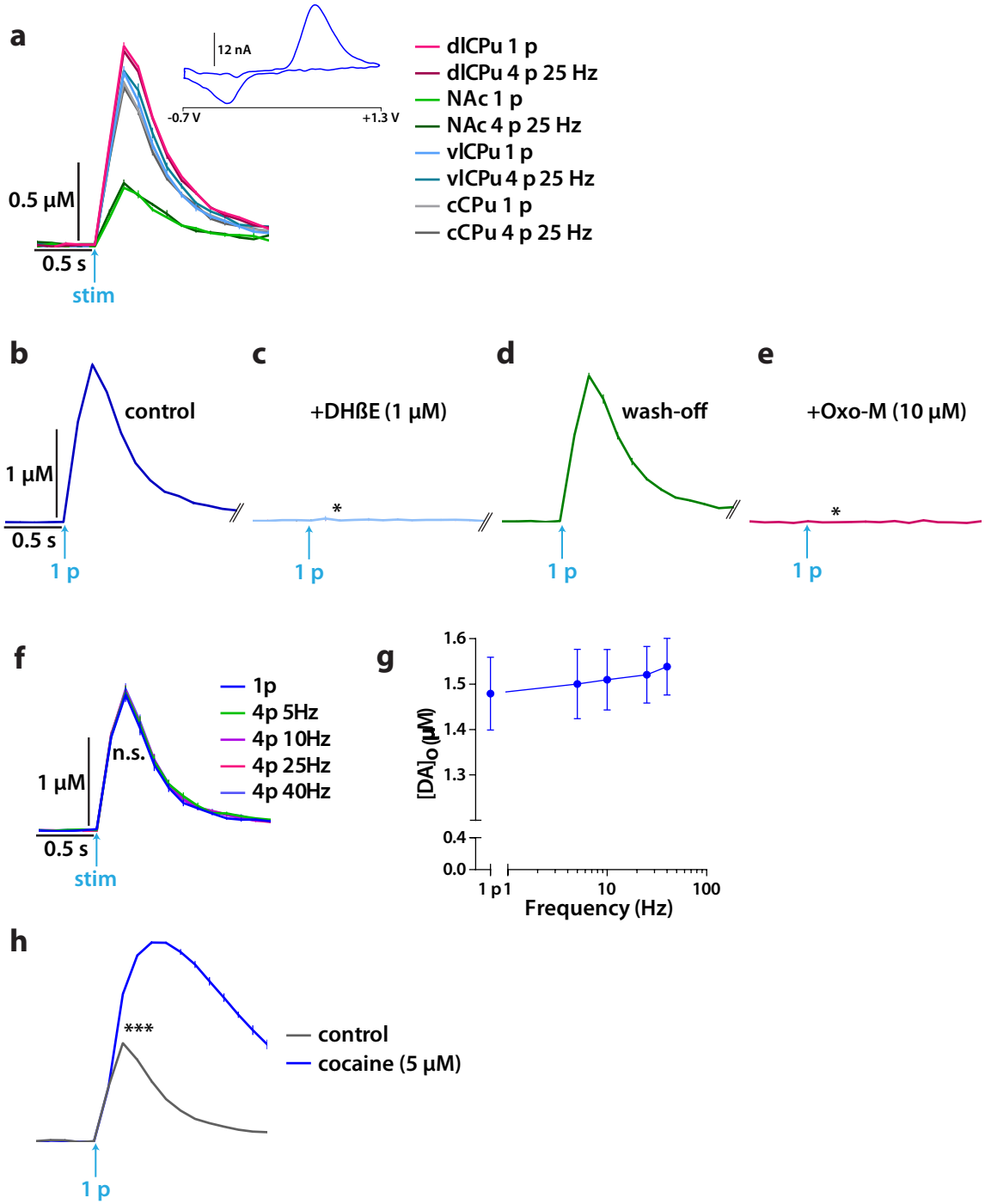

Figure 4.6 Light-evoked DA release is successfully triggered throughout dorsal and ventral striatum in ChAT-Cre rat following CPu injections of AAV2 ChR2 vector

(a) Mean $[DA]_o$ ± SEM versus time evoked by blue light stimuli of single pulse (1 p) or 4 pulses at 25 Hz (pulse widths 2 ms) across dorsal and ventral striatum in ChAT-Cre rat injected in CPu with AAV2 ChR2. **(b,c,d,e,f,h)** Mean $[DA]_o$ ± SEM versus time evoked by single pulse (1 p) or 4 pulse trains at 5, 10, 25 or 40 Hz blue light stimuli in CPu-injected ChAT-Cre rat, light evoked $[DA]_o$ recorded in dorsal CPu. **(b,c)** nAChR antagonist (DHßE, 1 µM) or **(d,e)** mAChR agonist (Oxo-M, 10 µM) applications abolished light-evoked $[DA]_o$ (Mann-Whitney, *p<0.05). **(c,d)** Upon nAChR antagonist wash-off light-evoked $[DA]_o$ returned to pre-drug baseline. **(f)** Light-evoked $[DA]_o$ was insensitive to stimulation frequency (one-way ANOVA, p>0.05). **(g)** Mean peak evoked $[DA]_o$ ± SEM versus stimulation frequency evoked by blue light single pulses and pulse trains of 4 pulses at 5-40 Hz showing that regardless of stimulation frequency light-evoked $[DA]_o$ were similar. **(h)** DAT inhibition (cocaine, 5 µM) significantly increased light-evoked $[DA]_o$ (Wilcoxon, ***p<0.001), increasing the amplitude and duration of the light-evoked DA transients.

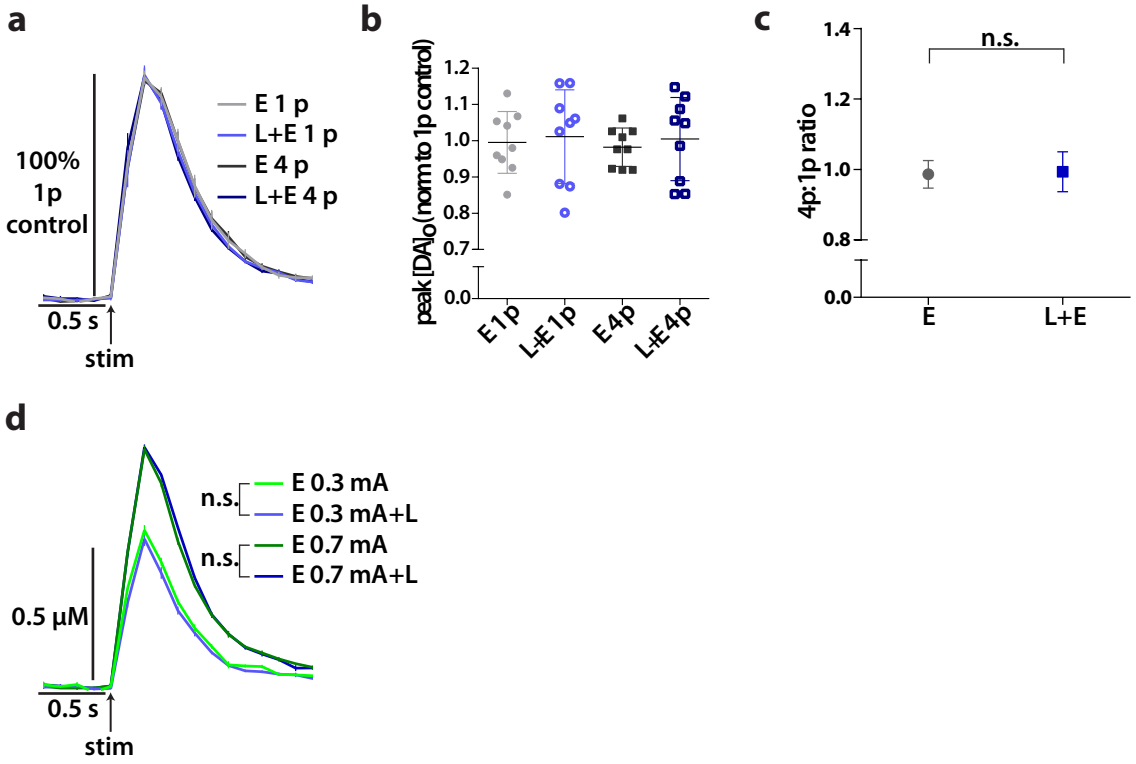

Figure 4.7 AAV2 ChR2-transduced brainstem cholinergic afferents do not drive light-evoked DA release in striatum and do not modulate electrically evoked $[DA]_o$ in ChAT-Cre rats
(a) Mean $[DA]_o$ ± SEM versus time evoked by single pulse (1 p) and high frequency burst (4 p at 100 Hz) electrical stimulation (E) with and without prior blue light (L) activation of ChR2-expressing striatal terminals originating in rostral PPN in ChAT-Cre rats injected with AAV2 ChR2. DA release was recorded in dorsal CPu (N=1). **(b)** Peak $[DA]_o$ of individual DA transients evoked with different stimulation protocols in dorsal CPu of ChAT-Cre rat injected with AAV2 ChR2 in rostral PPN. Error bars are SEM. Electrically evoked $[DA]_o$ was not significantly different between different stimulation protocols (Two-way ANOVA, $p>0.05$). **(c)** Ratio of $[DA]_o$ evoked by 4 p electrical stimulation to that evoked by 1 p electrical stimulation (4p:1p ratio) with and without light activation of ChR2-transduced brainstem afferents 500 ms or 1 s prior to electrical stimuli delivery was not significantly different ($p>0.05$; unpaired t-test). **(d)** Mean $[DA]_o$ ± SEM versus time evoked by single pulse electrical stimulation at 20% and 80% of maximal current response, 0.3 and 0.7 mA. Concurrent single blue light pulse (+L) delivery did not change electrically evoked $[DA]_o$ within a given current group (one-way ANOVA, $p>0.05$).

5. Investigation of mechanisms underlying striatal dopamine release deficits in a mouse model of Parkinson's disease overexpressing human wild type α-synuclein

5.1 Introduction

Unveiling mechanisms causing DA neuron degeneration is crucial for understanding PD aetiology and thus finding a cure. Animal models recapitulating human disease enable examination of PD pathology at different stages. Therefore, such models are a valuable resource for elucidating the earliest changes and/or pathological processes underlying final common pathway of DA neuron dysfunction. The *SNCA OVX* mouse is a new PD model developed by the Oxford Parkinson's Disease Centre and Wade-Martins group, first introduced in Chapter 1. These mice overexpress human wild type α-synuclein protein on mouse α-synuclein-knockout background and present with striatal DA release deficits from an early age (Janezic et al., 2013). Onset of evoked DA release deficits in the *SNCA OVX* line happens prior to SNc neuron loss or alterations in the firing rates of the midbrain DA neurons, which are only observed in aged mice around the time when motor deficits also become manifest (Janezic et al., 2013). Further, DA release deficits are not explained by decrease in striatal DA content or precursor enzymes (Janezic et al., 2013), suggesting impaired release is not the product of deficient transmitter synthesis or storage, but is the function of α-synuclein-dependent changes in transmitter handling. In this chapter I explore a few possible mechanisms which may underlie impaired DA release in the *SNCA OVX* line. In overview, the work presented here examines whether DA release deficits in the *SNCA OVX* mice compared to their age- and sex-matched *Snca -/-* littermate controls are due to a) changes in ACh receptor function (Sections 5.3.1 and 5.3.2), b) impaired DAT function (Sections 5.3.3.) or c) vesicle redistribution (Sections 5.3.4) following overexpression of human wild type α-synuclein.

5.1.1 Acetylcholine-dopamine balance in the *SNCA OVX* release deficits

SNCA OVX mice show impaired DA release in dorsal striatum from 3 months of age (Janezic et al., 2013). I used these mice to explore whether evoked DA deficits persist in the absence of local ACh influence, as dopaminergic dysfunction *per se* does not happen in isolation. Changes in DA transmission may stem from primary alterations in dopaminergic axon function following α-synuclein overexpression. However, profound influence of cholinergic system on regulation of striatal DA transmission suggests DA release deficits could also stem from underlying changes in ACh transmission.

Firstly, striatal ChIs dynamically gate DA release probability via nAChRs localized to dopaminergic terminals and mAChRs on ChIs (Rice and Cragg, 2004; Zhang and Sulzer, 2004; Exley et al., 2008; Threlfell et al., 2010). Synchronous ChI population activity can even drive ACh-evoked striatal DA release (Cachope et al., 2012; Threlfell et al., 2012). Therefore, primary changes in cholinergic tone can directly affect striatal DA transmission, and may plausibly underlie diminished DA release in the *SNCA OVX* line.

Secondly, DA itself robustly affects striatal ChI activity via D2- and D1-like receptors on ChIs. Changes in dopaminergic transmission may therefore alter cholinergic tone further affecting downstream regulation of DA by ACh. For example, acting at D2 receptors on ChIs (Yan et al., 1997), DA prolongs the duration of ChI pause, suppressing tonic activity and ACh release. D2-dependent reduction in Na^+ currents reduces the rate of spontaneous pacemaking activity in ChIs (Maurice et al., 2004), while D2-mediated inhibition of re-polarizing hyperpolarization-activated cation current I(h) prolongs the slow afterhyperpolarisation phase in ChI pause, delaying subsequent spiking (Deng et al.,

2007). D2 receptors can also reduce N-type Ca^{2+} channel activity thereby reducing the probability of ChI firing in response to afferent messages (Yan et al., 1997). Thus, D2 receptors exercise sustained negative control over ChI activity. Consistently, diminished ACh release follows systemic administration of a D2 agonist (DeBoer et al., 1996). Furthermore, pause induction in ChIs in dorsal striatum was shown to be directly mediated by DA acting at D2 receptors (Chuhma et al., 2014).

D1-like receptors could also prolong afterhyperpolarisation currents underlying ChI pause, possibly via enhancement of L-type Ca^{2+} conductance (Surmeier et al., 1995; Bennett and Wilson, 1998). Most likely, however, D1-like receptors, D5 subtype in particular (Yan et al., 1997), inhibit ChIs via negative regulation of RGS4-dependent signalling cascade by protein kinase A, which activates M_4 mAChRs which in turn autoinhibit ChI firing (Zhang et al., 2002a; Ding et al., 2006). DA could further modulate ChI activity via GABA. D1-like receptors potentiate Zn^{2+}-sensitive GABA currents in ChIs facilitating inhibition (Yan and Surmeier, 1997). DA can also indirectly affect GABA release via ChIs. By inhibiting ChI firing, thus ensuring the rapidly desensitizing nAChRs on fast-spiking parvalbumin-positive interneurons are in an active state, DA enables evoked GABA transmission to transiently halt further ACh release following a brief peak in ChI activity (Sullivan et al., 2008). The loss of negative feedback from the dopaminergic system can enhance ACh tone and/or alter spiking behaviour of ChIs. Correspondingly, DA depletion leads to emergence of synchronous oscillatory activity in ChI networks (Raz et al., 1996, 2001).

The above data agree with the PD phenomenon that as DA transmission decreases, ACh levels are on the rise (Lehmann and Langer, 1983). Prior to L-dopa

discovery, anticholinergic drugs were the main PD treatment; being particularly effective at alleviating tremor and are still used today (Pisani et al., 2007; Smith et al., 2012b). Notably, ACh-DA disequilibrium has supra-additive effects on striatal function, dysregulating balanced weighting of the incoming synaptic messages by MSNs and leading to aberrant BG output and plasticity. For instance, ACh can actively inhibit cortical drive of MSNs by decreasing glutamate release from cortical terminals (Higley et al., 2009). ChIs can also inhibit MSNS indirectly via activation fast-spiking parvalbumin-positive interneurons (Sullivan et al., 2008) and neuropeptide Y-expressing neurogliaform neurons (English et al., 2011), or even via recruitment of GABA release from DA terminals (Tritsch et al., 2012, 2014; Nelson et al., 2014b).

Therefore, deficient DA release in the dorsal striata of *SNCA OVX* mice could be the function of primary DA axis impairments, and/or be secondary to ACh-dependent mechanisms. The latter could either stem from primary changes in cholinergic transmission following α-synuclein overexpression, or be secondary to altered DA transmission which in turn changes ACh release rules, further affecting function of the striatal DA system. Evidence that there are changes to ACh axis in PD is presented below.

5.1.1.1 Nicotinic receptor changes in Parkinson's disease

Receptor binding assays from post-mortem human tissue detect reduction in nAChR signal in the caudate-putamen of PD patients (Rinne et al., 1991; Durany et al., 2000; Quik et al., 2004), although not all studies agree (Lange et al., 1993). The observed signal decrease, quantified as ~25% reduction in human (Durany et al., 2000) and ~50% reduction in MPTP-treated primates (McCallum et al., 2005), stems from a decline in receptor number, not changes in their binding properties (Rinne et al., 1991). Animal

studies employing 6-OHDA and MPTP lesions in rodents and primates, confirm selective loss of nAChR subtypes localized to dopaminergic terminals, in particular $\alpha6\beta2$- and $\alpha4\beta2$-containing subunits (Clarke and Pert, 1985; Zoli et al., 2002; Quik, 2003; McCallum et al., 2005). Thus, nigral degeneration also results in striatal nAChR loss. In PD, loss of nAChRs is also detectable in hippocampus and prefrontal cortex, underscoring the role of changes in cholinergic transmission in cognitive decline in this patient group (Calabresi et al., 2006).

The decline in striatal nAChR number could have wide-ranging consequences. In the light of nAChRs driving DA release (Cachope et al., 2012; Threlfell et al., 2012), nAChR loss could contribute to progressively falling DA release, an effect synergistic to the overall decline in nigrostriatal innervation. This prediction is consistent with greater impairment of habitual motor behaviours observed in advanced PD (Hadj-Bouziane et al., 2012). Preferential loss of DA innervation is observed in the sensorimotor striatum, corresponding to caudal putamen in human and dorsolateral striatum in rodent (Yin and Knowlton, 2006; Balleine and O'Doherty, 2010). Yet, the associative striatum, corresponding to head of caudate nucleus in human and dorsomedial striatum in rodent (Yin and Knowlton, 2006; Balleine and O'Doherty, 2010), while showing loss of DA innervation also has the highest ChI density, at least in human (Bernácer et al., 2007). Consequently, goal-directed behaviours governed by the associative regions could be spared more due to compensatory adaptations provided by the cholinergic system.

Of course, if the decline in nAChR number is due to degeneration of nAChR-expressing DA terminals, the possibility of cholinergic-mediated compensatory changes is meaningless. Yet, no time-matched comparisons of the extent of SNc neuronal loss

and decline in nAChR number exists. There are human PD studies showing 80-90% decrease in striatal DAT expression, while decline in nAChR number is on the order of 50-60% (Quik et al., 2004). These data argue that the lost nAChRs are only partly localized to degenerating DA terminals, and this is consistent with nAChRs being found on other structures, including parvalbumin-positive interneurons (Sullivan et al., 2008). Further, it is also possible that the surviving DA axons upregulate nAChR expression. Thus, the remaining nAChRs could still aid dopaminergic function, even if indirectly. Extensive spread of dopaminergic axonal arbours in a lattice-like arrangement throughout the striatum (Descarries et al., 1996; Moss and Bolam, 2008; Matsuda et al., 2009) and extrasynaptic ACh and DA spill-over would enable propagation of signals through the broad axonal DA network even with a few remaining axons having a large sphere of influence.

I examined whether underlying deficits in DA axons manifest as impaired DA release in dorsal striatum in the *SNCA OVX* line were explained by a cholinergic mechanism. This hypothesis was assessed by examining evoked DA levels in the absence of local ACh influence in 3-4 months-old *SNCA OVX* and *Snca -/-*mice (Section 5.3.1). This age group was chosen because 3 months-old young adult *SNCA OVX* mice already present with DA release deficits in dorsal striatum (Janezic et al., 2013).

5.1.1.2 Muscarinic receptor changes in Parkinson's disease

Radiography studies of PD post-mortem brains reveal ~30% reduction in M_2-class mAChR expression in dorsal caudate-putamen, consistent with findings from 6-OHDA lesioned rats (Joyce, 1991, 1993). M_2-class mAChRs are found throughout the striatum (Zhang et al., 2002b; Zhou et al., 2003). Data show some M_4 mAChR localization to MSNs

(Weiner et al., 1990; Levey et al., 1991; Santiago and Potter, 2001; Yan et al., 2001; Wang et al., 2006). Yet, ChIs have the highest expression levels of both M_2 and M_4 mAChR subtypes (Yan and Surmeier, 1996; Alcantara et al., 2001; Ding et al., 2006). Therefore, alterations in M_2-class mAChR expression following dopaminergic denervation are likely ChI-related. These changes, for example, could stem from loss of trophic factor signalling from degenerating SNc neurons to ChIs causing selective apoptosis of the latter (Gonzalez-Reyes et al., 2012), or stem from a decrease in mAChR expression.

Postsynaptic M_2 and M_4 mAChRs on ChIs (Levey et al., 1991; Hersch et al., 1994; Yan and Surmeier, 1996), constitute an autonomous feedback circuit negatively regulating striatal ACh release. mAChRs can directly trigger inhibitory post-synaptic potentials in ChIs or even silence them (Calabresi et al., 1998; Bonsi et al., 2008), following ACh binding to the upper half of mAChR trans-membrane domain (Wess et al., 1995). This negative regulation happens via Ca^{2+} currents reduction at Cav2.1 and Cav2.2 channels (Yan and Surmeier, 1996), which in turn regulate afterhyperpolarisation duration via re-polarizing potassium channels (SK) (Goldberg and Wilson, 2005). Thus, inhibition of Ca^{2+} currents at CaV2.2 channels by reducing SK channel activity reduces afterhyperpolarisation duration, promoting irregular spiking in ChIs (Ding et al., 2006). Consequently, reduction in mAChR expression could significantly compromise cholinergic autofeedback system.

Loss of M_2-class receptors need not be the sole process underlying cholinergic transmission changes. Subtle alterations in mAChR function, such as dysregulation of the signalling cascades employed by or regulating the activity of M_2-class receptors could

also arise following dopaminergic denervation. For example, DA depletion could trigger upregulation of RGS4 signalling in ChIs, leading to attenuation of M_2-class receptor function (Ding et al., 2006). There is also some data suggesting that signalling via glycoprotein Sonic hedgehog from DA neurons to ChIs could regulate RGS4 activity via protein kinase A engagement (Gonzalez-Reyes et al., 2012). Together, these findings point to dysregulation in G protein-dependent coupling between receptors and effectors at mAChRs following decline in nigrostriatal dopaminergic transmission resulting in decreased cholinergic autoinhibition.

The above data suggest that mAChR function could be altered in aged *SNCA OVX* mice, given the evidence for SNc neuronal loss in this model at 18 months and DA release deficits from 3 months onwards (Janezic et al., 2013). This hypothesis was evaluated by examining mAChR function in 18-26 months-old aged *SNCA OVX* and *Snca -/-* mice (Section 5.3.2). This age group was chosen because at this time point the *SNCA OVX* line presents with both SNc dopaminergic cell loss and reduced striatal DA release, thus changes in mAChR function are likely to be unveiled then.

5.1.2 Vesicle dysregulation hypothesis of a-synuclein-dependent dopamine dysfunction

Aberrantly high α-synuclein levels could also lead to DA neuron dysfunction via interference with vesicle handling processes. The family of synuclein proteins, comprising three highly homologous isoforms, α-, β-, and γ-synuclein (Maroteaux and Scheller, 1991), is expressed ubiquitously throughout the central and peripheral nervous systems in both human and rodent (Iwai et al., 1995; Li et al., 2002; Vivacqua et al., 2011; Mollenhauer et al., 2012). Expression of α-synuclein is localized to presynaptic

terminals and other cellular sub-compartments, including the nucleus, with a divergent expression pattern in different brain regions (Iwai et al., 1995; Kahle et al., 2000; Li et al., 2002; Mori et al., 2002; Totterdell and Meredith, 2005; Yu et al., 2007; Zhang et al., 2008; Vivacqua et al., 2011). Further, α-synuclein is associated with curved membranes of specific curvature, and in particular vesicles of small diameter (~25 nm) (Davidson, 1998; Westphal and Chandra, 2013). Presynaptic localization of α-synuclein points to its involvement in transmitter release, yet physiological role of α-synuclein remains undetermined.

The neurotransmitter release function of α-synuclein was initially inferred from localizing its expression to distal reserve pool of synaptic vesicles. Researchers hypothesized interaction with actin microfilaments being a mechanism for α-synuclein participation in release events (Lee et al., 2008; Bellani et al., 2010). Later studies demonstrated α-synuclein involvement in continuous SNARE complex assembly (Burré et al., 2010; Garcia-Reitböck et al., 2010) and promotion of vesicle accumulation at the active zone (Diao et al., 2013). Functionally, α-synuclein participation in vesicle handling is supported by studies showing global α-synuclein overexpression or knockout alters vesicle clustering and/or mobilization, in particular affecting DA releasability (Abeliovich et al., 2000; Yavich et al., 2004; Senior et al., 2008; Anwar et al., 2011; Janezic et al., 2013). Aberrant α-synuclein levels/species also lead to changes in synaptic transmission and plasticity (Cabin et al., 2002; Watson et al., 2009; Kurz et al., 2010; Diógenes et al., 2012). At the synapse, however, α-synuclein acts as a supplementary chaperone-like component maintaining long-term synaptic homeostasis (Chandra et al., 2004, 2005; Burré et al., 2010), rather than being essential for vesicle release *per se*.

Given the decrease in evoked DA levels in *SNCA OVX* mice, the topical question is whether deficits are due to α-synuclein-dependent changes in vesicle handling processes. With no evidence for reduced DA tissue content or availability of precursors such as TH in *SNCA OVX* mice (Janezic et al., 2013), a process other than transmitter synthesis and storage is involved. Thus, impaired DA release could stem from a decrease in the readily releasable and/or recycling vesicle pool sizes brought about by impaired vesicle re-clustering following endocytosis, or even by dispersion of endocytosed vesicles away from the active zone mediated by α-synuclein (Nemani et al., 2010). Considering that the functional role of α-synuclein in SNARE complex assembly is distinct from its pathological role (Burre et al., 2012), it is possible that vesicle cycling processes other than vesicle fusion with the presynaptic membrane are involved.

5.1.2.1 The timecourse of vesicle recruitment in the *SNCA OVX* model

While the EM data from *SNCA OVX* mice demonstrate an increase in DA vesicle clustering in the SNc terminals, there appears to be no overall change in the vesicle distance from the active zone or vesicle density/number (Janezic et al., 2013). Thus, the prediction about vesicle dispersal away from the release sites does not hold true. Yet, impaired DA release could also stem from increased vesicle clustering at axon terminal level. Dense vesicle clustering could change the timecourse of vesicle recruitment to the release sites, possibly due to increased mechanical force required for tethering of tightly juxtapositioned vesicles to the active zone. Thus, the *SNCA OVX* dopaminergic deficits may be due to impaired initial release, with densely clustered vesicles taking longer to be engaged to their respective docking sites. However, once recruited, increased vesicle clustering could better support sustained transmitter release during long synaptic depolarisations. Thus, it was predicted that sustained $[DA]_o$ could be different between

SNCA OVX and *Snca -/-* mice, and this hypothesis was evaluated by using long electrical pulse train stimulations lasting up to 1 s to potentially enable examination of the timecourse of DA vesicle recruitment to the release sites (Sections 5.3.4). These experiments were performed in 7-10 months-old mice, this age group was chosen as an intermediate age point between young (3-4 months) and old age (18-26 months).

5.1.3 Protein-protein interactions underlying impaired dopamine release: dopamine transporter and α-synuclein

Dopaminergic dysfunction precipitated by α-synuclein overexpression could emerge from changes in vesicle handling processes. Yet, DA neurons also express DAT, which directly interacts with α-synuclein, and consequently α-synuclein overexpression could alter release dynamics via DAT. DAT activity is essential for DA uptake from the extracellular space into the pre-synaptic neurons using Cl^-/Na^+ gradients (Amara and Kuhar, 1993; Gu et al., 1994). Beside prompt clearing of transmitter and termination of DA signal, DAT-mediated endocytosis supplies the recycling pool of vesicles with DA (Rizzoli and Betz, 2005; Wu and Wu, 2009). This ensures reliable transmitter release over time by providing the readily-releasable pool with recycled material, avoiding transmitter stores depletion during sustained neuronal firing. Changes in DAT could also cause a decrease in striatal DA release via a number of routes. Increased DAT activity would prematurely terminate DA signals via increased DA clearance, thus limiting the sphere of DA influence. Decreased DAT function could also impair evoked DA release, but this time via reduction in quantal size as vesicle loading with DA would be impaired.

Alpha-synuclein was found to directly interact with DAT via protein-protein complex formation upon its binding to the DAT C-terminus between residues 606-617

(Lee et al., 2001; Wersinger et al., 2003). The physiological relevance of DAT and α-synuclein interaction is unknown, although data suggest it could be detrimental to DA neurons. Specifically, formation of the DAT-α-synuclein complex may increase neuronal apoptosis (Lee et al., 2001), possibly via alterations in plasma membrane localization/activity of the transporter itself. However, the data regarding DAT localization changes upon α-synuclein binding are contradictory. Some studies find increased transporter availability at the cell surface (Lee et al., 2001), while others observe dynamic trafficking of DAT to the cytosol (Wersinger and Sidhu, 2003; Wersinger et al., 2003). Although the conflicting observations may arise from different transfection methods, both studies predict that α-synuclein can influence DAT. In particular, it appears that DAT availability could be altered by interaction with α-synuclein, although no FCV data collected to date hints at impaired DAT function in the *SNCA OVX* line (Anwar et al., 2011; Janezic et al., 2013). However, RNA knockdown of α-synuclein in cell lines results in decreased DAT activity and reduced toxicity of MPTP (Fountaine and Wade-Martins, 2007). Overall, an additional mechanism for disruption of dopaminergic transmission by α-synuclein overexpression may lie in its ability to modify DAT function.

5.1.3.1 CaMK2 inhibition as a tool for assessing the impact of α-synuclein on DAT function

Co-immunoprecipitation pull-down assays in addition to highlighting the interaction between α-synuclein and DAT (Lee et al., 2001; Wersinger et al., 2003), also established that calcium calmodulin kinase 2 (CaMK2) binds DAT in the same region as α-synuclein (Fog et al., 2006). Importantly, both CaMK2 and α-synuclein are expressed in midbrain dopaminergic neurons and their expression co-localizes with DAT (Kamata et

al., 2006; Bellucci et al., 2011). In particular, among the CaMK2 isoforms, SNc neurons widely express only γ and δ, and traces of β can also be found, while CaMK2α is not expressed in the SNc neurons (Kamata et al., 2006).

CaMK2 changes DAT membrane trafficking and other transporter properties by changing the phosphorylation status of DAT. DAT phosphorylation by CaMK2 enhances DA uptake in synaptosomal preparations (Uchikawa et al., 1995; Page et al., 2004), while inhibition of CaMK2 decreases DAT-mediated transmitter uptake in an activity-dependent manner (Padmanabhan et al., 2008). Thus, transient Ca^{2+} oscillations arising from AP firing regulate DAT molecule availability via CaMK2 signalling (Padmanabhan et al., 2008; Padmanabhan and Prasad, 2009). Given that the binding sites for α-synuclein and CaMK2 on DAT overlap, it is possible that the effects of CaMK2 inhibition on DAT function will be differentially regulated between the *SNCA OVX* and *Snca -/-* lines due to α-synuclein overexpression in the former. I hypothesised that inhibiting CaMK2 activity could reveal an underlying changes in DAT function in *SNCA OVX* compared to *Snca -/-* mice. This hypothesis was tested by pre-incubating slices from 3-4 months-old *SNCA OVX* and *Snca -/-* mice with CaMK2 inhibitor following preparation of slices for FCV, and subsequent assessment of DA release dynamics with and without DAT inhibition (Section 5.3.3).

5.1.4 Summary

Work presented in this chapter investigates the functional state of the cholinergic system in relation to previously described DA release deficits revealed by electrically evoked transients in dorsal striatum of *SNCA OVX* mice. In addition, using long pulse train stimulations I explore the possibility of sustained DA release differences,

and consequently potential changes in the timecourse of vesicle recruitment to the release sites, between *SNCA OVX* and *Snca -/-* lines. I also explore whether α-synuclein-mediated changes in DAT function underlie impaired DA release following a-synuclein overexpression.

5.2 Methods

Methods used were as described in Chapter 2, unless otherwise stated here.

5.2.1 Animals

Transgenic α-synuclein mice were created in the Wade-Martins laboratory using BAC technology. Briefly, pronuclei from C57Bl6/J mouse were injected with 135kb BAC DNA containing full human wild-type *SNCA* gene locus, flanked by endogenous promoter sequence. Resulting lines where stable BAC integration was confirmed by fluorescence *in situ* hybridization were backcrossed for nine generations onto mouse α-synuclein knockout line on C57Bl6/J background to create a mouse overexpressing human α-synuclein in the absence of mouse α-synuclein (Janezic et al., 2013). The *SNCA OVX* mice express human α-synuclein at 1.9 times the level of endogenous mouse α-synuclein in a C57Bl6/J mouse (Janezic et al., 2013). Age and sex-matched littermate *SNCA OVX* and *Snca -/-* mice were used in all experiments. 3-4 months-old pairs were used for examination of nAChR function in paired recording experiments. 18-26 months-old aged mice were used for characterization of mAChR function. 7-10 months-old mice were used for assessment of sustained DA properties. Finally, 3-4 months-old mice were also used for assessing DAT function in pilot CaMK2 inhibition experiments. N is the number of animals used for experimentation, and n is the total number of observations.

5.2.2 Experimental design

5.2.2.1 Nicotinic receptor function

nAChR involvement in DA release deficits in *SNCA OVX* versus *Snca -/-* mice was assessed by sampling evoked DA release in the presence of nAChR antagonist (DHβE, 1 μM), to remove any modulatory effects exercised by the cholinergic system on

nigrostriatal DA circuits via nAChRs. Specifically, I assessed concentrations of DA released directly via activation of striatal DA terminals. Recordings were acquired from both genotypes on the same day to ensure the comparison of the absolute DA concentrations is not affected by possible differences in CFM sensitivity or recording conditions, such as bath temperature fluctuations. DA release was sampled in 6 sites in the dorsal striatum (CPu), namely dorsomedial (dmCPu), dorsomidline (dmidCPu), dorsolateral (dlCPu), central (cCPu), ventromedial (vmCPu) and ventrolateral (vlCPu), and in 2 sites in the NAc core. Stimulation protocol comprised 3 stimulations separated by 2.5 min intervals that consisted of 1 pulse, 4 pulses at 100 Hz and 1 pulse. The peak evoked $[DA]_o$ following first and third 1 p stimulation were averaged to produce mean peak 1 p values for the 4p:1p ratio comparisons. Each stimulation sequence was delivered once per recording site, alternating the genotype and the site the recordings were acquired from. In the dlCPu and NAc core frequency response was also sampled by 4 pulse train stimulations at variable stimulation frequencies (5 Hz, 10Hz, 25 Hz, 40 Hz, 100 Hz) repeated once.

The data from these multi-site sampling experiments are absolute concentrations, in µM, of electrically evoked extracellular DA ($[DA]_o$). The recorded $[DA]_o$ transients were grouped together according to the stimulation protocol (1p vs. 4p) and the region of interest (CPu vs. NAc) for averaging and statistical analyses. The average transients represent the mean±SEM of single traces recorded from 9 different animals per genotype (N=9 per genotype). For statistical comparisons the mean peak evoked $[DA]_o$ values were used. The data were analysed using unpaired t-tests or two-way ANOVA, after normal data distribution was confirmed with Shapiro-Wick's test of normality.

5.2.2.2 Muscarinic receptor function

mAChR function in *SNCA OVX* versus *Snca -/-* mice was assessed by application of sequentially increasing concentrations of muscarinic agonist (Oxo-M, 0-10 µM). The following drug concentrations were used for dose-response curve: control (no drug), 60 nM, 100 nM, 600 nM, 1 µM, 10 µM. Low (1 pulse) and high (4 pulses at 100Hz) stimulation frequencies were employed as mAChR activation alters DA release in a frequency-sensitive manner, similar to antagonism of nAChRs (Threlfell et al., 2010). After the final Oxo-M dose application (10 µM), an additional nAChR antagonist dose (DHβE, 1 µM) was applied to assess whether the maximal Oxo-M effect was reached, as DHβE will prevent actions of any remaining ACh. All recordings were performed in the dlCPu. Different genotypes were used for experiments on different days, as the data are normalised to control (1p stimulation in drug-free condition) within each genotype for each experiment. Consequently, any day-to-day variation in CFM sensitivity which affects absolute concentrations is not critical here.

Due to progressive decrease in electrically evoked $[DA]_o$ over time in a given recording site (i.e. site decline) in old animals in particular, only a subset of drug concentrations was applied within any given experiment (60 nM, 600 nM, 10 µM or 100 nM, 1 µM, 10 µM). This was done to ensure that drug wash-on time and recording duration did not compromise data quality by bringing evoked $[DA]_o$ levels below CFM detection threshold. A total of 10 mouse pairs were used (N=10 per genotype), and where possible recordings from 2 different slices per animal were acquired (total recording sites=16 *SNCA OVX*; total recording sites=19 *Snca -/-*). Averaged $[DA]_o$ transients represent the mean±SEM of at least 3 evoked $[DA]_o$ traces per animal per slice per stimulation frequency for each drug concentration used. The data were analysed

using single-phase exponential decay and sigmoidal dose-response curve-fitting functions, unpaired t-test and two-way ANOVA.

5.2.2.3 Dopamine transporter experiments

For the α-synuclein-DAT interaction experiments, a selective inhibitor of CaMK2 (KN-62, 5 µM) with no known off-target effects on L-type Ca^{2+} channels, unlike KN-93 variant (Gao et al., 2006), was used. Slices were pre-incubated in KN-62 (5 µM) prior to recordings, and it was subsequently bath-applied throughout at 5 µM. Evoked $[DA]_o$ properties were assessed in the presence and absence of DAT influence. First, $[DA]_o$ was evoked by single pulse (1 p) and high frequency bursts of 4 pulses at 100 Hz (4 p 100 Hz) stimulations. The frequency sensitivity was then probed using 4 pulse trains at 5 Hz, 10Hz, 25 Hz, 40 Hz and 100 Hz. Secondly, the same protocols were repeated following bath application of DAT inhibitor (cocaine, 5 µM). All recordings were performed in the dlCPu. Slices from different genotypes were used on different days as data were normalised to 1 p control within a genotype for each experiment. A total of 4 *SNCA OVX* (N=2) and *Snca -/-* (N=2) mice were used. The averaged $[DA]_o$ transients represent the average of 4 $[DA]_o$ traces per animal per recording site, 2 slices were recorded from in each animal (total recording sites=4 per genotype). For statistical comparisons the mean peak $[DA]_o$ values were used. Data were statistically analysed using two-way ANOVA.

5.2.2.4 Sustained dopamine release properties

Sustained $[DA]_o$ in *SNCA OVX* versus *Snca -/-* mice was examined in the presence of D2 receptor antagonist (L-741,626, 1 µM). It was bath-applied throughout the experiment to eliminate any contribution from D2 receptors, which have the capacity to limit DA release during prolonged stimulation (Phillips et al., 2002; Wu et al., 2002;

Moquin and Michael, 2009; Anzalone et al., 2012), and to ensure that the recorded differences did not stem from regional variability in dopaminergic autofeedback. Changes in sustained DA release between *SNCA OVX* and *Snca -/-* mice could reflect changes in handling of vesicle pools following α-synuclein overexpression. $[DA]_o$ was evoked with single pulse stimulations and trains of 20 pulses at 20 Hz in three striatal regions, dlCPu, cCPu and vmCPu. The long stimulation protocol was adopted as changes in vesicle handling may not be apparent in discrete stimulation protocols using single pulse stimulation or short pulse bursts at high frequency. Different genotypes were used for experiments on different days as data is normalised to 1p control condition within a genotype for each experiment. Averaged $[DA]_o$ transients represent the mean±SEM of at least 4 $[DA]_o$ traces per animal per recording site. Recording were acquired in 4 different animals per genotype, 2 slices were recorded from in each animal (N=4, total recording sites=8 per genotype). For statistical comparisons the mean peak $[DA]_o$ values were used. The data were statistically analysed using single-phase exponential decay curve-fitting functions and two-way ANOVA.

5.2.3 Drugs

Oxo-M, L-741,626 and KN-62 were purchased from Tocris Bioscience or Ascent Scientific. Cocaine, DHβE and all other chemicals were purchased from Sigma-Aldrich. All solutions were prepared using distilled and de-ionized water. Drugs were dissolved in distilled water or DMSO (L-741,626; KN-62) to make stock aliquots at 1000-10000× final concentrations and stored at -20°C. The drug stocks were diluted in oxygenated aCSF from frozen aliquots immediately before use and were bath applied.

5.3 Results

5.3.1 nAChR modulation of *SNCA OVX* dopamine release deficits

5.3.1.1 Dopamine release deficits in dorsal striatum of *SNCA OVX* mice are not explained by changes in cholinergic tone at nAChRs

DA release deficits in *SNCA OVX* mice could stem from changes in ACh tone at nAChRs. I investigated whether abolishing ACh action at nAChRs would change evoked $[DA]_o$ compared to previously reported data where ACh axis was not manipulated (Janezic et al., 2013). Experiments sampling electrically evoked $[DA]_o$ from multiple striatal regions were conducted here in the presence of nAChR antagonist (DHβE, 1 μM). Mean $[DA]_o$±SEM evoked by single pulse (Figure 5.1a-b) or high frequency burst (4 pulses at 100 Hz) (Figure 5.2a-b) stimulations in dorsal (CPu) and ventral (NAc) striatum of *SNCA OVX* and *Snca -/-* mice were plotted versus time, with a breakdown of evoked $[DA]_o$ profiles within 6 sampling sites in CPu and 2 sites in NAc core (Figure 5.1c, 5.2c).

SNCA OVX mice had significantly lower single pulse evoked $[DA]_o$ compared to *Snca -/-* line in CPu ($t=2.49$ $df=106$; $p=0.014$, two-tailed; unpaired t-test; Figure 5.1a). Mean peak evoked $[DA]_o$±SEM in CPu was 1.49±0.08 μM (n=54) for *SNCA OVX* line and 1.80±0.10 μM (n=54) for *Snca -/-* line. The difference in single pulse evoked $[DA]_o$ in NAc core was not statistically significant ($t=1.84$ $df=34$; $p=0.075$, two-tailed; unpaired t-test; Figure 5.1b). However, the mean peak evoked $[DA]_o$ in NAc was lower in *SNCA OVX* line 1.26±0.13 μM (n=18) compared to *Snca -/-* mice 1.60±0.14 μM (n=18). Single pulse evoked $[DA]_o$ in the *SNCA OVX* mice compared to *Snca -/-* littermates was on average 16% lower in the CPu and 21% lower in the NAc.

p=0.013) and recording site (F(5,96)=4.54, p=0.000), but no interactions (F(5,96)=1.26, p=0.287). Post-hoc Bonferroni t-tests showed that dlCPu in particular was the main region contributing to significantly lower evoked $[DA]_o$ in *SNCA OVX* compared to *Snca -/-* mice ($p<0.05$) (Figure 5.1c,e). Likewise, for the high frequency burst data, the mean peak evoked $[DA]_o$ were overall significantly lower in the *SNCA OVX* compared to *Snca -/-* line, while in vmCPu *SNCA OVX* presented with better evoked DA release than *Snca -/-* line. Two-way ANOVA revealed the main effect of genotype (F(1,96)=4.80, p=0.031) and recording site (F(5,96)=2.53, p=0.034), but no interactions (F(5,96)=0.96, p=0.445) (Figure 5.2c,e). Post-hoc Bonferroni comparisons showed no single sampling region to be the main driver of the overall difference in evoked $[DA]_o$ between *SNCA OVX* and *Snca -/-* mice with high frequency burst stimulation protocol ($p>0.05$). In CPu sampling sites across both low and high stimulation frequencies dlCPu and dmidCPu always had the largest percentage difference between *SNCA OVX* and *Snca -/-* lines, with 20-34% reduction in *SNCA OVX* compared to *Snca -/-* littermate controls (Figure 5.1e, 5.2e). Thus, deficits in evoked $[DA]_o$ in the *SNCA OVX* line compared to *Snca -/-* in the absence of ACh tone at nAChRs were present at low and high stimulation frequencies, with dlCPu in particular contributing to the overall decline in evoked $[DA]_o$ in dorsal striatum of *SNCA OVX* mice.

Quantification of the electrically-evoked $[DA]_o$ in both dorsal (CPu) and ventral striatum (NAc) at low (1 p) and high (4 p 100 Hz) stimulation frequencies showed an overall 16% reduction in the *SNCA OVX* compared to *Snca -/-* (Figure 5.1d, 5.2d). For single pulse stimulation the mean peak evoked $[DA]_o$ was significantly different between *SNCA OVX* and *Snca -/-* lines. Two-way ANOVA revealed the main effect of genotype (F(1,140)=6.68, p=0.011), and post-hoc Bonferroni comparisons showed that in dorsal

striatum in particular the *SNCA OVX* line had significantly lower evoked $[DA]_o$ than *Snca -/-* controls ($p<0.05$) (Figure 5.1d). For high frequency burst stimulation two-way ANOVA revealed the main effect of genotype ($F(1,140)=4.82$, $p=0.030$), but post-hoc Bonferroni t-tests were not significant, revealing that the mean peak evoked $[DA]_o$ was overall significantly lower in *SNCA OVX* compared to *Snca -/-* mice, but not for any given region alone ($p>0.05$) (Figure 5.2d).

5.3.1.3 Release deficits are present regardless of stimulation protocol, but frequency sensitivity and dynamic gating of dopamine release probability in the absence of nAChR tone is similar between *SNCA OVX* and *Snca -/-* lines

To test whether DA release deficits in *SNCA OVX* line were stimulation frequency dependent, all peak evoked $[DA]_o$ were normalized to single pulse mean peak $[DA]_o$ from *Snca -/-* line. Two-way ANOVA on these data revealed the main effect of genotype ($F(1,96)=26.11$, $p<0.0001$) and stimulation frequency ($F(5,96)=19.92$, $p<0.0001$), but no interactions ($F(5,96)=0.56$, $p=0.728$) in the dlCPu (Figure 5.3a). Thus, overall evoked $[DA]_o$ was significantly lower in *SNCA OVX* than *Snca -/-* mice in dlCPu. Post-hoc Bonferroni comparisons showed that in particular the difference between *SNCA OVX* and *Snca -/-* was significant at 100 Hz stimulation ($p<0.01$). For the NAc core data, two-way ANOVA revealed the main effect of genotype ($F(1,96)=5.38$, $p=0.023$) and stimulation frequency ($F(5,96)=7.24$, $p<0.0001$), but no interactions ($F(5,96)=0.23$, $p=0.951$) (Figure 5.3b), suggesting overall lower evoked $[DA]_o$ in *SNCA OVX* than *Snca -/-* mice. Post-hoc Bonferroni t-tests, however, showed no significant difference for individual frequency groups ($p>0.05$). Therefore, evoked DA release deficits in the *SNCA OVX* line compared to *Snca -/-* mice were present irrespective of stimulation protocol in the absence of ACh tone at nAChRs. Further, two-way ANOVA on a larger number of data points was able to

detect the overall statistically significant reduction in evoked $[DA]_o$ in the NAc of *SNCA OVX* mice (6 frequencies, 9 data points in each group).

The frequency sensitivity of electrically evoked $[DA]_o$ reflects dynamic gating of DA by mechanisms that govern DA release probability (Pr), including cholinergic mechanisms, and other factors that will include summation of individual DA release events, clearance of DA by uptake and D2 receptor-dependent release autoinhibition. Typically, low Pr corresponds to high frequency sensitivity, while high Pr translates to low frequency sensitivity of transmitter release events. For dopaminergic system, therefore, frequency can be used as a read-out of Pr. I examined whether underlying changes to DA Pr in the absence of ACh influence contributed to DA release deficits by comparing the ratio of $[DA]_o$ evoked following 4 p 100 Hz stimulation to $[DA]_o$ evoked following 1 p stimulation (4p:1p ratio). The 4p:1p ratios were similar between genotypes for both CPu 2.87±0.14 vs. 2.76±0.18 for *SNCA OVX* vs. *Snca -/-*, and NAc 2.88±0.35 vs. 2.78±0.33 for *SNCA OVX* vs. *Snca -/-*, as revealed by two-way ANOVA showing no significant main effect of either recording site ($F(1,68)=0.002$, $p=0.9641$) or genotype ($F(1,68)=0.15$, $p=0.7047$) (Figure 5.3c). These data suggest that DA release probability was unaltered in the *SNCA OVX* compared to *Snca -/-* mice in the absence of cholinergic transmission.

Finally, I examined whether frequency sensitivity of electrically evoked $[DA]_o$ was altered in the *SNCA OVX* line compared to *Snca -/-* across full range of stimulation frequencies. Data were normalized to the mean peak $[DA]_o$ values evoked with single pulse stimulation within each genotype. Showing frequency sensitivity in the presence of nAChR blockade, the mean peak evoked $[DA]_o$ was nonetheless not significantly different

between genotypes within a given frequency group both in the dlCPu and NAc core. Two-way ANOVA analyses revealed the main effect of stimulation frequency ($F(5,96)=19.20$, $p<0.0001$), but not genotype ($F(1,96)=0.02$ $p=0.877$) in the dlCPu (Figure 5.3d). Similarly, for the NAc core two-way ANOVA showed the main effect of stimulation frequency ($F(5,96)=6.91$, $p<0.0001$), but not genotype ($F(1,96)=1.58$, $p=0.212$) (Figure 5.3e). Together these data show that frequency sensitivity of electrically evoked $[DA]_o$ in the absence of nAChR influence is not altered in the *SNCA OVX* mice compared to *Snca -/-* controls in both dlCPu and NAc core sampling sites, further suggesting no change in DA Pr in young adult mice following α-synuclein overexpression.

5.3.2 mAChR function in aged *SNCA OVX* mice

5.3.2.1 *SNCA OVX* mice present with exaggerated decline in evoked $[DA]_o$ over time

Research indicates that a decrease in mAChR activity could follow DA depletion (Ding et al., 2006; Gonzalez-Reyes et al., 2012). To address this, mAChR function was assessed in aged 18-26 months *SNCA OVX* and *Snca -/-* mice with sequential application of increasing mAChR agonist concentrations (Oxo-M, max 10 μM). In these experiments achieving steady evoked $[DA]_o$ sustainable over time proved difficult. Site decline characterized by progressive decline in evoked $[DA]_o$ with time was problematic for data acquisition prior to the first drug dose application, particularly in the *SNCA OVX* line. Because the plateau in evoked $[DA]_o$ were reached at different time points in different experiments, the protocol was set over time rather than anchored to recordings acquired after steady state in evoked $[DA]_o$ was reached. This step was taken to

minimize compromising of the data quality, as Oxo-M application leads to further decrease in evoked $[DA]_o$ and thus could bring DA signal below CFM detection threshold.

First, to examine predrug site decline dynamics, all transient peaks within a given experiment were normalized to the peak value of the first evoked DA transient and averaged across experiments. Single-phase exponential decay curve fitting for the single pulse data averaged across the 60 nM and 100 nM data sets revealed significantly faster decline in evoked $[DA]_o$ in the *SNCA OVX* compared to *Snca -/-* line ($F(3,8)=150.7$, $p<0.0001$; Figure 5.4a). Further, two-way ANOVA on the single pulse predrug data revealed the main effect of time ($F(5.198)= 426.4$, $p<0.0001$), genotype ($F(1,198)= 518.5$, $p<0.0001$) and a highly significant interaction ($F(5,198)= 58.22$, $p<0.0001$) (Figure 5.4a). Thus, the timecourse evoked $[DA]_o$ decline was significantly affected by genotype. Post-hoc Bonferroni comparisons showed that starting at 5 min, i.e. following 3rd stimulus delivery, *SNCA OVX* had significantly lower peak evoked $[DA]_o$ than *Snca -/-* mice for the data normalised to the first evoked DA transient ($p<0.0001$). A more pronounced decline in evoked $[DA]_o$ over time in the *SNCA OVX* line suggests that presynaptic vesicle pools could be handled differently in this model, a possibility further explored in section 5.3.4.

Secondly, the 60 nM and 100 nM data sets were analysed separately. Decline in predrug evoked $[DA]_o$ assessed by single-phase exponential decay curve fitting was again more pronounced in the *SNCA OVX* line than *Snca -/-* for both the 60 nM ($F(3,71)=30.92$, $p<0.0001$; Figure 5.4b) and 100 nM ($F(3,162)=7.76$, $p<0.0001$; Figure 5.4c) data sets. Site decline significantly compromises data interpretation, as drug effects cannot be isolated from $[DA]_o$ decline caused by other factors (e.g. old age, α-synuclein overexpression). However, when the decline rate from the single pulse predrug data curve fitting was

extrapolated to the whole experiment duration, the data averaged across multiple experiments showed that the plateau value for evoked $[DA]_o$ in control condition could be approximated retrospectively (Figure 5.4b,c). I then used this plateau values from curve fitting to normalize the drug data to, and thus correct for site decline. This transformation showed that for both 60 nM (Figure 5.4d) and 100 nM (Figure 5.4e) data sets the peak evoked $[DA]_o$ in *SNCA OVX* and *Snca -/-* mice were overlapping, suggesting no change in mAChR function in aged *SNCA OVX* animals. However, I further confirmed that similar dose responses to mAChR agonist application were true using 4p:1p ratio.

5.3.2.2 mAChRs function is not compromised in the aged *SNCA OVX* line compared to *Snca -/-* controls

To assess mAChR function more accurately, I used the 4p:1p ratio data to construct Oxo-M dose response curves for aged *SNCA OVX* and *Snca -/-* mice. This method works with the current data because although site decline decreases evoked $[DA]_o$ over time, the relationship between $[DA]_o$ evoked by single pulse (1 p) and high frequency burst (4 p 100 Hz) remains unchanged, as both are equally affected by evoked $[DA]_o$ rundown. Specifically, progressive decline in evoked $[DA]_o$ does not lead to decrease in 4p:1p ratio over time, and these ratios for predrug data were not significantly different between *SNCA OVX* and *Snca -/-* mice ($t=1.06$ $df=4$; $p=0.3498$, two-tailed; unpaired t-test; Figure 5.5a).

Plotting the 4p:1p ratio data against applied Oxo-M concentrations showed no significant difference in mAChR sigmoidal dose-response curves between *SNCA OVX* and *Snca -/-* mice in EC_{50} (half-maximal effective concentration) and Hill slope (rate of co-operative binding) values ($F(2,6)=2.25$, $p=0.1866$; Figure 5.5b). Nonetheless, the raw

4p:1p ratio data could not be used to meaningfully compare dose-response curves between *SNCA OVX* and *Snca -/-* lines for the reasons outlined below.

It was previously shown that the end of Oxo-M dose-response curve is equivalent to inhibition of nAChRs with DHβE, i.e. once a maximal Oxo-M dose is achieved blockade of nAChRs with DHβE has no additional effects (Threlfell et al., 2010). A final 1 µM DHβE dose was therefore used to define the top limit of the drug-response curve for Oxo-M in the *SNCA OVX* and *Snca -/-* lines. Because the effects of 10 µM Oxo-M+1 µM DHβE are different in *SNCA OVX* and *Snca -/-* lines, the data cannot be compared directly between genotypes without normalization. To compare Oxo-M dose response curves between *SNCA OVX* and *Snca -/-* lines, I normalized the data to its own maximal effect (100% value=4p:1p ratio at 10 µM Oxo-M+1 µM DHβE) and curve-fitted the normalized data (Figure 5.5c). Sigmoidal dose-response curve fitting showed there were no significant differences in the EC_{50} and Hill slope values between the dose-response curves for Oxo-M in *SNCA OVX* and *Snca -/-* mice ($F(2,6)=0.44$, $p=0.6657$). Therefore, mAChR function in the dlCPu was similar between *SNCA OVX* and *Snca -/-*, with no mAChR dysfunction identifiable in aged 18-26 months-old *SNCA OVX* mice.

5.3.3 Inhibition of CaMK2 activity did not differentially alter DAT function in *SNCA OVX* compared to *Snca -/-*

Another explanation for impaired DA release in *SNCA OVX* compared to *Snca -/-* mice is alteration in DAT function. Data acquired in our lab by Dr Sarah Threlfell have previously identified that cocaine is able to enhance evoked $[DA]_o$ to a greater extent in CPu of *SNCA OVX* than *Snca -/-* line (Figure 5.6a,b) and that % increase of evoked $[DA]_o$ by cocaine is significantly higher in *SNCA OVX* mice (Figure 5.6c). These data suggest that

DAT function may be greater in *SNCA OVX* line. I therefore aimed to examine effects of α-synuclein overexpression on DAT using CaMK2 inhibition as a tool.

Because both α-synuclein and CaMK2 have the same binding site on DAT, by inhibiting CaMK2 activity the impact of high α-synuclein levels on DAT might be unveiled. Specifically, CaMK2-dependent phosphorylation of DAT increases its function, and thus inhibition of CaMK2 activity could decrease the effects of cocaine on evoked $[DA]_o$ in *SNCA OVX* revealing α-synuclein-dependent DAT phosphorylation. This hypothesis was examined by pre-incubating slices from *SNCA OVX* and *Snca -/-* mice with CaMK2 inhibitor KN-62 (5 μM) following slice preparation, with subsequent bath application of KN-62 (5 μM) throughout. Evoked $[DA]_o$ was assessed in control and following DAT blockade with cocaine (5 μM). These data have no drug-free comparison, therefore control data are the single pulse evoked $[DA]_o$ in the presence of KN-62.

Application of cocaine potentiated evoked $[DA]_o$ significantly more in the *SNCA OVX* compared to *Snca -/-* line for both single pulse and high frequency burst stimulation protocols (Figure 5.6d,e). Two-way ANOVA revealed the main effect of cocaine application for single pulse ($F(1,28)=19.84$, $p=0.001$; Figure 5.6d) and high frequency burst (4 p 100 Hz) data ($F(1,28)=20.92$, $p<0.0001$; Figure 5.6e). Post-hoc Bonferroni t-tests showed the mean peak evoked $[DA]_o$ following cocaine application increased to a significantly greater degree in the *SNCA OVX* line compared to *Snca -/-* mice ($p<0.05$). The greater potentiation of basal evoked $[DA]_o$ in the *SNCA OVX* compared to *Snca -/-* mice by cocaine happened across all stimulation frequencies (Figure 5.6f).

In summary, DAT inhibition with cocaine significantly increases evoked $[DA]_o$ in both *Snca -/-* and *SNCA OVX* mice as previously shown by Dr Threlfell (Figure 5.6a,b).

Further, DAT inhibition with cocaine significantly increases evoked $[DA]_o$ in the presence of CaMK2 inhibitor KN-62 in both genotypes. Specifically, cocaine significantly potentiated evoked $[DA]_o$ in *Snca -/-* mice, as revealed by two-way ANOVA showing main effect of drug application ($F(1,84)=3787$, $p<0.0001$; Figure 5.6g). Post-hoc Bonferroni t-tests revealed that at 5 and 10 Hz stimulations in particular evoked $[DA]_o$ was significantly higher in cocaine compared to KN-62 ($p<0.05$, $p<0.01$). In *SNCA OVX* line there was a highly significant effect of cocaine on evoked $[DA]_o$ ($F(1,84)=106.9$, $p<0.0001$; two-way ANOVA; Figures 5.6h), and post-hoc Bonferroni t-tests showed that across all stimulation frequencies $[DA]_o$ evoked during DAT inhibition were significantly higher than in KN-62 ($p<0.01$, $p<0.001$, $p<0.05$). Finally, the percentage increase in evoked $[DA]_o$ during DAT inhibition was significantly greater in the *SNCA OVX* compared to *Snca -/-* line even in the presence of CaMK2 inhibitor KN-62 (Figure 5.6i). Two-way ANOVA revealed highly significant main effects of genotype ($F(1,84)=1.709e+006$, $p<0.0001$) and stimulation frequency ($F(5,84)=233379$, $p<0.0001$), and highly significant interaction ($F(5.84)=2833$, $p<0.0001$). Post-hoc Bonferroni t-tests showed that for all stimulation protocols percentage increase in evoked $[DA]_o$ was significantly higher in *SNCA OVX* compared to *Snca -/-* mice ($p<0.0001$).

Therefore, CaMK2 inhibition did not preclude differential DAT inhibition effects between *SNCA OVX* and *Snca -/-* mice by equalizing the evoked DA levels following cocaine application. Consequently, these data suggest that increased effects of cocaine in *SNCA OVX* are not due α-synuclein-induced DAT phosphorylation increasing DAT function, which could be manipulated by CaMK2 inhibition with KN-62.

5.3.4 Sustained DA release properties are different in *SNCA OVX* compared to *Snca -/-* mice

5.3.4.1 Different release profiles in striatal sub-regions revealed by long train stimuli

Regional differences in sustained $[DA]_o$ profiles in both *SNCA OVX* and *Snca -/-* mice are evident from plots of the mean $[DA]_o$ versus time evoked with electrical stimulation lasting 1 s (Figure 5.7a,b,c). Contribution from D2 receptors was removed with antagonist L-741,626 (1 μM) bath-applied throughout all recordings, yet regional differences in evoked $[DA]_o$ profiles were still present. Such regional variability in the shapes of evoked $[DA]_o$ transients in the absence of D2 signalling usually stems from differences in release probability and DAT expression gradient between different striatal regions (Cragg and Rice, 2004). The DAT activity is the highest in the dlCPu, and therefore $[DA]_o$ signal is already being terminated during the delivery of the electrical pulse train, resulting in a 'peaked' transient shape (Figure 5.7a). This example dramatically demonstrates the power of DAT in regulating the timecourse of $[DA]_o$ availability. In contrast, in the cCPu (Figure 5.7b) and vmCPu (Figure 5.7c), where DAT activity is lower, evoked $[DA]_o$ continues to increase throughout the duration of electrical stimulation delivery, and then the DA signal is terminated by uptake.

5.3.4.2 *SNCA OVX* may have better sustained $[DA]_o$ in dlCPu

I explored whether, within a given striatal region, $[DA]_o$ evoked by a 1 s-long pulse train varied over time as a function of genotype to determine if sustained DA release was different between *SNCA OVX* and *Snca -/-* mice. Transients were normalized

to their mean peak control 1p values, and then values of $[DA]_o$ from between 0.25 and 1.25 s after start of the stimulation were used for statistical comparisons.

In the dlCPu of *SNCA OVX* mice compared to *Snca -/-*, $[DA]_o$ were sustained slightly but significantly better (Figure 5.7a). Two-way ANOVA revealed the main effect of genotype ($F(1,135)= 57.00$, $p<0.0001$) and time ($F(8,135)= 489.7$, $p<0.0001$), but no interactions ($F(8,135)= 0.52$, $p=0.839$). Post-hoc Bonferroni comparisons showed that at 0.875 s, 1.000 s and 1.125 s after the stimulation start, mean evoked $[DA]_o$ was significantly higher in *SNCA OVX* mice compared to *Snca -/-* littermates ($p<0.05$, $p<0.01$, $p<0.05$).

In the cCPu, sustained $[DA]_o$ was not significantly different between *SNCA OVX* and *Snca -/-* mice, as two-way ANOVA revealed no main effect of genotype ($F(1,135)= 2.85$, $p=0.094$; Figure 5.7b). In the vmCPu, the trend in better sustained $[DA]_o$ reversed as *Snca -/-* mice presented with higher mean evoked $[DA]_o$ (Figure 5.7c). Two-way ANOVA revealed the main effect of genotype ($F(1,135)= 37.94$, $p<0.0001$) and time ($F(8,135)= 66.24$, $p<0.0001$), and no interactions ($F(8,135)= 0.10$, $p=0.999$), but post-hoc Bonferroni t-tests were not significant.

Higher variability in evoked $[DA]_o$ in cCPu and vmCPu, as evidenced by larger SEM error bars in Figures 5.7b and 5.7c, complicates drawing conclusions about the differences in underlying DA release between *SNCA OVX* and *Snca -/-* mice in these regions. Because FCV recordings capture $[DA]_o$ evoked from a population of DA release sites, lower variability in dlCPu indicates more homogenous populations, which can be more meaningfully compared across genotypes and different recording days. In contrast, high variability in evoked $[DA]_o$ in cCPu and vmCPu recordings requires caution in data

interpretation. The 'apparent' changes in sustained $[DA]_o$ between *SNCA OVX* and *Snca -/-* mice could disappear if a large enough population of recording sites is sampled, and variability in evoked $[DA]_o$ regresses towards the mean. Therefore, I focused on the comparison of $[DA]_o$ profiles from the dlCPu sampling sites, although in the subsequent experiments recordings were also performed in cCPu and vmCPu.

5.3.4.3 The timecourse of vesicle recruitment may be altered in *SNCA OVX*

It appears that *SNCA OVX* mice could be better able to sustain $[DA]_o$ in some striatal regions, such as dlCPu, during prolonged pulse train stimuli than *Snca -/-* controls (Figure 5.7a). The better sustained $[DA]_o$ in the dlCPu of *SNCA OVX* mice could potentially be explained by denser vesicle clustering in the *SNCA OVX* line in dorsal striatum (Janezic et al., 2013). A significant increase in vesicle clustering could provide a structural basis for more efficient recruitment of vesicles to the active zone during release events evoked by prolonged depolarization, such as 20 pulses at 20 Hz stimulation protocol lasting 1 s. These data suggest that one of the possible mechanisms for impaired DA release in dorsal striatum of *SNCA OVX* mice compared to *Snca -/-* littermates could be the difference in the timecourse of vesicle recruitment, with vesicles taking longer to be mobilized to the active zone in the *SNCA OVX* animals. However, once recruited, and with the added contribution from denser vesicle clustering, *SNCA OVX* could be better able to sustain $[DA]_o$ during prolonged stimulation in dlCPu.

5.3.4.4 Uptake reduction does not explain better sustained $[DA]_o$ in *SNCA OVX*

$[DA]_o$ evoked with prolonged stimulation depends on two factors: vesicle recruitment/release and uptake of released neurotransmitter with DAT. Thus, one of the

possible explanations for better sustained $[DA]_o$ in the dlCPu of *SNCA OVX* line is reduced uptake of $[DA]_o$ by DAT, rather than a change in the rate of vesicle release. To investigate this, I compared DA decay rates of concentration-matched transients evoked with single pulse stimulation in dlCPu, cCPu and vmCPu of *SNCA OVX* and *Snca -/-* mice (Figure 5.7d,e,f). Single-phase exponential-decay curve fitting of the falling phases of electrically evoked DA transients between 0.125 s and 2.125 s from the stimulus start showed that $[DA]_o$ uptake by DAT was happening significantly faster in the *SNCA OVX* compared to *Snca -/-* mice in dlCPu and vmCPu, while in cCPu *Snca -/-* controls had faster $[DA]_o$ uptake rate. The K (rate constant) values between the curves were significantly different in dlCPu ($K=4.48\ s^{-1}$ vs. $K=3.31\ s^{-1}$ for *SNCA OVX* vs. *Snca -/-*) ($F(2,186)=9.84$, $p<0.0001$; Figure 5.7d), cCPu ($K=3.32\ s^{-1}$ vs. $K=3.53\ s^{-1}$ for *SNCA OVX* vs. *Snca -/-*) ($F(2,186)=5.33$, $p=0.006$; Figure 5.7e) and vmCPu ($K=4.02\ s^{-1}$ vs. $K=3.12\ s^{-1}$ for *SNCA OVX* vs. *Snca -/-*) ($F(2,186)=3.69$, $p=0.027$; Figure 5.7f). Thus, *SNCA OVX* mice presented with enhanced and not reduced DAT function in dlCPu, which does not explain higher sustained $[DA]_o$ in dlCPu of the *SNCA OVX* line, but may explain increased effects of cocaine in *SNCA OVX*.

During stimulation lasting 1 s cholinergic autofeedback could also be involved in regulation of DA release. To test this, pilot control experiments were performed in wild-type C57Bl6/J mouse (N=1, total sampling sites=2) with mAChR antagonist (atropine, 1 µM). Two-way ANOVA on the mean evoked $[DA]_o$ between 0.25 s and 1.25 s after the stimulus start revealed no main effect of drug application in dlCPu ($F(1,54)=2.45$, $p=0.124$; Figure 5.7g) and vmCPu ($F(1,54)=3.23$, $p=0.078$; Figure 5.7i). However, in cCPu two-way ANOVA showed the main effect of drug ($F(1,54)=49.24$, $p<0.0001$), and post-hoc Bonferroni t-tests showed that at 0.75 s evoked $[DA]_o$ was significantly lower in atropine compared to control condition ($p<0.05$) (Figure 5.7h). The latter difference,

however, most likely stems from atropine recordings being acquired later in the experiment when evoked $[DA]_o$ was decreasing over time, rather than reflect a real difference between atropine and control recording conditions. From these data I conclude that muscarinic regulation of sustained $[DA]_o$ evoked with 20 pulses at 20 Hz stimulation protocol is likely absent.

5.3.4.5 Examination of sustained $[DA]_o$ in *Synapsin 3 -/-* mice supports altered vesicle recruitment hypothesis of impaired dopamine release in *SNCA OVX*

Further controls examined sustained $[DA]_o$ in Synapsin 3 knockout mice (*Synapsin 3 -/-*), where vesicle pools are known to be more readily available for release. Synapsin 3 negatively regulates DA release (Kile et al., 2010), with *Synapsin 3 -/-* mice showing an increase in the recycling vesicle pool size (Feng et al., 2002). Thus, in *Synapsin 3 -/-* mice vesicles are released more readily in response to stimulation. *Synapsin 3 -/-* line, therefore, would be a good control for addressing how changes in vesicle availability impact on sustained $[DA]_o$ to help address whether the difference in sustained $[DA]_o$ in the dlCPu of *SNCA OVX* and *Snca -/-* mice could stem from changes in vesicle handling following α-synuclein overexpression.

Across all three recording regions in dlCPu, cCPu and vmCPu, *Synapsin 3 -/-* mice (N=3, 2 slices recorded from per animal) showed faster evoked $[DA]_o$ rundown with long electrical stimulation train of 20 pulses at 20 Hz than the *SNCA OVX* line (Figure 5.8 a,b,c). Two-way ANOVA on the mean evoked $[DA]_o$ between 0.25 s and 1.25 s from the stimulation start revealed the main effect of genotype across all three sampling sites: dlCPu ($F(1,117)=21.72$, $p<0.0001$; Figure 5.8a), cCPu ($F(1,117)=82,39$, $p<0.0001$; Figure 5.8b) and vmCPu ($F(1,117)=5.06$, $p=0.026$; Figure 5.8c). Post-hoc Bonferroni comparisons

revealed that in cCPu evoked $[DA]_o$ was significantly lower in *Synapsin 3 -/-* line between 0.625 s and 1.25 s ($p<0.05$, $p<0.01$, $p<0.001$). Because in the *Synapsin 3 -/-* model the size of the recycling pool of vesicles is increased and vesicles are more readily available for release, sustained depolarization depletes DA release quicker because less is available for release later on in the stimulation train. These data support current hypothesis that the timecourse of vesicle recruitment to the release sites could be different between *SNCA OVX* and *Snca -/-* mice.

Extra exploratory experiments were performed to further examine the interaction between α-synuclein overexpression and vesicle handling which may impact DA releasability. *Synapsin 3 -/-* line does not have *Snca -/-* background, which limits data interpretation regarding the role of α-synuclein overexpression in regulation of vesicle handling. A more meaningful comparison would be with *Synapsin 3 -/-* line on *Snca -/-* background to ensure that the only difference between *SNCA OVX* and *Synapsin 3 -/-* was presence or absence of Synapsin 3, and not mouse α-synuclein. For the experiments performed by other lab members, *Synapsin 3 -/-* mice were bred to *Snca -/-* mice and some of the generated double-knockout *Synapsin 3 -/- Snca -/-* mice were used for exploring sustained $[DA]_o$ with 1 s-long pulse train stimuli. The experiments with 20 pulses at 20 Hz stimulation protocols were repeated in double-knockout mice (N=3, 2 slices recorded from per animal) and wild-type C57Bl6/J controls (N=2, 2 slices recorded from per animal).

I first acquired FCV recordings from the striatum of C57Bl6/J wild-type mice in order to examine whether sustained $[DA]_o$ evoked with 20 pulses at 20 Hz electrical stimulation were different between wild-type and *Synapsin 3 -/-* (Figure 5.8d,e,f) and

Snca -/- mice (Figure 5.8g,h,i). Two-way ANOVA on mean evoked $[DA]_o$ between 0.25 s and 1.25 s from the stimulation start revealed the main effect of genotype in dlCPu ($F(1,72)=4.35$, $p=0.0405$) showing significantly higher decline in sustained $[DA]_o$ in *Synapsin 3 -/-* compared to WT mice (Figure 5.8d), while in vmCPu *Synapsin 3 -/-* showed significantly better sustained $[DA]_o$ than WT ($F(1,72)=7.34$, $p=0.008$; Figure 5.8f). For the *Snca -/-* and WT comparison two-way ANOVA revealed the main effect of genotype only in the cCPu, where decline in sustained $[DA]_o$ was more pronounced in the *Snca -/-* mice ($F91,54)=7.24$, $p=0.009$; Figure 5.8h). Overall, however, evoked DA release profiles and sustained $[DA]_o$, especially in dorsal recording sites, were similar between wild-type controls and single knockout Synapsin 3-/- or *Snca -/-* lines. These data show the knockout of either *Synapsin 3 -/-* or *Snca -/-* alone does not dramatically alter sustained $[DA]_o$.

Next, I examined sustained $[DA]_o$ in *Snca -/-* single knockout and *Synapsin 3 -/- Snca -/-* double-knockout mice, to explore whether the latter could provide a better control for examining vesicle handling processes in the *SNCA OVX* line. *Synapsin 3 -/- Snca -/-* mice presented with an increase in the overall evoked $[DA]_o$ and better sustained $[DA]_o$ in dlCPu and cCPu (Figure 5.8j,k), but not vmCPu (Figure 5.8l). Two-way ANOVA on mean evoked $[DA]_o$ between 0.25 s and 1.25 s from the stimulation start showed the main effect of genotype in dlCPu ($F(1,90)=129.6$, $p<0.0001$; Figure 5.8j), cCPu ($F(1,90)=51.73$, $p<0.0001$; Figure 5.8k) and vmCPu ($F(1,90)=7.89$, $p=0.006$; Figure 5. 8l). Post-hoc Bonferroni t-tests showed that in the dlCPu starting from 0.5 s and in the cCPu from 0.875 s *Synapsin 3 -/- Snca -/-* mice had significantly better sustained $[DA]_o$ than *Snca -/-* mice ($p<0.05$, $p<0.01$, $p<0.001$). Together these data show double knockout of Synapsin 3 and α-synuclein had synergistic effect on vesicle handling and

recruitment. Thus, this double-knockout mouse line could not be used as a control for exploring the underpinnings of better sustained $[DA]_o$ in the *SNCA OVX* mice. Supra-additive effects suggest that both Synapsin 3 and α-synuclein may employ a common mechanism for control of intersynaptic vesicle dispersion and/or vesicle mobility. However, addressing these questions was beyond the scope of the current thesis work. Experiments are currently underway in the lab to examine the interactions between Synapsin 3 and α-synuclein in regulating striatal DA release following α-synuclein knockout and overexpression.

5.4 Discussion

DA release deficits in dorsal striatum of *SNCA OVX* mice were reported previously (Janezic et al., 2013). Data presented in this chapter further extended investigation of the *SNCA OVX* PD model by showing reduced DA release directly stems from a primary dysfunction of the dopaminergic system, and is not mediated via a cholinergic mechanism. Specifically, changes in ACh tone at nicotinic receptors on DA axons were not responsible for impaired DA release in dorsal striatum of young adult (3-4 months-old) *SNCA OVX* mice. However, the data acquired in the presence of nAChR antagonist also showed increased ACh tone in the NAc of *SNCA OVX* line, which could mask or compensate for an underlying impairment in evoked DA in ventral striatum.

Electrically-evoked $[DA]_o$ in dorsal striatum of *SNCA OVX* mice was significantly lower compared to *Snca -/-* controls in the absence of ACh transmission, consistent with published data acquired without nAChR antagonist (Janezic et al., 2013). Further examination of DA transients from individual sampling sites revealed that dlCPu in particular was the main contributor to the overall impaired DA release in dorsal striatum of *SNCA OVX* line. Work from our laboratory and others suggests that during electrical stimulation of striatal DA release, in addition to direct depolarization of dopaminergic terminals, cholinergic system could also be driving DA release via an ACh-dependent mechanism (Cachope et al., 2012; Threlfell et al., 2012). In fact, during electrical stimulation with cholinergic transmission intact, ChI-evoked DA release could be the dominant component of the recorded DA signal: both with direct light-evoked depolarization of striatal ChIs and electrical stimulation of striatal DA release, evoked DA transients are frequency insensitive, whereas light-evoked depolarization of DA axon

terminals only produces highly frequency sensitive DA release events. Cholinergic axis also powerfully regulate DA release probability and short-term plasticity via nAChRs on DA axons (Rice and Cragg, 2004; Zhang and Sulzer, 2004; Exley et al., 2008). Further, decrease in nAChR number in Parkinson's patients and animal models suggests that cholinergic transmission rules, including nAChR tone, could be altered (Rinne et al., 1991; Durany et al., 2000; Quik et al., 2004; McCallum et al., 2005). Therefore, the reported DA release deficits in the *SNCA OVX* line could stem not from a primary SNc neuron dysfunction that renders them less able to release DA upon depolarization, but could be 'under-written' or exacerbated by the ChI circuit. Current results, however, demonstrate that with the ACh axis disabled, DA transmission deficits are still present in dorsal striatum of *SNCA OVX* mice compared to *Snca -/-* littermates, confirming that factors directly regulating DA release within the DA axon terminal are at play.

The current study further revealed an underlying DA release deficit in ventral striatum of *SNCA OVX* line in the absence of cholinergic influence. With nAChR blockade, a trend towards significantly lower evoked $[DA]_o$ release was unmasked in the NAc of *SNCA OVX* mice. The percent decrease in evoked $[DA]_o$ in both dorsal and ventral striatum in *SNCA OVX* mice compared to *Snca -/-* was similar. Yet, the data for the NAc were underpowered with fewer data points and larger variance. Only two-way ANOVA on the frequency data set were able to reveal a significant decrease in evoked $[DA]_o$ in the NAc of *SNCA OVX*. A decrease in evoked $[DA]_o$ in ventral striatum of the *SNCA OVX* line has not been reported previously for the data where ACh transmission was intact, suggesting increased ACh transmission in the NAc of *SNCA OVX* could mask or compensate for DA release impairments in ventral striatum. This is consistent with observations of increased ACh levels in PD (Lehmann and Langer, 1983). Comparing the

current data from NAc sampling sites with the data recorded while ACh transmission was intact (Janezic et al., 2013), the amplitude of evoked $[DA]_o$ is similar to the previously reported data for both *SNCA OVX* and *Snca -/-* lines. However, the relative decrease in evoked $[DA]_o$ in the *SNCA OVX* line in the absence of cholinergic influence is more pronounced.

Thus, evoked $[DA]_o$ deficits in dorsal striatum of *SNCA OVX* mice were present regardless of ACh tone at nAChRs, whereas decreased $[DA]_o$ release in ventral striatum was only revealed by eliminating ACh influence at nAChRs. These data hence suggest that cholinergic transmission could differentially compensate for dysfunction of pre-synaptic DA terminals via nAChRs between dorsal and ventral striatum, possibly due to variable receptor subunit composition. For example, α4α5β2-containing subtypes of nAChR are predominantly found and govern DA transmission in the CPu, while in the NAc α4α6β2β3-containing subtypes of nAChR regulate DA transmission (Drenan et al., 2010; Exley et al., 2011, 2012). Additionally, differential innervation of dorsal and ventral striatal territories by midbrain projections, originating from SNc and VTA respectively (Nelson et al., 1996; Haber et al., 2000; McFarland and Haber, 2000), could also contribute to this distinction in external regulation of DA release deficits by ACh. Current data also showed that impaired $[DA]_o$ release in dorsal and ventral striatum of *SNCA OVX* mice compared to *Snca -/-* littermate controls is due to deficits in general transmitter releasability, rather than changes in release probability or frequency sensitivity of electrically evoked $[DA]_o$ following α-synuclein overexpression.

In aged 18-26 months-old *SNCA OVX* mice, the time point when SNc neuron degeneration is present in the transgenic model (Janezic et al., 2013), there were no

identifiable changes in mAChR function, assessed by sequential application of increasing concentrations of mAChR agonist Oxo-M. Because dose-response curves could not be fitted to untransformed data, I used percent-normalized data to determine whether changes in binding kinetics and half-maximal drug responses, indicative of changes in receptor coupling, were present in aged 18-26 months-old mice following α-synuclein overexpression. These comparisons revealed no change in mAChRs activity between *SNCA OVX* and *Snca -/-* lines. This finding is surprising in the light of previously published evidence for functional downregulation of muscarinic autoreceptor function following decline in DA transmission (Ding et al., 2006; Gonzalez-Reyes et al., 2012) and decline in mAChR number in Parkinson's disease per se (Joyce, 1991, 1993).

For this data set, however, the dose-response curve is incomplete: the maximal effect of Oxo-M is not reached in either *SNCA OVX* or *Snca -/-* mice, since application of DHβE should not have an additional effect if Oxo-M dose is maximal. This observation sets the *SNCA OVX* and *Snca -/-* lines apart from the WT C57Bl6/J mice where 10 μM of Oxo-M is the maximal effective dose of mAChR agonist (Threlfell et al., 2010). Further, plots of the raw data also suggest that 10 μM Oxo-M+ 1 μM DHβE effect was not equivalent in *SNCA OVX* and *Snca -/-* genotypes as judged by the 4p:1p ratio data. The differences in 4p:1p ratios obtained using absolute evoked $[DA]_o$ between *SNCA OVX* and *Snca -/-* mice could not be uncovered in 3-4 months-old animals following nAChR blockade with DHβE. Further, the 4p:1p ratios obtained using single pulse control normalized data were also unchanged in aged *SNCA OVX* compared to *Snca -/-* mice in drug-free control conditions. Yet, in the presence of DHβE the 4p:1p ratios were different in 18-26 months-old *SNCA OVX* and *Snca -/-* mice. It is difficult to unequivocally establish whether these differences stemmed from age-related changes exacerbated by

interference with cholinergic transmission, or were due to random sampling from different populations of DA releasing sites. Plots of the raw data also show that 10 μM Oxo-M effect was not equivalent in *SNCA OVX* and *Snca -/-* mice. Therefore, it is possible that failure to uncover changes in mAChR activity was the results of using insufficiently high drug doses, and required larger number of animals. However, due to limited availability of aged littermate paired *SNCA OVX* and *Snca -/-* mice we could not increase the number of observations.

Current experimental design may also not be sensitive enough to highlight subtle changes in mAChR function. In particular, changes in G protein-dependent coupling between receptors and effectors at mAChR could be obscured by site decline, and having to use the 4p:1p ratio data instead of the raw control normalized peak values. We may be unable to catch alterations in muscarinic receptor signalling using an indirect readout of changes in evoked DA release, in contrast to direct biochemical examination of intracellular signalling cascades supported by mAChRs. Alternatively, different mAChR subtypes, including M_2 and M_4 localized to ChIs (Levey et al., 1991; Hersch et al., 1994; Yan and Surmeier, 1996), could be differentially affected. Therefore, a broad-spectrum agonist like Oxo-M could be unable to uncover changes in mAChR function between the *SNCA OVX* and *Snca -/-* lines if the latter occur in receptor subtype-specific manner. For example, the study, which detected downregulation in RGS4 signalling at mAChRs following DA depletion, also found transient upregulation of M_2 expression (Gonzalez-Reyes et al., 2012). Interestingly, the highest Oxo-M dose applied (10 μM) was more effective in *SNCA OVX* than Snca-/- mice, which could be consistent with new data reporting ChI death following α-synuclein overexpression (Aldrin-Kirk et al., 2014).

I next examined whether more pronounced rise in evoked $[DA]_o$ following DAT inhibition with cocaine in the *SNCA OVX* line compared to *Snca -/-* could be reversed by inhibition of CaMK2 activity with KN-62 (5 μM). In particular, I explored whether potentiated cocaine effects in the *SNCA OVX* line could be due to increased DAT phosphorylation following α-synuclein overexpression, which could increase DAT function. CaMK2 has the same binding site on the DAT as α-synuclein, thus I hypothesised that inhibiting CaMK2a activity could unveil the effects of α-synuclein overexpression on DAT function. Specifically, I predicted that this manipulation would equalize DAT inhibition effects on evoked $[DA]_o$ between *SNCA OVX* and *Snca -/-* lines. Contrary to this prediction, evoked $[DA]_o$ following cocaine application was significantly higher in *SNCA OVX* compared to *Snca -/-* mice. Specifically, DAT inhibition led to an average increase of ~75% in evoked $[DA]_o$ in *SNCA OVX* mice, and ~25% increase in the *Snca -/-* line across all stimulation protocols. These data, therefore, replicate consistently observed significantly higher potentiation of evoked DA release with cocaine in the *SNCA OVX* compared to *Snca -/-* line made by Dr Threlfell. Thus, CaMK2 activity inhibition, at least under present experimental conditions, could not be used to examine functional interactions between DAT and α-synuclein, and was moreover suggestive of α-synuclein overexpression not impacting phosphorylation status of DAT. However, pre-injecting mice with KN-62 might be necessary to reveal this interaction, if the changes are highly time-dependent and require more than a few hours to take place. Yet, some biochemical analyses will be necessary to first examine whether DAT phosphorylation status is altered between *Snca -/-* and *SNCA OVX* lines.

The last stage of the project encompassed identification of mechanisms which may govern reduced DA releasability in dorsal striatum of *SNCA OVX* line. Gross

similarity of DA release profiles evoked with 1 s-long electrical stimulation across three striatal sub-regions in dlCPu, cCPu and vmCPu between *SNCA OVX* and *Snca -/-* lines suggests global regulation of DA transmission by diffusion and uptake remains intact in this transgenic PD model. Yet, there was an indication of better sustained $[DA]_o$ in the dlCPu of *SNCA OVX* mice compared to *Snca -/-*. Prior studies reporting increase in evoked DA following synuclein knock-down (Senior et al., 2008; Anwar et al., 2011) and decrease in evoked DA following α-synuclein overexpression (Janezic et al., 2013), would predict a more pronounced reduction in DA release upon sustained stimulation in *SNCA OVX* mice. The EM data showing increased vesicle clustering in the *SNCA OVX* line (Janezic et al., 2013) could reconcile the contradiction between the earlier studies and currently obtained results. The increased vesicle clustering being able to support better sustained DA release in the dlCPu of the *SNCA OVX* line is corroborated by the data from *Synapsin 3 -/-* mice. For the *Synapsin 3 -/-* line, in which vesicles are more readily available for release (Feng et al., 2002; Kile et al., 2010), site rundown happened quicker during long stimulation pulse train lasting 1 s. Comparison of the data from *SNCA OVX*, *Snca -/-* and *Synapsin 3 -/-* lines suggest a possibility that vesicle handling processes may be altered following α-synuclein overexpression. These data find resonance with experiments performed in 18-26 months-old *SNCA OVX* and *Snca -/-* mice, where progressive decline in evoked $[DA]_o$ over time is more pronounced and happens significantly faster in the transgenic line, pointing to α-synuclein-dependent changes in vesicle handling.

In order to ensure that the only difference between the compared mouse lines was presence or absence of Synapsin 3, not α-synuclein, double-knockout mice were used. *Synapsin 3 -/- Snca -/-* mice unexpectedly presented with both increased evoked DA levels and better sustained $[DA]_o$. Previously reported studies could explain the

increase in the overall evoked DA release levels, with Synapsin 3 being the negative regulator of DA release (Kile et al., 2010), and knockout of α-synuclein resulting in an increase in evoked DA levels (Senior et al., 2008; Anwar et al., 2011). Yet, an explanation for better sustained $[DA]_o$ in the *Synapsin 3 -/- Snca -/-* double-knockout line is lacking. The only study looking at the interaction of α-synuclein and synapsins suggests that a-synuclein overexpression leads to protein aggregate formation at the presynaptic terminals, and thus reduces the expression of synapsin proteins (Spinelli et al., 2014). Thus, due to lack of data on functional interactions between α-synuclein and Synapsin 3 I cannot speculate as to why the double knockout of these proteins is able to support better sustained $[DA]_o$. Consequently, the *Synapsin 3 -/- Snca -/-* mice also could not be used as a control for evaluating sustained $[DA]_o$ properties in the *SNCA OVX* line. From the data currently presented I can only conclude that Synapsin 3 and α-synuclein may have common mechanisms in affecting synapse function via regulation of vesicle mobility and/or dispersion and/or handing, and that Synapsin 3 and α-synuclein are likely the negative regulators of each other's function.

Together with the previously published (Janezic et al., 2013) and currently present data showing DA release deficits in dorsal striatum of *SNCA OVX* mice with short stimulation protocols, better sustained $[DA]_o$ in dlCPu in the *SNCA OVX* line with 1 s-long stimulation points to a distinction between instantaneous and sustained DA release properties. In particular, the initial DA release, evoked by single pulse or short high frequency burst stimulation protocols, is clearly compromised in the *SNCA OVX* line compared to *Snca -/-* littermates both in the presence and absence of ACh influence. Yet, during continuous 1 s-long stimulation DA transients recorded in the dlCPu were

indicative of better sustained $[DA]_o$ in the *SNCA OVX* line compared to *Snca -/-*. I focus on dlCPu due to low variability in evoked $[DA]_o$ in this region, which therefore provides a more reliable functional read-out and enables more accurate comparison of sustained $[DA]_o$ properties across animals, experimental days and sampling sites. The data presented here indicate that *SNCA OVX* could be able to recruit additional vesicles for supporting sustained release in dlCPu during long hyperpolarization of DA axon terminals, while with short stimulation protocols *SNCA OVX* line consistently presents with deficits in evoked DA release. Thus, I hypothesize that the timecourse of vesicle recruitment to the release sites could be different between the *Snca -/-* and *SNCA OVX* lines and this distinction could stem from differences in vesicle clustering profiles.

SNCA OVX mice present with significantly higher vesicle clustering in DA axon terminals compared to *Snca -/-* littermates (Janezic et al., 2013). Thus, it is possible that mechanisms recruiting vesicles to the active zone and regulating vesicle fusion with the plasma membrane are compromised in the *SNCA OVX* line. Consequently, initial DA release probed with short electrical stimulation shows DA release deficits in the *SNCA OVX* compared to *Snca -/-* mice. However, once the vesicle docking machinery has succeeded in tethering first vesicles to the active zone and due to close proximity of other vesicles following α-synuclein-mediated increase in vesicle clustering, sustained $[DA]_o$ could be better in *SNCA OVX* mice. This hypothesis provides a testable framework for understanding evoked DA release deficits in this PD model overexpressing human α-synuclein. There are no reported DA 'content' abnormalities, yet the functional characterization of the dopaminergic system reveals impaired DA release in *SNCA OVX* compared to *Snca -/-* mice. More data is required to explore this possibility, potentially using longer stimulation protocols. This work, however, was not undertaken as a part of

this project because long stimulations lasting a few seconds engage additional neurotransmitter systems, such as glutamatergic signalling which in turn engages nitric oxide release from MSNs, that can modify DA release profiles via secondary signalling cascades (Rice et al., 2011), and thus obscure the primary release deficits intrinsic to the DA axon terminals.

5.5 Summary

The data presented in this chapter further extend the work on DA neurotransmission deficits in the *SNCA OVX* mouse model of PD. Specifically, in this chapter I demonstrate that deficits in evoked DA release in dorsal striatum of *SNCA OVX* mice compared to *Snca -/-* controls are present regardless of the state of cholinergic transmission. However, these data also show that DA release deficits in ventral striatum could be uncovered in *SNCA OVX* mice following arrest of cholinergic transmission, suggesting that up-regulation of ACh tone at nAChRs could obscure primary DA release deficits in the NAc and/or compensate for release deficits in evoked DA. Examination of mAChR function following dopaminergic denervation after SNc neuronal degeneration and during reduced striatal DA transmission in aged mice revealed no difference between *SNCA OVX* and *Snca -/-* lines, although this data set is limited. Inhibition of CaMK2 activity also did not prove to be a suitable tool for examining interactions between DAT and α-synuclein, suggesting that DAT phosphorylation was not altered by α-synuclein overexpression, contributing to increased cocaine effects in *SNCA OVX* mice. Finally, investigation of sustained DA release properties potentially highlights a dissociation between release events evoked with short (up to 80 ms) and long (1 s) stimulation protocols, whereby initial release is consistently shown to be compromised

in the *SNCA OVX* line compared to *Snca -/-* mice, while sustained $[DA]_o$ could be better in the dlCPu of *SNCA OVX* mice compared to *Snca -/-* littermates.

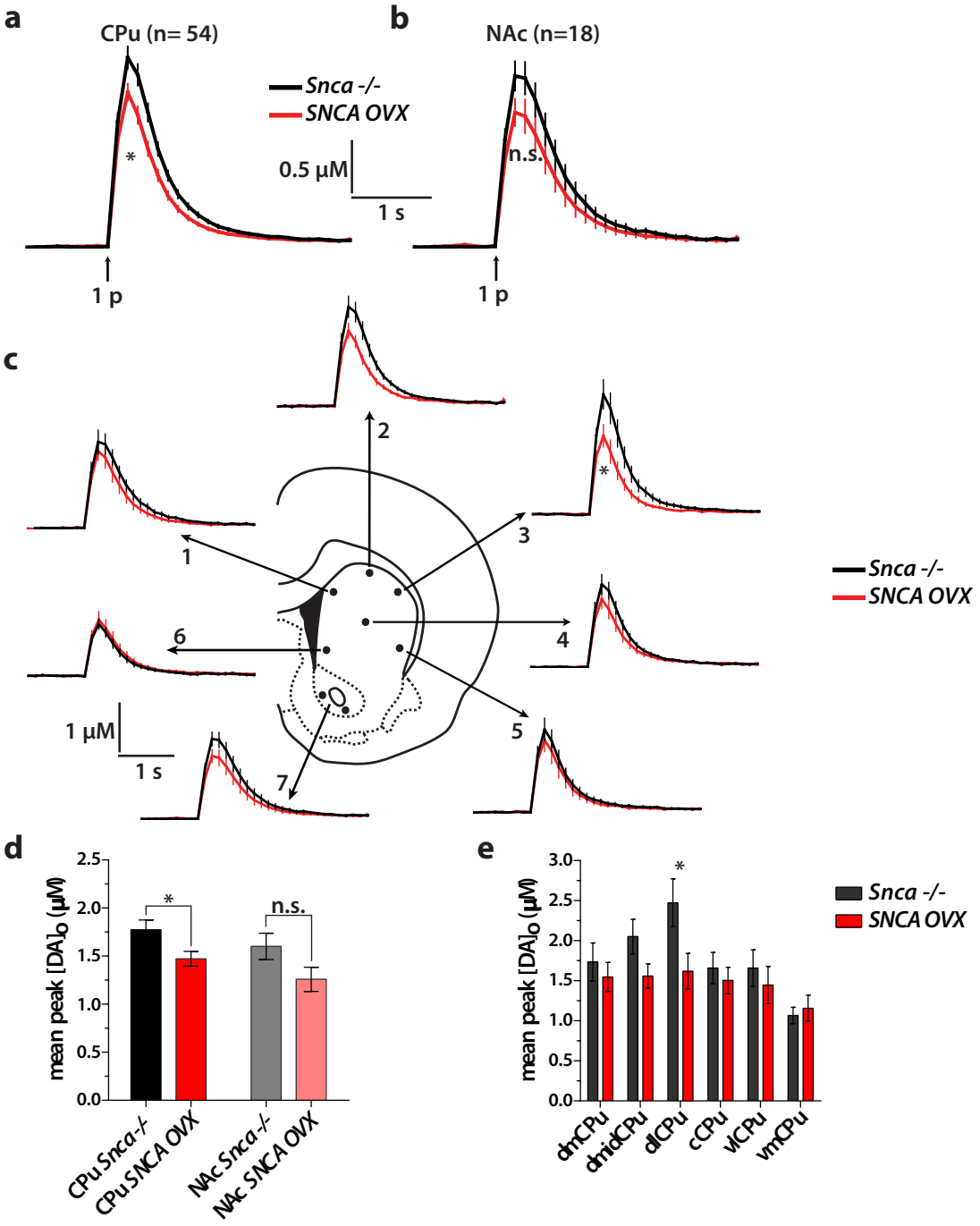

Figure 5.1 Deficits in 1 p-evoked $[DA]_o$ in *SNCA OVX* line persist in the absence of ACh tone at nAChRs

(a,b) Mean $[DA]_o$ ± SEM versus time evoked by single pulse stimulation (1 p) in CPu **(a)** and NAc **(b)** of *Snca -/-* (N=9) and *SNCA OVX* (N=9) mice at 3-4 months of age with nAChR antagonist (DHβE, 1 µM) present throughout. Mean peak evoked $[DA]_o$ was significantly lower in *SNCA OVX* compared to *Snca -/-* in the CPu **(a)** (*p<0.05; unpaired t-test), but not the NAc **(b)** (p>0.05; unpaired t-test). **(c)** Regional breakdown of mean 1 p-evoked $[DA]_o$ ± SEM versus time within 6 sampling sites in the CPu (dmCPu, dmidCPu, dlCPu, cCPu, vlCPu, vmCPu) and 2 sites in the NAc core. dlCPu was the main contributor to the overall 1 p-evoked $[DA]_o$ deficits in dorsal striatum of *SNCA OVX* mice (Two-way ANOVA, *post-hoc* Bonferroni t-tests). **(d,e)** Mean peak 1 p-evoked $[DA]_o$ ± SEM grouped by genotype and recording site. **(d)** *SNCA OVX* mice on average had 16% lower evoked $[DA]_o$ than *Snca -/-* controls in the CPu and 21% in the NAc, but reduction in evoked $[DA]_o$ was statistically significant only in CPu (Two-way ANOVA, *post-hoc* Bonferroni t-tests). **(e)** In CPu of *SNCA OVX* mice dlCPu and dmidCPu had the largest reduction in evoked $[DA]_o$ compared to *Snca -/-*, 34% and 24% respectively. The reduction in evoked $[DA]_o$ in dlCPu of *SNCA OVX* was statistically significant (Two-way ANOVA, *post-hoc* Bonferroni t-tests, *p<0.05).

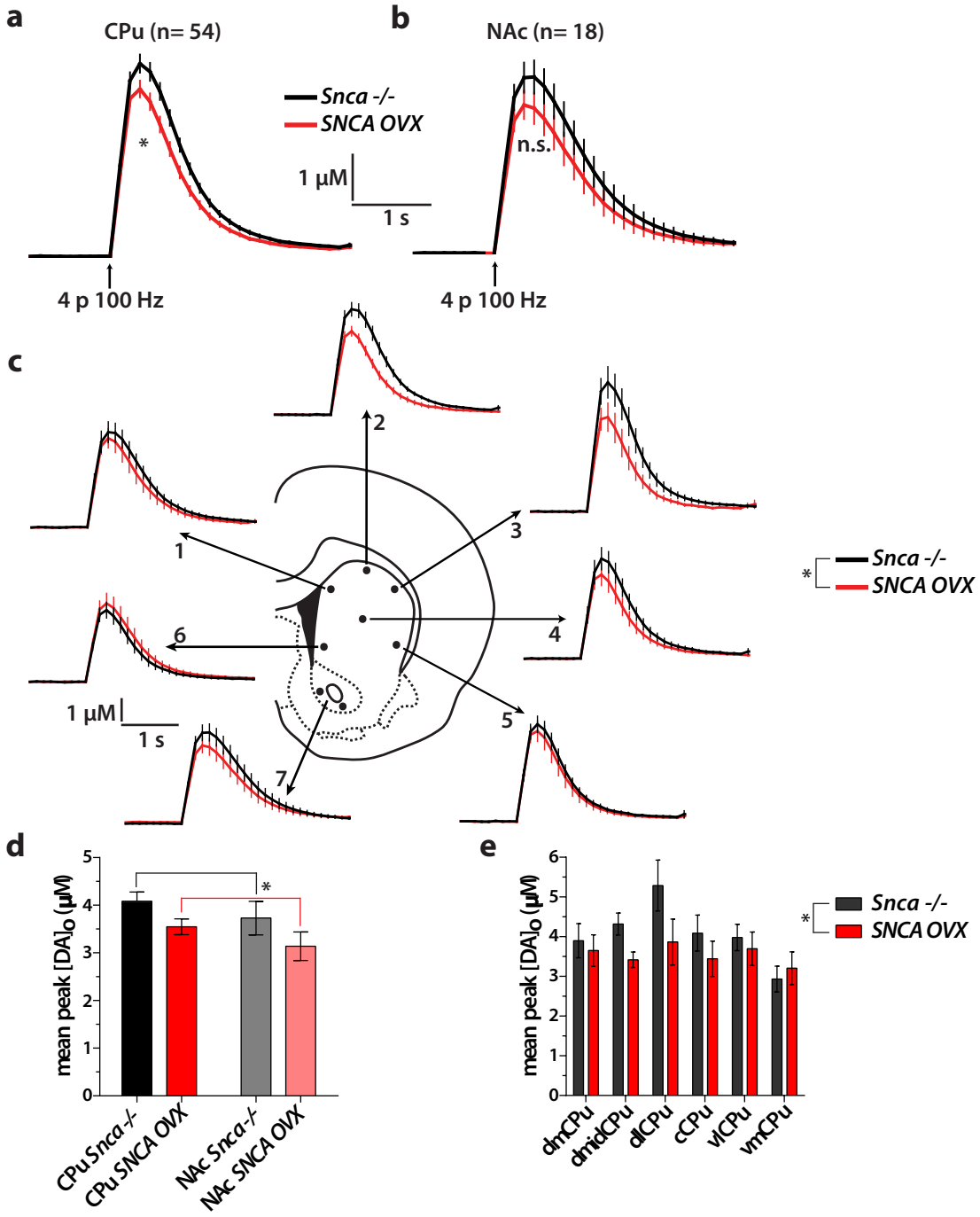

Figure 5.2 Deficits in 4 p-evoked $[DA]_o$ in *SNCA OVX* line persist in the absence of ACh tone at nAChRs

(a,b) Mean $[DA]_o$ ± SEM versus time evoked by high frequency burst stimulation (4 p 100 Hz) in CPu **(a)** and NAc **(b)** of *Snca -/-* (N=9) and *SNCA OVX* (N=9) mice at 3-4 months of age with nAChR antagonist (DHβE, 1 µM) present throughout. Mean peak evoked $[DA]_o$ was significantly lower in *SNCA OVX* than *Snca -/-* line in the CPu **(a)** (*p<0.05; unpaired t-test), but not the NAc **(b)** (p>0.05; unpaired t-test). **(c)** Regional breakdown of mean 4 p-evoked $[DA]_o$ ± SEM versus time within 6 sampling sites in the CPu (dmCPu, dmidCPu, dlCPu, cCPu, vlCPu, vmCPu) and 2 sites in the NAc core. Overall, across all CPu sites evoked $[DA]_o$ was significantly lower in *SNCA OVX* than *Snca -/-* mice (Two-way ANOVA, *p>0.05). **(d,e)** Mean peak 4 p-evoked $[DA]_o$ ± SEM grouped by genotype and recording site. **(d)** *SNCA OVX* mice on average had 13% lower evoked $[DA]_o$ than *Snca -/-* mice in the CPu and 15% in the NAc. Overall, *SNCA OVX* mice had lower evoked $[DA]_o$ than *Snca -/-* controls (Two-way ANOVA, *p>0.05). **(e)** In CPu of *SNCA OVX* mice dlCPu and dmidCPu had the largest reduction in evoked $[DA]_o$ compared to *Snca -/-* controls, 26% and 20% respectively. Two-way ANOVA revealed the main effect of genotype (*p>0.05), but no single region contributed significantly to the overall 4 p-evoked $[DA]_o$ deficits in the *SNCA OVX* line.

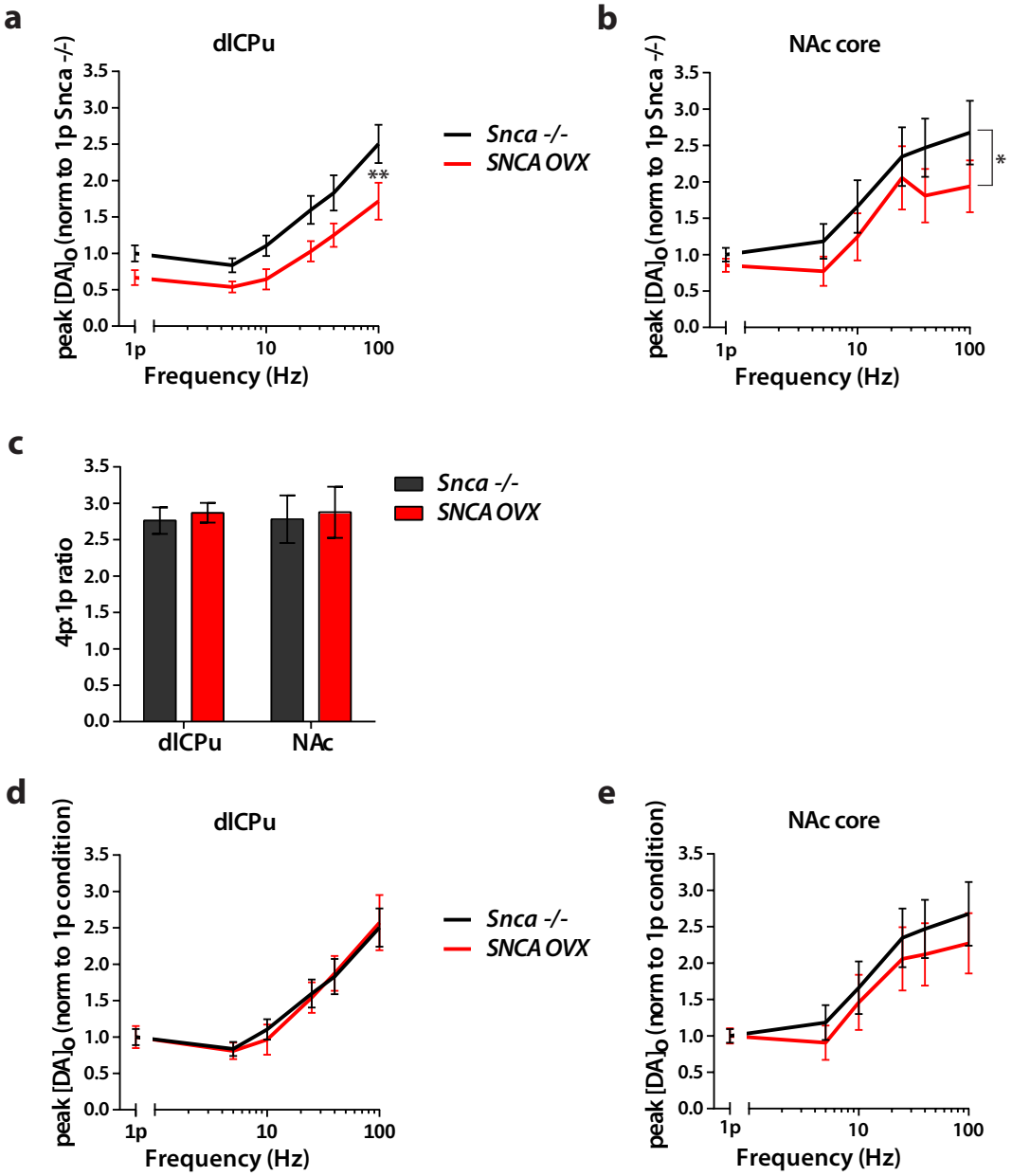

Figure 5.3 $[DA]_o$ release deficits in the *SNCA OVX* line in the absence of ACh tone at nAChRs are present across all stimulation frequencies, but frequency sensitivity and release probability of evoked $[DA]_o$ is unaltered compared to *Snca -/-* controls

(a,b) Mean peak $[DA]_o$ ± SEM versus stimulation frequency evoked by 4 pulses electrical stimulation trains at 5, 10, 25, 40 and 100 Hz in CPu **(a)** and NAc **(b)** of *Snca -/-* (N=9) and *SNCA OVX* (N=9) mice at 3-4 months of age with nAChR antagonist (DHβE, 1 μM) present throughout. Data are normalized to 1 p evoked $[DA]_o$ in the *Snca -/-*. DA release deficits in the *SNCA OVX* mice were present irrespective of stimulation frequency (Two-way ANOVA, *p<0.05, *post-hoc* Bonferroni t-tests,**p<0.01). **(c)** Ratio of $[DA]_o$ evoked by 4 pulses at 100 Hz to $[DA]_o$ evoked by 1 pulse stimulation for the dlCPu and NAc core grouped by genotype. 4p:1p ratio was not significantly different between *SNCA OVX* and *Snca -/-* lines for both dlCPu and NAC core recording sites (Two-way ANOVA, p>0.05), suggesting no changes in DA release probability. **(d,e)** Mean peak $[DA]_o$ ± SEM versus stimulation frequency evoked by 4 pulses electrical stimulation trains at 5, 10, 25, 40 and 100Hz in CPu **(d)** and NAc **(e).** Data are normalized to 1 p evoked $[DA]_o$ within each genotype. Frequency sensitivity of evoked $[DA]_o$ was unaltered in the *SNCA OVX* line compared to *Snca -/-* mice (Two-way ANOVA, p>0.05).

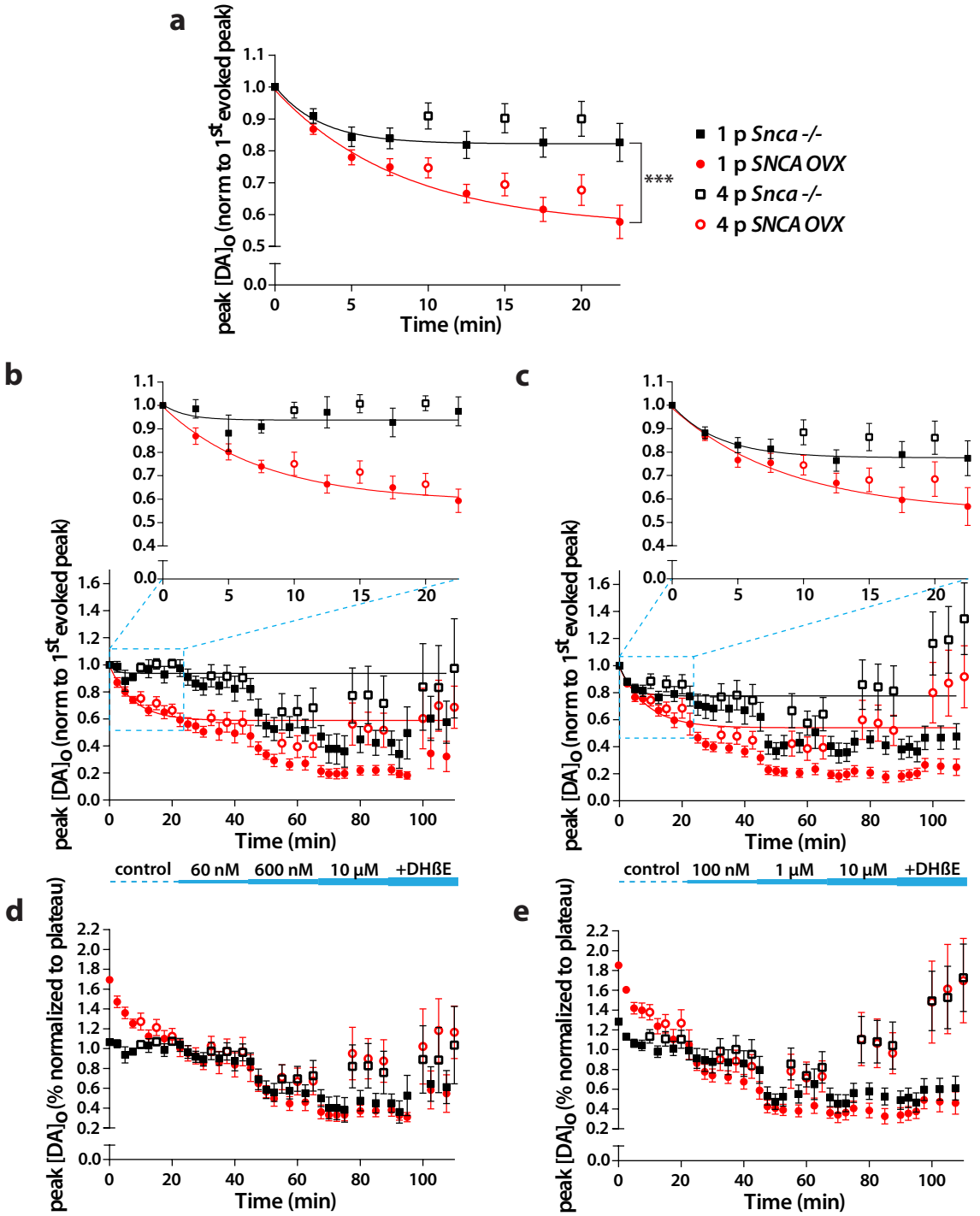

Figure 5.4 Progressive decline in evoked $[DA]_o$ over time is more pronounced in aged 18-26 months old *SNCA OVX* compared to *Snca-/-* mice

(a) Mean peak $[DA]_o$ ± SEM versus time evoked in the dlCPu of 18-26 months old *Snca -/-* (N=10) and *SNCA OVX* (N=10) mice with 1 p or 4 p 100 Hz stimulations. Data are normalized to the peak of the first evoked $[DA]_o$ transient. Exponential decay curve fit to 1 p data shows significantly higher predrug site decline in *SNCA OVX* than *Snca -/-* mice (***p<0.001). **(b,c)** Mean peak $[DA]_o$ ± SEM versus time evoked in the dlCPu with 1 p or 4 p 100 Hz stimulations during sequential application of increasing Oxo-M doses at 60 nM, 600 nM and 10 µM **(b)** or 100 nM, 1µM and 10 µM **(c)**. Data are normalized to the peak of the first evoked $[DA]_o$ transient. Exponential decay curve fit to 1 p predrug data shows significantly higher site decline in *SNCA OVX* for both data sets (***p<0.001). **(d,e)** As decline in evoked $[DA]_o$ almost reaches plateau in predrug condition, the data were normalized to their respective predrug plateau values to correct for site decline. This transformation shows that for both 60 nM **(d)** and 100 nM **(e)** data sets mAChR response to agonist application is the same, as the data for *SNCA OVX* and *Snca -/-* overlap.

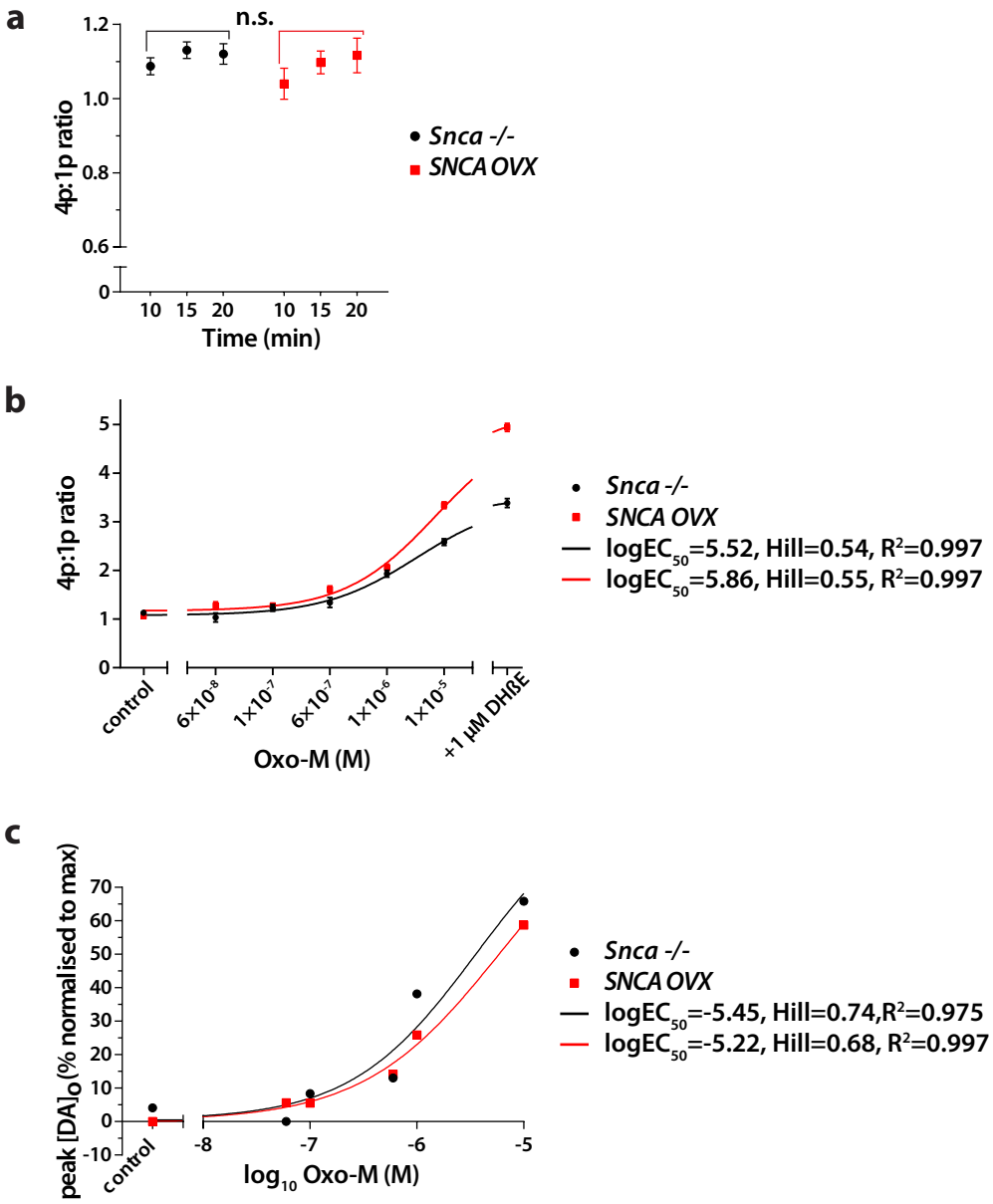

Figure 5.5 mAChR function is not altered in *SNCA OVX* compared to *Snca -/-* mice at 18-26 months
(a) Ratio of $[DA]_o$ evoked by 4 pulses at 100 Hz to $[DA]_o$ evoked by 1 pulse stimulation in the dlCPu of 18-26 months-old *SNCA OVX* (N=10) and *Snca -/-* (N=10) mice at 3 time points prior to the first drug dose application. The 4p:1p ratios were not significantly different between *SNCA OVX* and *Snca -/-* lines (unpaired t-test, p>0.05), and remained relatively steady. **(b)** Ratio of $[DA]_o$ ± SEM evoked by high frequency burst (4 p 100 Hz) to $[DA]_o$ ± SEM evoked by single pulse (1 p) versus applied concentration of mAChR agonist Oxo-M (60 nM, 100 nM, 600 nM, 1µM, 10µM) in the dlCPu of aged 18-26 months old *SNCA OVX* (N=10) and *Snca -/-* (N=10) mice. The 4p:1p ratio values at + 1 µM DHßE data point, which defines the top limit of the drug response curve, are different between genotypes and therefore the dose-response curves for Oxo-M between *SNCA OVX* and *Snca -/-* cannot be meaningfully compared without normalizing the data. **(c)** To compare dose-response curves between genotypes the 4p:1p ratio data were % normalized using the max value, i.e. the data point value at 10 µM Oxo-M+ 1 µM DHßE. For each data set the largest value represents 100% and the lowest value is 0%, Oxo-M concentration values were log-transformed. Normalized data were fitted with sigmoidal dose-response curve. The $logEC_{50}$ and Hill slope values were not significantly different between *SNCA OVX* and *Snca -/-* Oxo-M dose-response curves (p>0.05), and thus mAChR function was not altered between transgenic and control lines at 18-26 months of age.

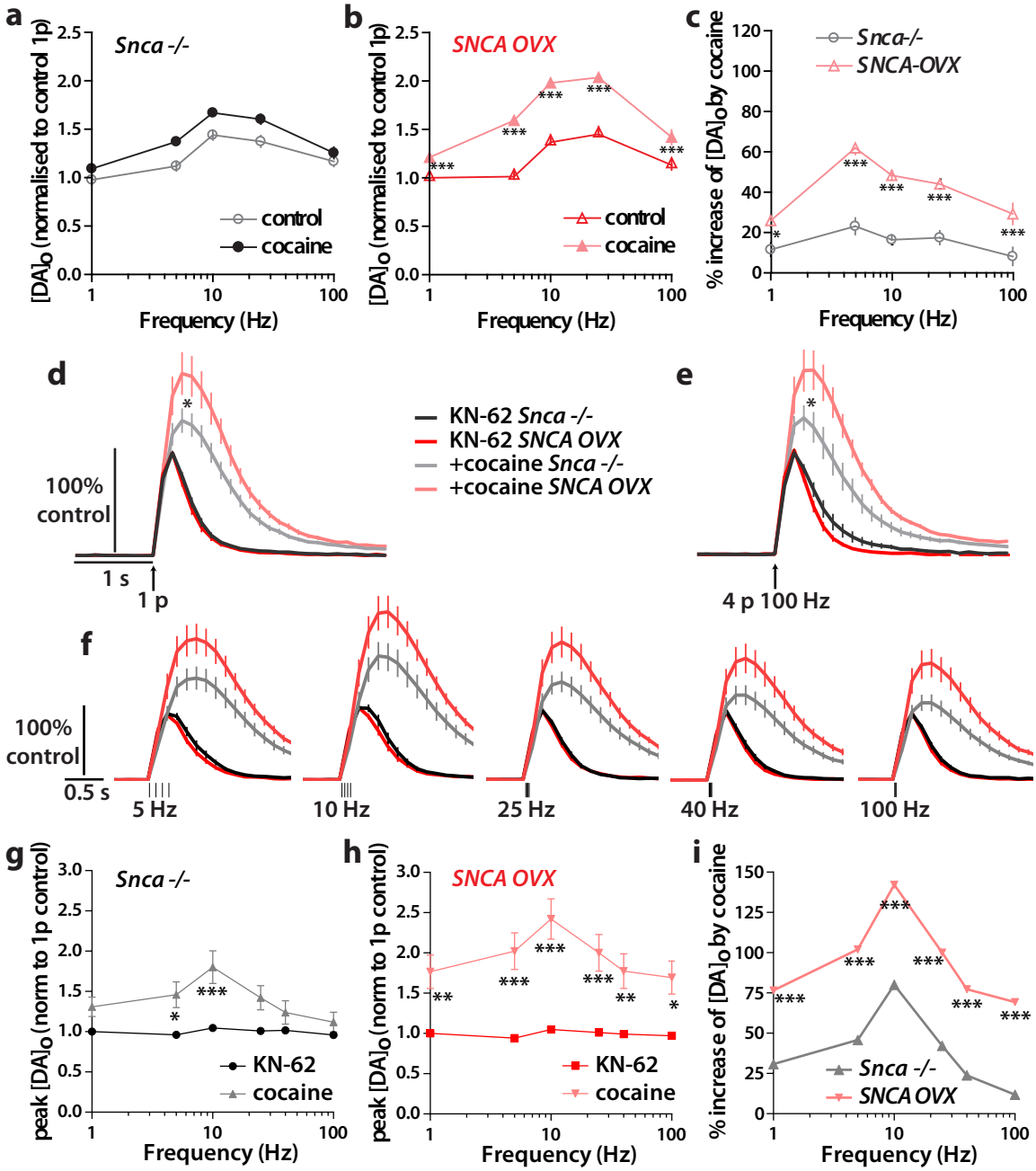

Figure 5.6 Inhibition of CaMK2 activity does not prevent the increased potentiation of evoked $[DA]_o$ by cocaine in *SNCA OVX* compared to *Snca -/-* mice

(a,b) Mean peak evoked $[DA]_o$ ± SEM versus frequency following1 pulse or 4 pulses at 5-100 Hz stimulations are not significantly different after DAT inhibition (cocaine, 5 µM) in CPu of **(a)** *Snca-/-* (Two-way ANOVA, p>0.05), but is significantly greater in **(b)** *SNCA OVX* mice (Two-way ANOVA, *post-hoc* Bonferroni t-tests). **(c)** The percentage increase of mean peak evoked $[DA]_o$ by cocaine is significantly greater in *SNCA OVX* mice (Two-way ANOVA, *post-hoc* Bonferroni t-tests).**(d-i)** All slices were pre-incubated with CaMK2 inhibitor (KN-62, 5 µM), also bath-applied at 5 µM. Data are normalized to 1 p evoked $[DA]_o$ in control, i.e. KN-62, condition within genotype. **(d,e)** Mean $[DA]_o$ ± SEM versus time evoked by 1 p **(d)** or 4 p at 100 Hz **(e)** stimulation in dlCPu of *SNCA OVX* (N=2) and *Snca -/-* (N=2) mice at 3-4 months of age in KN-62 and following DAT inhibition (cocaine, 5 µM). Cocaine potentiated evoked $[DA]_o$ significantly more in *SNCA OVX* than *Snca -/-* mice both for 1 p **(d)** and 4 p 100 Hz **(e)** protocols (Two-way ANOVA, *post-hoc* Bonferroni t-tests). **(f)** Mean $[DA]_o$ ± SEM versus time evoked by trains of 4 pulses at 1-100 Hz in KN-62 and cocaine. **(g,h)** Mean peak $[DA]_o$ ± SEM versus stimulation frequency, summary of (f). Cocaine significantly increased evoked $[DA]_o$ in both *Snca -/-* **(g)** and *SNCA OVX* **(h)** mice (Two-way ANOVA,*post-hoc* Bonferroni t-tests). **(i)** The percentage increase of mean peak evoked $[DA]_o$ was significantly greater in *SNCA OVX* than *Snca -/-* mice (Two-way ANOVA, *post-hoc* Bonferroni t-tests, *p<0.05, **p<0.01, ***p<0.001).

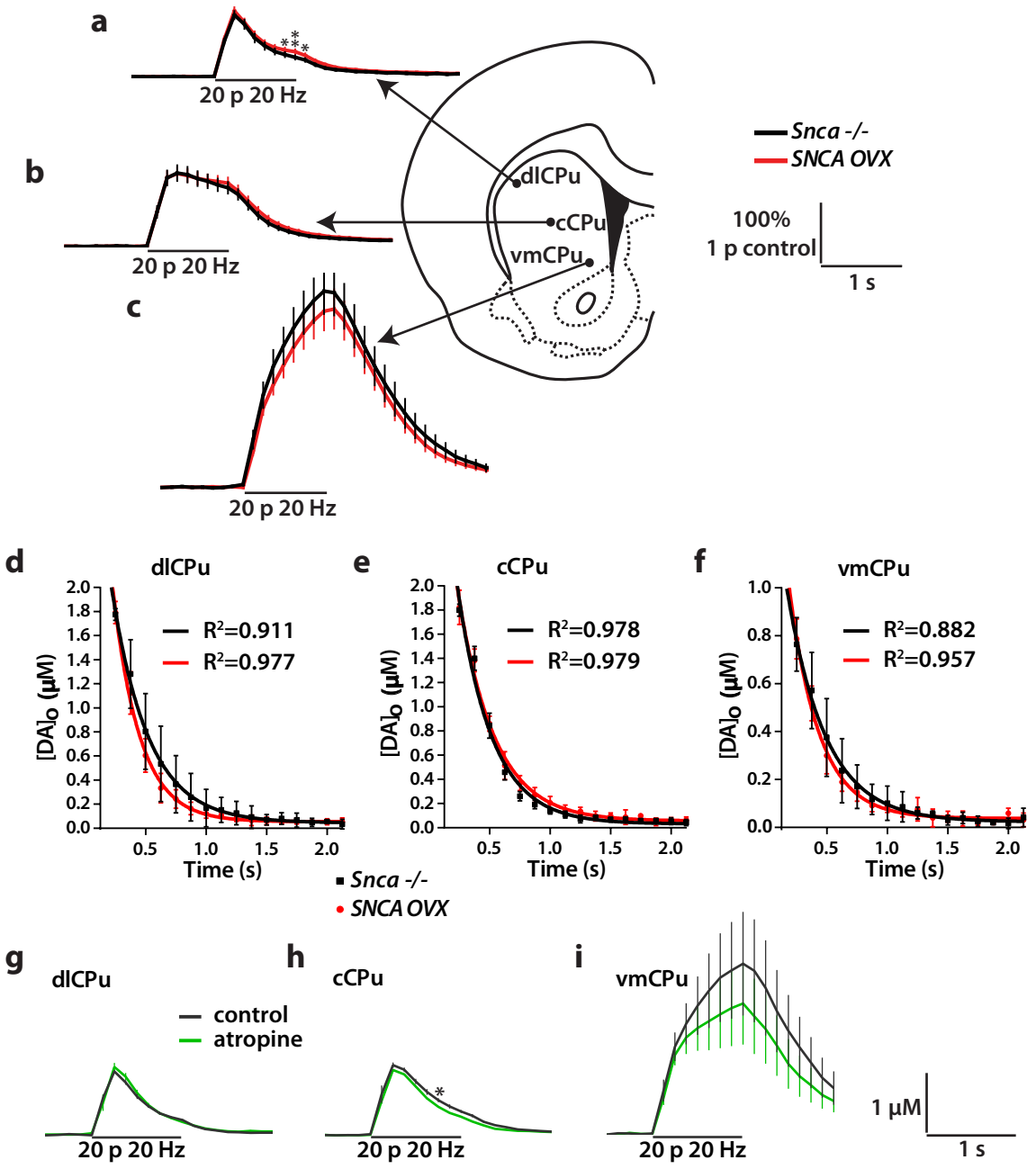

Figure 5.7 *SNCA OVX* mice show better sustained $[DA]_o$ during 1 s long electrical stimulation train in the dlCPu compared to *Snca -/-* controls

(a,b,c) Mean $[DA]_o$ ± SEM versus time evoked by electrical pulse train stimulation of 20 pulses at 20 Hz in dlCPu **(a)**, cCPu **(b)** and vmCPu **(c)** of *Snca -/-* (N=4) and *SNCA OVX* (N=4) mice at 7-10 months of age. D2 receptor antagonist (L-741,626, 1 µM) was bath-applied throughout to abolish autoinhibition of DA release. Sustained $[DA]_o$ was significantly higher in the dlCPu of *SNCA OVX* than *Snca -/-* mice at 0.875 - 1.125 s from the start of the stimulation **(a)**, and overall lower in the vmCPu (Two-way ANOVA, *post-hoc* Bonferroni t-tests). **(d,e,f)** Single-phase exponential decay curve fit of concentration-matched 1 pulse evoked $[DA]_o$ transients between 0.125-2.125 s from the start of the stimulation in dlCPu (***p<0.001) **(d)**, cCPu (**p<0.01) **(e)** and vmCPu (*p<0.05) **(f)** of *Snca -/-* (N=4) and *SNCA OVX* (N=4) mice at 7-10 months of age showed that in dlCPu and vmCPu *SNCA OVX* had higher rate of DA clearance by DAT than *Snca -/-*, while in cCPu the reverse was true. Overall, DAT function was not significantly decreased in the *SNCA OVX* line. **(g,h,i)** Mean $[DA]_o$ ± SEM versus time evoked by stimulation of 20 pulses at 20 Hz in dlCPu **(g)**, cCPu **(h)** and vmCPu **(i)** of C57Bl6/J wild-type mouse (N=1) in control and following application of muscarinic agonist (atropine, 1 µM). D2 receptor antagonist (L-741,626, 1 µM) present throughout. These pilot data show that with 1 s -long stimulation endogenous muscarinic receptor regulation of evoked DA is absent (Two-way ANOVA, *post-hoc* Bonferroni t-tests, *p<0.05,***p<0.001).

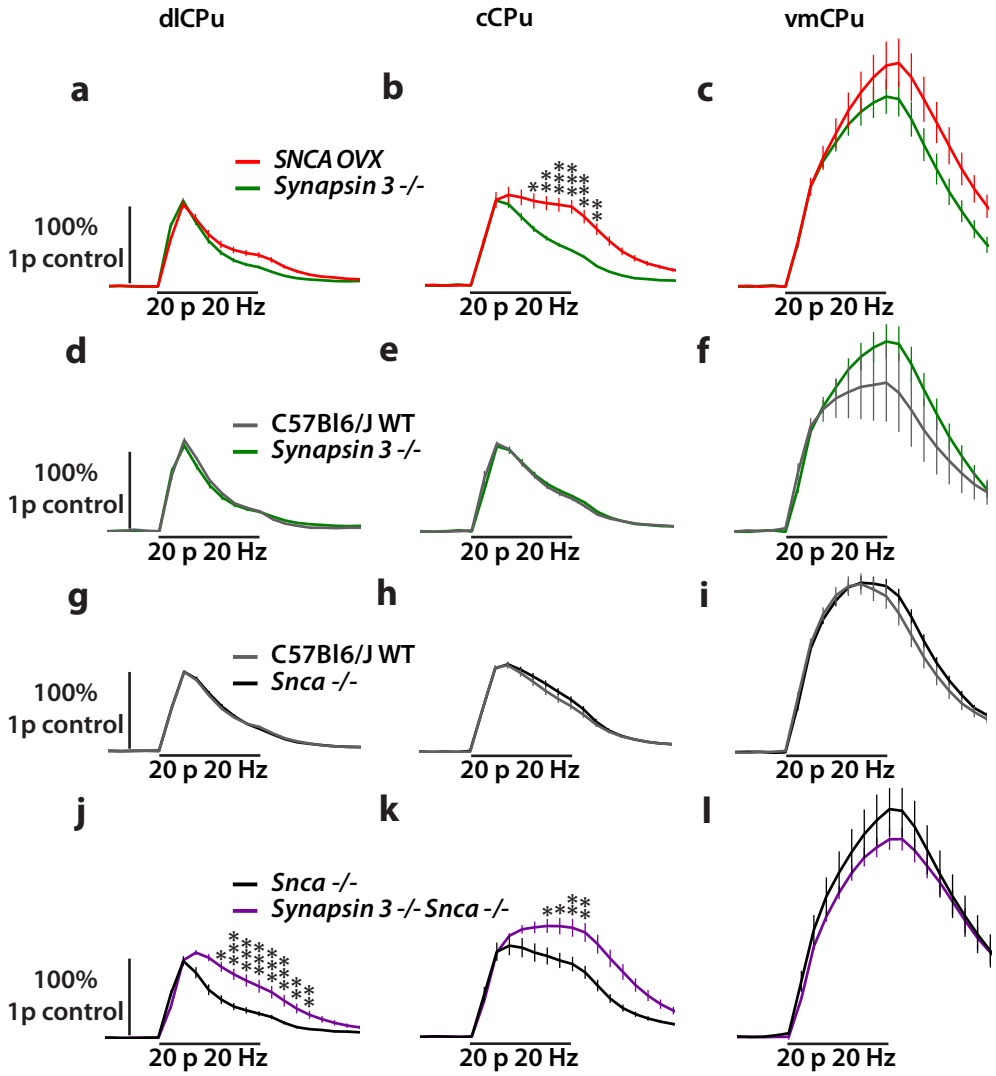

Figure 5.8 *SNCA OVX* line present with enhanced sustained $[DA]_o$ compared to *Synapsin 3 -/-* mice where vesicles are more readily available for release, while double-knockout of α-synuclein and Synapsin 3 has synergistic effects on evoked $[DA]_o$

(a-l) D2 receptor antagonist (L-741,626, 1 µM) present throughout. **(a,b,c)** Mean $[DA]_o$ ± SEM versus time evoked by 20 p at 20 Hz stimulation in dlCPu **(a),** cCPu **(b)** and vmCPu **(c)** of *SNCA OVX* (N=4) mice at 7-10 months and *Synapsin 3 -/-* (N=2) mice at 3-4 months of age. Sustained $[DA]_o$ at 0.25-1.25 s from the stimulation start was significantly lower in *Synapsin 3 -/-* line compared to *SNCA OVX* mice in dlCPu (Two-way ANOVA, ***p<0.001), cCPu (Two-way ANOVA, *post-hoc* Bonferroni t-tests) and vmCPu (Two-way ANOVA, *p<0.05). **(d,e,f)** Mean $[DA]_o$ ± SEM versus time evoked by 20 p at 20 Hz stimulation in dlCPu **(d),** cCPu **(e)** and vmCPu **(f)** of WT C57Bl6/J (N=3) and *Synapsin 3 -/-* (N=3) mice at 3-4 months of age. Sustained $[DA]_o$ at 0.25-1.25 s from the stimulation start was overall significantly different between WT and *Synapsin 3 -/-* mice in dlCPu (Two-way ANOVA, *p<0.05) and vmCPu (Two-way ANOVA,**p<0.01). **(g,h,i)** Mean $[DA]_o$ ± SEM versus time evoked by 20 p at 20 Hz stimulation in dlCPu **(g),** cCPu **(h)** and vmCPu **(i)** of WT C57Bl6/J (N=2) and *Snca -/-* (N=2) mice at 3-4 months of age (paired recordings - both genotypes on the same day). Sustained $[DA]_o$ at 0.25-1.25 s from the stimulation start was overall significantly different between WT and *Snca -/-* mice in cCPu (Two-way ANOVA, *p<0.05). **(j,k,l)** Mean $[DA]_o$ ± SEM versus time evoked by 20 p at 20 Hz stimulation in dlCPu **(j),** cCPu **(k)** and vmCPu **(l)** of *Snca -/-* (N=4) mice at 7-10 months and *Synapsin 3 -/- Snca -/-* (N=3) mice at 3-4 months of age. Sustained $[DA]_o$ at 0.25-1.25 s from the stimulation start was significantly higher in the *Synapsin 3 -/- Snca -/-* mice compared to *Snca -/-* in dlCPu (Two-way ANOVA, *post-hoc* Bonferroni t-tests), cCPu (Two-way ANOVA, *post-hoc* Bonferroni t-tests, *p<0.05,**p<0.01, ***p<0.001) and vmCPu (Two-way ANOVA, **p<0.01).

6. General Discussion

6.1 General discussion overview

The work presented in this thesis is concerned with understanding cholinergic regulation of striatal DA transmission in health and disease. Chapters 3 and 4 presented the data from exploration of candidate circuits for driving ACh-evoked striatal DA release using optogenetics. Chapter 5 examined whether ACh-dependent mechanisms could underlie DA release deficits in a mouse model of Parkinson's disease overexpressing human wild type α-synuclein protein using electrical stimulation approach. These data further extend our understanding of the interplay between striatal ACh and DA in normal and pathological states. The discussion section of individual chapters interpreted experimental results and provided a framework for understanding experimental approach and data in the light of currently published literature. The General Discussion aims to briefly review the key findings and their wider implications, thus using presented data to synthesize a bigger picture that this body of scholarly work contributes to understanding of the BG.

6.2 Acetylcholine-evoked drive of striatal dopamine release is physiologically relevant

The first goal of this thesis work was to explore physiological relevance of a recently identified ACh-evoked drive of striatal DA release (Cachope et al., 2012; Threlfell et al., 2012). Thus, I examined whether ACh-evoked striatal DA release could be triggered by driving ChI population activity via stimulation of afferents of thalamic or cortical origin. These experiments also intended to explore the relative roles of thalamostriatal and corticostriatal inputs in recruiting ACh-dependent DA release.

Optogenetic experiments using AAV5 ChR2 vector injections in CaMK2a-Cre mice revealed that both thalamostriatal and corticostriatal afferents could drive ChI-evoked DA release. These DA events detected with FCV at CFMs were dependent on glutamate and ACh, and were putatively evoked by synchronous activity in a population of striatal ChIs recruited by stimulation of their excitatory inputs. Together, these data suggest that cholinergic drive of striatal DA could potentially be engaged *in vivo*. In particular, behaviours synchronizing ChI activity following synaptic input barrages from cortical or thalamic afferents could also drive local striatal DA release. However, due to methodological complications associated with combined axonal transport of AAV5-packaged ChR2 construct in the non-specific CaMK2a-Cre driver line, I switched to using exclusively anterogradely transported AAV2-packaged ChR2 vector. Nonetheless, as AAV2 ChR2 experiments yielded no light-evoked DA events, at present it remains unknown whether thalamostriatal and corticostriatal afferents to ChIs are capable of driving locally mediated DA release independently of each other.

Thus, we learned that cholinergic drive of striatal DA release is possible via engagement of circuits removed one synapse away from the primary driver mechanism, suggesting it could be recruited *in vivo* and is physiologically relevant. However, we could not establish what are the relative roles of thalamostriatal and corticostriatal circuits in driving local striatal DA release. This is an important question to elucidate, especially in the light of data suggesting tri-fold number of synaptic contacts on ChIs of thalamic origin compared to cortical afferents (Doig et al., 2014). The question arising is whether with such vast difference in the synapse number each projection carries an equal weight in driving glutamate-dependent ACh-evoked DA events, and if so, how this 'equalized' output function is achieved. Electrophysiology data will be vital for

quantification of these relationships; yet again the difficulties of comparing the data from single cell- and population-based response monitoring would have to be addressed. Future work therefore could examine glutamatergic drive of ChI population activity for local striatal DA release using more sophisticated experimental paradigms.

6.2.1 Alternative approaches: genetic engineering and trans-synaptic targeting

To improve upon the current experimental design, several strategies can be exploited. Firstly, given limited availability of Cre-driver lines for selective targeting of cortical versus thalamic structures with bi-directionally transported AAV5 ChR2 vector, which this far has been the most successful in indirect drive of ACh-evoked DA release, genetic engineering can be called upon. For example, finding genetic markers which selectively define neuronal populations of interest, i.e. striatally-projecting M1 or Pf neurons, and subsequently targeting Cre-expression to those neurons using BAC or knock-in techniques. This fundamental change in experimental approach, however, relies on the assumption that co-activation of M1 and Pf inputs to ChIs in not required for successful drive of ACh-evoked DA by glutamatergic afferents.

Alternatively, trans-synaptic targeting of convergent inputs could also be achieved using dual injection strategies in ChAT-Cre driver line. First, injections of Cre-dependent rabies virus plasmid carrying gene sequence for either Cre- or FLP-recombinase in striatum would selectively label and transduce ChI afferents of cortical and thalamic origin via retrograde trans-synaptic transport (Kato et al., 2011; Osakada et al., 2011; Watabe-Uchida et al., 2012; Kress et al., 2013). Subsequent injections of Cre- or FLP-dependent ChR2 vectors in both M1 and Pf of these mice would enable selective

examination of roles of cortical and thalamic inputs using dual band-width optogenetic activation with red-shifted and blue-shifted ChR2 variants, such as Chrimson and Chronos (Klapoetke et al., 2014). In this case, minimally overlapping activation spectra could be used to either activate each pathway in isolation, or using broad-spectrum filter concurrently activate both M1 and Pf afferents. Furthermore, this experimental set up could be paired with DREADDs for selective inhibition of a single afferent pathway (Armbruster et al., 2007; Ferguson et al., 2011, 2013), to enable exploration of the necessary and sufficient circuit components for driving glutamate-dependent ACh-evoked striatal DA. The major shortcoming of this approach, however, would be the number of surgical procedures and large intracerebral injection volumes required, and the associated time and experimental error.

Knowing the specifics is indispensable for understanding the exact circumstances of when thalamic and/or cortical drive of terminal DA release could happen, and hence for developing experimental paradigms that could explore ChI-evoked drive of striatal DA *in vivo* using behavioural manipulations. However, the bigger picture itself lies in discovering what messages could be conveyed to the local computational circuitry via this route.

6.2.2 Are dopamine-independent behaviours really dopamine independent?

Axo-axonic drive of transmitter release from striatal dopaminergic terminals by cholinergic system raises the question of whether intact behavioural control following overtraining is really DA independent, if local DA signalling can be provided by a ChI-dependent mechanism. Thus, when DA release events are no longer supported by the

midbrain messages conveying zero reward prediction error (Schultz, 1998; Wickens et al., 2007; Steinberg et al., 2013), striatal DA release can still be evoked by local ACh-dependent signalling cascades.

ChIs acquire characteristic burst-pause firing pattern with conditioning (Morris et al., 2004; Goldberg and Reynolds, 2011). Hence, during the early learning stages pause in ChI activity could enable dynamic translation of increased firing rate of the midbrain DA neurons in striatal DA events of larger amplitude (Cragg, 2006). In turn, synchronized burst firing of ChIs, occurring either initially or upon rebound excitation, could take over driving DA release locally once the midbrain neurons are no longer responsive to stimuli or context which provide no new learning. Of course, this is one of many possible explanations for changes in DA neuron firing properties with overtraining still resulting in intact performance of putatively DA-dependent behaviours. Yet, the possibility that local ACh-dependent drive of DA release continues to encode all the necessary information and provides DA for normal circuit function is appealing.

6.2.3 Synchronized spiking or pauses in cholinergic interneuron activity that matter for acetylcholine-evoked drive of striatal dopamine?

Up to now, the core emphasis was placed on active information transfer from ChIs to DA terminals, which relies on synchronized ChI population activity and activation of pre-synaptic nAChRs on DA axons for driving locally evoked DA events. However, current results are still relevant when pauses in ChI activity, historically accepted to be the main correlate of ChI role in learning and behaviour (Wilson et al., 1990; Aosaki et al., 1998; Tan and Bullock, 2008; Schulz et al., 2011), are considered.

It is possible that the main purpose of cortical and thalamic afferents recruiting ChI population activity lies not in driving of ACh-evoked striatal DA release *per se*. Rather, it could be a way for the cholinergic system, by creating a pause-like state in ACh transmission, to enhance gain in processing of DA signals conveyed by SNc/VTA activity via transient desensitization of nAChRs on dopaminergic terminals (Cragg, 2006). Of course, the probability of this 'additional' signalling event occurring depends on the relative timing of these discrete DA release episodes. Specifically, it could only take place if DA terminals recover within 100 ms of the initial nAChRs-mediated drive of a DA release event to support the subsequent DA release directly evoked by midbrain spiking activity. Then, striatal DA signals could be amplified during the time when nAChRs are refractory. Critically, differential processing supported by distinct signal integration strategies employed by cortical versus thalamic inputs in recruiting ChI population activity would still hold true. Further, these two roles of the local ACh-mediated DA signalling cascades, i.e. local drive of DA release and gain amplification of DA signals of midbrain origin, are not mutually exclusive.

6.2.4 Defining the context in which di-synaptic drive of local striatal dopamine could support behavioural performance

The context in which glutamate-dependent ChI-evoked drive of DA release is of relevance to behaviour yet remains the subject of speculation. I propose that there are several roles these locally mediated DA signalling events may fulfil. Firstly, these events could support unperturbed striatal information processing when the nigrostriatal pathway no longer supplies DA signals. Secondly, cortical and thalamic drive of striatal DA release could also serve as global and/or local feedback circuit for acquisition of

learned behaviours. For example, evidence that selection of subsets of highly active cortical inputs happens via activation of D2 receptors (Bamford et al., 2004), suggests that cortex itself, or even Pf afferents, could selectively reinforce input filtering via this route. The same mechanism could also enhance burst firing by cortical pyramidal neurons in layer V (Vitrac et al., 2014), further increasing the probability of glutamate-dependent ChI-evoked DA events occurring. Recently published findings of DA directly driving pause response in ChIs in dorsal striatum (Chuhma et al., 2014) additionally suggest that local DA signalling could enhance conditioned response acquisition by the cholinergic system. In this case, the primary role of Pf afferents in facilitating acquisition of characteristic burst-pause response sequence by ChIs (Graybiel et al., 1994; Matsumoto et al., 2001) could happen not only via direct entrainment, but also via recruitment of ACh-evoked DA release, at least in dorsal striatum, region linked to encoding of state prediction information (Bradfield et al., 2013).

Rather than conveying mutually redundant information, cortical or thalamic drive of ChI-evoked DA release likely relays signals about distinct aspects of behaviourally salient events. Cortical inputs could predominantly encode internal occurrences, forming a top-down processing loop for attention and anticipation of significant events (Kimura et al., 2004): strong initial input would lead to a DA event. In contrast, multimodal nature of Pf inputs would make Pf striatal afferents an ideal candidate for conveying information about external events. Bottom-up sensory-driven processing underwritten by sustained activation of the circuit upon detection of discrepancy, would terminate top-down cortical drive giving precedence to Pf signals (Kimura et al., 2004). In addition, by triggering DA release Pf projections could mediate feed-forward facilitation for creating a sensory-motor preparatory set for the arrival of cortical signals by aiding

activation of MSNs via D1 receptors or selective filtering of highly active cortical inputs via D2 receptors (Hernández-López et al., 1997; Bamford et al., 2004). Cortex, in turn, via DA route could provide signals for salience attribution in conjunction with Pf inputs conveying arousal and attention, to facilitate associative learning during online behavioural performance.

6.2.5 Analogue versus digital code for signal transfer

With respect to digital versus analogue mode for signal transfer between cortical or thalamic inputs and striatal ChIs, several possible configurations exist. Cortical neurons in layer V of motor and sensory areas show tonic low frequency firing or bursting behaviour *in vitro* and *in vivo* (Agmon and Connors, 1989; Pockberger, 1991; Hattox and Nelson, 2007; Hedrick and Waters, 2011), possibly due to distinct laminar distribution of their synaptic inputs (Larkum et al., 2001). Similarly, thalamic Pf neurons can be induced to fire at frequencies of up to 40 Hz showing bursts of 2-5 spikes, but most recordings demonstrate 2-3 spikes/s firing mode (Doig et al., 2014) and discharges of groups of spikes at low frequency (Lacey et al., 2007). Hence, depending on stimuli intensity, distinct signal transfer modes could be used by M1 and Pf afferents in communicating with their downstream ChI targets.

According to Sherman (2001), tonic low frequency firing facilitates linear signal summation leading to larger excitatory post-synaptic potentials, which is equivalent to an analogue code. In turn, burst firing integration, characterized by a step function, is analogous to a digital all-or-none code. Pf inputs to ChIs may employ analogue coding, which is well suited to conveying alerting messages as signal amplitude could represent the degree of urgency. Low frequency firing typically observed in Pf units is consistent

with this prediction (Ni et al., 2000; Parr-Brownlie et al., 2009). However, existence of distinct types of Pf neurons suggests that caudal intralaminar thalamus could also employ digital coding for neurons with a bursting discharge pattern (Beatty et al., 2009). Cortical afferents are also likely to utilize a mixture of digital and analogue codes, although based on high frequency discharges recorded in single cortical units digital coding may dominate. In this case, cortical drive of striatal DA release could be employed to relieve synaptic depression which follows high frequency burst firing (Wickens et al., 1996) or even further potentiate spiking activity of cortical neurons (Vitrac et al., 2014).

Nonetheless, low release probability at cortical synapses and high release probability at thalamic terminals (Fremeau et al., 2004a, 2004b; Ding et al., 2008), may equalize the differences in the firing modes and corresponding information transfer strategies between the two afferent inputs to striatal ChIs. As such, high release probability at thalamic terminals suggests that in between responding more synapses are silent/refractory, similar to digital code. In contrast, low release probability at cortical terminals may mean these projections are better suited to analogue representation, as there is scope for further increase in response amplitude with increasing stimulation or input intensity.

Together, the above data suggest that exclusively one mode of information transfer between corticostriatal or thalamostriatal afferents and ChIs is unlikely. This arrangement corresponds with organization of information transfer between ChIs and DA axons, downstream of cortical or thalamic inputs. The relay code will always be translated to digital between ChIs and DA axon terminals, as I show that ACh-evoked DA

release events are all-or-none responses. Therefore, relying exclusively on analogue code by either thalamic or cortical afferents to striatal ChIs may be redundant, as this information is never conveyed to the downstream dopaminergic targets, unless it has some functionality at the level of regulating ChI activity and not ACh-evoked DA release.

6.2.6 Acetylcholine-evoked dopamine release is not a species artefact

One of the important concerns for all optogenetic experiments using transgenic mouse lines is whether generated results are genuine, or are a consequence of transgene expression, changes in native protein expression patterns, etc. Therefore, an important experiment for demonstrating physiological relevance of ACh-evoked DA events, in addition to showing recruitment of DA release by stimulation of ChI afferents in CaMK2a-Cre mice, was to show that ACh-dependent DA release following direct activation of ChI populations is not specific to ChAT-Cre or ChAT-ChR2 mouse lines. Large amplitude light-evoked DA release events were recorded throughout dorsal and ventral striatum of ChAT-Cre rat (Witten et al., 2011) expressing ChR2 in ChIs following striatal injections of AAV2 ChR2. Hence, I confirmed that ACh-evoked drive of striatal DA release is not a species artefact, and is observed in both mouse and rat following direct activation of striatal ChIs expressing ChR2 with blue light. Significantly, AAV2-packaged ChR2 construct was successfully employed to drive light-evoked striatal DA release with direct activation of ChIs in mouse and rat ChAT-Cre lines, yet failed to do so when used for recruitment of ChI activity by stimulation of their afferent excitatory inputs.

6.3 AAV5 ChR2, AAV2 ChR2 and hyperpolarization experiments: implications for probing circuit function using optogenetics

The foremost difference in using AAV5-packaged and AAV2-packaged ChR2 constructs in CaMK2a-Cre driver line was their success and failure in driving glutamate-dependent ACh-evoked striatal DA release. Thus, for indirect drive of striatal DA via recruitment of ChI population activity by activation of their excitatory glutamatergic afferents only the AAV5 ChR2 vector was successful. In contrast, AAV2 ChR2 experiments in several permutations consistently generated negative data. Yet, the AAV2 ChR2 vector was functional as when used in ChAT-Cre mouse and rat, DA events evoked by direct depolarization of striatal ChIs with light were robust. The discordant results from the AAV5 ChR2 and AAV2 ChR2 series of experiments first of all suggest that vector properties play a major role in determining the success of experimental outcomes, and thus call for scrupulous examination of negative data and careful design of circuit mapping experiments. Secondly, they also emphasize that further work is required to delineate the exact circumstances of when and whether independent drive of striatal DA release via ChIs by cortical and thalamic inputs is achievable.

It is possible that AAV2 ChR2 simply failed to transduce large enough population of striatally-projecting neurons to achieve sufficient synchronization of excitatory activity in post-synaptic ChIs. However, AAV2 ChR2-transduced afferents also may not have been able to recruit any post-synaptic excitation in striatal ChIs. Future studies should therefore incorporate electrophysiology to back up FCV data and distinguish between a number of alternative explanations. Furthermore, electrophysiology data

would be able to offer clues regarding the necessity of cortical and thalamic inputs co-activation for driving glutamate-dependent ACh-evoked DA release.

A direct comparison between AAV5 ChR2 and AAV2 ChR2 experiments is not possible, not only due to different transduction efficiencies of the two vectors, but also distinct recruitment of intracellular transport machinery by AAV5 and AAV2. Notably, all AAV-based vectors reported to provide high levels of ChR2 transduction both in rodent and primate brains, including AAV5, AAV6, AAV8 and AAV9 serotypes (Paterna et al., 2004; Taymans et al., 2007; McFarland et al., 2009; Markakis et al., 2010; Towne et al., 2010; Masamizu et al., 2011; Salegio et al., 2012), are subject to combined anterograde-retrograde axonal transport which perhaps renders them most efficient in facilitating virus spread. Extending our understanding of mechanisms regulating neuronal transduction with AAV-packaged vectors, including molecules governing intracellular transport modes, would greatly aid future studies by enabling informed choice of construct to suit a particular experimental design.

The inability to drive light-evoked DA release following optical stimulation of hyperpolarizing opsins Arch 3.0 and eNpHR 3.0 selectively expressed in striatal ChIs in ChAT-Cre mouse line was ubiquitous. Yet, these studies would also benefit from companion electrophysiology. We can be fairly certain that inhibition of ChIs activity was achievable with these hyperpolarizing ion pumps, while the state of rebound spiking, if any, is completely unknown. Averaging single cell responses could obscure main effects and complicate extrapolation of single-cell electrophysiology results to a direct comparison with FCV read-out of a population-based response in ACh-evoked striatal DA release. An alternative approach would be to perform experiments geared towards

monitoring of spiking activity from a large population of neurons simultaneously in real time. In this respect, Ca^{2+} imaging with genetically encoded indicators could be a promising tool and should be considered for further extending the current work. Nonetheless, these experiments also face challenges because Ca^{2+} imaging needs to be combined with optogenetic stimulation, and currently there are no reports of opsin and voltage sensitive Ca^{2+} indicators co-expression in the same neuronal population. Further, newly emerging chloride-selective variants of ChR2 (Berndt et al., 2014; Wietek et al., 2014) could significantly benefit the investigation of evoked DA release induced by rebound spiking in striatal ChI populations, as these hyperpolarizing tools are more likely to provide sufficient hyperpolarization not only to pause ChI activity, but also achieve sufficient membrane depolarization to induce intrinsically-generated rebound excitation.

6.4 Cholinergic modulation of striatal dopamine release: implications for *SNCA OVX* work

Further examination of DA release deficits in the *SNCA OVX* line showed that changes in ACh tone at nAChRs were not a mechanism underlying impaired evoked DA release in dorsal striatum of this PD model, overexpressing human wild type α-synuclein protein. Instead evoked DA impairments stemmed from a primary dysfunction at the level of DA axon terminals. However, I unexpectedly uncovered potential deficits in evoked DA release in ventral striatum of the same model in experimental paradigm where ACh action at nAChRs was removed. These data indicate that changes in ACh tone at nAChRs could mask or compensate for DA release deficits in ventral striatum of *SNCA OVX* mice, while in dorsal striatum cholinergic system appears to have little effect on α-synuclein-dependent DA neuron dysfunction.

More extended examination of these findings is needed, but they potentially offer new insights into treatment strategies targeting DA dysfunction in PD with anticholinergic agents. In theory, these data could change our understanding of PD therapeutics, suggesting that in some disease cases where α-synuclein overexpression is involved, the effects of anticholinergic drugs may be different between dorsal and ventral striatum, with little effect on the former and exacerbating an underlying dopaminergic dysfunction in the latter. However, firm conclusions on this account cannot be drawn without a large scale biochemical and electrophysiological profiling of the two striatal regions to identify primary and compensatory changes underlying alterations in evoked DA release, and finding an explanation for how cholinergic tone may distinctly affect evoked DA properties between CPu and NAc. Significantly, cholinergic impact on striatal DA release in PD may also be mediated via ACh-evoked drive of striatal DA release, especially via thalamostriatal projections (Threlfell et al., 2012). There is a number of reports from human PD cases identifying Pf neuron degeneration in this patient group (Henderson et al., 2000a, 2000b; Halliday, 2009). Further, Pf overactivity has also been reported for animal models of PD (Bacci et al., 2004; Lanciego et al., 2008), perhaps suggesting compensatory changes that transiently upregulate neuronal activity to support striatal DA release. These observations suggest that ACh impact on DA dysfunction in PD cases resulting from α-synuclein overexpression may be even greater.

Another intriguing observation that emerged from the work on this model of PD is concerned with α-synuclein-dependent changes in vesicle handling, which may be a candidate mechanism for impaired DA release in *SNCA OVX* mice. Specifically, the data suggest that the properties of evoked and sustained $[DA]_o$ may be differentially affected

by α-synuclein overexpression. While impairing initial release, possibly due to increased vesicle clustering precluding efficient vesicle recruitment to the docking sites with short-lasting depolarization, sustained $[DA]_o$ is actually higher in the *SNCA OVX* line compared to *Snca -/-* controls. The future work must examine these differences further to explore if they could be more apparent with more extended stimulation protocols, and potentially using techniques that enable more precise quantification of quantal release over time, including electrophysiology and amperometry. In turn, if this theory holds up in the face of evidence, these new insights could be used for therapeutic targeting of evoked DA deficits with treatments that reduce vesicle clustering in dopaminergic terminals that are induced by α-synuclein-dependent changes in vesicle handling.

6.5 Concluding remarks

The data presented in this thesis underscore the importance of understanding the wider context for ACh-DA interactions in health and disease states. These interactions have a significant impact on the overall function of the BG, primarily via their effect on striatal circuitry, and therefore require further hypothesis-driven exploration. From the work conducted as part of this thesis research we learned that dopaminergic pathways in dorsal and ventral striatum may be differentially affected by α-synuclein overexpression in *SNCA OVX* mouse model of PD, possibly due to distinct compensatory changes in ACh tone. Further, this work drew a distinction between instantaneous DA release events recruited with short stimulation protocols, which consistently show evoked DA deficits, and sustained DA release following prolonged depolarization, which may be better in *SNCA OVX* compared to *Snca -/-* mice. This hypothesis provides a testable framework for understanding α-synuclein-dependent

dysfunction of DA neurons during early disease stages, potentially explaining why deficits in evoked DA release are present prior to SNc degeneration and even in the face of normal DA tissue content. In turn, AAV5 ChR2 work suggested that cortical and thalamic afferents to ChIs may work co-operatively to drive ACh-evoked striatal DA release. It remains to be established what the relative contributions of each individual pathway to ChI-evoked rive of striatal DA release are. Further work on this front would benefit from combining optogenetics, FCV and electrophysiology, and use of selective transduction methods where behaviour of viral vectors can be better controlled. From the current work we learned that some of the methodological complications cannot be predicted in advance, and thus may require flexible evolution of experimental approaches to tackle research questions at hand.

Bibliography

Abeliovich A, Schmitz Y, Fariñas I, Choi-Lundberg D, Ho WH, Castillo PE, Shinsky N, Verdugo JM, Armanini M, Ryan A, Hynes M, Phillips H, Sulzer D, Rosenthal A (2000) Mice lacking alpha-synuclein display functional deficits in the nigrostriatal dopamine system. Neuron 25:239–252.

Adrover MF, Shin JH, Alvarez VA (2014) Glutamate and dopamine transmission from midbrain dopamine neurons share similar release properties but are differentially affected by cocaine. J Neurosci 34:3183–3192.

Agmon A, Connors BW (1989) Repetitive burst-firing neurons in the deep layers of mouse somatosensory cortex. Neurosci Lett 99:137–141.

Al-Mansoori KM, Hasan MY, Al-Hayani A, El-Agnaf OMA (2013) The role of α-synuclein in neurodegenerative diseases: from molecular pathways in disease to therapeutic approaches. Curr Alzheimer Res 10:559–568.

Albin RL, Young AB, Penney JB (1989) The functional anatomy of basal ganglia disorders. Trends Neurosci 12:366–375.

Albin RL, Young AB, Penney JB (1995) The functional anatomy of disorders of the basal ganglia. Trends Neurosci 18:63–64.

Alcantara a a, Mrzljak L, Jakab RL, Levey a I, Hersch SM, Goldman-Rakic PS (2001) Muscarinic m1 and m2 receptor proteins in local circuit and projection neurons of the primate striatum: anatomical evidence for cholinergic modulation of glutamatergic prefronto-striatal pathways. J Comp Neurol 434:445–460.

Aldridge JW, Berridge KC, Rosen AR (2004) Basal ganglia neural mechanisms of natural movement sequences. Can J Physiol Pharmacol 82:732–739.

Aldrin-Kirk P, Davidsson M, Holmqvist S, Li J-Y, Björklund T (2014) Novel AAV-Based Rat Model of Forebrain Synucleinopathy Shows Extensive Pathologies and Progressive Loss of Cholinergic Interneurons. Lewis P, ed. PLoS One 9:e100869.

Alloway KD, Smith JB, Watson GDR (2014) Thalamostriatal projections from the medial posterior and parafascicular nuclei have distinct topographic and physiologic properties. J Neurophysiol 111:36–50.

Altman J, Bayer SA (1981) Development of the brain stem in the rat. V. Thymidine-radiographic study of the time of origin of neurons in the midbrain tegmentum. J Comp Neurol 198:677–716.

Amara SG, Kuhar MJ (1993) Neurotransmitter transporters: recent progress. Annu Rev Neurosci 16:73–93.

Anstrom KK, Woodward DJ (2005) Restraint increases dopaminergic burst firing in awake rats. Neuropsychopharmacology 30:1832–1840.

Anwar S, Peters O, Millership S, Ninkina N, Doig N, Connor-Robson N, Threlfell S, Kooner G, Deacon RM, Bannerman DM, Bolam JP, Chandra SS, Cragg SJ, Wade-Martins R, Buchman VL (2011) Functional alterations to the nigrostriatal system in mice lacking all three members of the synuclein family. J Neurosci 31:7264–7274.

Anzalone A, Ramos M, Mei C De, Hopf FW, Iaccarino C, Halbout B, Jacobsen J, Kinoshita C, Welter M, Caron MG, Bonci A, Sulzer D, Borrelli E, Lizardi-Ortiz JE, De Mei C (2012) Dual Control of Dopamine Synthesis and Release by Presynaptic and Postsynaptic Dopamine D2 Receptors. J Neurosci 32:9023–9034.

Aosaki T, Graybiel AM, Kimura M (1994a) Effect of the nigrostriatal dopamine system on acquired neural responses in the striatum of behaving monkeys. Science 265:412–415.

Aosaki T, Kimura M, Graybiel AM (1995) Temporal and spatial characteristics of tonically active neurons of the primate's striatum. J Neurophysiol 73:1234–1252.

Aosaki T, Kiuchi K, Kawaguchi Y (1998) Dopamine D1-like receptor activation excites rat striatal large aspiny neurons in vitro. J Neurosci 18:5180–5190.

Aosaki T, Tsubokawa H, Ishida A, Watanabe K, Graybiel AM, Kimura M (1994b) Responses of tonically active neurons in the primate's striatum undergo systematic changes during behavioral sensorimotor conditioning. J Neurosci 14:3969–3984.

Apicella P (2002) Tonically active neurons in the primate striatum and their role in the processing of information about motivationally relevant events. Eur J Neurosci 16:2017–2026.

Apicella P (2007) Leading tonically active neurons of the striatum from reward detection to context recognition. Trends Neurosci 30:299–306.

Arbuthnott GW, Wickens J (2007) Space, time and dopamine. Trends Neurosci 30:62–69.

Armbruster BN, Li X, Pausch MH, Herlitze S, Roth BL (2007) Evolving the lock to fit the key to create a family of G protein-coupled receptors potently activated by an inert ligand. Proc Natl Acad Sci U S A 104:5163–5168.

Armstrong-James M, Millar J (1979) Carbon fibre microelectrodes. J Neurosci Methods 1:279–287.

Armstrong-James M, Millar J, Kruk ZL (1980) Quantification of noradrenaline iontophoresis. Nature 288:181–183.

Arroyo-Jim nez MM, Bourgeois JP, Marubio LM, Le Sourd AM, Ottersen OP, Rinvik E, Fairén A, Changeux JP (1999) Ultrastructural localization of the alpha4-subunit of the neuronal acetylcholine nicotinic receptor in the rat substantia nigra. J Neurosci 19:6475–6487.

Aschauer DF, Kreuz S, Rumpel S (2013) Analysis of transduction efficiency, tropism and axonal transport of AAV serotypes 1, 2, 5, 6, 8 and 9 in the mouse brain. PLoS One 8:e76310.

Avshalumov M V, Chen BT, Marshall SP, Peña DM, Rice ME (2003) Glutamate-dependent inhibition of dopamine release in striatum is mediated by a new diffusible messenger, H2O2. J Neurosci 23:2744–2750.

Avshalumov M V, Patel JC, Rice ME (2008) AMPA receptor-dependent H2O2 generation in striatal medium spiny neurons but not dopamine axons: one source of a retrograde signal that can inhibit dopamine release. J Neurophysiol 100:1590–1601.

Baba M, Nakajo S, Tu PH, Tomita T, Nakaya K, Lee VM, Trojanowski JQ, Iwatsubo T (1998) Aggregation of alpha-synuclein in Lewy bodies of sporadic Parkinson's disease and dementia with Lewy bodies. Am J Pathol 152:879–884.

Bacci J-J, Kachidian P, Kerkerian-Le Goff L, Salin P (2004) Intralaminar thalamic nuclei lesions: widespread impact on dopamine denervation-mediated cellular defects in the rat basal ganglia. J Neuropathol Exp Neurol 63:20–31.

Balleine BW, O'Doherty JP (2010) Human and rodent homologies in action control: corticostriatal determinants of goal-directed and habitual action. Neuropsychopharmacology 35:48–69.

Bamford NS, Zhang H, Schmitz Y, Wu N, Cepeda C, Levine MS, Schmauss C, Zakharenko SS, Zablow L, Sulzer D (2004) Heterosynaptic dopamine neurotransmission selects sets of corticostriatal terminals. 42:653–663.

Bayer S, Wills K, Triarhou L, Ghetti B (1995) Time of neuron origin and gradients of neurogenesis in midbrain dopaminergic neurons in the mouse. Exp Brain Res 105.

Beach TG, Adler CH, Sue LI, Peirce JB, Bachalakuri J, Dalsing-Hernandez JE, Lue LF, Caviness JN, Connor DJ, Sabbagh MN, Walker DG (2008) Reduced striatal tyrosine hydroxylase in incidental Lewy body disease. Acta Neuropathol 115:445–451.

Beatty J a, Sylwestrak EL, Cox CL (2009) Two distinct populations of projection neurons in the rat lateral parafascicular thalamic nucleus and their cholinergic responsiveness. Neuroscience 162:155–173.

Bell MI, Richardson PJ, Lee K (2002) Functional and molecular characterization of metabotropic glutamate receptors expressed in rat striatal cholinergic interneurones. J Neurochem 81:142–149.

Bellani S, Sousa VL, Ronzitti G, Valtorta F, Meldolesi J, Chieregatti E (2010) The regulation of synaptic function by alpha-synuclein. Commun Integr Biol 3:106–109.

Bello EP, Mateo Y, Gelman DM, Noaín D, Shin JH, Low MJ, Alvarez V a, Lovinger DM, Rubinstein M (2011) Cocaine supersensitivity and enhanced motivation for reward in mice lacking dopamine D2 autoreceptors. Nat Neurosci 14:1033–1038.

Bellucci A, Navarria L, Falarti E, Zaltieri M, Bono F, Collo G, Spillantini MG, Grazia M, Missale C, Spano P (2011) Redistribution of DAT/α-synuclein complexes visualized by "in situ" proximity ligation assay in transgenic mice modelling early Parkinson's disease. PLoS One 6:e27959.

Beltramo R, D'Urso G, Dal Maschio M, Farisello P, Bovetti S, Clovis Y, Lassi G, Tucci V, De Pietri Tonelli D, Fellin T (2013) Layer-specific excitatory circuits differentially control recurrent network dynamics in the neocortex. Nat Neurosci 16.

Bennett BD, Bolam JP (1993) Characterization of calretinin-immunoreactive structures in the striatum of the rat. Brain Res 609:137–148.

Bennett BD, Callaway JC, Wilson CJ (2000) Intrinsic membrane properties underlying spontaneous tonic firing in neostriatal cholinergic interneurons. Neurosci Res 20:8493–8503.

Bennett BD, Wilson CJ (1998) Synaptic regulation of action potential timing in neostriatal cholinergic interneurons. J Neurosci 18:8539–8549.

Bennett BD, Wilson CJ (1999) Spontaneous activity of neostriatal cholinergic interneurons in vitro. J Neurosci 19:5586–5596.

Benson DL, Isackson PJ, Gall CM, Jones EG (1992) Contrasting patterns in the localization of glutamic acid decarboxylase and Ca2+/calmodulin protein kinase gene expression in the rat central nervous system. Neuroscience 46:825–849.

Benson DL, Isackson PJ, Hendry SH, Jones EG (1991) Differential gene expression for glutamic acid decarboxylase and type II calcium-calmodulin-dependent protein kinase in basal ganglia, thalamus, and hypothalamus of the monkey. J Neurosci 11:1540–1564.

Berendse HW, Galis-de Graaf Y, Groenewegen HJ (1992) Topographical organization and relationship with ventral striatal compartments of prefrontal corticostriatal projections in the rat. J Comp Neurol 316:314–347.

Berendse HW, Groenewegen HJ (1990) Organization of the thalamostriatal projections in the rat, with special emphasis on the ventral striatum. J Comp Neurol 299:187–228.

Bernácer J, Prensa L, Giménez-Amaya JM (2007) Cholinergic interneurons are differentially distributed in the human striatum. PLoS One 2:e1174.

Bernard R, Veh RW (2012) Individual neurons in the rat lateral habenular complex project mostly to the dopaminergic ventral tegmental area or to the serotonergic raphe nuclei. J Comp Neurol 520:2545–2558.

Bernard V, Bolam JP (1998) Subcellular and subsynaptic distribution of the NR1 subunit of the NMDA receptor in the neostriatum and globus pallidus of the rat: co-localization at synapses with the GluR2/3 subunit of the AMPA receptor. Eur J Neurosci 10:3721–3736.

Berndt A, Lee SY, Ramakrishnan C, Deisseroth K (2014) Structure-guided transformation of channelrhodopsin into a light-activated chloride channel. Science 344:420–424.

Berridge KC, Robinson TE (1998) What is the role of dopamine in reward: hedonic impact, reward learning, or incentive salience? Brain Res Brain Res Rev 28:309–369.

Bertorelli R, Zambelli M, Di Chiara G, Consolo S (1992) Dopamine depletion preferentially impairs D1- over D2-receptor regulation of striatal in vivo acetylcholine release. J Neurochem 59:353–357.

Bevan MD, Bolam JP (1995) Cholinergic, GABAergic, and glutamate-enriched inputs from the mesopontine tegmentum to the subthalamic nucleus in the rat. J Neurosci 15:7105–7120.

Björklund A, Lindvall O (1984) Dopamine-containing systems in the CNS. Handb Chem Neuroanat Class Transm Rat.

Bodner RA, Outeiro TF, Altmann S, Maxwell MM, Cho SH, Hyman BT, McLean PJ, Young AB, Housman DE, Kazantsev AG (2006) Pharmacological promotion of inclusion formation: a therapeutic approach for Huntington's and Parkinson's diseases. Proc Natl Acad Sci U S A 103:4246–4251.

Bolam JP, Francis CM, Henderson Z (1991) Cholinergic input to dopaminergic neurons in the substantia nigra: a double immunocytochemical study. Neuroscience 41:483–494.

Bolam JP, Hanley JJ, Booth P a, Bevan MD (2000) Synaptic organisation of the basal ganglia. J Anat 196 (Pt 4:527–542.

Bolam JP, Wainer BH, Smith AD (1984) Characterization of cholinergic neurons in the rat neostriatum. A combination of choline acetyltransferase immunocytochemistry, Golgi-impregnation and electron microscopy. Neuroscience 12:711–718.

Bond A (1980) Modern polarographic methods in analytical chemistry.

Bonsi P, Cuomo D, De Persis C, Centonze D, Bernardi G, Calabresi P, Pisani a (2005) Modulatory action of metabotropic glutamate receptor (mGluR) 5 on mGluR1 function in striatal cholinergic interneurons. Neuropharmacology 49 Suppl 1:104–113.

Bonsi P, Cuomo D, Martella G, Madeo G, Schirinzi T, Puglisi F, Ponterio G, Pisani A (2011) Centrality of striatal cholinergic transmission in Basal Ganglia function. Front Neuroanat 5:6.

Bonsi P, Martella G, Cuomo D, Platania P, Sciamanna G, Bernardi G, Wess J, Pisani A (2008) Loss of muscarinic autoreceptor function impairs long-term depression but not long-term potentiation in the striatum. J Neurosci 28:6258–6263.

Borisovska M, Bensen a. L, Chong G, Westbrook GL (2013) Distinct Modes of Dopamine and GABA Release in a Dual Transmitter Neuron. J Neurosci 33:1790–1796.

Borland LM, Michael AC (2004) Voltammetric study of the control of striatal dopamine release by glutamate. J Neurochem 91:220–229.

Boyden ES, Zhang F, Bamberg E, Nagel G, Deisseroth K (2005) Millisecond-timescale, genetically targeted optical control of neural activity. Nat Neurosci 8:1263–1268.

Bradfield LAA, Bertran-Gonzalez J, Chieng B, Balleine BWW (2013) The Thalamostriatal Pathway and Cholinergic Control of Goal-Directed Action: Interlacing New with Existing Learning in the Striatum. Neuron 79:1–14.

Brischoux F, Chakraborty S, Brierley DI, Ungless MA (2009) Phasic excitation of dopamine neurons in ventral VTA by noxious stimuli. Proc Natl Acad Sci U S A 106:4894–4899.

Britt JP, Benaliouad F, McDevitt RA, Stuber GD, Wise RA, Bonci A (2012) Synaptic and Behavioral Profile of Multiple Glutamatergic Inputs to the Nucleus Accumbens. Neuron 76:790–803.

Britt JP, McGehee DS (2008) Presynaptic opioid and nicotinic receptor modulation of dopamine overflow in the nucleus accumbens. J Neurosci 28:1672–1681.

Broekman MLD, Comer LA, Hyman BT, Sena-Esteves M (2006) Adeno-associated virus vectors serotyped with AAV8 capsid are more efficient than AAV-1 or -2 serotypes for widespread gene delivery to the neonatal mouse brain. Neuroscience 138:501–510.

Brog JS, Salyapongse a, Deutch a Y, Zahm DS (1993) The patterns of afferent innervation of the core and shell in the "accumbens" part of the rat ventral striatum: immunohistochemical detection of retrogradely transported fluoro-gold. J Comp Neurol 338:255–278.

Brown MTC, Tan KR, O'Connor EC, Nikonenko I, Muller D, Lüscher C (2012) Ventral tegmental area GABA projections pause accumbal cholinergic interneurons to enhance associative learning. Nature:1–5.

Brown P (2007) Abnormal oscillatory synchronisation in the motor system leads to impaired movement. Curr Opin Neurobiol 17:656–664.

Bull DR, Palij P, Sheehan MJ, Millar J, Stamford JA, Kruk ZL, Humphrey PP (1990) Application of fast cyclic voltammetry to measurement of electrically evoked dopamine overflow from brain slices in vitro. J Neurosci Methods 32:37–44.

Burger C, Gorbatyuk OS, Velardo MJ, Peden CS, Williams P, Zolotukhin S, Reier PJ, Mandel RJ, Muzyczka N (2004) Recombinant AAV viral vectors pseudotyped with viral capsids from serotypes 1, 2, and 5 display differential efficiency and cell tropism after delivery to different regions of the central nervous system. Mol Ther 10:302–317.

Burre J, Sharma M, Sudhof TC (2012) Systematic Mutagenesis of -Synuclein Reveals Distinct Sequence Requirements for Physiological and Pathological Activities. J Neurosci 32:15227–15242.

Burré J, Sharma M, Tsetsenis T, Buchman V, Etherton MR, Südhof TC (2010) Alpha-synuclein promotes SNARE-complex assembly in vivo and in vitro. Science 329:1663–1667.

Cabin DE, Shimazu K, Murphy D, Cole NB, Gottschalk W, McIlwain KL, Orrison B, Chen A, Ellis CE, Paylor R, Lu B, Nussbaum RL (2002) Synaptic vesicle depletion correlates with attenuated synaptic responses to prolonged repetitive stimulation in mice lacking alpha-synuclein. J Neurosci 22:8797–8807.

Cachope R, Mateo Y, Mathur BNN, Irving J, Wang H-L, Morales M, Lovinger DMM, Cheer JFF (2012) Selective Activation of Cholinergic Interneurons Enhances Accumbal Phasic Dopamine Release: Setting the Tone for Reward Processing. Cell Rep 2:33–41.

Calabresi P, Centonze D, Gubellini P, Marfia G a, Pisani a, Sancesario G, Bernardi G (2000a) Synaptic transmission in the striatum: from plasticity to neurodegeneration.

Calabresi P, Centonze D, Gubellini P, Pisani A, Bernardi G (2000b) Acetylcholine-mediated modulation of striatal function. Trends Neurosci 23:120–126.

Calabresi P, Centonze D, Pisani a, Sancesario G, North R a, Bernardi G (1998) Muscarinic IPSPs in rat striatal cholinergic interneurones. J Physiol 510 (Pt 2:421–427.

Calabresi P, Mercuri NB, Sancesario G, Bernardi G (1993) Electrophysiology of dopamine-denervated striatal neurons. Implications for Parkinson's disease. Brain 116 (Pt 2:433–452.

Calabresi P, Picconi B, Parnetti L, Di Filippo M (2006) A convergent model for cognitive dysfunctions in Parkinson's disease: the critical dopamine-acetylcholine synaptic balance. Lancet Neurol 5:974–983.

Calabresi P, Picconi B, Tozzi A, Di Filippo M (2007) Dopamine-mediated regulation of corticostriatal synaptic plasticity. Trends Neurosci 30:211–219.

Campbell BC, McLean CA, Culvenor JG, Gai WP, Blumbergs PC, Jäkälä P, Beyreuther K, Masters CL, Li QX (2001) The solubility of alpha-synuclein in multiple system atrophy differs from that of dementia with Lewy bodies and Parkinson's disease. J Neurochem 76:87–96.

Cardin JA, Carlén M, Meletis K, Knoblich U, Zhang F, Deisseroth K, Tsai L-H, Moore CI (2009) Driving fast-spiking cells induces gamma rhythm and controls sensory responses. Nature 459:663–667.

Cardin JA, Carlén M, Meletis K, Knoblich U, Zhang F, Deisseroth K, Tsai L-H, Moore CI (2010) Targeted optogenetic stimulation and recording of neurons in vivo using cell-type-specific expression of Channelrhodopsin-2. Nat Protoc 5:247–254.

Carr DB, Sesack SR (2000) Projections from the rat prefrontal cortex to the ventral tegmental area: target specificity in the synaptic associations with mesoaccumbens and mesocortical neurons. J Neurosci 20:3864–3873.

Carretta D, Sbriccoli a, Santarelli M, Pinto F, Granato a, Minciacchi D (1996) Crossed thalamo-cortical and cortico-thalamic projections in adult mice. Neurosci Lett 204:69–72.

Castle M, Aymerich MS, Sanchez-Escobar C, Gonzalo N, Obeso JA, Lanciego JL (2005) Thalamic innervation of the direct and indirect basal ganglia pathways in the rat: Ipsi- and contralateral projections. J Comp Neurol 483:143–153.

Centonze D, Grande C, Usiello A, Gubellini P, Erbs E, Martin AB, Pisani A, Tognazzi N, Bernardi G, Moratalla R, Borrelli E, Calabresi P (2003) Receptor subtypes involved in the presynaptic and postsynaptic actions of dopamine on striatal interneurons. J Neurosci 23:6245–6254.

Centonze D, Gubellini P, Bernardi G, Calabresi P (1999) Permissive role of interneurons in corticostriatal synaptic plasticity. Brain Res Brain Res Rev 31:1–5.

Centonze D, Picconi B, Gubellini P, Bernardi G, Calabresi P (2001) Dopaminergic control of synaptic plasticity in the dorsal striatum. Eur J Neurosci 13:1071–1077.

Cepeda C, André VM, Yamazaki I, Wu N, Kleiman-Weiner M, Levine MS (2008) Differential electrophysiological properties of dopamine D1 and D2 receptor-containing striatal medium-sized spiny neurons. Eur J Neurosci 27:671–682.

Champtiaux N, Gotti C, Cordero-Erausquin M, David DJ, Przybylski C, Léna C, Clementi F, Moretti M, Rossi FM, Le Novère N, McIntosh JM, Gardier AM, Changeux J-P (2003) Subunit composition of functional nicotinic receptors in dopaminergic neurons investigated with knock-out mice. J Neurosci 23:7820–7829.

Chan CS, Surmeier DJ, Yung W-H (2005) Striatal information signaling and integration in globus pallidus: timing matters. Neurosignals 14:281–289.

Chandra S, Fornai F, Kwon H-B, Yazdani U, Atasoy D, Liu X, Hammer RE, Battaglia G, German DC, Castillo PE, Südhof TC (2004) Double-knockout mice for alpha- and beta-synucleins: effect on synaptic functions. Proc Natl Acad Sci U S A 101:14966–14971.

Chandra S, Gallardo G, Fernández-Chacón R, Schlüter OM, Südhof TC (2005) Alpha-synuclein cooperates with CSPalpha in preventing neurodegeneration. Cell 123:383–396.

Cheatwood JL, Corwin J V, Reep RL (2005) Overlap and interdigitation of cortical and thalamic afferents to dorsocentral striatum in the rat. Brain Res 1036:90–100.

Cheatwood JL, Reep RL, Corwin J V (2003) The associative striatum: cortical and thalamic projections to the dorsocentral striatum in rats. Brain Res 968:1–14.

Cheer JF, Wassum KM, Heien MLA V, Phillips PEM, Wightman RM (2004) Cannabinoids enhance subsecond dopamine release in the nucleus accumbens of awake rats. J Neurosci 24:4393–4400.

Cheer JF, Wassum KM, Sombers LA, Heien MLA V, Ariansen JL, Aragona BJ, Phillips PEM, Wightman RM (2007) Phasic dopamine release evoked by abused substances requires cannabinoid receptor activation. J Neurosci 27:791–795.

Chen BT, Moran KA, Avshalumov M V, Rice ME (2006) Limited regulation of somatodendritic dopamine release by voltage-sensitive Ca channels contrasted with strong regulation of axonal dopamine release. J Neurochem 96:645–655.

Chen BT, Rice ME (2001) Novel Ca2+ dependence and time course of somatodendritic dopamine release: substantia nigra versus striatum. J Neurosci 21:7841–7847.

Chen Q, Veenman L, Knopp K, Yan Z, Medina L, Song WJ, Surmeier DJ, Reiner A (1998) Evidence for the preferential localization of glutamate receptor-1 subunits of AMPA receptors to the dendritic spines of medium spiny neurons in rat striatum. Neuroscience 83:749–761.

Chéramy A, Romo R, Godeheu G, Baruch P, Glowinski J (1986) In vivo presynaptic control of dopamine release in the cat caudate nucleus--II. Facilitatory or inhibitory influence of L-glutamate. Neuroscience 19:1081–1090.

Chevalier G, Deniau JM (1990) Disinhibition as a basic process in the expression of striatal functions. Trends Neurosci 13:277–280.

Chow BY, Han X, Dobry AS, Qian X, Chuong AS, Li M, Henninger MA, Belfort GM, Lin Y, Monahan PE, Boyden ES (2010) High-performance genetically targetable optical neural silencing by light-driven proton pumps. Nature 463:98–102.

Chuhma N, Mingote S, Moore H, Rayport S (2014) Dopamine Neurons Control Striatal Cholinergic Neurons via Regionally Heterogeneous Dopamine and Glutamate Signaling. Neuron 81:901–912.

Chuhma N, Zhang H, Masson J, Zhuang X, Sulzer D, Hen R, Rayport S (2004) Dopamine neurons mediate a fast excitatory signal via their glutamatergic synapses. J Neurosci 24:972–981.

Ciesielska A, Mittermeyer G, Hadaczek P, Kells AP, Forsayeth J, Bankiewicz KS (2011) Anterograde axonal transport of AAV2-GDNF in rat basal ganglia. Mol Ther 19:922–927.

Cisek P, Kalaska JF (2010) Neural mechanisms for interacting with a world full of action choices. Annu Rev Neurosci 33:269–298.

Clapp-Lilly KL, Roberts RC, Duffy LK, Irons KP, Hu Y, Drew KL (1999) An ultrastructural analysis of tissue surrounding a microdialysis probe. J Neurosci Methods 90:129–142.

Clark JJ, Collins AL, Sanford CA, Phillips PEM (2013) Dopamine encoding of pavlovian incentive stimuli diminishes with extended training. J Neurosci 33:3526–3532.

Clarke PB, Hommer DW, Pert A, Skirboll LR (1987) Innervation of substantia nigra neurons by cholinergic afferents from pedunculopontine nucleus in the rat: neuroanatomical and electrophysiological evidence. Neuroscience 23:1011–1019.

Clarke PBS, Pert A (1985) Autoradiographic evidence for nicotine receptors on nigrostriatal and mesolimbic dopaminergic neurons. Brain Res 348:355–358.

Cohen BN, Mackey EDW, Grady SR, McKinney S, Patzlaff NE, Wageman CR, McIntosh JM, Marks MJ, Lester HA, Drenan RM (2012) Nicotinic cholinergic mechanisms causing elevated dopamine release and abnormal locomotor behavior. Neuroscience 200:31–41.

Consolo S, Baldi G, Giorgi S, Nannini L (1996a) The cerebral cortex and parafascicular thalamic nucleus facilitate in vivo acetylcholine release in the rat striatum through distinct glutamate receptor subtypes. Eur J Neurosci 8:2702–2710.

Consolo S, Baronio P, Guidi G, Di Chiara G, Consolo, S., Baronio, P., Guidi, G. & di Chiara G (1996b) ROLE OF THE PARAFASCICULAR THALAMIC NUCLEUS D1-DEPENDENT CONTROL OF IN VIVO ACETYLCHOLINE Abstract--We. Neuroscience 71:157–165.

Contant C, Umbriaco D, Garcia S, Watkins KC, Descarries L (1996) Ultrastructural characterization of the acetylcholine innervation in adult rat neostriatum. Neuroscience 71:937–947.

Cornwall J, Phillipson OT (1988) Afferent projections to the dorsal thalamus of the rat as shown by retrograde lectin transport. II. The midline nuclei. Brain Res Bull 21:147–161.

Cowan RL, Wilson CJ, Emson PC, Heizmann CW (1990) Parvalbumin-containing GABAergic interneurons in the rat neostriatum. J Comp Neurol 302:197–205.

Cragg S, Rice ME, Greenfield SA (1997a) Heterogeneity of electrically evoked dopamine release and reuptake in substantia nigra, ventral tegmental area, and striatum. J Neurophysiol 77:863–873.

Cragg SJ (2003) Variable dopamine release probability and short-term plasticity between functional domains of the primate striatum. J Neurosci 23:4378–4385.

Cragg SJ (2006) Meaningful silences: how dopamine listens to the ACh pause. Trends Neurosci 29:125–131.

Cragg SJ, Baufreton J, Xue Y, Bolam JP, Bevan MD (2004) Synaptic release of dopamine in the subthalamic nucleus. Eur J Neurosci 20:1788–1802.

Cragg SJ, Greenfield S a (1997) Differential autoreceptor control of somatodendritic and axon terminal dopamine release in substantia nigra, ventral tegmental area, and striatum. J Neurosci 17:5738–5746.

Cragg SJ, Hawkey CR, Greenfield SA (1997b) Comparison of serotonin and dopamine release in substantia nigra and ventral tegmental area: region and species differences. J Neurochem 69:2378–2386.

Cragg SJ, Hille CJ, Greenfield SA (2000) Dopamine Release and Uptake Dynamics within Nonhuman Primate Striatum In Vitro. J Neurosci 20:8209–8217.

Cragg SJ, Hille CJ, Greenfield SA (2002) Functional Domains in Dorsal Striatum of the Nonhuman Primate Are Defined by the Dynamic Behavior of Dopamine. J Neurosci 22:5705–5712.

Cragg SJ, Nicholson C, Kume-kick J, Tao L, Rice E, Ford CP, Gantz SC, Phillips PEM, Williams JT, Rice ME (2011) Dopamine-Mediated Volume Transmission in Midbrain Is Regulated by Distinct Extracellular Geometry and Uptake Dopamine-Mediated Volume Transmission in Midbrain Is Regulated by Distinct Extracellular Geometry and Uptake. J Neurophysiol:1761–1771.

Cragg SJ, Nicholson C, Kume-Kick J, Tao L, Rice ME (2001) Dopamine-mediated volume transmission in midbrain is regulated by distinct extracellular geometry and uptake. J Neurophysiol 85:1761–1771.

Cragg SJ, Rice ME (2004) DAncing past the DAT at a DA synapse. Trends Neurosci 27:270–277.
Crespi F, Martin KF, Marsden CA (1988) Measurement of extracellular basal levels of serotonin in vivo using nafion-coated carbon fibre electrodes combined with differential pulse voltammetry. Neuroscience 27:885–896.
Cui G, Jun SB, Jin X, Pham MD, Vogel SS, Lovinger DM, Costa RM (2013) Concurrent activation of striatal direct and indirect pathways during action initiation. Nature 494:238–242.
Daberkow DP, Brown HD, Bunner KD, Kraniotis S a., Doellman M a., Ragozzino ME, Garris P a., Roitman MF (2013) Amphetamine Paradoxically Augments Exocytotic Dopamine Release and Phasic Dopamine Signals. J Neurosci 33:452–463.
Dautan D, Huerta-Ocampo I, Witten IB, Deisseroth K, Bolam JP, Gerdjikov T, Mena-Segovia J (2014) A major external source of cholinergic innervation of the striatum and nucleus accumbens originates in the brainstem. J Neurosci 34:4509–4518.
Davidson BL, Stein CS, Heth JA, Martins I, Kotin RM, Derksen TA, Zabner J, Ghodsi A, Chiorini JA (2000) Recombinant adeno-associated virus type 2, 4, and 5 vectors: transduction of variant cell types and regions in the mammalian central nervous system. Proc Natl Acad Sci U S A 97:3428–3432.
Davidson WS (1998) Stabilization of alpha -Synuclein Secondary Structure upon Binding to Synthetic Membranes. J Biol Chem 273:9443–9449.
Day JJ, Roitman MF, Wightman RM, Carelli RM (2007) Associative learning mediates dynamic shifts in dopamine signaling in the nucleus accumbens. Nat Neurosci 10:1020–1028.
Day JJ, Wheeler RA, Roitman MF, Carelli RM (2006) Nucleus accumbens neurons encode Pavlovian approach behaviors: evidence from an autoshaping paradigm. Eur J Neurosci 23:1341–1351.
Day M, Wokosin D, Plotkin JL, Tian X, Surmeier DJ (2008) Differential excitability and modulation of striatal medium spiny neuron dendrites. J Neurosci 28:11603–11614.
De Rijk MC, Launer LJ, Berger K, Breteler MM, Dartigues JF, Baldereschi M, Fratiglioni L, Lobo A, Martinez-Lage J, Trenkwalder C, Hofman A (2000) Prevalence of Parkinson's disease in Europe: A collaborative study of population-based cohorts. Neurologic Diseases in the Elderly Research Group. Neurology 54:S21–3.
DeBoer P, Abercrombie ED (1996) Physiological release of striatal acetylcholine in vivo: modulation by D1 and D2 dopamine receptor subtypes. J Pharmacol Exp Ther 277:775–783.
DeBoer P, Heeringa MJ, Abercrombie ED (1996) Spontaneous release of acetylcholine in striatum is preferentially regulated by inhibitory dopamine D2 receptors. Eur J Pharmacol 317:257–262.
Del-Fava F, Hasue RH, Ferreira JGP, Shammah-Lagnado SJ (2007) Efferent connections of the rostral linear nucleus of the ventral tegmental area in the rat. Neuroscience 145:1059–1076.
DeLong MR (1990) Primate models of movement disorders of basal ganglia origin. Trends Neurosci 13:281–285.
Deng P, Zhang Y, Xu ZC (2007) Involvement of I(h) in dopamine modulation of tonic firing in striatal cholinergic interneurons. J Neurosci 27:3148–3156.
Descarries L, Gisiger V, Steriade M (1997) Diffuse transmission by acetylcholine in the CNS. Prog Neurobiol 53:603–625.
Descarries L, Mechawar N (2000) Ultrastructural evidence for diffuse transmission by monoamine and acetylcholine neurons of the central nervous system. Prog Brain Res 125:27–47.
Descarries L, Watkins KC, Garcia S, Bosler O, Doucet G (1996) Dual character, asynaptic and synaptic, of the dopamine innervation in adult rat neostriatum: a quantitative autoradiographic and immunocytochemical analysis. J Comp Neurol 375:167–186.
Deschênes M, Bourassa J, Doan VD, Parent A (1996) A single-cell study of the axonal projections arising from the posterior intralaminar thalamic nuclei in the rat. Eur J Neurosci 8:329–343.

Deschenes M, Bourassa J, Parent A (1996) Striatal and cortical projections of single neurons from the central lateral thalamic nucleus in the rat. Neuroscience 72:679–687.

Di Chiara G, Morelli M, Consolo S (1994) Modulatory functions of neurotransmitters in the striatum: ACh/dopamine/NMDA interactions. Trends Neurosci 17:228–233.

Di Pasquale G, Davidson BL, Stein CS, Martins I, Scudiero D, Monks A, Chiorini JA (2003) Identification of PDGFR as a receptor for AAV-5 transduction. Nat Med 9:1306–1312.

Diao J, Burré J, Vivona S, Cipriano DJ, Sharma M, Kyoung M, Südhof TC, Brunger AT (2013) Native α-synuclein induces clustering of synaptic-vesicle mimics via binding to phospholipids and synaptobrevin-2/VAMP2. Elife 2:e00592.

Diester I, Kaufman MT, Mogri M, Pashaie R, Goo W, Yizhar O, Ramakrishnan C, Deisseroth K, Shenoy K V (2011) An optogenetic toolbox designed for primates. Nat Neurosci 14:387–397.

Ding J, Guzman JN, Tkatch T, Chen S, Goldberg J a, Ebert PJ, Levitt P, Wilson CJ, Hamm HE, Surmeier DJ (2006) RGS4-dependent attenuation of M4 autoreceptor function in striatal cholinergic interneurons following dopamine depletion. Nat Neurosci 9:832–842.

Ding J, Peterson JD, Surmeier DJ (2008) Corticostriatal and thalamostriatal synapses have distinctive properties. J Neurosci 28:6483–6492.

Ding JB, Guzman JN, Peterson JD, Goldberg J a, Surmeier DJ (2010) Thalamic gating of corticostriatal signaling by cholinergic interneurons. Neuron 67:294–307.

Diógenes MJ, Dias RB, Rombo DM, Vicente Miranda H, Maiolino F, Guerreiro P, Näsström T, Franquelim HG, Oliveira LMA, Castanho MARB, Lannfelt L, Bergström J, Ingelsson M, Quintas A, Sebastião AM, Lopes L V, Outeiro TF (2012) Extracellular alpha-synuclein oligomers modulate synaptic transmission and impair LTP via NMDA-receptor activation. J Neurosci 32:11750–11762.

Dobi A, Margolis EB, Wang H-L, Harvey BK, Morales M (2010) Glutamatergic and nonglutamatergic neurons of the ventral tegmental area establish local synaptic contacts with dopaminergic and nondopaminergic neurons. J Neurosci 30:218–229.

Doig NM, Magill PJ, Apicella P, Bolam JP, Sharott a. (2014) Cortical and Thalamic Excitation Mediate the Multiphasic Responses of Striatal Cholinergic Interneurons to Motivationally Salient Stimuli. J Neurosci 34:3101–3117.

Doig NM, Moss J, Bolam JP (2010) Cortical and thalamic innervation of direct and indirect pathway medium-sized spiny neurons in mouse striatum. J Neurosci 30:14610–14618.

Doyon J, Bellec P, Amsel R, Penhune V, Monchi O, Carrier J, Lehéricy S, Benali H (2009) Contributions of the basal ganglia and functionally related brain structures to motor learning. Behav Brain Res 199:61–75.

Drenan RM, Grady SR, Steele AD, McKinney S, Patzlaff NE, McIntosh JM, Marks MJ, Miwa JM, Lester HA (2010) Cholinergic modulation of locomotion and striatal dopamine release is mediated by alpha6alpha4* nicotinic acetylcholine receptors. J Neurosci 30:9877–9889.

Drukarch B, Schepens E, Stoof JC (1990) Muscarinic receptor activation attenuates D2 dopamine receptor mediated inhibition of acetylcholine release in rat striatum: indications for a common signal transduction pathway. Neuroscience 37:1–9.

Dubé L, Smith a D, Bolam JP (1988) Identification of synaptic terminals of thalamic or cortical origin in contact with distinct medium-size spiny neurons in the rat neostriatum. J Comp Neurol 267:455–471.

Dubois B, Pillon B (1997) Cognitive deficits in Parkinson's disease. J Neurol 244:2–8.

Durany N, Zöchling R, Boissl KW, Paulus W, Ransmayr G, Tatschner T, Danielczyk W, Jellinger K, Deckert J, Riederer P (2000) Human post-mortem striatal α4β2 nicotinic acetylcholine receptor density in schizophrenia and Parkinson's syndrome. Neurosci Lett 287:109–112.

Ellender TJ, Harwood J, Kosillo P, Capogna M, Bolam JP (2013) Heterogeneous properties of central lateral and parafascicular thalamic synapses in the striatum. J Physiol 591:257–272.

Ellender TJ, Huerta-Ocampo I, Deisseroth K, Capogna M, Bolam JP (2011) Differential Modulation of Excitatory and Inhibitory Striatal Synaptic Transmission by Histamine. J Neurosci 31:15340–15351.

English DF, Ibanez-Sandoval O, Stark E, Tecuapetla F, Buzsáki G, Deisseroth K, Tepper JM, Koos T (2011) GABAergic circuits mediate the reinforcement-related signals of striatal cholinergic interneurons. Nat Neurosci.

Erro E, Lanciego JL, Giménez-Amaya JM (1999) Relationships between thalamostriatal neurons and pedunculopontine projections to the thalamus: a neuroanatomical tract-tracing study in the rat. Exp brain Res 127:162–170.

Everitt BJ, Morris KA, O'Brien A, Robbins TW (1991) The basolateral amygdala-ventral striatal system and conditioned place preference: further evidence of limbic-striatal interactions underlying reward-related processes. Neuroscience 42:1–18.

Everitt BJ, Robbins TW (2005) Neural systems of reinforcement for drug addiction: from actions to habits to compulsion. Nat Neurosci 8:1481–1489.

Ewing AG, Bigelow JC, Wightman RM (1983) Direct in vivo monitoring of dopamine released from two striatal compartments in the rat. Science 221:169–171.

Exley R, Clements M a, Hartung H, McIntosh JM, Cragg SJ (2008) Alpha6-containing nicotinic acetylcholine receptors dominate the nicotine control of dopamine neurotransmission in nucleus accumbens. Neuropsychopharmacology 33:2158–2166.

Exley R, Maubourguet N, David V, Eddine R, Evrard A, Pons S, Marti F, Threlfell S, Cazala P, McIntosh JM, Changeux J-P, Maskos U, Cragg SJ, Faure P (2011) Distinct contributions of nicotinic acetylcholine receptor subunit alpha4 and subunit alpha6 to the reinforcing effects of nicotine. Proc Natl Acad Sci U S A 108:7577–7582.

Exley R, McIntosh JM, Marks MJ, Maskos U, Cragg SJ (2012) Striatal α5 nicotinic receptor subunit regulates dopamine transmission in dorsal striatum. J Neurosci 32:2352–2356.

Fallon JH (1988) Topographic organization of ascending dopaminergic projections. Ann N Y Acad Sci 537:1–9.

Fallon JH, Moore RY (1978) Catecholamine innervation of the basal forebrain. IV. Topography of the dopamine projection to the basal forebrain and neostriatum. J Comp Neurol 180:545–580.

Fearnley JM, Lees AJ (1991) Ageing and Parkinson's disease: substantia nigra regional selectivity. Brain 114 (Pt 5:2283–2301.

Feng J, Chi P, Blanpied TA, Xu Y, Magarinos AM, Ferreira A, Takahashi RH, Kao H-T, McEwen BS, Ryan TA, Augustine GJ, Greengard P (2002) Regulation of neurotransmitter release by synapsin III. J Neurosci 22:4372–4380.

Feng LR, Federoff HJ, Vicini S, Maguire-Zeiss KA (2010) Alpha-synuclein mediates alterations in membrane conductance: a potential role for alpha-synuclein oligomers in cell vulnerability. Eur J Neurosci 32:10–17.

Ferguson SM, Eskenazi D, Ishikawa M, Wanat MJ, Phillips PEM, Dong Y, Roth BL, Neumaier JF (2011) Transient neuronal inhibition reveals opposing roles of indirect and direct pathways in sensitization. Nat Neurosci 14:22–24.

Ferguson SM, Phillips PEM, Roth BL, Wess J, Neumaier JF (2013) Direct-Pathway Striatal Neurons Regulate the Retention of Decision-Making Strategies. J Neurosci 33:11668–11676.

Fino E, Venance L (2010) Spike-timing dependent plasticity in the striatum. Front Synaptic Neurosci 2:6.

Fino E, Venance L (2011) Spike-timing dependent plasticity in striatal interneurons. Neuropharmacology 60:780–788.

Floresco SB, West AR, Ash B, Moore H, Grace AA (2003) Afferent modulation of dopamine neuron firing differentially regulates tonic and phasic dopamine transmission. Nat Neurosci 6:968–973.

Fog JU, Khoshbouei H, Holy M, Owens WA, Vaegter CB, Sen N, Nikandrova Y, Bowton E, McMahon DG, Colbran RJ, Daws LC, Sitte HH, Javitch JA, Galli A, Gether U (2006) Calmodulin kinase II interacts with the dopamine transporter C terminus to regulate amphetamine-induced reverse transport. Neuron 51:417–429.

Ford CP, Gantz SC, Phillips PEM, Williams JT (2010) Control of extracellular dopamine at dendrite and axon terminals. J Neurosci 30:6975–6983.

Fortin GD, Desrosiers CC, Yamaguchi N, Trudeau L-E (2006) Basal somatodendritic dopamine release requires snare proteins. J Neurochem 96:1740–1749.

Fountaine TM, Wade-Martins R (2007) RNA interference-mediated knockdown of alpha-synuclein protects human dopaminergic neuroblastoma cells from MPP(+) toxicity and reduces dopamine transport. J Neurosci Res 85:351–363.

Frankle WG, Laruelle M, Haber SN (2006) Prefrontal cortical projections to the midbrain in primates: evidence for a sparse connection. Neuropsychopharmacology 31:1627–1636.

Freeze BS, Kravitz A V, Hammack N, Berke JD, Kreitzer AC (2013) Control of basal ganglia output by direct and indirect pathway projection neurons. J Neurosci 33:18531–18539.

Fremeau RT, Kam K, Qureshi T, Johnson J, Copenhagen DR, Storm-Mathisen J, Chaudhry FA, Nicoll RA, Edwards RH (2004a) Vesicular glutamate transporters 1 and 2 target to functionally distinct synaptic release sites. Science 304:1815–1819.

Fremeau RT, Voglmaier S, Seal RP, Edwards RH (2004b) VGLUTs define subsets of excitatory neurons and suggest novel roles for glutamate. Trends Neurosci 27:98–103.

Fuchs J, Nilsson C, Kachergus J, Munz M, Larsson E-M, Schüle B, Langston JW, Middleton FA, Ross OA, Hulihan M, Gasser T, Farrer MJ (2007) Phenotypic variation in a large Swedish pedigree due to SNCA duplication and triplication. Neurology 68:916–922.

Fujiwara H, Hasegawa M, Dohmae N, Kawashima A, Masliah E, Goldberg MS, Shen J, Takio K, Iwatsubo T (2002) alpha-Synuclein is phosphorylated in synucleinopathy lesions. Nat Cell Biol 4:160–164.

Fujiyama F, Fritschy JM, Stephenson FA, Bolam JP (2000) Synaptic localization of GABA(A) receptor subunits in the striatum of the rat. J Comp Neurol 416:158–172.

Galvan A, Smith Y (2011) The primate thalamostriatal systems: Anatomical organization, functional roles and possible involvement in Parkinson's disease. Basal Ganglia 1:179–189.

Gao L, Blair LAC, Marshall J (2006) CaMKII-independent effects of KN93 and its inactive analog KN92: Reversible inhibition of L-type calcium channels. Biochem Biophys Res Commun 345:1606–1610.

Garcia-Reitböck P, Anichtchik O, Bellucci A, Iovino M, Ballini C, Fineberg E, Ghetti B, Della Corte L, Spano P, Tofaris GK, Goedert M, Spillantini MG (2010) SNARE protein redistribution and synaptic failure in a transgenic mouse model of Parkinson's disease. Brain 133:2032–2044.

Gasbarri A, Verney C, Innocenzi R, Campana E, Pacitti C (1994) Mesolimbic dopaminergic neurons innervating the hippocampal formation in the rat: a combined retrograde tracing and immunohistochemical study. Brain Res 668:71–79.

Gasparini S, Migliore M, Magee JC (2004) On the initiation and propagation of dendritic spikes in CA1 pyramidal neurons. J Neurosci 24:11046–11056.

Gates MA, Coupe VM, Torres EM, Fricker-Gates RA, Dunnett SB (2004) Spatially and temporally restricted chemoattractive and chemorepulsive cues direct the formation of the nigro-striatal circuit. Eur J Neurosci 19:831–844.

Geibel S, Friedrich T, Ormos P, Wood PG, Nagel G, Bamberg E (2001) The voltage-dependent proton pumping in bacteriorhodopsin is characterized by optoelectric behavior. Biophys J 81:2059–2068.

Gerdeman GL, Partridge JG, Lupica CR, Lovinger DM (2003) It could be habit forming: drugs of abuse and striatal synaptic plasticity. Trends Neurosci 26:184–192.

Gerfen C, Engber T, Mahan L, Susel Z, Chase T, Monsma F, Sibley D (1990) D1 and D2 dopamine receptor-regulated gene expression of striatonigral and striatopallidal neurons. Science (80-) 250:1429–1432.

Gerfen CR, Baimbridge KG, Miller JJ (1985) The neostriatal mosaic: compartmental distribution of calcium-binding protein and parvalbumin in the basal ganglia of the rat and monkey. Proc Natl Acad Sci U S A 82:8780–8784.

Gerfen CR, Baimbridge KG, Thibault J (1987a) The neostriatal mosaic: III. Biochemical and developmental dissociation of patch-matrix mesostriatal systems. J Neurosci 7:3935–3944.

Gerfen CR, Herkenham M, Thibault J (1987b) The neostriatal mosaic: II. Patch- and matrix-directed mesostriatal dopaminergic and non-dopaminergic systems. J Neurosci 7:3915–3934.

Gerfen CR, Surmeier DJ (2011) Modulation of striatal projection systems by dopamine. Annu Rev Neurosci 34:441–466.

Gerhardt GA, Oke AF, Nagy G, Moghaddam B, Adams RN (1984) Nafion-coated electrodes with high selectivity for CNS electrochemistry. Brain Res 290:390–395.

German DC, Manaye KF (1993) Midbrain dopaminergic neurons (nuclei A8, A9, and A10): three-dimensional reconstruction in the rat. J Comp Neurol 331:297–309.

Gertler TS, Chan CS, Surmeier DJ (2008) Dichotomous anatomical properties of adult striatal medium spiny neurons. J Neurosci 28:10814–10824.

Giehm L, Svergun DI, Otzen DE, Vestergaard B (2011) Low-resolution structure of a vesicle disrupting α-synuclein oligomer that accumulates during fibrillation. Proc Natl Acad Sci U S A 108:3246–3251.

Giménez-Amaya JM, McFarland NR, de las Heras S, Haber SN (1995) Organization of thalamic projections to the ventral striatum in the primate. J Comp Neurol 354:127–149.

Giorguieff MF, Le Floc'h ML, Glowinski J, Besson MJ (1977) Involvement of cholinergic presynatpic receptors of nicotinic and muscarinic types in the control of the spontaneous release of dopamine from striatal dopaminergic terminals in the rat. J Pharmacol Exp Ther 200:535–544.

Gispert S, Del Turco D, Garrett L, Chen A, Bernard DJ, Hamm-Clement J, Korf H-W, Deller T, Braak H, Auburger G, Nussbaum RL (2003) Transgenic mice expressing mutant A53T human alpha-synuclein show neuronal dysfunction in the absence of aggregate formation. Mol Cell Neurosci 24:419–429.

Goldberg J a, Reynolds JNJ (2011) Spontaneous firing and evoked pauses in the tonically active cholinergic interneurons of the striatum. Neuroscience.

Goldberg JA, Ding JB, Surmeier DJ (2012) Muscarinic Receptors Fryer AD, Christopoulos A, Nathanson NM, eds. 208:223–241.

Goldberg JA, Wilson CJ (2005) Control of spontaneous firing patterns by the selective coupling of calcium currents to calcium-activated potassium currents in striatal cholinergic interneurons. J Neurosci 25:10230–10238.

Gong S, Doughty M, Harbaugh CR, Cummins A, Hatten ME, Heintz N, Gerfen CR (2007) Targeting Cre recombinase to specific neuron populations with bacterial artificial chromosome constructs. J Neurosci 27:9817–9823.

Gonon F, Buda M, Cespuglio R, Jouvet M, Pujol J-F (1980) In vivo electrochemical detection of catechols in the neostriatum of anaesthetized rats: dopamine or DOPAC? Nature 286:902–904.

Gonon F, Cespuglio R, Ponchon JL, Buda M, Jouvet M, Adams RN, Pujol JF (1978) [In vivo continuous electrochemical determination of dopamine release in rat neostriatum]. C R Acad Sci Hebd Seances Acad Sci D 286:1203–1206.

Gonzalez-Reyes LEE, Verbitsky M, Blesa J, Jackson-Lewis V, Paredes D, Tillack K, Phani S, Kramer ERR, Przedborski S, Kottmann AHH (2012) Sonic Hedgehog Maintains Cellular and Neurochemical Homeostasis in the Adult Nigrostriatal Circuit. Neuron 75:306–319.

Gotti C, Guiducci S, Tedesco V, Corbioli S, Zanetti L, Moretti M, Zanardi A, Rimondini R, Mugnaini M, Clementi F, Chiamulera C, Zoli M (2010) Nicotinic acetylcholine receptors in the mesolimbic pathway: primary role of ventral tegmental area alpha6beta2* receptors in mediating systemic nicotine effects on dopamine release, locomotion, and reinforcement. J Neurosci 30:5311–5325.

Gotti C, Moretti M, Clementi F, Riganti L, McIntosh JM, Collins AC, Marks MJ, Whiteaker P (2005) Expression of nigrostriatal alpha 6-containing nicotinic acetylcholine receptors is selectively reduced, but not eliminated, by beta 3 subunit gene deletion. Mol Pharmacol 67:2007–2015.

Götz T, Kraushaar U, Geiger J, Lübke J, Berger T, Jonas P (1997) Functional properties of AMPA and NMDA receptors expressed in identified types of basal ganglia neurons. J Neurosci 17:204–215.

Grace AA, Bunney BS (1984a) The control of firing pattern in nigral dopamine neurons: single spike firing. J Neurosci 4:2866–2876.

Grace AA, Bunney BS (1984b) The control of firing pattern in nigral dopamine neurons: burst firing. J Neurosci 4:2877–2890.

Gradinaru V, Thompson KR, Zhang F, Mogri M, Kay K, Schneider MB, Deisseroth K (2007) Targeting and readout strategies for fast optical neural control in vitro and in vivo. J Neurosci 27:14231–14238.

Grahn JA, Parkinson JA, Owen AM (2009) The role of the basal ganglia in learning and memory: neuropsychological studies. Behav Brain Res 199:53–60.

Graveland GA, DiFiglia M (1985) The frequency and distribution of medium-sized neurons with indented nuclei in the primate and rodent neostriatum. Brain Res 327:307–311.

Graybiel AM (2008) Habits, rituals, and the evaluative brain. Annu Rev Neurosci 31:359–387.

Graybiel AM, Aosaki T, Flaherty AW, Kimura M (1994) The basal ganglia and adaptive motor control. Science 265:1826–1831.

Graybiel AM, Ragsdale CW (1978) Histochemically distinct compartments in the striatum of human, monkeys, and cat demonstrated by acetylthiocholinesterase staining. Proc Natl Acad Sci U S A 75:5723–5726.

Groves PM, Linder JC (1983) Dendro-dendritic synapses in substantia nigra: descriptions based on analysis of serial sections. Exp brain Res 49:209–217.

Groves PM, Linder JC, Young SJ (1994) 5-hydroxydopamine-labeled dopaminergic axons: three-dimensional reconstructions of axons, synapses and postsynaptic targets in rat neostriatum. Neuroscience 58:593–604.

Gu H, Wall SC, Rudnick G (1994) Stable expression of biogenic amine transporters reveals differences in inhibitor sensitivity, kinetics, and ion dependence. J Biol Chem 269:7124–7130.

Gurney K, Prescott TJ, Redgrave P (2001) A computational model of action selection in the basal ganglia. I. A new functional anatomy. Biol Cybern 84:401–410.

Guzman MS, De Jaeger X, Raulic S, Souza I a, Li AX, Schmid S, Menon RS, Gainetdinov RR, Caron MG, Bartha R, Prado VF, Prado M a M (2011) Elimination of the vesicular acetylcholine transporter in the striatum reveals regulation of behaviour by cholinergic-glutamatergic co-transmission. PLoS Biol 9:e1001194.

Haber SN, Fudge JL, McFarland NR (2000) Striatonigrostriatal pathways in primates form an ascending spiral from the shell to the dorsolateral striatum. J Neurosci 20:2369–2382.

Hadj-Bouziane F, Benatru I, Brovelli A, Klinger H, Thobois S, Broussolle E, Boussaoud D, Meunier M (2012) Advanced Parkinson's disease effect on goal-directed and habitual processes involved in visuomotor associative learning. Front Hum Neurosci 6:351.

Halliday GM (2009) Thalamic changes in Parkinson's disease. Parkinsonism Relat Disord 15 Suppl 3:S152–5.

Han X, Boyden ES (2007) Multiple-color optical activation, silencing, and desynchronization of neural activity, with single-spike temporal resolution. PLoS One 2:e299.

Hartung H, Threlfell S, Cragg SJ (2011) Nitric oxide donors enhance the frequency dependence of dopamine release in nucleus accumbens. Neuropsychopharmacology 36:1811–1822.

Hashimoto M, Hsu LJ, Xia Y, Takeda A, Sisk A, Sundsmo M, Masliah E (1999) Oxidative stress induces amyloid-like aggregate formation of NACP/alpha-synuclein in vitro. Neuroreport 10:717–721.

Hattori T, Fibiger HC, McGeer PL (1975) Demonstration of a pallido-nigral projection innervating dopaminergic neurons. J Comp Neurol 162:487–504.

Hattox AM, Nelson SB (2007) Layer V neurons in mouse cortex projecting to different targets have distinct physiological properties. J Neurophysiol 98:3330–3340.

Hedrick T, Waters J (2011) Spiking patterns of neocortical L5 pyramidal neurons in vitro change with temperature. Front Cell Neurosci 5:1.

Helmchen F, Svoboda K, Denk W, Tank DW (1999) In vivo dendritic calcium dynamics in deep-layer cortical pyramidal neurons. Nat Neurosci 2:989–996.

Henderson JM, Carpenter K, Cartwright H, Halliday GM (2000a) Loss of thalamic intralaminar nuclei in progressive supranuclear palsy and Parkinson's disease: clinical and therapeutic implications. Brain 123 (Pt 7:1410–1421.

Henderson JM, Carpenter K, Cartwright H, Halliday GM (2000b) Degeneration of the centré median-parafascicular complex in Parkinson's disease. Ann Neurol 47:345–352.

Henny P, Brown MTC, Northrop A, Faunes M, Ungless M a, Magill PJ, Bolam JP (2012) Structural correlates of heterogeneous in vivo activity of midbrain dopaminergic neurons. Nat Neurosci 15:613–619.

Herdon H, Nahorski SR (1989) Investigations of the roles of dihydropyridine and omega-conotoxin-sensitive calcium channels in mediating depolarisation-evoked endogenous dopamine release from striatal slices. Naunyn Schmiedebergs Arch Pharmacol 340:36–40.

Herkenham M, Pert CB (1981) Mosaic distribution of opiate receptors, parafascicular projections and acetylcholinesterase in rat striatum. Nature 291:415–418.

Hernández-López S, Bargas J, Surmeier DJ, Reyes a, Galarraga E (1997) D1 receptor activation enhances evoked discharge in neostriatal medium spiny neurons by modulating an L-type Ca2+ conductance. J Neurosci 17:3334–3342.

Hersch SM, Ciliax BJ, Gutekunst C a, Rees HD, Heilman CJ, Yung KK, Bolam JP, Ince E, Yi H, Levey a I (1995) Electron microscopic analysis of D1 and D2 dopamine receptor proteins in the dorsal striatum and their synaptic relationships with motor corticostriatal afferents. J Neurosci 15:5222–5237.

Hersch SM, Gutekunst CA, Rees HD, Heilman CJ, Levey AI (1994) Distribution of m1-m4 muscarinic receptor proteins in the rat striatum: light and electron microscopic immunocytochemistry using subtype-specific antibodies. J Neurosci 14:3351–3363.

Higley MJ, Gittis AH, Oldenburg I a, Balthasar N, Seal RP, Edwards RH, Lowell BB, Kreitzer AC, Sabatini BL (2011) Cholinergic interneurons mediate fast VGluT3-dependent glutamatergic transmission in the striatum. PLoS One 6:e19155.

Higley MJ, Soler-Llavina GJ, Sabatini BL (2009) Cholinergic modulation of multivesicular release regulates striatal synaptic potency and integration. Nat Neurosci 12:1121–1128.

Hikida T, Kimura K, Wada N, Funabiki K, Nakanishi S (2010) Distinct roles of synaptic transmission in direct and indirect striatal pathways to reward and aversive behavior. Neuron 66:896–907.

Hill JA, Zoli M, Bourgeois JP, Changeux JP (1993) Immunocytochemical localization of a neuronal nicotinic receptor: the beta 2-subunit. J Neurosci 13:1551–1568.

Hirsch E, Graybiel AM, Agid YA (1988) Melanized dopaminergic neurons are differentially susceptible to degeneration in Parkinson's disease. Nature 334:345–348.

Hnasko TS, Chuhma N, Zhang H, Goh GY, Sulzer D, Palmiter RD, Rayport S, Edwards RH (2010) Vesicular glutamate transport promotes dopamine storage and glutamate corelease in vivo. Neuron 65:643–656.

Hnasko TS, Hjelmstad GO, Fields HL, Edwards RH (2012) Ventral Tegmental Area Glutamate Neurons: Electrophysiological Properties and Projections. J Neurosci 32:15076–15085.

Hoffman AF, Gerhardt GA (1999) Differences in pharmacological properties of dopamine release between the substantia nigra and striatum: an in vivo electrochemical study. J Pharmacol Exp Ther 289:455–463.

Hoffman AF, Lupica CR, Gerhardt GA (1998) Dopamine transporter activity in the substantia nigra and striatum assessed by high-speed chronoamperometric recordings in brain slices. J Pharmacol Exp Ther 287:487–496.

Hollerman JR, Schultz W (1998) Dopamine neurons report an error in the temporal prediction of reward during learning. Nat Neurosci 1:304–309.

Holmes NM, Fam J (2013) How Does Dopamine Release in the Nucleus Accumbens Core Relate to Encoding of a Pavlovian Incentive Stimulus? J Neurosci 33:10191–10192.

Hoover DB, Muth EA, Jacobowitz DM (1978) A mapping of the distribution of acetycholine, choline acetyltransferase and acetylcholinesterase in discrete areas of rat brain. Brain Res 153:295–306.

Horvitz JC (2002) Dopamine gating of glutamatergic sensorimotor and incentive motivational input signals to the striatum. Behav Brain Res 137:65–74.

Houser CR (1990) Cholinergic synapses in the central nervous system: studies of the immunocytochemical localization of choline acetyltransferase. J Electron Microsc Tech 15:2–19.

Howe MW, Tierney PL, Sandberg SG, Phillips PEM, Graybiel AM (2013) Prolonged dopamine signalling in striatum signals proximity and value of distant rewards. Nature 500:575–579.

Hutson TH, Verhaagen J, Yáñez-Muñoz RJ, Moon LDF (2012) Corticospinal tract transduction: a comparison of seven adeno-associated viral vector serotypes and a non-integrating lentiviral vector. Gene Ther 19:49–60.

Hyland BI, Reynolds JNJ, Hay J, Perk CG, Miller R (2002) Firing modes of midbrain dopamine cells in the freely moving rat. Neuroscience 114:475–492.

Ibáñez-Sandoval O, Tecuapetla F, Unal B, Shah F, Koós T, Tepper JM (2011) A Novel Functionally Distinct Subtype of Striatal Neuropeptide Y Interneuron. J Neurosci 31:16757–16769.

Iravani MM, Kruk ZL (1997) Real-time measurement of stimulated 5-hydroxytryptamine release in rat substantia nigra pars reticulata brain slices. Synapse 25:93–102.

Isomura Y, Takekawa T, Harukuni R, Handa T, Aizawa H, Takada M, Fukai T (2013) Reward-Modulated Motor Information in Identified Striatum Neurons. J Neurosci 33:10209–10220.

Iwai A, Masliah E, Yoshimoto M, Ge N, Flanagan L, de Silva HA, Kittel A, Saitoh T (1995) The precursor protein of non-A beta component of Alzheimer's disease amyloid is a presynaptic protein of the central nervous system. Neuron 14:467–475.

Jaffe EH, Marty A, Schulte A, Chow RH (1998) Extrasynaptic vesicular transmitter release from the somata of substantia nigra neurons in rat midbrain slices. J Neurosci 18:3548–3553.

Janezic S et al. (2013) Deficits in dopaminergic transmission precede neuron loss and dysfunction in a new Parkinson model. Proc Natl Acad Sci U S A 110:E4016–25.

Jeong J, Shi W-X, Hoffman R, Oh J, Gore JC, Bunney BS, Peterson BS (2012) Bursting as a source of non-linear determinism in the firing patterns of nigral dopamine neurons. Eur J Neurosci 36:3214–3223.

Jiang BYZ, North RA (1991) Membrane properties and synaptic responses of rat striatal neruons in vitro. Physiology 443:533–553.

Jimenez-Castellanos J, Graybiel AM (1987) Subdivisions of the dopamine-containing A8-A9-A10 complex identified by their differential mesostriatal innervation of striosomes and extrastriosomal matrix. Neuroscience 23:223–242.

Joel D, Weiner I (1994) The organization of the basal ganglia-thalamocortical circuits: open interconnected rather than closed segregated. Neuroscience 63:363–379.

John CE, Budygin EA, Mateo Y, Jones SR (2006) Neurochemical characterization of the release and uptake of dopamine in ventral tegmental area and serotonin in substantia nigra of the mouse. J Neurochem 96:267–282.

Jones EG, Coulter JD, Burton H, Porter R (1977) Cells of origin and terminal distribution of corticostriatal fibers arising in the sensory-motor cortex of monkeys. J Comp Neurol 173:53–80.

Jones EG, Leavitt RY (1974) Retrograde axonal transport and the demonstration of non-specific projections to the cerebral cortex and striatum from thalamic intralaminar nuclei in the rat, cat and monkey. J Comp Neurol 154:349–377.

Joshua M, Adler A, Mitelman R, Vaadia E, Bergman H (2008) Midbrain dopaminergic neurons and striatal cholinergic interneurons encode the difference between reward and aversive events at different epochs of probabilistic classical conditioning trials. J Neurosci 28:11673–11684.

Joyce JN (1991) Differential response of striatal dopamine and muscarinic cholinergic receptor subtypes to the loss of dopamine. I. Effects of intranigral or intracerebroventricular 6-hydroxydopamine lesions of the mesostriatal dopamine system. Exp Neurol 113:261–276.

Joyce JN (1993) Differential response of striatal dopamine and muscarinic cholinergic receptor subtypes to the loss of dopamine. III. Results in Parkinson's disease cases. Brain Res 600:156–160.

Kahle PJ, Neumann M, Ozmen L, Muller V, Jacobsen H, Schindzielorz A, Okochi M, Leimer U, van Der Putten H, Probst A, Kremmer E, Kretzschmar HA, Haass C (2000) Subcellular localization of wild-type and Parkinson's disease-associated mutant alpha -synuclein in human and transgenic mouse brain. J Neurosci 20:6365–6373.

Kamata A, Takeuchi Y, Fukunaga K (2006) Identification of the isoforms of Ca2+/calmodulin-dependent protein kinase II and expression of brain-derived neurotrophic factor mRNAs in the substantia nigra. J Neurochem 96:195–203.

Kamishina H, Yurcisin GH, Corwin J V, Reep RL (2008) Striatal projections from the rat lateral posterior thalamic nucleus. Brain Res 1204:24–39.

Kato S, Kuramochi M, Kobayashi K, Fukabori R, Okada K, Uchigashima M, Watanabe M, Tsutsui Y, Kobayashi K (2011) Selective neural pathway targeting reveals key roles of thalamostriatal projection in the control of visual discrimination. J Neurosci 31:17169–17179.

Kawagoe KT, Garris PA, Wiedemann DJ, Wightman RM (1992) Regulation of transient dopamine concentration gradients in the microenvironment surrounding nerve terminals in the rat striatum. Neuroscience 51:55–64.

Kawaguchi Y (1992) Large aspiny cells in the matrix of the rat neostriatum in vitro: physiological identification, relation to the compartments and excitatory postsynaptic currents. J Neurophysiol 67:1669–1682.

Kawaguchi Y (1993) Physiological, morphological, and histochemical characterization of three classes of interneurons in rat neostriatum. J Neurosci 13:4908–4923.

Kawai H, Lazar R, Metherate R (2007) Nicotinic control of axon excitability regulates thalamocortical transmission. Nat Neurosci 10:1168–1175.

Kawano M, Kawasaki A, Sakata-Haga H, Fukui Y, Kawano H, Nogami H, Hisano S (2006) Particular subpopulations of midbrain and hypothalamic dopamine neurons express vesicular glutamate transporter 2 in the rat brain. J Comp Neurol 498:581–592.

Kayed R, Head E, Thompson JL, McIntire TM, Milton SC, Cotman CW, Glabe CG (2003) Common structure of soluble amyloid oligomers implies common mechanism of pathogenesis. Science 300:486–489.

Kelly RS, Wightman RM (1987) Detection of dopamine overflow and diffusion with voltammetry in slices of rat brain. Brain Res 423:79–87.

Kemp JM, Powell TP (1970) The cortico-striate projection in the monkey. Brain 93:525–546.

Kemp JM, Powell TP (1971a) The structure of the caudate nucleus of the cat: light and electron microscopy. Philos Trans R Soc London Ser B Biol Sci 262:383–401.

Kemp JM, Powell TP (1971b) The synaptic organization of the caudate nucleus. Philos Trans R Soc Lond B Biol Sci 262:383–401.

Kennedy RT, Jones SR, Wightman RM (1992) Simultaneous measurement of oxygen and dopamine: coupling of oxygen consumption and neurotransmission. Neuroscience 47:603–612.

Kile BM, Guillot TS, Venton BJ, Wetsel WC, Augustine GJ, Wightman RM (2010) Synapsins differentially control dopamine and serotonin release. J Neurosci 30:9762–9770.

Kim KM, Baratta M V, Yang A, Lee D, Boyden ES, Fiorillo CD (2012) Optogenetic mimicry of the transient activation of dopamine neurons by natural reward is sufficient for operant reinforcement. PLoS One 7:e33612.

Kim SH, Jang JY, Jang M, Um KB, Chung S, Kim HJ, Park MK (2013) Homeostatic regulation mechanism of spontaneous firing determines glutamate responsiveness in the midbrain dopamine neurons. Cell Calcium 54:295–306.

Kimchi EY, Torregrossa MM, Taylor JR, Laubach M (2009) Neuronal correlates of instrumental learning in the dorsal striatum. J Neurophysiol 102:475–489.

Kimura M, Minamimoto T, Matsumoto N, Hori Y (2004) Monitoring and switching of cortico-basal ganglia loop functions by the thalamo-striatal system. Neurosci Res 48:355–360.

Kimura M, Rajkowski J, Evarts E (1984) Tonically discharging putamen neurons exhibit set-dependent responses. Proc Natl Acad Sci U S A 81:4998–5001.

Kimura M, Yamada H, Matsumoto N (2003) Tonically active neurons in the striatum encode motivational contexts of action. Brain Dev 25 Suppl 1:S20–3.

Kirik D, Rosenblad C, Burger C, Lundberg C, Johansen TE, Muzyczka N, Mandel RJ, Björklund A (2002) Parkinson-like neurodegeneration induced by targeted overexpression of alpha-synuclein in the nigrostriatal system. J Neurosci 22:2780–2791.

Kish SJ, Shannak K, Hornykiewicz O (1988) Uneven pattern of dopamine loss in the striatum of patients with idiopathic Parkinson's disease. Pathophysiologic and clinical implications. N Engl J Med 318:876–880.

Kissinger PT, Hart JB, Adams RN (1973) Voltammetry in brain tissue--a new neurophysiological measurement. Brain Res 55:209–213.

Kita H (1996) Glutamatergic and GABAergic postsynaptic responses of striatal spiny neurons to intrastriatal and cortical stimulation recorded in slice preparations. Neuroscience 70:925–940.

Kita JM, Kile BM, Parker LE, Wightman RM (2009) In vivo measurement of somatodendritic release of dopamine in the ventral tegmental area. Synapse 63:951–960.

Kitabatake Y, Hikida T, Watanabe D, Pastan I, Nakanishi S (2003) Impairment of reward-related learning by cholinergic cell ablation in the striatum. Proc Natl Acad Sci U S A 100:7965–7970.

Klapoetke NC et al. (2014) Independent optical excitation of distinct neural populations. Nat Methods.

Knowlton BJ, Mangels JA, Squire LR (1996) A neostriatal habit learning system in humans. Science 273:1399–1402.

Kolisnyk B, Guzman MS, Raulic S, Fan J, Magalhaes a. C, Feng G, Gros R, Prado VF, Prado M a. M (2013) ChAT-ChR2-EYFP Mice Have Enhanced Motor Endurance But Show Deficits in Attention and Several Additional Cognitive Domains. J Neurosci 33:10427–10438.

Korecka J, Schouten M, Eggers R, Ulusoy A, Bossers K, Verhaagen J (2011) Viral Gene Therapy (Xu K, ed). InTech.

Kravitz A V, Freeze BS, Parker PRL, Kay K, Thwin MT, Deisseroth K, Kreitzer AC (2010) Regulation of parkinsonian motor behaviours by optogenetic control of basal ganglia circuitry. Nature 466:622–626.

Kravitz A V, Tye LD, Kreitzer AC (2012) Distinct roles for direct and indirect pathway striatal neurons in reinforcement. Nat Neurosci 15:816–818.

Krebs MO, Desce JM, Kemel ML, Gauchy C, Godeheu G, Cheramy a, Glowinski J (1991) Glutamatergic control of dopamine release in the rat striatum: evidence for presynaptic N-methyl-D-aspartate receptors on dopaminergic nerve terminals. J Neurochem 56:81–85.

Kreitzer AC, Malenka RC (2007) Endocannabinoid-mediated rescue of striatal LTD and motor deficits in Parkinson's disease models. Nature 445:643–647.

Kress GJ, Yamawaki N, Wokosin DL, Wickersham IR, Shepherd GMG, Surmeier DJ (2013) Convergent cortical innervation of striatal projection neurons. Nat Neurosci 16:665–667.

Krüger R, Kuhn W, Müller T, Woitalla D, Graeber M, Kösel S, Przuntek H, Epplen JT, Schöls L, Riess O (1998) Ala30Pro mutation in the gene encoding alpha-synuclein in Parkinson's disease. Nat Genet 18:106–108.

Kudernatsch M, Sutor B (1994) Cholinergic modulation of dopamine overflow in the rat neostriatum: a fast cyclic voltammetric study in vitro. Neurosci Lett 181:107–112.

Kurz A, Double KL, Lastres-Becker I, Tozzi A, Tantucci M, Bockhart V, Bonin M, García-Arencibia M, Nuber S, Schlaudraff F, Liss B, Fernández-Ruiz J, Gerlach M, Wüllner U, Lüddens H, Calabresi P, Auburger G, Gispert S (2010) A53T-alpha-synuclein overexpression impairs dopamine signaling and striatal synaptic plasticity in old mice. PLoS One 5:e11464.

Kusnoor S V, Parris J, Muly EC, Morgan JI, Deutch a Y (2010) Extracerebellar role for Cerebellin1: modulation of dendritic spine density and synapses in striatal medium spiny neurons. J Comp Neurol 518:2525–2537.

Lacey CJ, Bolam JP, Magill PJ (2007) Novel and distinct operational principles of intralaminar thalamic neurons and their striatal projections. J Neurosci 27:4374–4384.

Lacey CJ, Boyes J, Gerlach O, Chen L, Magill PJ, Bolam JP (2005) GABA(B) receptors at glutamatergic synapses in the rat striatum. Neuroscience 136:1083–1095.

Lam HA, Wu N, Cely I, Kelly RL, Hean S, Richter F, Magen I, Cepeda C, Ackerson LC, Walwyn W, Masliah E, Chesselet M-F, Levine MS, Maidment NT (2011) Elevated tonic extracellular dopamine concentration and altered dopamine modulation of synaptic activity precede dopamine loss in the striatum of mice overexpressing human α-synuclein. J Neurosci Res 89:1091–1102.

Lanciego JL, Gonzalo N, Castle M, Sanchez-Escobar C, Aymerich MS, Obeso JA (2004) Thalamic innervation of striatal and subthalamic neurons projecting to the rat entopeduncular nucleus. Eur J Neurosci 19:1267–1277.

Lanciego JL, Rodríguez-Oroz MC, Blesa FJ, Alvarez-Erviti L, Guridi J, Barroso-Chinea P, Smith Y, Obeso JA (2008) Lesion of the centromedian thalamic nucleus in MPTP-treated monkeys. Mov Disord 23:708–715.

Lange KW, Wells FR, Jenner P, Marsden CD (1993) Altered Muscarinic and Nicotinic Receptor Densities in Cortical and Subcortical Brain Regions in Parkinson's Disease. J Neurochem 60:197–203.

Langer LF, Graybiel AM (1989) Distinct nigrostriatal projection systems innervate striosomes and matrix in the primate striatum. Brain Res 498:344–350.

Lapper SR& BJ (1992) INPUT FROM THE FRONTAL CORTEX AND THE NUCLEUS TO CHOLINERGIC INTERNEURONS IN THE DORSAL OF THE RAT. Neuroscience 51:533–545.

Larkum ME, Zhu JJ, Sakmann B (2001) Dendritic mechanisms underlying the coupling of the dendritic with the axonal action potential initiation zone of adult rat layer 5 pyramidal neurons. J Physiol 533:447–466.

Lashuel HA, Petre BM, Wall J, Simon M, Nowak RJ, Walz T, Lansbury PT (2002) Alpha-synuclein, especially the Parkinson's disease-associated mutants, forms pore-like annular and tubular protofibrils. J Mol Biol 322:1089–1102.

Lee FJ, Liu F, Pristupa ZB, Niznik HB (2001) Direct binding and functional coupling of alpha-synuclein to the dopamine transporters accelerate dopamine-induced apoptosis. FASEB J 15:916–926.

Lee S-J, Jeon H, Kandror K V (2008) Alpha-synuclein is localized in a subpopulation of rat brain synaptic vesicles. Acta Neurobiol Exp (Wars) 68:509–515.

Lehmann J, Langer SZ (1983) The striatal cholinergic interneuron: synaptic target of dopaminergic terminals? Neuroscience 10:1105–1120.

Lei W, Jiao Y, Del Mar N, Reiner A (2004) Evidence for differential cortical input to direct pathway versus indirect pathway striatal projection neurons in rats. J Neurosci 24:8289–8299.

Leventhal DK, Gage GJ, Schmidt R, Pettibone JR, Case AC, Berke JD (2012) Basal ganglia beta oscillations accompany cue utilization. Neuron 73:523–536.

Levey AI, Kitt CA, Simonds WF, Price DL, Brann MR (1991) Identification and localization of muscarinic acetylcholine receptor proteins in brain with subtype-specific antibodies. J Neurosci 11:3218–3226.

Leviel V, Gobert a, Guibert B (1990) The glutamate-mediated release of dopamine in the rat striatum: further characterization of the dual excitatory-inhibitory function. Neuroscience 39:305–312.

Levine MS, Li Z, Cepeda C, Cromwell HC, Altemus KL (1996) Neuromodulatory actions of dopamine on synaptically-evoked neostriatal responses in slices. Synapse 24:65–78.

Li J-Y, Henning Jensen P, Dahlström A (2002) Differential localization of alpha-, beta- and gamma-synucleins in the rat CNS. Neuroscience 113:463–478.

Li X, Qi J, Yamaguchi T, Wang H-L, Morales M (2013) Heterogeneous composition of dopamine neurons of the rat A10 region: molecular evidence for diverse signaling properties. Brain Struct Funct 218:1159–1176.

Lin JY (2011) A user's guide to channelrhodopsin variants: features, limitations and future developments. Exp Physiol 96:19–25.

Liu X, Jones EG (1997) Alpha isoform of calcium-calmodulin dependent protein kinase II (CAM II kinase-alpha) restricted to excitatory synapses in the CA1 region of rat hippocampus. Neuroreport 8:1475–1479.

Liu XB, Jones EG (1996) Localization of alpha type II calcium calmodulin-dependent protein kinase at glutamatergic but not gamma-aminobutyric acid (GABAergic) synapses in thalamus and cerebral cortex. Proc Natl Acad Sci U S A 93:7332–7336.

Ljungberg T, Ungerstedt U (1976) Sensory inattention produced by 6-hydroxydopamine-induced degeneration of ascending dopamine neurons in the brain. Exp Neurol 53:585–600.

Lo Bianco C, Ridet J-L, Schneider BL, Deglon N, Aebischer P (2002) alpha -Synucleinopathy and selective dopaminergic neuron loss in a rat lentiviral-based model of Parkinson's disease. Proc Natl Acad Sci U S A 99:10813–10818.

Lokwan SJ, Overton PG, Berry MS, Clark D (1999) Stimulation of the pedunculopontine tegmental nucleus in the rat produces burst firing in A9 dopaminergic neurons. Neuroscience 92:245–254.

Lonart G, Zigmond MJ (1991) High Glutamate Concentrations Evoke Ca++-lndependent Dopamine Release from Striatal Slices : A Possible Role of Reverse Dopamine Transport. J Pharmacol Exp Ther 256:1132–1138.

Lundblad M, Decressac M, Mattsson B, Björklund A (2012) Impaired neurotransmission caused by overexpression of α-synuclein in nigral dopamine neurons. Proc Natl Acad Sci U S A 109:3213–3219.

Macchi G, Bentivoglio M, Molinari M, Minciacchi D (1984) The thalamo-caudate versus thalamo-cortical projections as studied in the cat with fluorescent retrograde double labeling. Exp brain Res 54:225–239.

Madisen L, Zwingman TA, Sunkin SM, Oh SW, Zariwala HA, Gu H, Ng LL, Palmiter RD, Hawrylycz MJ, Jones AR, Lein ES, Zeng H (2010) A robust and high-throughput Cre reporting and characterization system for the whole mouse brain. Nat Neurosci 13:133–140.

Marin O, Anderson SA, Rubenstein JL (2000) Origin and molecular specification of striatal interneurons. J Neurosci 20:6063–6076.

Markakis EA, Vives KP, Bober J, Leichtle S, Leranth C, Beecham J, Elsworth JD, Roth RH, Samulski RJ, Redmond DE (2010) Comparative transduction efficiency of AAV vector serotypes 1-6 in the substantia nigra and striatum of the primate brain. Mol Ther 18:588–593.

Maroteaux L, Scheller RH (1991) The rat brain synucleins; family of proteins transiently associated with neuronal membrane. Brain Res Mol Brain Res 11:335–343.

Masamizu Y, Okada T, Kawasaki K, Ishibashi H, Yuasa S, Takeda S, Hasegawa I, Nakahara K (2011) Local and retrograde gene transfer into primate neuronal pathways via adeno-associated virus serotype 8 and 9. Neuroscience 193:249–258.

Matsuda W, Furuta T, Nakamura KC, Hioki H, Fujiyama F, Arai R, Kaneko T (2009) Single nigrostriatal dopaminergic neurons form widely spread and highly dense axonal arborizations in the neostriatum. J Neurosci 29:444–453.

Matsumoto M, Hikosaka O (2009) Two types of dopamine neuron distinctly convey positive and negative motivational signals. Nature 459:837–841.

Matsumoto N, Hanakawa T, Maki S, Graybiel AM, Kimura M (1999) Role of [corrected] nigrostriatal dopamine system in learning to perform sequential motor tasks in a predictive manner. J Neurophysiol 82:978–998.

Matsumoto N, Minamimoto T, Graybiel a M, Kimura M (2001) Neurons in the thalamic CM-Pf complex supply striatal neurons with information about behaviorally significant sensory events. J Neurophysiol 85:960–976.

Mattis J, Tye KM, Ferenczi EA, Ramakrishnan C, Shea DJO, Prakash R, Gunaydin LA, Hyun M, Fenno LE, Gradinaru V, Yizhar O, Deisseroth K (2012) Principles for applying optogenetic tools derived from direct comparative analysis of microbial opsins. Online 9.

Maurice N, Mercer J, Chan CS, Hernandez-Lopez S, Held J, Tkatch T, Surmeier DJ (2004) D2 dopamine receptor-mediated modulation of voltage-dependent Na+ channels reduces autonomous activity in striatal cholinergic interneurons. J Neurosci 24:10289–10301.

McCallum SE, Parameswaran N, Bordia T, McIntosh JM, Grady SR, Quik M (2005) Decrease in alpha3*/alpha6* nicotinic receptors but not nicotine-evoked dopamine release in monkey brain after nigrostriatal damage. Mol Pharmacol 68:737–746.

McFarland NR, Haber SN (2000) Convergent inputs from thalamic motor nuclei and frontal cortical areas to the dorsal striatum in the primate. J Neurosci 20:3798–3813.

McFarland NR, Lee J-S, Hyman BT, McLean PJ (2009) Comparison of transduction efficiency of recombinant AAV serotypes 1, 2, 5, and 8 in the rat nigrostriatal system. J Neurochem 109:838–845.

McGeorge a J, Faull RL (1989) The organization of the projection from the cerebral cortex to the striatum in the rat. Neuroscience 29:503–537.

Mechawar N, Watkins KC, Descarries L (2002) Ultrastructural features of the acetylcholine innervation in the developing parietal cortex of rat. J Comp Neurol 443:250–258.

Mejías-Aponte CA, Drouin C, Aston-Jones G (2009) Adrenergic and noradrenergic innervation of the midbrain ventral tegmental area and retrorubral field: prominent inputs from medullary homeostatic centers. J Neurosci 29:3613–3626.

Mena-Segovia J, Ross HM, Magill PJ, Bolam JP (2005) THE PEDUNCULOPONTINE NUCLEUS : Towards a Functional Integration with the Basal Ganglia. In: The Basal Ganglia VIII (Bolam, J.P., Inghan, C.A. and Magill PJ, ed), pp 533–544. New York: Springer Science and Business Media.

Mena-Segovia J, Winn P, Bolam JP (2008) Cholinergic modulation of midbrain dopaminergic systems. Brain Res Rev 58:265–271.

Mercer L, del Fiacco M, Cuello AC (1979) The smooth endoplasmic reticulum as a possible storage site for dendritic dopamine in substantia nigra neurones. Experientia 35:101–103.

Mercuri N, Bernardi G, Calabresi P, Cotugno A, Levi G, Stanzione P (1985) Dopamine decreases cell excitability in rat striatal neurons by pre- and postsynaptic mechanisms. Brain Res 358:110–121.

Meredith GE, Wouterlood FG (1990) Hippocampal and midline thalamic fibers and terminals in relation to the choline acetyltransferase-immunoreactive neurons in nucleus accumbens of the rat: a light and electron microscopic study. J Comp Neurol 296:204–221.

Messamore E (1993) Cholinesterase inhibitor effects on extracellular acetylcholine in rat striatum. Neuropharmacology 32:291–296.

Michael DJ, Wightman RM (1999) Electrochemical monitoring of biogenic amine neurotransmission in real time. J Pharm Biomed Anal 19:33–46.

Middleton FA, Strick PL (2000) Basal ganglia and cerebellar loops: motor and cognitive circuits. Brain Res Brain Res Rev 31:236–250.

Miles PR, Mundorf ML, Wightman RM (2002) Release and uptake of catecholamines in the bed nucleus of the stria terminalis measured in the mouse brain slice. Synapse 44:188–197.

Millar J, Stamford JA, Kruk ZL, Wightman RM (1985) Electrochemical, pharmacological and electrophysiological evidence of rapid dopamine release and removal in the rat caudate nucleus following electrical stimulation of the median forebrain bundle. Eur J Pharmacol 109:341–348.

Minamimoto T, Hori Y, Kimura M (2009) Roles of the thalamic CM-PF complex-Basal ganglia circuit in externally driven rebias of action. Brain Res Bull 78:75–79.

Mink JW (1996) THE BASAL GANGLIA: FOCUSED SELECTION AND INHIBITION OF COMPETING MOTOR PROGRAMS. Prog Neurobiol 50:381–425.

Mink JW (2003) The Basal Ganglia and involuntary movements: impaired inhibition of competing motor patterns. Arch Neurol 60:1365–1368.

Mitch Taylor I, Jaquins-Gerstl A, Sesack SR, Michael AC (2012) Domain-dependent effects of DAT inhibition in the rat dorsal striatum. J Neurochem 122:283–294.

Mollenhauer B, Trautmann E, Otte B, Ng J, Spreer A, Lange P, Sixel-Döring F, Hakimi M, Vonsattel J-P, Nussbaum R, Trenkwalder C, Schlossmacher MG (2012) α-Synuclein in human cerebrospinal fluid is principally derived from neurons of the central nervous system. J Neural Transm 119:739–746.

Montague PR, McClure SM, Baldwin PR, Phillips PEM, Budygin EA, Stuber GD, Kilpatrick MR, Wightman RM (2004) Dynamic gain control of dopamine delivery in freely moving animals. J Neurosci 24:1754–1759.

Moquin KF, Michael AC (2009) Tonic autoinhibition contributes to the heterogeneity of evoked dopamine release in the rat striatum. J Neurochem 110:1491–1501.

Moquin KF, Michael AC (2011) An inverse correlation between the apparent rate of dopamine clearance and tonic autoinhibition in subdomains of the rat striatum: a possible role of transporter-mediated dopamine efflux. J Neurochem 117:133–142.

Morales I, Yanos C, Rodriguez-Sabate C, Sanchez A, Rodriguez M (2013) Striatal glutamate degenerates thalamic neurons. J Neuropathol Exp Neurol 72:286–297.

Mori F, Tanji K, Yoshimoto M, Takahashi H, Wakabayashi K (2002) Immunohistochemical comparison of alpha- and beta-synuclein in adult rat central nervous system. Brain Res 941:118–126.

Morita K, Morishima M, Sakai K, Kawaguchi Y (2013) Dopaminergic Control of Motivation and Reinforcement Learning: A Closed-Circuit Account for Reward-Oriented Behavior. J Neurosci 33:8866–8890.

Morris G, Arkadir D, Nevet A, Vaadia E, Bergman H (2004) Coincident but distinct messages of midbrain dopamine and striatal tonically active neurons. Neuron 43:133–143.

Moss J, Bolam JP (2008) A dopaminergic axon lattice in the striatum and its relationship with cortical and thalamic terminals. J Neurosci 28:11221–11230.

Moss J, Ungless MA, Bolam JP (2011) Dopaminergic axons in different divisions of the adult rat striatal complex do not express vesicular glutamate transporters. Eur J Neurosci 33:1205–1211.

Moukhles H, Bosler O, Bolam JP, Vallée A, Umbriaco D, Geffard M, Doucet G (1997) Quantitative and morphometric data indicate precise cellular interactions between serotonin terminals and postsynaptic targets in rat substantia nigra. Neuroscience 76:1159–1171.

Mrzljak L, Levey AI, Goldman-Rakic PS (1993) Association of m1 and m2 muscarinic receptor proteins with asymmetric synapses in the primate cerebral cortex: morphological evidence for cholinergic modulation of excitatory neurotransmission. Proc Natl Acad Sci U S A 90:5194–5198.

Nagel G, Szellas T, Huhn W, Kateriya S, Adeishvili N, Berthold P, Ollig D, Hegemann P, Bamberg E (2003) Channelrhodopsin-2, a directly light-gated cation-selective membrane channel. Proc Natl Acad Sci U S A 100:13940–13945.

Nagode DA, Tang A-H, Yang K, Alger BE (2014) Optogenetic identification of an intrinsic cholinergically driven inhibitory oscillator sensitive to cannabinoids and opioids in hippocampal CA1. J Physiol 592:103–123.

Nair-Roberts RG, Chatelain-Badie SD, Benson E, White-Cooper H, Bolam JP, Ungless MA (2008) Stereological estimates of dopaminergic, GABAergic and glutamatergic neurons in the ventral tegmental area, substantia nigra and retrorubral field in the rat. Neuroscience 152:1024–1031.

Nakamura K, Nemani VM, Azarbal F, Skibinski G, Levy JM, Egami K, Munishkina L, Zhang J, Gardner B, Wakabayashi J, Sesaki H, Cheng Y, Finkbeiner S, Nussbaum RL, Masliah E, Edwards RH (2011) Direct membrane association drives mitochondrial fission by the Parkinson disease-associated protein alpha-synuclein. J Biol Chem 286:20710–20726.

Nakamura S, Ito Y, Shirasaki R, Murakami F (2000) Local directional cues control growth polarity of dopaminergic axons along the rostrocaudal axis. J Neurosci 20:4112–4119.

Nelson AB, Bussert TG, Kreitzer AC, Seal RP (2014a) Striatal Cholinergic Neurotransmission Requires VGLUT3. J Neurosci 34:8772–8777.

Nelson ABB, Hammack N, Yang CFF, Shah NMM, Seal RPP, Kreitzer ACC (2014b) Striatal cholinergic interneurons Drive GABA release from dopamine terminals. Neuron 82:63–70.

Nelson EL, Liang CL, Sinton CM, German DC (1996) Midbrain dopaminergic neurons in the mouse: computer-assisted mapping. J Comp Neurol 369:361–371.

Nemani VM, Lu W, Berge V, Nakamura K, Onoa B, Lee MK, Chaudhry F a, Nicoll R a, Edwards RH (2010) Increased expression of alpha-synuclein reduces neurotransmitter release by inhibiting synaptic vesicle reclustering after endocytosis. Neuron 65:66–79.

Ni ZG, Gao DM, Benabid AL, Benazzouz A (2000) Unilateral lesion of the nigrostriatal pathway induces a transient decrease of firing rate with no change in the firing pattern of neurons of the parafascicular nucleus in the rat. Neuroscience 101:993–999.

Nicola SM (2007) The nucleus accumbens as part of a basal ganglia action selection circuit. Psychopharmacology (Berl) 191:521–550.

Nicola SM, Surmeier J, Malenka RC (2000) Dopaminergic modulation of neuronal excitability in the striatum and nucleus accumbens. Annu Rev Neurosci 23:185–215.

Nieoullon A, Cheramy A, Glowinski J (1978) Release of dopamine evoked by electrical stimulation of the motor and visual areas of the cereberal cortex in both caudate nuclei and in the substantia nigra in the cat. Brain Res 145:69–83.

Nirenberg MJ, Chan J, Liu Y, Edwards RH, Pickel VM (1997) Vesicular monoamine transporter-2: immunogold localization in striatal axons and terminals. Synapse 26:194–198.

Nirenberg MJ, Vaughan RA, Uhl GR, Kuhar MJ, Pickel VM (1996) The dopamine transporter is localized to dendritic and axonal plasma membranes of nigrostriatal dopaminergic neurons. J Neurosci 16:436–447.

Niv Y (2007) Cost, benefit, tonic, phasic: what do response rates tell us about dopamine and motivation? Ann N Y Acad Sci 1104:357–376.

Noga BR, Pinzon A, Mesigil RP, Hentall ID (2004) Steady-state levels of monoamines in the rat lumbar spinal cord: spatial mapping and the effect of acute spinal cord injury. J Neurophysiol 92:567–577.

O'Neill RD, Grünewald RA, Fillenz M, Albery WJ (1982) Linear sweep voltammetry with carbon paste electrodes in the rat striatum. Neuroscience 7:1945–1954.
Okada K, Toyama K, Inoue Y, Isa T, Kobayashi Y (2009) Different pedunculopontine tegmental neurons signal predicted and actual task rewards. J Neurosci 29:4858–4870.
Olsson M, Björklund A, Campbell K (1998) Early specification of striatal projection neurons and interneuronal subtypes in the lateral and medial ganglionic eminence. Neuroscience 84:867–876.
Omelchenko N, Sesack SR (2005) Laterodorsal tegmental projections to identified cell populations in the rat ventral tegmental area. J Comp Neurol 483:217–235.
Omelchenko N, Sesack SR (2010) Periaqueductal gray afferents synapse onto dopamine and GABA neurons in the rat ventral tegmental area. J Neurosci Res 88:981–991.
Oorschot DE (1996) Total number of neurons in the neostriatal, pallidal, subthalamic, and substantia nigral nuclei of the rat basal ganglia: a stereological study using the cavalieri and optical disector methods. J Comp Neurol 366:580–599.
Ormel L, Stensrud MJ, Bergersen LH, Gundersen V (2012) VGLUT1 is localized in astrocytic processes in several brain regions. Glia 60:229–238.
Osakada F, Mori T, Cetin AH, Marshel JH, Virgen B, Callaway EM (2011) New rabies virus variants for monitoring and manipulating activity and gene expression in defined neural circuits. Neuron 71:617–631.
Packard MG, Knowlton BJ (2002) Learning and memory functions of the Basal Ganglia. Annu Rev Neurosci 25:563–593.
Packer AM, Roska B, Häusser M (2013) Targeting neurons and photons for optogenetics. Nat Neurosci 16:805–815.
Padmanabhan S, Lambert NA, Prasad BM (2008) Activity-dependent regulation of the dopamine transporter is mediated by Ca(2+)/calmodulin-dependent protein kinase signaling. Eur J Neurosci 28:2017–2027.
Padmanabhan S, Prasad BM (2009) Sustained depolarization decreases calcium/calmodulin-dependent protein kinase II activity and gene expression in dopamine neurons. Neuroscience 163:277–285.
Page G, Barc-Pain S, Pontcharraud R, Cante A, Piriou A, Barrier L (2004) The up-regulation of the striatal dopamine transporter's activity by cAMP is PKA-, CaMK II- and phosphatase-dependent. Neurochem Int 45:627–632.
Pan W-X, Hyland BI (2005) Pedunculopontine tegmental nucleus controls conditioned responses of midbrain dopamine neurons in behaving rats. J Neurosci 25:4725–4732.
Pan WX, Mao T, Dudman JT (2010) Inputs to the dorsal striatum of the mouse reflect the parallel circuit architecture of the forebrain. Front Neuroanat 4:147.
Paquet M, Smith Y (2003) Group I metabotropic glutamate receptors in the monkey striatum: subsynaptic association with glutamatergic and dopaminergic afferents. J Neurosci 23:7659–7669.
Parent A, Mackey A, De Bellefeuille L (1983) The subcortical afferents to caudate nucleus and putamen in primate: a fluorescence retrograde double labeling study. Neuroscience 10:1137–1150.
Parent M, Descarries L (2008) Acetylcholine innervation of the adult rat thalamus: distribution and ultrastructural features in dorsolateral geniculate, parafascicular, and reticular thalamic nuclei. J Comp Neurol 511:678–691.
Parent M, Parent A (2005) Single-axon tracing and three-dimensional reconstruction of centre median-parafascicular thalamic neurons in primates. J Comp Neurol 481:127–144.
Parent M, Parent A (2006) Single-axon tracing study of corticostriatal projections arising from primary motor cortex in primates. J Comp Neurol 496:202–213.

Park J, Kile BM, Wightman RM (2009) In vivo voltammetric monitoring of norepinephrine release in the rat ventral bed nucleus of the stria terminalis and anteroventral thalamic nucleus. Eur J Neurosci 30:2121–2133.

Park J, Takmakov P, Wightman RM (2011) In vivo comparison of norepinephrine and dopamine release in rat brain by simultaneous measurements with fast-scan cyclic voltammetry. J Neurochem 119:932–944.

Parr-Brownlie LC, Poloskey SL, Bergstrom DA, Walters JR (2009) Parafascicular thalamic nucleus activity in a rat model of Parkinson's disease. Exp Neurol 217:269–281.

Patel JC, Rossignol E, Rice ME, Machold RP (2012) Opposing regulation of dopaminergic activity and exploratory motor behavior by forebrain and brainstem cholinergic circuits. Nat Commun 3:1172.

Patel JC, Witkovsky P, Coetzee WA, Rice ME (2011) Subsecond regulation of striatal dopamine release by pre-synaptic KATP channels. J Neurochem 118:721–736.

Paterna J-C, Feldon J, Büeler H (2004) Transduction profiles of recombinant adeno-associated virus vectors derived from serotypes 2 and 5 in the nigrostriatal system of rats. J Virol 78:6808–6817.

Paxinos G, Franklin KBJ (2008) The Mouse Brain in Stereotaxic Coordinates. Elsevier Academic Press.

Perrone-Capano C, Tino A, Amadoro G, Pernas-Alonso R, di Porzio U (1996) Dopamine transporter gene expression in rat mesencephalic dopaminergic neurons is increased by direct interaction with target striatal cells in vitro. Brain Res Mol Brain Res 39:160–166.

Peters JL, Miner LH, Michael AC, Sesack SR (2004) Ultrastructure at carbon fiber microelectrode implantation sites after acute voltammetric measurements in the striatum of anesthetized rats. J Neurosci Methods 137:9–23.

Petreanu L, Huber D, Sobczyk A, Svoboda K (2007) Channelrhodopsin-2-assisted circuit mapping of long-range callosal projections. Nat Neurosci 10:663–668.

Phelps PE, Houser CR, Vaughn JE (1985) Immunocytochemical localization of choline acetyltransferase within the rat neostriatum: a correlated light and electron microscopic study of cholinergic neurons and synapses. J Comp Neurol 238:286–307.

Phelps PE, Vaughn JE (1986) Immunocytochemical localization of choline acetyltransferase in rat ventral striatum: a light and electron microscopic study. J Neurocytol 15:595–617.

Phillips PE, Stamford JA (2000) Differential recruitment of N-, P- and Q-type voltage-operated calcium channels in striatal dopamine release evoked by "regular" and "burst" firing. Brain Res 884:139–146.

Phillips PEM, Hancock PJ, Stamford JA (2002) Time window of autoreceptor-mediated inhibition of limbic and striatal dopamine release. Synapse 44:15–22.

Picciotto MR, Zoli M, Rimondini R, Léna C, Marubio LM, Pich EM, Fuxe K, Changeux JP (1998) Acetylcholine receptors containing the beta2 subunit are involved in the reinforcing properties of nicotine. Nature 391:173–177.

Pickel VM (2000) Extrasynaptic distribution of monoamine transporters and receptors. Prog Brain Res 125:267–276.

Pickel VM, Chan J, Nirenberg MJ (2002) Region-specific targeting of dopamine D2-receptors and somatodendritic vesicular monoamine transporter 2 (VMAT2) within ventral tegmental area subdivisions. Synapse 45:113–124.

Pihel K, Walker QD, Wightman RM (1996) Overoxidized Polypyrrole-Coated Carbon Fiber Microelectrodes for Dopamine Measurements with Fast-Scan Cyclic Voltammetry. Anal Chem 68:2084–2089.

Pinto A, Jankowski M, Sesack SR (2003) Projections from the paraventricular nucleus of the thalamus to the rat prefrontal cortex and nucleus accumbens shell: ultrastructural characteristics and spatial relationships with dopamine afferents. J Comp Neurol 459:142–155.

Pisani a, Bonsi P, Centonze D, Bernardi G, Calabresi P (2001) Functional coexpression of excitatory mGluR1 and mGluR5 on striatal cholinergic interneurons. Neuropharmacology 40:460–463.

Pisani a, Bonsi P, Centonze D, Calabresi P, Bernardi G (2000) Activation of D2-like dopamine receptors reduces synaptic inputs to striatal cholinergic interneurons. J Neurosci 20:RC69.

Pisani A, Bernardi G, Ding J, Surmeier DJ (2007) Re-emergence of striatal cholinergic interneurons in movement disorders. Trends Neurosci 30:545–553.

Pisani A, Bonsi P, Catania MV, Giuffrida R, Morari M, Marti M, Centonze D, Bernardi G, Kingston AE, Calabresi P (2002) Metabotropic glutamate 2 receptors modulate synaptic inputs and calcium signals in striatal cholinergic interneurons. J Neurosci 22:6176–6185.

Pisani A, Bonsi P, Centonze D, Gubellini P, Bernardi G, Calabresi P (2003) Targeting striatal cholinergic interneurons in Parkinson's disease: Focus on metabotropic glutamate receptors. Neuropharmacology 45:45–56.

Platt NJ, Gispert S, Auburger G, Cragg SJ (2012) Striatal dopamine transmission is subtly modified in human A53Tα-synuclein overexpressing mice. PLoS One 7:e36397.

Pockberger H (1991) Electrophysiological and morphological properties of rat motor cortex neurons in vivo. Brain Res 539:181–190.

Podda M V, Riccardi E, D'Ascenzo M, Azzena GB, Grassi C (2010) Dopamine D1-like receptor activation depolarizes medium spiny neurons of the mouse nucleus accumbens by inhibiting inwardly rectifying K+ currents through a cAMP-dependent protein kinase A-independent mechanism. Neuroscience 167:678–690.

Polymeropoulos MH et al. (1997) Mutation in the alpha-synuclein gene identified in families with Parkinson's disease. Science 276:2045–2047.

Qing K, Mah C, Hansen J, Zhou S, Dwarki V, Srivastava A (1999) Human fibroblast growth factor receptor 1 is a co-receptor for infection by adeno-associated virus 2. Nat Med 5:71–77.

Quik M (2003) Differential Declines in Striatal Nicotinic Receptor Subtype Function after Nigrostriatal Damage in Mice. Mol Pharmacol 63:1169–1179.

Quik M, Bordia T, Forno L, McIntosh JM (2004) Loss of alpha-conotoxinMII- and A85380-sensitive nicotinic receptors in Parkinson's disease striatum. J Neurochem 88:668–679.

Quik M, Vailati S, Bordia T, Kulak JM, Fan H, McIntosh JM, Clementi F, Gotti C (2005) Subunit composition of nicotinic receptors in monkey striatum: effect of treatments with 1-methyl-4-phenyl-1,2,3,6-tetrahydropyridine or L-DOPA. Mol Pharmacol 67:32–41.

Quilty MC, King AE, Gai W-P, Pountney DL, West AK, Vickers JC, Dickson TC (2006) Alpha-synuclein is upregulated in neurones in response to chronic oxidative stress and is associated with neuroprotection. Exp Neurol 199:249–256.

Quinn JJ, Pittenger C, Lee AS, Pierson JL, Taylor JR (2013) Striatum-dependent habits are insensitive to both increases and decreases in reinforcer value in mice. Eur J Neurosci 37:1012–1021.

Rabinowitz JE, Rolling F, Li C, Conrath H, Xiao W, Xiao X, Samulski RJ (2002) Cross-packaging of a single adeno-associated virus (AAV) type 2 vector genome into multiple AAV serotypes enables transduction with broad specificity. J Virol 76:791–801.

Raimondo J V, Kay L, Ellender TJ, Akerman CJ (2012) Optogenetic silencing strategies differ in their effects on inhibitory synaptic transmission. Nat Neurosci 15:1102–1104.

Raju D V, Ahern TH, Shah DJ, Wright TM, Standaert DG, Hall RA, Smith Y (2008) Differential synaptic plasticity of the corticostriatal and thalamostriatal systems in an MPTP-treated monkey model of parkinsonism. Eur J Neurosci 27:1647–1658.

Raju D V, Shah DJ, Wright TM, Hall RA, Smith Y (2006) Differential synaptology of vGluT2-containing thalamostriatal afferents between the patch and matrix compartments in rats. J Comp Neurol 499:231–243.

Rakovska A, Javitt D, Raichev P, Ang R, Balla A, Aspromonte J, Vizi S (2003) Physiological release of striatal acetylcholine (in vivo): effect of somatostatin on dopaminergic-cholinergic interaction. Brain Res Bull 61:529–536.

Ramanathan S, Hanley JJ, Deniau J-M, Bolam JP (2002) Synaptic convergence of motor and somatosensory cortical afferents onto GABAergic interneurons in the rat striatum. J Neurosci 22:8158–8169.

Raz a, Feingold a, Zelanskaya V, Vaadia E, Bergman H (1996) Neuronal synchronization of tonically active neurons in the striatum of normal and parkinsonian primates. J Neurophysiol 76:2083–2088.

Raz A, Frechter-Mazar V, Feingold A, Abeles M, Vaadia E, Bergman H (2001) Activity of pallidal and striatal tonically active neurons is correlated in mptp-treated monkeys but not in normal monkeys. J Neurosci 21:RC128.

Redgrave P, Vautrelle N, Reynolds JNJ (2011) Functional properties of the basal ganglia's re-entrant loop architecture: selection and reinforcement. Neuroscience 198:138–151.

Reep RL, Cheatwood JL, Corwin J V (2003) The associative striatum: organization of cortical projections to the dorsocentral striatum in rats. J Comp Neurol 467:271–292.

Reiner A, Hart NM, Lei W, Deng Y (2010) Corticostriatal projection neurons - dichotomous types and dichotomous functions. Front Neuroanat 4:142.

Reiner A, Jiao Y, Del Mar N, Laverghetta AV, Lei WL (2003) Differential morphology of pyramidal tract-type and intratelencephalically projecting-type corticostriatal neurons and their intrastriatal terminals in rats. J Comp Neurol 457:420–440.

Reynolds JNJ, Hyland BI, Wickens JR (2004) Modulation of an afterhyperpolarization by the substantia nigra induces pauses in the tonic firing of striatal cholinergic interneurons. J Neurosci 24:9870–9877.

Reynolds JNJ, Wickens JR (2002) Dopamine-dependent plasticity of corticostriatal synapses. Neural Netw 15:507–521.

Reynolds JNJ, Wickens JR (2004) The corticostriatal input to giant aspiny interneurons in the rat: a candidate pathway for synchronising the response to reward-related cues. Brain Res 1011:115–128.

Rice ME, Cragg SJ (2004) Nicotine amplifies reward-related dopamine signals in striatum. Nat Neurosci 7:583–584.

Rice ME, Cragg SJ (2008) Dopamine spillover after quantal release: rethinking dopamine transmission in the nigrostriatal pathway. Brain Res Rev 58:303–313.

Rice ME, Cragg SJ, Greenfield SA (1997) Characteristics of electrically evoked somatodendritic dopamine release in substantia nigra and ventral tegmental area in vitro. J Neurophysiol 77:853–862.

Rice ME, Nicholson C (1991) Diffusion characteristics and extracellular volume fraction during normoxia and hypoxia in slices of rat neostriatum. J Neurophysiol 65:264–272.

Rice ME, Oke AF, Bradberry CW, Adams RN (1985) Simultaneous voltammetric and chemical monitoring of dopamine release in situ. Brain Res 340:151–155.

Rice ME, Patel JC, Cragg SJ (2011) Dopamine release in the basal ganglia. Neuroscience 198:112–137.

Rice ME, Richards CD, Nedergaard S, Hounsgaard J, Nicholson C, Greenfield SA (1994) Direct monitoring of dopamine and 5-HT release in substantia nigra and ventral tegmental area in vitro. Exp brain Res 100:395–406.

Rinne JO, Myllykyla¨ T, Lo¨nnberg P, Marjama¨ki P (1991) A postmortem study of brain nicotinic receptors in Parkinson's and Alzheimer's disease. Brain Res 547:155–158.

Rizzoli SO, Betz WJ (2005) Synaptic vesicle pools. Nat Rev Neurosci 6:57–69.

Robbins TW, Everitt BJ (1996) Neurobehavioural mechanisms of reward and motivation. Curr Opin Neurobiol 6:228–236.

Roberts PJ, Anderson SD (1979) Stimulatory effect of L-glutamate and related amino acids on [3H]dopamine release from rat striatum: an in vitro model for glutamate actions. J Neurochem 32:1539–1545.

Roberts RC, Force M, Kung L (2002) Dopaminergic synapses in the matrix of the ventrolateral striatum after chronic haloperidol treatment. Synapse 45:78–85.

Royce GJ (1983) Cells of origin of corticothalamic projections upon the centromedian and parafascicular nuclei in the cat. Brain Res 258:11–21.

Royer S, Zemelman B V, Barbic M, Losonczy A, Buzsáki G, Magee JC (2010) Multi-array silicon probes with integrated optical fibers: light-assisted perturbation and recording of local neural circuits in the behaving animal. Eur J Neurosci 31:2279–2291.

Sadikot a F, Parent a, Smith Y, Bolam JP (1992) Efferent connections of the centromedian and parafascicular thalamic nuclei in the squirrel monkey: a light and electron microscopic study of the thalamostriatal projection in relation to striatal heterogeneity. J Comp Neurol 320:228–242.

Sadikot AF, Rymar V V (2009) The primate centromedian-parafascicular complex: anatomical organization with a note on neuromodulation. Brain Res Bull 78:122–130.

Salegio E a, Samaranch L, Kells a P, Mittermeyer G, San Sebastian W, Zhou S, Beyer J, Forsayeth J, Bankiewicz KS (2012) Axonal transport of adeno-associated viral vectors is serotype-dependent. Gene Ther 20:348–352.

Salminen O, Murphy KL, McIntosh JM, Drago J, Marks MJ, Collins AC, Grady SR (2004) Subunit composition and pharmacology of two classes of striatal presynaptic nicotinic acetylcholine receptors mediating dopamine release in mice. Mol Pharmacol 65:1526–1535.

Sanchez CE, Tierney TS, Gale JT, Alavian KN, Sahin A, Lee J-S, Mulligan RC, Carter BS (2011a) Recombinant adeno-associated virus type 2 pseudotypes: comparing safety, specificity, and transduction efficiency in the primate striatum. Laboratory investigation. J Neurosurg 114:672–680.

Sanchez G, Rodriguez MJ, Pomata P, Rela L, Murer MG (2011b) Reduction of an afterhyperpolarization current increases excitability in striatal cholinergic interneurons in rat parkinsonism. J Neurosci 31:6553–6564.

Santiago MP, Potter LT (2001) Biotinylated m4-toxin demonstrates more M4 muscarinic receptor protein on direct than indirect striatal projection neurons. Brain Res 894:12–20.

Satake W et al. (2009) Genome-wide association study identifies common variants at four loci as genetic risk factors for Parkinson's disease. Nat Genet 41:1303–1307.

Schenk JO, Miller E, Rice ME, Adams RN (1983) Chronoamperometry in brain slices: quantitative evaluations of in vivo electrochemistry. Brain Res 277:1–8.

Scherman D, Desnos C, Darchen F, Pollak P, Javoy-Agid F, Agid Y (1989) Striatal dopamine deficiency in Parkinson's disease: role of aging. Ann Neurol 26:551–557.

Schilman E a, Uylings HBM, Galis-de Graaf Y, Joel D, Groenewegen HJ (2008) The orbital cortex in rats topographically projects to central parts of the caudate-putamen complex. Neurosci Lett 432:40–45.

Schmidt R, Leventhal DK, Mallet N, Chen F, Berke JD (2013) Canceling actions involves a race between basal ganglia pathways. Nat Neurosci 16:1118–1124.

Schmitz Y, Schmauss C, Sulzer D (2002) Altered dopamine release and uptake kinetics in mice lacking D2 receptors. J Neurosci 22:8002–8009.

Schönfuss D, Reum T, Olshausen P, Fischer T, Morgenstern R (2001) Modelling constant potential amperometry for investigations of dopaminergic neurotransmission kinetics in vivo. J Neurosci Methods 112:163–172.

Schönig K, Weber T, Frömmig A, Wendler L, Pesold B, Djandji D, Bujard H, Bartsch D (2012) Conditional gene expression systems in the transgenic rat brain. BMC Biol 10:77.

Schultz W (1998) Predictive reward signal of dopamine neurons. J Neurophysiol 80:1–27.

Schultz W (2006) Behavioral theories and the neurophysiology of reward. Annu Rev Psychol 57:87–115.

Schultz W, Apicella P, Ljungberg T (1993) Responses of monkey dopamine neurons to reward and conditioned stimuli during successive steps of learning a delayed response task. J Neurosci 13:900–913.

Schulz JM, Oswald MJ, Reynolds JNJ (2011) Visual-Induced Excitation Leads to Firing Pauses in Striatal Cholinergic Interneurons. J Neurosci 31:11133–11143.

Schulz JM, Reynolds JNJ (2013) Pause and rebound: sensory control of cholinergic signaling in the striatum. Trends Neurosci 36:41–50.

Schwab M, Agid Y, Glowinski J, Thoenen H (1977) Retrograde axonal transport of 125I-tetanus toxin as a tool for tracing fiber connections in the central nervous system; connections of the rostral part of the rat neostriatum. Brain Res 126:211–224.

Seki A, Miyauchi S, Hayashi S, Kikukawa T, Kubo M, Demura M, Ganapathy V, Kamo N (2007) Heterologous expression of Pharaonis halorhodopsin in Xenopus laevis oocytes and electrophysiological characterization of its light-driven Cl- pump activity. Biophys J 92:2559–2569.

Senior SL, Ninkina N, Deacon R, Bannerman D, Buchman VL, Cragg SJ, Wade-Martins R (2008) Increased striatal dopamine release and hyperdopaminergic-like behaviour in mice lacking both alpha-synuclein and gamma-synuclein. Eur J Neurosci 27:947–957.

Sesack SR, Aoki C, Pickel VM (1994) Ultrastructural localization of D2 receptor-like immunoreactivity in midbrain dopamine neurons and their striatal targets. J Neurosci 14:88–106.

Sharott A, Doig NM, Mallet N, Magill PJ (2012) Relationships between the Firing of Identified Striatal Interneurons and Spontaneous and Driven Cortical Activities In Vivo. J Neurosci 32:13221–13236.

Sherman SM (2001) Tonic and burst firing: dual modes of thalamocortical relay. Trends Neurosci 24:122–126.

Shiflett MW, Brown R a, Balleine BW (2010) Acquisition and performance of goal-directed instrumental actions depends on ERK signaling in distinct regions of dorsal striatum in rats. J Neurosci 30:2951–2959.

Shimamoto S a., Ryapolova-Webb ES, Ostrem JL, Galifianakis NB, Miller KJ, Starr P a. (2013) Subthalamic Nucleus Neurons Are Synchronized to Primary Motor Cortex Local Field Potentials in Parkinson's Disease. J Neurosci 33:7220–7233.

Shimizu N, Duan SM, Hori T, Oomura Y (1990) Glutamate modulates dopamine release in the striatum as measured by brain microdialysis. Brain Res Bull 25:99–102.

Shu Z, Taylor IM, Michael AC (2013) The dopamine patchwork of the rat nucleus accumbens core. Eur J Neurosci 38:3221–3229.

Sidibé M, Smith Y (1999) Thalamic inputs to striatal interneurons in monkeys: synaptic organization and co-localization of calcium binding proteins. Neuroscience 89:1189–1208.

Simón-Sánchez J et al. (2009) Genome-wide association study reveals genetic risk underlying Parkinson's disease. Nat Genet 41:1308–1312.

Smeal RM, Keefe K a, Wilcox KS (2008) Differences in excitatory transmission between thalamic and cortical afferents to single spiny efferent neurons of rat dorsal striatum. Eur J Neurosci 28:2041–2052.

Smith AD, Bolam JP (1990) The neural network of the basal ganglia as revealed by the study of synaptic connections of identified neurones. Trends Neurosci 13:259–265.

Smith KS, Graybiel AM (2013) A Dual Operator View of Habitual Behavior Reflecting Cortical and Striatal Dynamics. Neuron:1–14.

Smith KS, Virkud A, Deisseroth K, Graybiel AM (2012a) Reversible online control of habitual behavior by optogenetic perturbation of medial prefrontal cortex.

Smith Y (2007) The Thalamus. :419–442.

Smith Y, Bevan MD, Shink E, Bolam JP (1998) COMMENTARY MICROCIRCUITRY OF THE DIRECT AND INDIRECT PATHWAYS OF THE BASAL GANGLIA. Science (80-) 86:353–387.

Smith Y, Raju D, Nanda B, Pare J-F, Galvan A, Wichmann T (2009) The thalamostriatal systems: anatomical and functional organization in normal and parkinsonian states. Brain Res Bull 78:60–68.

Smith Y, Raju D V, Pare J-F, Sidibe M (2004) The thalamostriatal system: a highly specific network of the basal ganglia circuitry. Trends Neurosci 27:520–527.

Smith Y, Wichmann T, Factor SA, Delong MR (2012b) Parkinson's disease therapeutics: new developments and challenges since the introduction of levodopa. Neuropsychopharmacology 37:213–246.

Smits SM, Burbach JPH, Smidt MP (2006) Developmental origin and fate of meso-diencephalic dopamine neurons. Prog Neurobiol 78:1–16.

Sodeik B (2000) Mechanisms of viral transport in the cytoplasm. Trends Microbiol 8:465–472.

Somogyi P, Bolam JP, Smith AD (1981) Monosynaptic cortical input and local axon collaterals of identified striatonigral neurons. A light and electron microscopic study using the Golgi-peroxidase transport-degeneration procedure. J Comp Neurol 195:567–584.

Somogyi P, Takagi H (1982) A note on the use of picric acid-paraformaldehyde-glutaraldehyde fixative for correlated light and electron microscopic immunocytochemistry. Neuroscience 7:1779–1783.

Spillantini MG, Crowther RA, Jakes R, Hasegawa M, Goedert M (1998) alpha-Synuclein in filamentous inclusions of Lewy bodies from Parkinson's disease and dementia with lewy bodies. Proc Natl Acad Sci U S A 95:6469–6473.

Spinelli KJ, Taylor JK, Osterberg VR, Churchill MJ, Pollock E, Moore C, Meshul CK, Unni VK (2014) Presynaptic Alpha-Synuclein Aggregation in a Mouse Model of Parkinson's Disease. J Neurosci 34:2037–2050.

Stamford J, Crespi F, Marsden C (1992) In vivo voltammetric methods for monitoring monoamine release and metabolism. Monit neuronal Act.

Stamford JA (1989) In vivo voltammetry--prospects for the next decade. Trends Neurosci 12:407–412.

Stamford JA, Kruk ZL, Millar J (1985) Ascorbic acid does not modulate stimulated dopamine release: in vivo voltammetric data in the rat. Neurosci Lett 60:357–362.

Stamford JA, Palij P, Davidson C, Jorm CM, Millar J (1993) Simultaneous "real-time" electrochemical and electrophysiological recording in brain slices with a single carbon-fibre microelectrode. J Neurosci Methods 50:279–290.

Steffensen SC, Svingos AL, Pickel VM, Henriksen SJ (1998) Electrophysiological characterization of GABAergic neurons in the ventral tegmental area. J Neurosci 18:8003–8015.

Steinberg EE, Keiflin R, Boivin JR, Witten IB, Deisseroth K, Janak PH (2013) A causal link between prediction errors, dopamine neurons and learning. Nat Neurosci 16:966–973.

Steriade M, Paré D, Parent A, Smith Y (1988) Projections of cholinergic and non-cholinergic neurons of the brainstem core to relay and associational thalamic nuclei in the cat and macaque monkey. Neuroscience 25:47–67.

Stewart TC, Choo X, Eliasmith C (2010) Symbolic Reasoning in Spiking Neurons: A Model of the Cortex/Basal Ganglia/Thalamus Loop. Engineering:1100–1105.

Stopper CM, Floresco SB (2014) What's better for me? Fundamental role for lateral habenula in promoting subjective decision biases. Nat Neurosci 17:33–35.

Straub C, Tritsch NX, Hagan NA, Gu C, Sabatini BL (2014) Multiphasic modulation of cholinergic interneurons by nigrostriatal afferents. J Neurosci 34:8557–8569.

Stuber GD, Hnasko TS, Britt JP, Edwards RH, Bonci A (2010) Dopaminergic terminals in the nucleus accumbens but not the dorsal striatum corelease glutamate. J Neurosci 30:8229–8233.

Sullivan M a, Chen H, Morikawa H (2008) Recurrent inhibitory network among striatal cholinergic interneurons. J Neurosci 28:8682–8690.

Summerford C, Bartlett JS, Samulski RJ (1999) AlphaVbeta5 integrin: a co-receptor for adeno-associated virus type 2 infection. Nat Med 5:78–82.

Summerford C, Samulski RJ (1998) Membrane-associated heparan sulfate proteoglycan is a receptor for adeno-associated virus type 2 virions. J Virol 72:1438–1445.

Surmeier DJ, Bargas J, Hemmings HC, Nairn AC, Greengard P (1995) Modulation of calcium currents by a D1 dopaminergic protein kinase/phosphatase cascade in rat neostriatal neurons. Neuron 14:385–397.

Surmeier DJ, Ding J, Day M, Wang Z, Shen W (2007) D1 and D2 dopamine-receptor modulation of striatal glutamatergic signaling in striatal medium spiny neurons. Trends Neurosci 30:228–235.

Svingos AL, Chavkin C, Colago EE, Pickel VM (2001a) Major coexpression of kappa-opioid receptors and the dopamine transporter in nucleus accumbens axonal profiles. Synapse 42:185–192.

Svingos AL, Colago EE, Pickel VM (2001b) Vesicular acetylcholine transporter in the rat nucleus accumbens shell: subcellular distribution and association with mu-opioid receptors. Synapse 40:184–192.

Swanson LW (1982) The projections of the ventral tegmental area and adjacent regions: a combined fluorescent retrograde tracer and immunofluorescence study in the rat. Brain Res Bull 9:321–353.

Takács VT, Szőnyi A, Freund TF, Nyiri G, Gulyás AI (2014) Quantitative ultrastructural analysis of basket and axo-axonic cell terminals in the mouse hippocampus. Brain Struct Funct.

Takagi H, Somogyi P, Somogyi J, Smith AD (1983) Fine structural studies on a type of somatostatin-immunoreactive neuron and its synaptic connections in the rat neostriatum: a correlated light and electron microscopic study. J Comp Neurol 214:1–16.

Takmakov P, McKinney CJ, Carelli RM, Wightman RM (2011) Instrumentation for fast-scan cyclic voltammetry combined with electrophysiology for behavioral experiments in freely moving animals. Rev Sci Instrum 82:074302.

Tamás G, Szabadics J (2004) Summation of unitary IPSPs elicited by identified axo-axonic interneurons. Cereb Cortex 14:823–826.

Tan CO, Bullock D (2008) A dopamine-acetylcholine cascade: simulating learned and lesion-induced behavior of striatal cholinergic interneurons. J Neurophysiol 100:2409–2421.

Tanaka D (1987) Differential laminar distribution of corticostriatal neurons in the prefrontal and pericruciate gyri of the dog. J Neurosci 7:4095–4106.

Taniguchi H, He M, Wu P, Kim S, Paik R, Sugino K, Kvitsiani D, Kvitsani D, Fu Y, Lu J, Lin Y, Miyoshi G, Shima Y, Fishell G, Nelson SB, Huang ZJ (2011) A resource of Cre driver lines for genetic targeting of GABAergic neurons in cerebral cortex. Neuron 71:995–1013.

Taschenberger G, Garrido M, Tereshchenko Y, Bähr M, Zweckstetter M, Kügler S (2012) Aggregation of αSynuclein promotes progressive in vivo neurotoxicity in adult rat dopaminergic neurons. Acta Neuropathol 123:671–683.

Taylor IM, Ilitchev AI, Michael AC (2013) Restricted diffusion of dopamine in the rat dorsal striatum. ACS Chem Neurosci 4:870–878.

Taylor TN, Potgieter D, Anwar S, Senior SL, Janezic S, Threlfell S, Ryan B, Parkkinen L, Deltheil T, Cioroch M, Livieratos A, Oliver PL, Jennings KA, Davies KE, Ansorge O, Bannerman DM, Cragg SJ, Wade-Martins R (2014) Region-specific deficits in dopamine, but not norepinephrine, signaling in a novel A30P α-synuclein BAC transgenic mouse. Neurobiol Dis 62:193–207.

Taymans J-M, Vandenberghe LH, Haute C Van Den, Thiry I, Deroose CM, Mortelmans L, Wilson JM, Debyser Z, Baekelandt V (2007) Comparative analysis of adeno-associated viral vector serotypes 1, 2, 5, 7, and 8 in mouse brain. Hum Gene Ther 18:195–206.

Tecuapetla F, Patel JC, Xenias H, English D, Tadros I, Shah F, Berlin J, Deisseroth K, Rice ME, Tepper JM, Koos T (2010) Glutamatergic signaling by mesolimbic dopamine neurons in the nucleus accumbens. J Neurosci 30:7105–7110.

Tehovnik EJ, Tolias AS, Sultan F, Slocum WM, Logothetis NK (2006) Direct and Indirect Activation of Cortical Neurons by Electrical Microstimulation. J Neurophysiol 96:512–521.

Thomas TM, Smith Y, Levey a I, Hersch SM (2000) Cortical inputs to m2-immunoreactive striatal interneurons in rat and monkey. Synapse 37:252–261.

Threlfell S, Clements M a, Khodai T, Pienaar IS, Exley R, Wess J, Cragg SJ (2010) Striatal muscarinic receptors promote activity dependence of dopamine transmission via distinct receptor subtypes on cholinergic interneurons in ventral versus dorsal striatum. J Neurosci 30:3398–3408.

Threlfell S, Cragg S (2007) Using fast-scan cyclic voltammetry to investigate somatodendritic dopamine release. Electrochem Methods Neurosci.

Threlfell S, Cragg SJ (2011) Dopamine signaling in dorsal versus ventral striatum: the dynamic role of cholinergic interneurons. Front Syst Neurosci 5:11.

Threlfell S, Lalic T, Platt NJ, Jennings K a, Deisseroth K, Cragg SJ (2012) Striatal dopamine release is triggered by synchronized activity in cholinergic interneurons. Neuron 75:58–64.

Tong J, Wong H, Guttman M, Ang LC, Forno LS, Shimadzu M, Rajput AH, Muenter MD, Kish SJ, Hornykiewicz O, Furukawa Y (2010) Brain alpha-synuclein accumulation in multiple system atrophy, Parkinson's disease and progressive supranuclear palsy: a comparative investigation. Brain 133:172–188.

Totterdell S, Meredith GE (2005) Localization of alpha-synuclein to identified fibers and synapses in the normal mouse brain. Neuroscience 135:907–913.

Towne C, Schneider BL, Kieran D, Redmond DE, Aebischer P (2010) Efficient transduction of non-human primate motor neurons after intramuscular delivery of recombinant AAV serotype 6. Gene Ther 17:141–146.

Tricomi E, Balleine BW, O'Doherty JP (2009) A specific role for posterior dorsolateral striatum in human habit learning. Eur J Neurosci 29:2225–2232.

Tritsch NX, Ding JB, Sabatini BL (2012) Dopaminergic neurons inhibit striatal output through non-canonical release of GABA. Nature 490:262–266.

Tritsch NX, Oh W-J, Gu C, Sabatini BL (2014) Midbrain dopamine neurons sustain inhibitory transmission using plasma membrane uptake of GABA, not synthesis. Elife 3:e01936.

Tsai H-C, Zhang F, Adamantidis A, Stuber GD, Bonci A, de Lecea L, Deisseroth K (2009) Phasic firing in dopaminergic neurons is sufficient for behavioral conditioning. Science 324:1080–1084.

Tsigelny IF, Sharikov Y, Wrasidlo W, Gonzalez T, Desplats PA, Crews L, Spencer B, Masliah E (2012) Role of α-synuclein penetration into the membrane in the mechanisms of oligomer pore formation. FEBS J 279:1000–1013.

Tsunematsu T, Tabuchi S, Tanaka KF, Boyden ES, Tominaga M, Yamanaka A (2013) Long-lasting silencing of orexin/hypocretin neurons using archaerhodopsin induces slow-wave sleep in mice. Behav Brain Res 255:64–74.

Uchikawa T, Kiuchi Y, Yura A, Nakachi N, Yamazaki Y, Yokomizo C, Oguchi K (1995) Ca(2+)-dependent enhancement of [3H]dopamine uptake in rat striatum: possible involvement of calmodulin-dependent kinases. J Neurochem 65:2065–2071.

Umbriaco D, Watkins KC, Descarries L, Cozzari C, Hartman BK (1994) Ultrastructural and morphometric features of the acetylcholine innervation in adult rat parietal cortex: an electron microscopic study in serial sections. J Comp Neurol 348:351–373.

Van der Kooy D, Fishell G (1987) Neuronal birthdate underlies the development of striatal compartments. Brain Res 401:155–161.

Van der Werf YD, Witter MP, Groenewegen HJ (2002) The intralaminar and midline nuclei of the thalamus. Anatomical and functional evidence for participation in processes of arousal and awareness. Brain Res Brain Res Rev 39:107–140.

Van Rooijen BD, Claessens MMAE, Subramaniam V (2010) Membrane Permeabilization by Oligomeric α-Synuclein: In Search of the Mechanism. PLoS One 5:e14292.

Veening JG, Cornelissen FM, Lieven P a (1980) The topical organization of the afferents to the caudatoputamen of the rat. A horseradish peroxidase study. Neuroscience 5:1253–1268.

Venda LL, Cragg SJ, Buchman VL, Wade-Martins R (2010) α-Synuclein and dopamine at the crossroads of Parkinson's disease. Trends Neurosci 33:559–568.

Venton BJ, Zhang H, Garris P a., Phillips PEM, Sulzer D, Wightman RM (2003) Real-time decoding of dopamine concentration changes in the caudate-putamen during tonic and phasic firing. J Neurochem 87:1284–1295.

Verma a, Moghaddam B (1998) Regulation of striatal dopamine release by metabotropic glutamate receptors. Synapse 28:220–226.

Vitrac C, Péron S, Frappé I, Fernagut P-O, Jaber M, Gaillard A, Benoit-Marand M (2014) Dopamine control of pyramidal neuron activity in the primary motor cortex via D2 receptors. Front Neural Circuits 8:13.

Vivacqua G, Casini A, Vaccaro R, Fornai F, Yu S, D'Este L (2011) Different sub-cellular localization of alpha-synuclein in the C57BL\6J mouse's central nervous system by two novel monoclonal antibodies. J Chem Neuroanat 41:97–110.

Voorn P, Kalsbeek A, Jorritsma-Byham B, Groenewegen HJ (1988) The pre- and postnatal development of the dopaminergic cell groups in the ventral mesencephalon and the dopaminergic innervation of the striatum of the rat. Neuroscience 25:857–887.

Voorn P, Vanderschuren LJMJ, Groenewegen HJ, Robbins TW, Pennartz CMA (2004) Putting a spin on the dorsal-ventral divide of the striatum. Trends Neurosci 27:468–474.

Wainer BH, Bolam JP, Freund TF, Henderson Z, Totterdell S, Smith AD (1984) Cholinergic synapses in the rat brain: a correlated light and electron microscopic immunohistochemical study employing a monoclonal antibody against choline acetyltransferase. Brain Res 308:69–76.

Wall NR, De La Parra M, Callaway EM, Kreitzer AC (2013) Differential Innervation of Direct- and Indirect-Pathway Striatal Projection Neurons. Neuron:1–14.

Walters RW, Yi SM, Keshavjee S, Brown KE, Welsh MJ, Chiorini JA, Zabner J (2001) Binding of adeno-associated virus type 5 to 2,3-linked sialic acid is required for gene transfer. J Biol Chem 276:20610–20616.

Wang W, Darvas M, Storey GP, Bamford IJ, Gibbs JT, Palmiter RD, Bamford NS (2013) Acetylcholine Encodes Long-Lasting Presynaptic Plasticity at Glutamatergic Synapses in the Dorsal Striatum after Repeated Amphetamine Exposure. J Neurosci 33:10405–10426.

Wang X, Sun Q-Q (2012) Characterization of axo-axonic synapses in the piriform cortex of Mus musculus. J Comp Neurol 520:832–847.

Wang Z, Kai L, Day M, Ronesi J, Yin HH, Ding J, Tkatch T, Lovinger DM, Surmeier DJ (2006) Dopaminergic control of corticostriatal long-term synaptic depression in medium spiny neurons is mediated by cholinergic interneurons. Neuron 50:443–452.

Wassef M, Berod A, Sotelo C (1981) Dopaminergic dendrites in the pars reticulata of the rat substantia nigra and their striatal input. Combined immunocytochemical localization of tyrosine hydroxylase and anterograde degeneration. Neuroscience 6:2125–2139.

Watabe-Uchida M, Zhu L, Ogawa SK, Vamanrao A, Uchida N (2012) Whole-Brain Mapping of Direct Inputs to Midbrain Dopamine Neurons. Neuron 74:858–873.

Watson JB, Hatami A, David H, Masliah E, Roberts K, Evans CE, Levine MS (2009) Alterations in corticostriatal synaptic plasticity in mice overexpressing human alpha-synuclein. Neuroscience 159:501–513.

Weber T, Schönig K, Tews B, Bartsch D (2011) Inducible gene manipulations in brain serotonergic neurons of transgenic rats. PLoS One 6:e28283.

Weiner DM, Levey AI, Brann MR (1990) Expression of muscarinic acetylcholine and dopamine receptor mRNAs in rat basal ganglia. Proc Natl Acad Sci U S A 87:7050–7054.

Wersinger C, Prou D, Vernier P, Sidhu A (2003) Modulation of dopamine transporter function by alpha-synuclein is altered by impairment of cell adhesion and by induction of oxidative stress. FASEB J 17:2151–2153.

Wersinger C, Sidhu A (2003) Attenuation of dopamine transporter activity by alpha-synuclein. Neurosci Lett 340:189–192.

Wess J, Blin N, Mutschler E, Blüml K (1995) Muscarinic acetylcholine receptors: structural basis of ligand binding and G protein coupling. Life Sci 56:915–922.

Westphal CH, Chandra SS (2013) Monomeric synucleins generate membrane curvature. J Biol Chem 288:1829–1840.

Wickens JR, Begg AJ, Arbuthnott GW (1996) Dopamine reverses the depression of rat corticostriatal synapses which normally follows high-frequency stimulation of cortex in vitro. Neuroscience 70:1–5.

Wickens JR, Horvitz JC, Costa RM, Killcross S (2007) Dopaminergic mechanisms in actions and habits. J Neurosci 27:8181–8183.

Wictorin K, Rklund ABJ (1989) Connectivity of striatal grafts implanted into the ibotenic acid-lesioned cortical afferents. Neuroscience 30:297–311.

Wietek J, Wiegert JS, Adeishvili N, Schneider F, Watanabe H, Tsunoda SP, Vogt A, Elstner M, Oertner TG, Hegemann P (2014) Conversion of channelrhodopsin into a light-gated chloride channel. Science 344:409–412.

Wightman RM, Amatore C, Engstrom RC, Hale PD, Kristensen EW, Kuhr WG, May LJ (1988) Real-time characterization of dopamine overflow and uptake in the rat striatum. Neuroscience 25:513–523.

Wilson CJ (2005) The mechanism of intrinsic amplification of hyperpolarizations and spontaneous bursting in striatal cholinergic interneurons. Neuron 45:575–585.

Wilson CJ, Chang HT, Kitai ST (1990) Firing patterns and synaptic potentials of identified giant aspiny interneurons in the rat neostriatum. J Neurosci 10:508–519.

Wilson CJ, Groves PM, Fifková E (1977) Monoaminergic synapses, including dendro-dendritic synapses in the rat substantia nigra. Exp brain Res 30:161–174.

Witten IB, Steinberg EE, Lee SY, Davidson TJ, Zalocusky KA, Brodsky M, Yizhar O, Cho SL, Gong S, Ramakrishnan C, Stuber GD, Tye KM, Janak PH, Deisseroth K (2011) Recombinase-driver rat lines: tools, techniques, and optogenetic application to dopamine-mediated reinforcement. Neuron 72:721–733.

Woolf NJ (1991) Cholinergic systems in mammalian brain and spinal cord. Prog Neurobiol 37:475–524.

Wright AK, Norrie L, Ingham CA, Hutton EA, Arbuthnott GW (1999) Double anterograde tracing of outputs from adjacent “barrel columns” of rat somatosensory cortex. Neostriatal projection patterns and terminal ultrastructure. Neuroscience 88:119–133.

Wright AK, Ramanathan S, Arbuthnott GW (2001) Identification of the source of the bilateral projection system from cortex to somatosensory neostriatum and an exploration of its physiological actions. Neuroscience 103:87–96.

Wu Q, Reith MEA, Walker QD, Kuhn CM, Carroll FI, Garris PA (2002) Concurrent autoreceptor-mediated control of dopamine release and uptake during neurotransmission: an in vivo voltammetric study. J Neurosci 22:6272–6281.

Wu X-S, Wu L-G (2009) Rapid endocytosis does not recycle vesicles within the readily releasable pool. J Neurosci 29:11038–11042.

Wu Y, Parent A (2000) Striatal interneurons expressing calretinin, parvalbumin or NADPH-diaphorase: a comparative study in the rat, monkey and human. Brain Res 863:182–191.

Yamada T, McGeer PL, Baimbridge KG, McGeer EG (1990) Relative sparing in Parkinson's disease of substantia nigra dopamine neurons containing calbindin-D28K. Brain Res 526:303–307.
Yamaguchi T, Sheen W, Morales M (2007) Glutamatergic neurons are present in the rat ventral tegmental area. Eur J Neurosci 25:106–118.
Yamaguchi T, Wang H-L, Morales M (2013) Glutamate neurons in the substantia nigra compacta and retrorubral field. Eur J Neurosci 38:3602–3610.
Yan Z, Flores-Hernandez J, Surmeier DJ (2001) Coordinated expression of muscarinic receptor messenger RNAs in striatal medium spiny neurons. Neuroscience 103:1017–1024.
Yan Z, Song WJ, Surmeier J (1997) D2 dopamine receptors reduce N-type Ca2+ currents in rat neostriatal cholinergic interneurons through a membrane-delimited, protein-kinase-C-insensitive pathway. J Neurophysiol 77:1003–1015.
Yan Z, Surmeier DJ (1996) Muscarinic (m2/m4) receptors reduce N- and P-type Ca2+ currents in rat neostriatal cholinergic interneurons through a fast, membrane-delimited, G-protein pathway. J Neurosci 16:2592–2604.
Yan Z, Surmeier DJ (1997) D5 dopamine receptors enhance Zn2+-sensitive GABA(A) currents in striatal cholinergic interneurons through a PKA/PP1 cascade. Neuron 19:1115–1126.
Yang H, Michael A (2007) In vivo fast-scan cyclic voltammetry of dopamine near microdialysis probes. Electrochem Methods Neurosci.
Yarom O, Cohen D (2011) Putative cholinergic interneurons in the ventral and dorsal regions of the striatum have distinct roles in a two choice alternative association task. Front Syst Neurosci 5:36.
Yavich L, Tanila H, Vepsäläinen S, Jäkälä P (2004) Role of alpha-synuclein in presynaptic dopamine recruitment. J Neurosci 24:11165–11170.
Yin HH, Knowlton BJ (2006) The role of the basal ganglia in habit formation. Nat Rev Neurosci 7:464–476.
Yin HH, Knowlton BJ, Balleine BW (2004) Lesions of dorsolateral striatum preserve outcome expectancy but disrupt habit formation in instrumental learning. Eur J Neurosci 19:181–189.
Yin HH, Knowlton BJ, Balleine BW (2005a) Blockade of NMDA receptors in the dorsomedial striatum prevents action-outcome learning in instrumental conditioning. Eur J Neurosci 22:505–512.
Yin HH, Knowlton BJ, Balleine BW (2006) Inactivation of dorsolateral striatum enhances sensitivity to changes in the action-outcome contingency in instrumental conditioning. Behav Brain Res 166:189–196.
Yin HH, Ostlund SB, Knowlton BJ, Balleine BW (2005b) The role of the dorsomedial striatum in instrumental conditioning. Eur J Neurosci 22:513–523.
Yizhar O, Fenno LE, Davidson TJ, Mogri M, Deisseroth K (2011) Optogenetics in neural systems. Neuron 71:9–34.
Yu S, Li X, Liu G, Han J, Zhang C, Li Y, Xu S, Liu C, Gao Y, Yang H, Uéda K, Chan P (2007) Extensive nuclear localization of alpha-synuclein in normal rat brain neurons revealed by a novel monoclonal antibody. Neuroscience 145:539–555.
Yung KK, Bolam JP, Smith AD, Hersch SM, Ciliax BJ, Levey AI (1995) Immunocytochemical localization of D1 and D2 dopamine receptors in the basal ganglia of the rat: light and electron microscopy. Neuroscience 65:709–730.
Zahm DS, Cheng AY, Lee TJ, Ghobadi CW, Schwartz ZM, Geisler S, Parsely KP, Gruber C, Veh RW (2011) Inputs to the midbrain dopaminergic complex in the rat, with emphasis on extended amygdala-recipient sectors. J Comp Neurol 519:3159–3188.
Zarranz JJ, Alegre J, Gómez-Esteban JC, Lezcano E, Ros R, Ampuero I, Vidal L, Hoenicka J, Rodriguez O, Atarés B, Llorens V, Gomez Tortosa E, del Ser T, Muñoz DG, de Yebenes JG (2004) The new mutation, E46K, of alpha-synuclein causes Parkinson and Lewy body dementia. Ann Neurol 55:164–173.

Zhang F, Gradinaru V, Adamantidis AR, Durand R, Airan RD, de Lecea L, Deisseroth K (2010) Optogenetic interrogation of neural circuits: technology for probing mammalian brain structures. Nat Protoc 5:439–456.

Zhang F, Wang L-P, Boyden ES, Deisseroth K (2006) Channelrhodopsin-2 and optical control of excitable cells. Nat Methods 3:785–792.

Zhang F, Wang L-P, Brauner M, Liewald JF, Kay K, Watzke N, Wood PG, Bamberg E, Nagel G, Gottschalk A, Deisseroth K (2007) Multimodal fast optical interrogation of neural circuitry. Nature 446:633–639.

Zhang H, Sulzer D (2003) Glutamate spillover in the striatum depresses dopaminergic transmission by activating group I metabotropic glutamate receptors. J Neurosci 23:10585–10592.

Zhang H, Sulzer D (2004) Frequency-dependent modulation of dopamine release by nicotine. Nat Neurosci 7:581–582.

Zhang L, Zhang C, Zhu Y, Cai Q, Chan P, Uéda K, Yu S, Yang H (2008) Semi-quantitative analysis of alpha-synuclein in subcellular pools of rat brain neurons: an immunogold electron microscopic study using a C-terminal specific monoclonal antibody. Brain Res 1244:40–52.

Zhang W, Basile AS, Gomeza J, Volpicelli LA, Levey AI, Wess J (2002a) Characterization of central inhibitory muscarinic autoreceptors by the use of muscarinic acetylcholine receptor knock-out mice. J Neurosci 22:1709–1717.

Zhang W, Yamada M, Gomeza J, Basile AS, Wess J (2002b) Multiple muscarinic acetylcholine receptor subtypes modulate striatal dopamine release, as studied with M1-M5 muscarinic receptor knock-out mice. J Neurosci 22:6347–6352.

Zhang Y, Meredith GE, Mendoza-Elias N, Rademacher DJ, Tseng KY, Steece-Collier K (2013) Aberrant Restoration of Spines and their Synapses in L-DOPA-Induced Dyskinesia: Involvement of Corticostriatal but Not Thalamostriatal Synapses. J Neurosci 33:11655–11667.

Zhao S, Ting JT, Atallah HE, Qiu L, Tan J, Gloss B, Augustine GJ, Deisseroth K, Luo M, Graybiel AM, Feng G (2011) Cell type–specific channelrhodopsin-2 transgenic mice for optogenetic dissection of neural circuitry function. Nat Methods 8:745–752.

Zhou F-M, Wilson C, Dani J a. (2003) Muscarinic and Nicotinic Cholinergic Mechanisms in the Mesostriatal Dopamine Systems. Neurosci 9:23–36.

Zhou F-M, Wilson CJ, Dani J a (2002) Cholinergic interneuron characteristics and nicotinic properties in the striatum. J Neurobiol 53:590–605.

Zhou FM, Liang Y, Dani J a (2001) Endogenous nicotinic cholinergic activity regulates dopamine release in the striatum. Nat Neurosci 4:1224–1229.

Zimmerman JB, Wightman RM (1991) Simultaneous electrochemical measurements of oxygen and dopamine in vivo. Anal Chem 63:24–28.

Znamenskiy P, Zador AM (2013) Corticostriatal neurons in auditory cortex drive decisions during auditory discrimination. Nature 497:482–485.

Zoli M, Moretti M, Zanardi A, McIntosh JM, Clementi F, Gotti C (2002) Identification of the Nicotinic Receptor Subtypes Expressed on Dopaminergic Terminals in the Rat Striatum. J Neurosci 22:8785–8789.